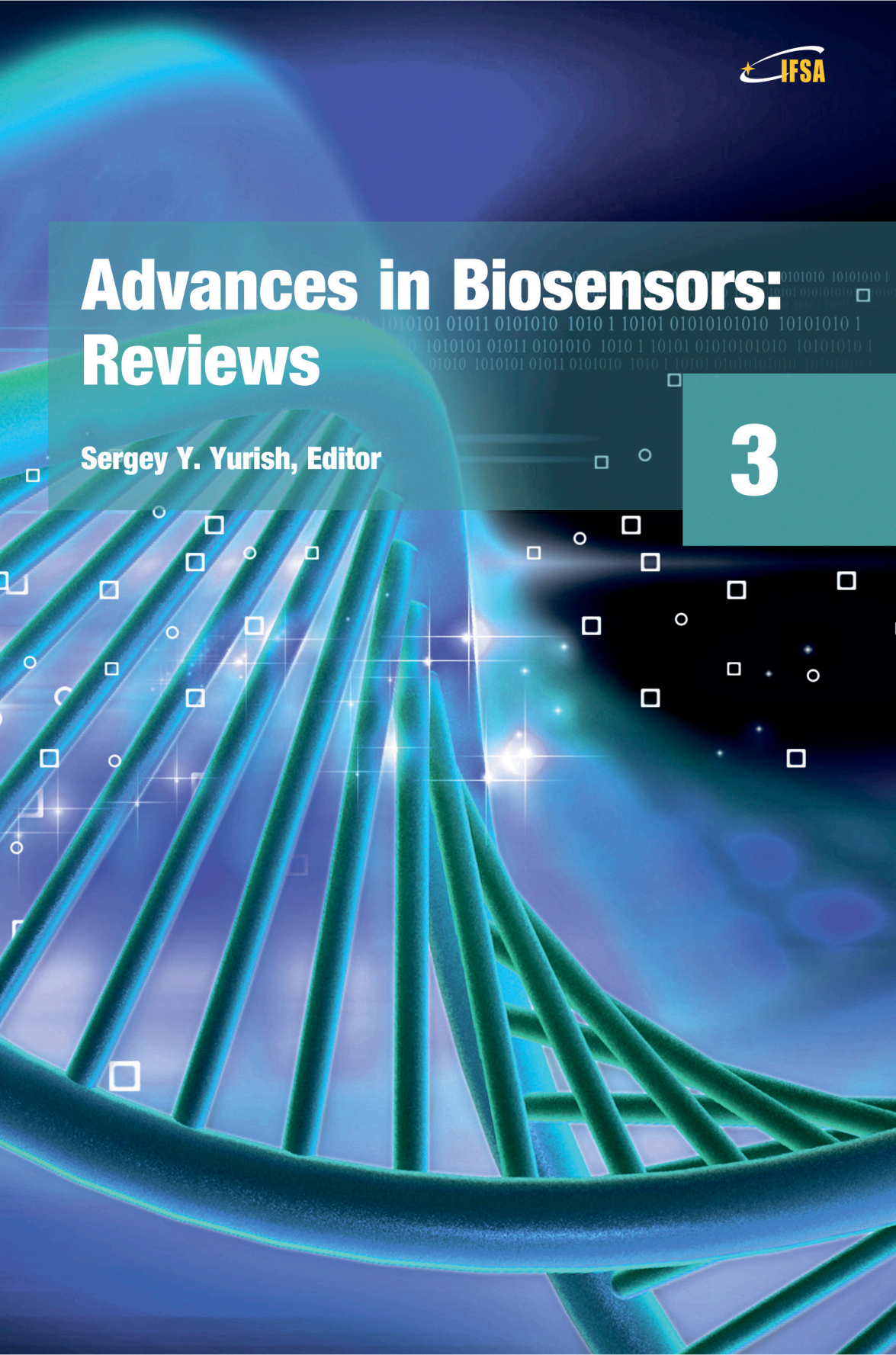
IFSA
Advances in Biosensors: Reviews
Sergey Y. Yurish, Editor
3

Advances in Biosensors: Reviews

Volume 3

S. Yurish
Editor

Advances in Biosensors: Reviews

Volume 3

International Frequency Sensor Association Publishing

S. Yurish, *Editor*
Advances in Biosensors: Reviews. Volume 3

Published by IFSA Publishing, S. L., 2020
E-mail (for print book orders and customer service enquires):
ifsa.books@sensorsportal.com

Visit our Home Page on http://www.sensorsportal.com

ISBN: 978-84-09-25125-4
e-ISBN: 978-84-09-25124-7
BN-20201107-XX
BIC: TCBS

Contents

Contents **5**
Preface **11**
Contributors **13**

1. Biomimetic Olfactory Biosensors and Bioelectronic Noses **15**
1.1. Introduction 15
1.2. The Olfactory System A Source of Inspiration 17
1.2.1. How Do We Smell ? *17*
1.2.2. The Mystery of Odor Discrimination (Odor Coding) *18*
1.2.3. Structure and Signaling Process of Olfactory Receptors *20*
1.2.4. Important Implication of Other Proteins *21*
1.3. Biomimetic Olfactory Biosensors and Bioelectronic Noses 23
1.3.1. Olfactory Tissues and Cells-based Olfactory Biosensors and Bioelectronic Noses *24*
1.3.2. Olfactory Receptor Based Olfactory Biosensors and Bioelectronic Noses *26*
1.3.2.1. Membrane Fractions 28
1.3.2.2. Nanovesicles 33
1.3.2.3. Nanodiscs 38
1.3.3. Odorant Binding Proteins Based Olfactory Biosensors and Bioelectronic Noses *44*
1.3.3.1. Odorant Analysis in the Liquid Phase 45
1.3.3.2. Odorant Analysis in the Gas Phase 49
1.4. Conclusions and Perspectives 51
Acknowledgments 53
References 54

2. Multifunctional Flexible Nanocomposite Sensors for Biomedical Applications **65**
2.1. Introduction 65
2.2. Fabrication of Polymer Composite Films 67
2.3. Characterization of Nanocomposite Films 70
2.3.1. Dielectric, Conductivity and Pyroelectric Characterization *70*
2.3.2. Figures-of-merits of Nanocomposites *71*
2.3.3. Piezoresistive Characterizations *71*
2.4. Conclusions 73
Acknowledgments 77
References 78

3. Novel Ni-based Nanostructures for Non-enzymatic Glucose Detection 81
3.1. Introduction 81
3.1.1. Diabetes and Enzymatic Glucose Sensors 81
3.1.2. Non-enzymatic Glucose Detection 83
3.1.3. Ni-based Electrodes 85
3.2. Methodology 87
3.2.1. Experimental Setup 87
3.2.2. Experimental Procedure 87
3.3. Advances in Non-enzymatic Glucose Detection by Ni-based Nanostructures 89
3.3.1. Porous Structures 89
3.3.2. Hierarchical Structures 94
3.3.3. Other Approaches 96
3.4. Conclusions 98
References 99

4. Wearable Sensors for Individual Grip Force Profiling 107
4.1. Introduction 107
4.2. Functional Characteristics of Human Grip Force 108
4.3. Wearable Grip Force Sensors for Individual Grip Force Profiling in Real Time during Bimanual Task Execution 112
4.4. Data Analysis and Visualization 117
4.5. Conclusions 121
References 122

5. Microfluidic Technologies for Clinical Biology and Biomedical Applications 125
5.1. Introduction 125
5.2. The Impact of Microfluidics on Biomedical Research 126
5.3. Microfluidic Technology for Stem Cell Research 127
5.4. Microfluidic Technology for Cancer Research 128
5.5. Microfluidic Technology for Fertility Research 130
5.6. Microfluidic Technology for Single Cell Analysis 131
5.7. Microfluidic Technology for Tissue Engineering 132
5.8. Microfluidic Technology for Pathogen Detections (Diagnostic Applications) 134
5.9. Microfluidic Technology for Protein Detection (Diagnostic Applications) 136
5.10. Microfluidic Technology for Organ on Chip 138
5.11. Microfluidics for Drug Delivery System 141
5.12. Conclusion and Future Perspective 143
References 144

6. A Simple and Accurate Method to Assess Autonomic Nervous System through Sudomotor Function 149
6.1. Introduction 149
6.2. Foundations: The Eccrine Sweat Glands 150
6.2.1. Physiological Behavior 151

6.2.2. Agonist and Antagonist Neurotransmitter Activations *152*
6.2.3. Electrical Stimulations *154*
6.3. Insight into the Sudoscan Measure: Electrochemical Hairless Skin Model at Low Voltages 154
6.3.1. Global Qualitative Considerations *155*
6.3.2. General Law of Conservation *156*
6.3.3. Geometrical Model of Eccrine Gland, Variables and Currents *157*
6.3.3.1. Geometry and Variables 157
6.3.3.2. The Currents 158
6.3.3.3. Ohm's Law and Electrical Field 160
6.3.4. Governing Conservation Equations *160*
6.3.4.1. Mass Conservation 160
6.3.4.2. Momentum Conservation 162
6.3.4.3. Momentum Steady Equation: Concentration Constancy 163
6.3.4.4. Mass Steady Equation 165
6.3.5. Steady State Additional Analytics for the Conservation of Mass Equation *166*
6.3.5.1. The Voltage inside the Gland is Almost Constant 167
6.3.5.2. The Axial Current is Almost Piecewise Linear 168
6.3.6. Skin Conductance: Gland Wall Ion Permeability *169*
6.3.7. Normalization *170*
6.3.8. Section Conclusion *172*
6.4. The Sudoscan Technology 172
6.4.1. Sudoscan Medical Device Description *173*
6.4.2. The Signal Measured and Its Main Parameters *175*
6.4.3. A Much Desired and Important Property of the Measure: Reproducibility *177*
6.4.4. Section Conclusion *178*
6.5. Clinical Applications for Various Pathologies and Treatments 179
6.5.1. Principle of the Method as It Is Explained to Clinician Users *180*
6.5.2. Clinical Development *180*
6.5.2.1. Normative Data and Accuracy of the Method 181
6.5.2.2. Performance in the Assessment of Sweat Function and Small Fiber Neuropathies as Compared to Usual Reference Methods 182
6.5.2.3. Performance in the Detection of Peripheral Neuropathy in Patients with Diabetes 185
6.5.2.4. Performance in the Detection of Cardiac Autonomic Neuropathy in Patients with Diabetes 186
6.5.2.5. Performance in the Diagnosis of Peripheral Neuropathy in Patients with Neurodegenerative Diseases 188
6.5.2.6. Performance in the Follow-up of Patients with Peripheral Neuropathy 189
6.5.3. New Clinical Developments *190*
6.5.4. Conclusion on Clinical Applications *191*
6.6. General Conclusion 191
Acknowledgements 192
References 192
Appendix 1. General Law of Conservation 196

Appendix 2. Mass Equation Source Term 201
Appendix 3. A Result Proof 202
Appendix 4. A Result Proof 203
Appendix 5. A Result Proof 203
Appendix 6. A Result Proof 204

7. Zinc Oxide (ZnO) Nano Particles for Anxiolytic Effect 205
7.1. Introduction 205
7.2. Nature of Anxiety: A Brief Look 206
7.3. Zinc and Human Metabolism 208
7.4. Synthesis of Nano Zinc Oxide 210
7.4.1. Chemical Precipitation 211
7.4.2. Sol-gel Method 212
7.4.3. Pyrolysis Methods 212
7.4.4. Mechanochemical Method 213
7.4.5. Biological Method 215
7.5. Nano Zinc Oxide for Anxiety Treatment 216
7.6. Conclusions and Future Perspectives 218
References 219

8. Enzyme Biosensors 223
8.1. Introduction 223
8.2. Basic Principle of Biosensors 224
8.2.1. Bioreceptors 224
8.2.2. Transducers 226
8.3. Enzymes as Biorecognition Elements 226
8.3.1. Effects of Immobilization on Enzyme Biosensor Response 228
8.3.2. Working Principle of Recognition 229
8.4. Classification of Enzyme Biosensors 230
8.4.1. Classification on the Basis of Evolution 230
8.4.1.1. 1st Generation Biosensors 231
8.4.1.2. 2nd Generation Biosensors 232
8.4.1.3. 3rd Generation Biosensors 233
8.4.2. Classification of Biosensor on the Basis of Transducing Mechanism 234
8.4.2.1. Electrochemical Enzyme Biosensors 234
8.4.2.2. Optical-detection Biosensors 236
8.4.2.3. Piezoelectric Biosensors 237
8.4.2.4. Thermal-detection Biosensors 237
8.4.3. Classification on the Basis of Monitoring Method 237
8.5. Advantages of Enzyme Biosensors [73-75] 239
8.6. Limitations of Enzyme Biosensors [76] 239
8.7. Factors Responsible for Enzyme Biosensor Failure 240
8.8. Applications of Enzyme Biosensors 241
8.8.1. Biomedical and Diagnostics 241
8.8.2. Agriculture and Environment 249
8.8.3. Food and Other Industries 252

8.9. Future Prospects 255
References 256

9. Nanobiosensors 273
9.1. Introduction 273
9.2. Types of Nanobiosensors based on Nanostructured Materials 275
9.2.1. Carbon Nanotubes Based Nanobiosensors 277
9.2.2. Graphene Based Nanobiosensors 283
9.2.3. Metal Nanoparticles Based Nanobiosensors 288
9.2.4. Metal Oxide Nanomaterials based Nanobiosensors 299
9.2.5. Enzyme Nanoparticles based Nanobiosensors 308
9.3. Applications of Nanobiosensors 312
9.3.1. Biomedical and Diagnostic Application 312
9.3.2. Environmental Applications 313
9.3.3. Food Contamination Monitoring Applications 314
9.3.4. Miscellaneous Applications 314
9.4. Conclusion and Future Prospects 315
References 316

Index 335

Preface

After successful publication of *'Advances in Biosensors: Reviews'*, Open Access Book Series Vol. 1 in 2017 and Vol.2 in 2018, and feedback from our authors and readers, we have decided to publish the third volume of this popular Book Series in 2020.

According to a new report by Grand View Research, Inc., the global biosensors market size is anticipated to reach US$ 36.0 billion by 2027, expanding at a CAGR 7.9%, various applications in the medical field, high demand for miniature diagnostic devices, and rapid technological advancements are the key driving factors for the market.

The 3rd volume of '*Advances in Biosensors: Reviews'*, Book Series contains 9 chapters written by 27 authors from 6 countries: France, India, Italy, Malaysia, Turkey and USA.

Chapter 1 devoted to the development of biomimetic olfactory biosensors and electronic noses. Authors introduce the mechanism of smell and odor discrimination principles and describe the main components of the olfactory system that are currently used as raw sensing materials for the design of biosensors namely the olfactory receptors and some other proteins such as odorant binding proteins and enzymes involved in biological olfaction. A review on the development of biomimetic olfactory biosensors and bioelectronic noses based on olfactory tissues and cells, olfactory receptors, and odorant binding proteins.

Chapter 2 describes the development and characterization of the multifunctional flexible nanocomposite film. To improve the sensitivity, the novel P(VDF-TrFE) film-sensors embedded with carbon nanoparticles were synthesized and fabricated via the solution casting technique. The fabricated films were characterized for dielectric, piezoresistive and electrical properties to predict the performance of the sensors for pressure and thermal detection. The possible applications of fabricated films in various biomedical devices are briefly described.

Chapter 3 is dedicated to the novel Ni-based nanostructures for non-enzymatic glucose detection. The Ni-based nanostructures with large surface area and porous structure have shown improved electrochemical properties, which allow to boost the sensitivity of glucose sensors.

Chapter 4 provides an overview of the current state of the art in grip force profiling to highlight important functional aspects. Various sensor glove systems for the real-time monitoring of surgical task skill evolution in novices training in a simulator task are also described.

Chapter 5 discuss how microfluidic technologies contributed in the fields such as drug discovery, high throughput screening and diagnostics, tissue and organ developments, as well as provides a solutions to perform rapid and efficient experiments on less sample volumes.

First, the Chapter 6 presents key information about the physiology of sweat glands and their control *via* small C fibers releasing Cholinergic and Adrenergic neurotransmitters. Then a full physical model of sweat gland behavior in the presence of low direct voltage applied to the skin will be developed and its physico-electrochemical properties demonstrated. It is followed by a description of the Sudoscan patented technology. Finally, the main results of the principal clinical development programs performed over the last 10 years using this very easy to use technology are summarized.

Chapter 7 presents an overview of considering ZnO nano-particles for anxiety treatment. After a brief look at the concept of anxiety, the synthesis of ZnO nano-particles such as wet chemical methods mechanochemistry and biological methods has been given. The techniques have been presented in a way that is comprehensible to researchers with various fields of study.

Chapter 8 is about the enzyme biosensors, its basic principle, classification, components and types of biorecognition elements. The advantages and limitations are also discussed in the chapter. This chapter is followed by the Chapter 9 on nanobiosensors of different types and its applications from the same authors. The future perspectives of nanobiosensors are also outlined.

I hope that readers will enjoy this new volume and that can be a valuable tool for those who are involved in research and development of different biosensors and biosensing systems.

I am looking for any advices, comments, suggestions and notices from the readers to make the next volumes of becoming popular *'Advances in Biosensors: Reviews'* Book Series.

Sergey Y. Yurish,
Editor, IFSA Publishing *Barcelona, Spain*

Contributors

Mohan Aggarwal, Department of Physics, Chemistry, and Mathematics (Materials Science Group), Alabama A & M University, USA

Suzi Amado, Clinical Psychologist, MEF University, Istanbul, Turkey, E-mail: suziamado@gmail.com

Hanna Ayoub, Impeto Medical, Paris, France

Ashok K. Batra, College of Engineering, Technology and Physical Sciences, Alabama A&M University, Normal (Huntsville), Alabama, USA

Philippe Brunswick, Impeto Medical, Paris, France

Arnaud Buhot, Univ. Grenoble Alpes, CEA, CNRS, IRIG, SyMMES, UMR5819, F-38000 Grenoble, France

Mohamed Yousuff Caffiyar, C. Abdul Hakeem College of Engineering and Technology, Melvisharam, Vellore, Tamil Nadu, India

Jean-Henri Calvet, Impeto Medical, Paris, France

Michel Cassir, PSL Research University, Chimie Paristech-CNRS, Institut de Recherche de Chimie de Paris, Paris, France

Birgitta Dresp-Langley, Centre National de la Recherche Scientifique (CNRS), France
UMR 7357 ICube Lab, CNRS and University of Strasbourg, France

Marielle El Kazzy, Univ. Grenoble Alpes, CEA, CNRS, IRIG, SyMMES, UMR5819, F-38000 Grenoble, France

Burcu Ertuğ, Nişantaşı University, Istanbul, Turkey,
E-mail: burcu.ertug@nisantasi.edu.tr

Kunal Grover, Henry Ford Health System, Detroit, MI 48202, USA

Yanxia Hou, Univ. Grenoble Alpes, CEA, CNRS, IRIG, SyMMES, UMR5819, F-38000 Grenoble, France

Charlotte Hurot, Univ. Grenoble Alpes, CEA, CNRS, IRIG, SyMMES, UMR5819, F-38000 Grenoble, France

A. Jabeena, VIT University, Vellore, Tamil Nadu, India

Ismail Hussain Kamal Basha, Universiti Teknologi PETRONAS, 32610 Seri Iskandar, Perak Darul Ridzuan, Malaysia

Aschalew Kassu, Department of Mechanical, Civil Engineering and Construction Management College of Engineering, Technology and Physical Sciences Alabama A&M University, Normal (Huntsville), AL 35762, USA

Kamel Khalfallah, Impeto Medical, Paris, France

Salvo Mirabella, Department of Physics and Astronomy "Ettore Majorana", University of Catania, Italy

Marie-Laure Névoret, REGENXBIO, Rockville, MD (Maryland), USA

Sharvare Palwai, Department of Physics, Chemistry, and Mathematics (Materials Science Group), Alabama A & M University, USA

Ashok Saini, Department of Microbiology, Institute of Home Economics, University of Delhi, New Delhi, India

Mario Urso, Department of Physics and Astronomy "Ettore Majorana", University of Catania, Italy

Kavita Vasdev, Department of Microbiology, Gargi College, University of Delhi, New Delhi, India

Jonathan S. Weerakkody, Univ. Grenoble Alpes, CEA, CNRS, IRIG, SyMMES, UMR5819, F-38000 Grenoble, France

Sandeep Yadav, Department of Biochemistry, Institute of Home Economics, University of Delhi, New Delhi, India

Chapter 1

Biomimetic Olfactory Biosensors and Bioelectronic Noses

Marielle El Kazzy, Charlotte Hurot, Jonathan S. Weerakkody, Arnaud Buhot and Yanxia Hou

1.1. Introduction

The environment in which we live is rich in odorants emitted from various natural and unnatural sources (plants, bacteria, industrial activities and other human activities). Odors are mainly composed of hydrophobic volatile organic compounds (VOCs) with molecular weights of less than 300 Da. They cover many chemical classes including organic acids, alcohols, aldehydes, ethers, esters, amides, amines, hydrocarbons, halogenated hydrocarbons, ketones, nitriles, aromatics, phenols, other nitrogen-containing compounds, and sulfur-containing compounds. Nowadays, the analysis of VOCs is of great interest to a diverse variety of fields, such as environmental monitoring, public safety and security, the food and beverage industry, the cosmetics and perfume industry, medical diagnostics and health monitoring, etc.

Traditional analytical methods, such as gas chromatography coupled to mass spectroscopy (GC-MS), are very accurate, reliable and able to identify different substances in a sample. Moreover, when combined with olfactometry, they can provide not only detailed chemical information but also sensory information. Nevertheless, these techniques require expensive equipment as well as expertise in operating them. They are often time-consuming and laborious to perform. On the other hand,

Yanxia Hou
Univ. Grenoble Alpes, CEA, CNRS, IRIG, SyMMES, UMR5819, Grenoble, France

the human nose is often used to analyze odorants and assess the quality of products in the food, beverage, cosmetics, and perfume industries. However, its use is limited by the fact that panelists are expensive to train and employ, and sometimes they can give biases in results highlighting the subjectiveness of the human sense of smell. Consequently, these approaches are not practical for use in a large scale. In such a context, there is an increasing demand for a device that could mimic the human nose and provide an objective, quantitative, rapid, and reliable analysis of odorants.

An interesting alternative could be electronic noses (eNs), which consist of an array of cross-reactive chemical sensors combined with an appropriate transduction system, and use advanced mathematical procedures based on pattern recognition and/or multivariate statistics for signal processing. Over the last three decades, eNs have demonstrated their great potential and efficiency as analytical tools for the analysis of VOCs in many fields [1-4]. However, for most existing eNs the main drawback is the lack of good selectivity. To overcome it, in the last decade, an increasing number of research activities have been concentrated on the development of olfactory biosensors and bioelectronic noses by incorporating biological material from the olfactory system (i.e. proteins, derivatives of cells and tissues, etc.) as sensing material in the device [5-9].

To clarify the terms, in this chapter, an olfactory biosensor refers to a single sensor system, while a bioelectronic nose refers to a multiplexed system with an array of olfactory biosensors.

Thanks to the current knowledge about the biological olfaction and recent achievements in genetic engineering, biotechnology and nanotechnology, such bioelectronic noses can better mimic the biological olfactory system with improved performances such as high sensitivity and selectivity. However, the integration of these sensing biomaterials to a bioelectronic nose device remains challenging due to the complex and fragile structure that governs their proper functionality.

After introduction, in the second part of this chapter, for better understanding the different strategies and technical solutions employed for the development of biomimetic olfactory biosensors and electronic noses, we will present the source of inspiration: the olfactory system. We will introduce the mechanism of smell and odor discrimination principles. Then we will describe the main components of the olfactory

system that are currently used as raw sensing materials for the design of biosensors namely the olfactory receptors (ORs) and some other proteins such as odorant binding proteins (OBPs) and enzymes involved in biological olfaction. In the third part, we will give a review on the development of biomimetic olfactory biosensors and bioelectronic noses based on olfactory tissues and cells, olfactory receptors, and odorant binding proteins. For each system, we will highlight the immobilization strategy employed to conserve the biological properties of the sensing material as well as its performances for the analysis of odorants. Finally, we will make a general conclusion and give some perspectives.

1.2. The Olfactory System A Source of Inspiration

1.2.1. How Do We Smell ?

Among the human senses, the mechanisms of sight, hearing, and touch that are based on physical stimulus are well understood. Today, we are able to fabricate devices that can record and reproduce the signals to mimic these senses, for example, camera for sight, microphone for hearing, and tactile sensor in smart phones and tablet PCs for touch. In contrast, the mechanism by which the biological nose can detect and identify odorant molecules based on chemical stimulus has long remained unknown. In fact, in 1970, when the organic chemist Robert Luft was asked, how olfactory perception is achieved, he replied “If you answer to this question, the Nobel Price is yours” [10]. And indeed, in 2004, Linda B. Buck and Richard Axel received the Nobel Prize in Physiology or Medicine [11] for their ground-breaking work on the molecular basis of odor recognition in 1991 [12]. In their famous study, they identified, for the first time, a multigene family that encodes the core proteins of the olfactory system: the olfactory receptors. They isolated and cloned 18 different ORs that bound odorants. For which, they also determined their structural features and other properties that will be detailed later.

As shown in Fig. 1.1, ORs are incorporated into the plasma membrane of the dendritic extrusions of olfactory neurons (ONs) called cilia. Each olfactory neuron expresses about a million copies of only one type of receptor. To enable the detection of odorant molecules, those non motile cilia are projected into the mucus that covers the nasal epithelium. On the other extremity, the unmyelinated axons of all the ONs carrying the

same type of ORs penetrate the ethmoid bone and reach the olfactory bulb where they converge into clusters called glomerulus. The glomeruli are then connected to the olfactory cortex via mitral and tufted cells that constitute second order neurons needed for processing the incoming signals [13, 14].

When the respiratory air enters the nasal cavity, the carried odorant molecules are dissolved in the mucus or transported by some other proteins to the vicinity of the ORs. Depending on their affinity, the ligands bind more or less strongly to the receptor and trigger a signalling cascade in the ONs. This generates an electrical impulse that is transmitted to the olfactory cortex where the signal is processed and the olfactory message is decoded.

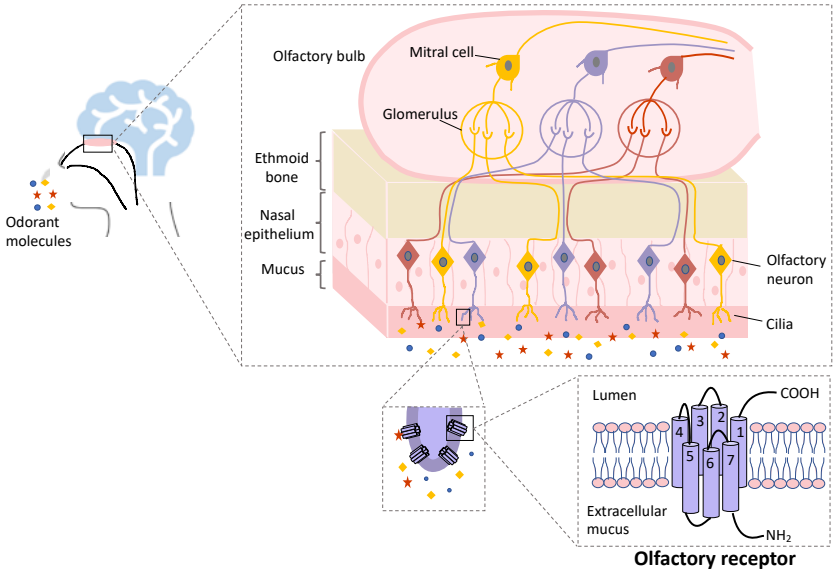

Fig. 1.1. Scheme of the structure of the olfactory system.

1.2.2. The Mystery of Odor Discrimination (Odor Coding)

Often underrated and overlooked compared to the other senses, our noses actually hold many hidden "super powers". Indeed, with roughly 400 different types of ORs, our odor detector can discriminate more than ten thousand different odors and can even distinguish between two

odorant enantiomers. For example, the (S)-(+)-2-methyl butanoic acid is perceived as tender and fruity while its enantiomer (R)-(-)-2-methyl butanoic acid smells like cheese or sweat [15]. But the most striking fact is that our olfactory system can detect some odorants such as 2-isobutyl-3-metoxypyrazine (IBMP – bell pepper odor) at sub nanomolar concentrations (0.01 nM in aqueous solution) [16]. This is equivalent to detect a few milligrams in an Olympic size swimming pool! Furthermore, it was recently reported that humans can discriminate more than 1 trillion olfactory stimuli [17].

To break the olfactory code, scientists have suggested many theories and proposed different models such as the "lock-key" model presented by Amoore [18] and the vibrational theory [19] by Malcolm Dyson. Despite all these models, the mystery behind the outstanding resolution and diversity of odor perception remained unsolved until the identification of the multigene family by Buck and Axel [12]. This discovery has opened new doors to study and investigate interaction modes between the ORs and odorant molecules.

With this intention, thanks to electrophysiological measurements, Firestein *et al.* [20] concluded that olfactory receptors are broadly tuned and can interact with a large spectrum of distinct odorant molecules. Similarly, using calcium imaging Krautwurst *et al.* [21], Malnic *et al.* [22] and Touhara [23] have confirmed that most ORs are indeed selective but not specific. In fact, one receptor can interact with more than one odorant molecule and each odorant molecule can be recognized by multiple olfactory receptors. This observation has led to the conclusion that the olfactory system uses a combinatorial code to discriminate and identify odors. This result can finally explain why odorant molecules having similar structures (such as enantiomers) could elicit a completely different physiological response.

In fact, it is this cross-reactive principle that has inspired the design of electronic noses. Such devices rely on an array of wide-spectrum sensing materials (the "ORs") coupled to a transducer (the "neurons") and associated with a pattern-recognition system (the "brain") to identify the odor. One sensing material must be able to bind different odorant molecules, and reversely, one odorant molecule can bind different sensing materials.

1.2.3. Structure and Signaling Process of Olfactory Receptors

For better understanding the olfaction mechanism in vertebrate at a molecular level, in this part, the structure and signalling process of vertebrate ORs will be presented. The work of Buck and Axel suggested the existence of a superfamily of odorant receptors characterized by seven transmembrane domains and exhibiting variability in regions that potentially represent the binding site of odorant molecules. They have also supported the idea that an intracellular G protein could be involved in the transduction mechanism. Since this breakthrough, many studies have been performed to identify, characterize and deorphanize the members of this large receptor family in both vertebrate and invertebrate [20, 21, 24-27]. Encoded by a multigene family [12, 28], ORs are heptahelical transmembrane G-protein-coupled receptors (GPCRs) that bind odorants. They belong to the class A, like rhodopsin or adrenergic receptors and constitute the largest family of GPCRs identified in the mammalian genome (~1000 genes) [13, 26, 29, 30]. Today, we know that the human genome harbors 396 functional OR genes [31].

The transduction mechanism of ORs in vertebrates and especially in humans has been extensively studied and described [30, 13, 32-36]. It is schematically illustrated in Fig. 1.2. Like all the members of GPCRs family, ORs transduce the binding event via the activation of a molecular switch: the guanine nucleotide-binding protein also called G-protein. Olfactory G-proteins (G_{olf}) are heterotrimeric proteins that consist of three subunits: alpha ($G\alpha_{olf}$), beta (β) and gamma (γ) [37, 38]. The last two subunits often form a stable dimer: The $G\beta\gamma$ complex. The binding of an odorant molecule induces a conformational change in the receptor that will activate its associated G-protein. When the G-protein is activated, the guanosine diphosphate (GDP) initially bound to the alpha subunit is replaced by a guanosine triphosphate (GTP). As a consequence, the α subunit dissociates from the G-protein complex and activates an enzyme: the adenylyl cyclase (AC). AC catalyzes the conversion of adenosine triphosphate (ATP) into the cyclic-3′, 5′-Adenosyl monophosphate (cAMP) neurotransmitter. The increasing concentration of cAMP triggers the opening of the cAMP-dependent membrane cation channels and thus enabling the entry of sodium and calcium ions (Na^+ and Ca^{2+}) into the ciliary lumen. Moreover, the influx of Ca^{2+} induces the opening of the Ca^{2+}-dependent Cl^- channels, which allows the exit of chloride ions Cl^- and a further depolarization of the cell. If the resulting membrane potential is large enough, an electrical

signal is generated and propagates, via the axons, to the olfactory cortex in the brain.

It should be noted here that the change in conformation that occurs upon an odorant binding event is a very important fact that allows the use of ORs for bioelectronic nose development. Indeed, the conformational change elicits a change in the electrical properties of the protein [39]. Thus, using different transduction strategies, it is possible to obtain measurable and detectable signals.

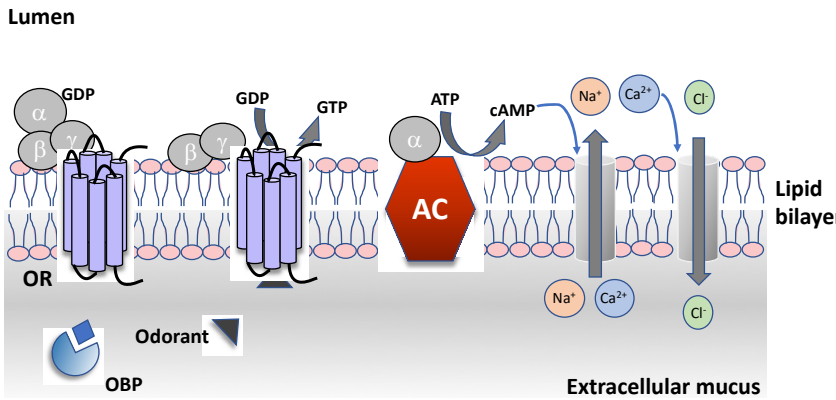

Fig. 1.2. Transduction mechanism of olfactory receptors.

1.2.4. Important Implication of Other Proteins

Some other proteins such as odorant binding proteins and odorant degrading enzymes also play a very important role in the olfaction mechanism. Their structure and functions are presented below.

Odorant binding proteins were detected for the first time by Pelosi *et al.* [40] in 1982 while searching for olfactory receptors using radioactively labeled odorant 2-isobutyl-3-metoxypyrazine (IBMP). Since then, the initially called pyrazine binding proteins were widely studied both in vertebrates (cow/bovine [41, 42], rat [43], rabbit [44], mouse [45, 46], humans [47], etc.) and insects (honeybee [48], drosophila [49], mosquitos [50], moth [51], etc.); and their amino acid sequence, structure and ligand affinities were extensively investigated. Additionally, many interesting reviews that summarize and discuss the work reported in the literature have been published [16, 52-58].

Highly concentrated in the nasal mucus of vertebrates [47] and in the sensory lymph of insects [55, 57], OBPs are small soluble proteins with low molecular weight (around 20 kDa) [16]. They are able to bind different classes of odorants in a reversible manner with a micromolar range dissociation constant [16, 52]. Vertebrate OBPs belong to the lipocalin family which also includes proteins such as bilin-binding protein (BBP) and retinol-binding protein (RBP) [59]. Despite presenting a great divergence in their amino acid sequence vertebrates OBPs share a common three-dimensional structure. This special architecture consists of a β-barrel formed by eight antiparallel β-sheets and a short α-helical domain at the C-terminus [60, 61]. On the other hand, insect OBPs are characterized by a structure that involves a hydrophobic cavity composed of six α-helical domains stabilized by three disulfide bonds [55-57].

Despite their well-defined structure, the physiological functions of OBPs in olfaction and chemoreception are not yet fully understood. Nevertheless, based on their characteristics (solubility, cross reactivity, molecular weight…) and their homology to carrier proteins such as alpha 2-microglobulin, some hypotheses have been proposed. Pevsner *et al.* [42, 62] first suggested that, like hemoglobin transports oxygen, OBPs may play a role in odorant transport and facilitate their diffusion across the aqueous mucus since odorant molecules are mainly hydrophobic. In addition, this could help in preserving these chemical messengers from enzymatic degradation [55]. In insects, a special class of binding proteins known as PBPs (pheromone binding proteins) was identified. Just like OBPs, PBPs transport pheromones through the sensillar lymph to reach their receptors and protect them from degrading enzymes [63, 57]. Finally, OBPs are also suspected to act as scavengers for odorants [33, 54]. They are thought to participate in olfactory signal termination by removing the odorant molecules from the mucus.

Indeed, another important part in the olfaction process is the signal termination. In fact, one of the remarkable features of the biological nose is its ability to rapidly recover after exposure to odorant molecules. This desensitization task also involves another protein family including protein kinase (such as protein kinase A or protein kinase C) and specialized G-protein receptor kinase (such as rhodopsin kinase) [53, 57, 64]. Those odorant degrading enzymes act directly on the ORs by phosphorylation, which stops their biological activity. It is important to note that phosphorylation of the receptors can also be induced by some odorants.

In order to ensure a real time detection and avoid the saturation of the olfactory receptors, the olfactory system must be constantly regenerated from odorant stimuli. Additionally, odorant molecules and pheromones are xenobiotic compounds thus, they must be eliminated from the system. In vertebrate, this task is assured by cytochrome P-450 enzymes which are a subset of monooxygenases [53, 64]. First identified in the liver, those enzymes have been found to be very active in the olfactory epithelium in the vicinity of the ORs [65]. Moreover, in many insects, enzymes such as esterase and oxidase that degrade sex pheromones were detected in the antenna and sensillar lymph [53, 57, 63].

To summarize, the remarkable performances in term of sensitivity and selectivity make the biological nose an extraordinary analytical system. Indeed, with millions of years of evolution, it has excellent performance for odor detection, discrimination, and recognition. Therefore, it presents a great source of inspiration for the design of highly accurate odor analysis tools. In the following part of this chapter, we will present the progress on the development of biomimetic olfactory biosensors and bioelectronic noses.

1.3. Biomimetic Olfactory Biosensors and Bioelectronic Noses

Since the mechanism of olfaction was unveiled, numerous teams from around the world have started to develop a new generation of odor analysis tools by mimicking the human nose. For this, they incorporated sensitive biomaterials from the olfactory system including ORs, OBPs, enzymes, and olfactory tissues into electronic devices. Indeed, so far, the sensitivity and selectivity of those bio-components for specific ligands can hardly be matched by any artificial material. In the last few decades, increasing research activities have concentrated on the exploitation of these biomaterials for the development of novel olfactory biosensors and bioelectronic noses. These systems have improved performances compared to classical eNs, which often employ chemical materials such as metal oxides, polymers, etc. However, their development is quite challenging due to several issues, namely the protein production in large quantities, the poor stability of biomaterials, the short lifetime and the poor reproducibility of biosensors. Fortunately, thanks to recent important advances in biotechnologies, nanotechnologies, and data processing, great progress has been made on their development, as summarized by several reviews [5, 27, 66-72]. In this part, we will present and discuss the ingenious strategies proposed by different teams

to tackle these technical challenges for building robust, sensitive and selective olfactory biosensors and bioelectronic noses.

1.3.1. Olfactory Tissues and Cells-based Olfactory Biosensors and Bioelectronic Noses

One biomimetic option that has been investigated for developing olfactory biosensors and bioelectronic noses consist in using olfactory tissues and cells as sensing materials [5, 73-79].

P. Wang's group designed a biomimetic cell-based olfactory biosensor by combining different olfactory tissues with an electronic transduction system. In the first example [77] they investigated the use of olfactory neurons and olfactory bulb cells as sensing material. Light-addressable potentiometric sensor (LAPS), a surface potential detector, was used as the transducer. This technique enables the detection of odorant binding by monitoring the extracellular potential of the cells. Olfactory neurons and bulb cells were collected from rat pups and cultivated on the silicon surface of LAPS chip (Fig. 1.3 a), which was coated with a mixture of poly-l-ornithine and laminin to improve its biocompatibility and thus promote cell adhesion. The performances of this olfactory biosensor were tested upon the injection of different concentrations of acetic acid. As a result, the system showed a linear dose-response. In addition, the sensitivity of the device to glutamic acid (Glu) (an important neurotransmitter in the olfactory bulb) was also tested. The device was capable to detect Glu at a concentration of 25 μM.

In a second study [78], they coupled olfactory mucosa tissue to a LAPS device (Fig. 1.3 b). The olfactory tissue was extracted from Sprague–Dawley rats and the isolated mucosa was deposited on the sensor surface with cilia receptors side up. To improve the attachment of the tissues, the surface was initially coated with dissolved cellulose nitrate and dried in air. Butanedione and acetic acid solutions were used to stimulate the system. It was shown that the olfactory mucosa tissues conserved their function and the obtained system was sensitive and responded to odorant stimulus. Moreover, when freshly isolated tissue was used, the biosensor could respond to odors for up to at least 2 h on LAPS.

In another example, for developing a cell-based olfactory biosensor, T. H. Park's group used artificial olfactory cells [79]. They expressed the rat olfactory receptor OR I7, combined with a rho-tag import sequence

at the N-terminus, on the surface of HEK-293 cells. These cells were attached to the surface of the sensor chip covered with poly-D-lysine. Various odorants including heptanal, octanal, nonanal, decanal, and helional were analyzed. These odorant molecules, initially dissolved in DMSO, were diluted in a running buffer containing Ca^{2+}. To evaluate the performances of the obtained olfactory biosensor, surface plasmon resonance (SPR) was adopted as transduction technique. In this system, the signal detected by the transducer was not linked to the conformational change of the olfactory receptor but was rather due to the influx of calcium induced by the odorant binding event. Since the olfactory receptors are expressed on the surface of cells they are, thus, located several micrometers away from the sensor surface, which is much greater than the detectable SPR evanescent field of ~200 nm (c.f. Fig. 1.4). Therefore, the system cannot detect the conformational change generated by the odorant binding. However, this binding event still triggered the intracellular signal transduction involving the Ca^{2+} ion influx, which caused changes in the intracellular composition. Such changes may generate a variation in the local refractive index leading to an SPR signal. As expected, the system presented a higher affinity to octanal (the specific ligand of OR I7) with a linear response in the range of 10^{-1} to 10^{-4} M. This study showed that it is possible to use SPR for cell-based olfactory biosensors. Most importantly, the authors have underlined and confirmed the role of calcium ions in the signalling process of olfactory receptor. A result that they proved in a previous study [80], where they investigated the cAMP and IP_3 pathways triggered by odorants binding to ORs expressed in heterologous cells (HEK-239).

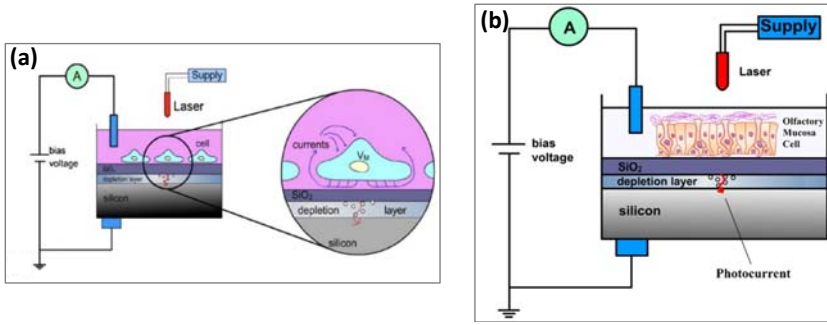

Fig. 1.3. Olfactory cells and tissues-based biosensors (a) [77], (b) [78].

To summarize, the cell-based olfactory biosensors are very interesting. In particular, they allow studying the process of odorant recognition at a single cell level. However, their practical on-field applications are quite limited by the short lifetime of these sensing materials and the strict and complex conditions required for cell culture.

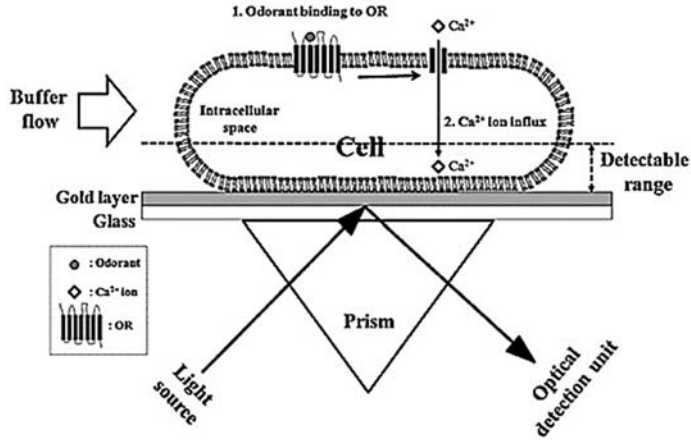

Fig. 1.4. Schematic illustration of a cell-based olfactory biosensor using SPR as transduction system [79].

1.3.2. Olfactory Receptor Based Olfactory Biosensors and Bioelectronic Noses

ORs are quite suitable for the development of olfactory biosensors and bioelectronic noses for several reasons. Firstly, they have high sensitivity and selectivity for odorant molecules. Secondly, their conformational change induced by odorant binding elicits a change in the electrical properties of the protein [39]. Therefore, it is possible to couple them with an appropriate transduction system to obtain a measurable and detectable signal. Thirdly, genetic engineering of proteins enables the addition of tags or other specific sequences to facilitate their purification as well as their immobilization on the sensors. Nevertheless, the exploration and exploitation of ORs for the development of bioelectronic noses is still very challenging from a technical point of view. This is mainly related to their production in large quantities and their stability in suboptimal environmental conditions after being incorporated into bioelectronic noses.

Indeed, the use of OR-based bioelectronic nose for industrial applications requires an efficient and high throughput protein production. During the first studies, the expression of ORs in heterologous cells was found to be very challenging, mainly due to their hydrophobic nature. Gimelbrant *et al.*[81] reported that when expressed in commonly used eukaryotic cell lines the ORs remained trapped in the endoplasmic reticulum or in the Golgi apparatus and could not be translocated into the plasma membrane. Moreover, a study on *C. elegans* [82] showed the importance of membrane associated proteins in targeting the olfactory receptors to the plasma membrane of olfactory neurons cilia. However, in order to investigate the binding affinities and transduction mechanisms of olfactory receptors, several teams succeeded to express those membrane proteins in non-neuronal cells. For this, different strategies were explored. For instance, using the baculovirus expression vector system (BEVS), Ramming *et al*. [26] succeeded to express ORs in surrogate Sf9 insect cells. Krautwurst [21] empirically found that a rhodopsin N-terminal extension can facilitate the traffic of the receptors, to the plasma membrane of human embryonic kidney (HEK-293) cells. Wetzel *et al.* [83] functionally expressed human OR17-40 fused with the membrane import sequence of 5- hydroxytriptamine receptor ($5\text{-}HT_3$) in HEK-293 cells and *Xenopus laevis* oocytes. Moreover, a receptor-transporting protein 1S (RTP1S) that is known to promote the translocation of OR in mammalian cells has been used to assist and increase the expression of the receptors [84]. Since then, great progress has been made. Today, several strategies exist for the expression of ORs [85], including cell-based expression [86-89], extracts from tissue or cells, cell-free expression and chemical synthesis [7, 90, 91]. Finally, prokaryotic systems such as *Escherichia coli* and yeast cells can also be used.

For the elaboration of olfactory biosensors and bioelectronic nose based on ORs, clearly, the incorporation of ORs into the sensor is another crucial yet tricky task. It can highly affect the sensitivity, stability and reproducibility of the corresponding device. ORs are membrane proteins and as such, depend on a lipid bilayer environment to maintain their structural stability and functionality. Here, we will present state of the art on the development of olfactory biosensors and bioelectronic noses based on ORs. In particular, we will focus on different innovative strategies reported in the literature to maintain their biological activities when immobilized on a sensor.

1.3.2.1. Membrane Fractions

In order to maintain the three-dimensional structure of ORs, the general idea is to keep them in a lipidic environment. The first strategy consists in expressing the ORs in a heterologous system and then breaking the plasma membrane into fractions carrying ORs, also called nanosomes in the literature. In this way, ORs are embedded in natural membranes. Thanks to genetic engineering, it is possible to make expression of ORs with special tags fused at their terminus. Certain tags such as polyhistidine and c-Myc tags may help in immobilizing and/or orientating ORs on the biosensor surface in an appropriate way to make their binding sites accessible for odorant molecules. Alternatively, if a specific antibody against the OR of interest exists, it can also be used for efficient OR immobilization. In the past two decades, various olfactory biosensors based on membrane fractions were developed using different ORs including I7 rat olfactory receptors (ORI7) [92], human olfactory receptor OR1740 [93-96] ODR-10 of *C. elegans* [97-100] and human olfactory receptor 2AG1 (hOR2AG1) [101, 102]. Here we will present some of them as examples.

In close collaboration, N. Jaffrezic's group and E. Pajot-Augy's group [92] succeeded to express rat ORI7 in yeast *Saccharomyces cerevisiae.* They had previously optimized the experimental conditions. When inducting receptor expression under low temperature at 15 °C, a low expression level was obtained but the expressed ORs were properly addressed to the plasma membrane, as confirmed by Western blotting and immunolocalization methods [103]. Furthermore, they proved that ORI7 conserved their biological activities well in the membrane fractions. Thus, they incorporated such membrane fractions to develop an olfactory biosensor based on electrochemical impedance spectroscopy (EIS). To ensure the appropriate orientation of ORs after immobilization, they first anchored antibodies specific to the OR on the biosensor through self-assembled multilayers. This immobilization strategy was first validated using another GPCR: rhodopsin [104]. In practice, as presented in Fig. 1.5a, first the gold electrode was functionalized with mixed self-assembled monolayers (SAMs) composed of 16-mercaptohexadecanoic acid (MHDA) and 1,2-dioleoyl-*sn*-glycero-3-phosphoethanolamine-*N*-(biotinyl) sodium salt (biotinyl-PE). The free space on the surface was blocked with goat antibodies. In the following step, neutravidin was introduced and bound to the biotin moieties on the mixed SAMs. Thanks to its four identical binding sites for biotin, biotinylated polyclonal antibody (Biot-Ab) specific to OR I7

was then immobilized on the gold surface. Finally, the membrane fractions carrying ORs were incorporated into the gold electrode by binding to the specific antibody with controlled orientation. EIS was used to evaluate the sensitivity and selectivity of the obtained olfactory biosensor towards odorants (specific heptanal and octanal, non-specific helional for negative control) in aqueous solution. The hydrophobic odorants were initially dissolved in dimethyl sulfoxide (DMSO) in order to facilitate their dissolution in aqueous solution. The authors have proven that ORs are active after their incorporation into the biosensor thanks to the immobilization strategy. The obtained system showed good sensitivity and selectivity for aldehydes with a linear response for concentrations between 10^{-13} and 10^{-4} M. It was stable during 7 days.

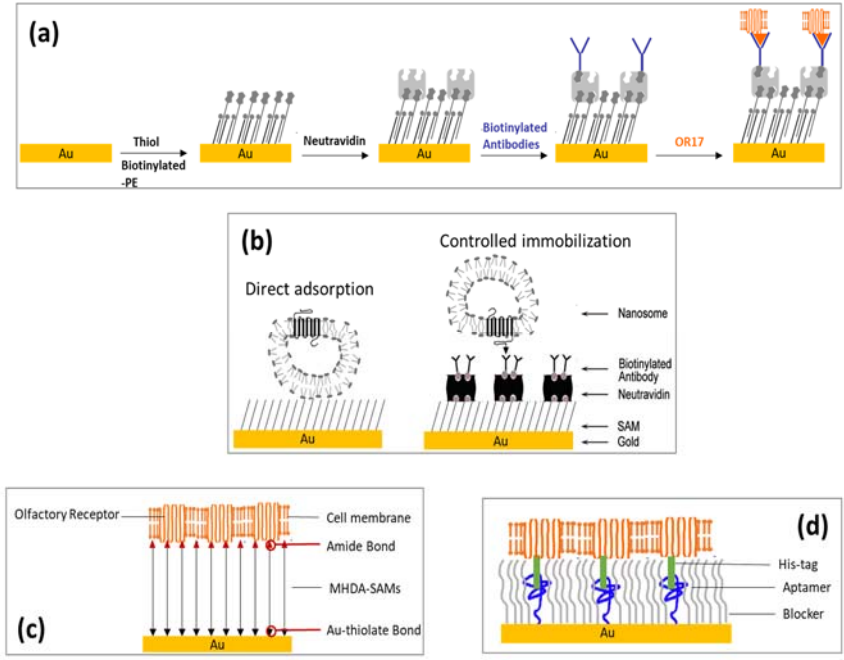

Fig. 1.5. Different strategies developed for the immobilization of membrane fractions carrying ORs: (a) antibody-directed specific immobilization [92], (b) comparison of physical adsorption and antibody-directed specific immobilization [96], (c) covalent bond [99], and (d) aptamer-assisted specific immobilization [100].

In another study [96], these two groups expressed OR1740 with a c-Myc-tag fused at its N-terminus using the same method. The membrane fractions carrying OR1740 had a uniform size with a diameter of ~50 nm. Moreover, in some control experiments, rat OR I7 and doubly tagged OR1740, with a c-Myc tag fused at its N-terminus and a HA-tag at its C-terminus, were also used. Here, a complete study was carried out in order to further optimize the immobilization method presented above. The main objective was to obtain an optimal immobilization procedure, which allowed for a good control over the density and especially the orientation of ORs, with a minimal non-specific interaction between odorant analytes and the underlayers. For this, three distinct SAMs carrying biotinyl groups at different densities were evaluated and compared. SPR was used for real time monitoring of step-by-step surface functionalization as well as for evaluating the performance of the obtained olfactory biosensor. Helional, an odorant specific to OR1740, was used in solution at a concentration of 5 μM. In this study, the authors clearly showed the importance of immobilization to achieve proper orientation of ORs. They compared the performance of two olfactory biosensors, the first prepared by antibody-directed specific immobilization of ORs and the second by simple physical adsorption of ORs on SAMs (see Fig. 1.5b). The biosensor response was increased up to 50 % for the former. Moreover, OR1740 was functional only when immobilized via a tag attached to its C-terminus, but not via its N-terminus. Finally, the authors demonstrated that the best immobilization method selected in this study was also well adapted for micro- and nanosensor formats.

Other groups used another type of ORs for the development of olfactory biosensors: ODR-10 of *C. elegans* in membrane fractions. A first example is a study led by the group of T. H. Park [97], in which ODR-10 was successfully expressed in *Escherichia coli* but with a low expression level, as confirmed by SDS-PAGE and Western blot. The authors have insisted on the advantages of expressing the OR in bacteria compared to in the mammalian cell system such as human embryonic kidney (HEK-293) cells, which were used in their previous work [105]. Indeed, the former is much easier since it requires neither an import sequence for the expression of ORs on the cell membrane nor the construction of a stable cell line, which is often time consuming and expensive. For the immobilization of the membrane fractions carrying ORs on the biosensor surface, they considered a simple method based on physical adsorption, without precise control over the orientation of ORs on the biosensor surface. For this, they expressed ODR-10 fused with a

GST-tag at the N-terminus and a 6×His-tag at the C-terminus. They lysed the bacterial cells by sonication and simply spread the obtained membrane fractions carrying ODR-10 on the gold plate of the quartz crystal. The ODR-10 of *C. elegans* is well characterized with a high affinity for diacetyl (butane-2,3-dione) [106]. In this study, quartz crystal microbalance (QCM) was used as transduction technique to evaluate the sensitivity and specificity of the obtained olfactory biosensor to various odorants, including diacetyl (specific analyte) and hexanal, heptanal, octanal and decanal (all for negative control). The odorant molecules initially dissolved in DMSO were diluted in sterilized water. Then, saturated vapors equilibrated with the odorant solutions were injected into the QCM system. The obtained olfactory biosensor showed good sensitivity and selectivity to the specific ligand (diacetyl) and exhibited a linear behavior in the range between 10^{-12} and 10^{-5} M. Finally, it is noteworthy that the authors demonstrated that there were non-specific interactions between the odorants and the phospholipid membrane which was also observed by Wu [107].

Three other examples presented below were led by P. Wang's group. To show the importance of the immobilization technique for proper orientation of ORs and its impact on the sensitivity and stability of the biosensor, they employed three different immobilization strategies.

In their first study [98], they expressed the ODR-10 of *C. elegans* on the plasma membrane of human breast cancer MCF-7 cells. A *flag-tag* was fused on its N-terminal for the easy visualization of its expression on the plasma membrane and a *rho-tag* import sequence was inserted to improve the expression level of ODR-10. The efficient expression of the receptors in the MCF-7 cells at the mRNA level was confirmed by reverse transcription-polymerase chain reaction (RT-PCR). Besides, fluorescent staining experiments revealed that the ORs were effectively expressed in the cells at high levels and evenly distributed across the plasma membrane. After sonication, the membrane fractions containing ODR-10 were immobilized by physical adsorption on gold layer without precise control over the orientation of ORs. Surface acoustic wave (SAW) was used as transduction technique. The performance of the obtained olfactory biosensor was evaluated using various odorants, including specific diacetyl and non-specific ethanol, butanol, pentanedione, hexanal, and isoamyl acetate. The odorant samples were freshly prepared in Tedlar bags by a liquid organic gas blender and were injected into the detection chamber by a syringe pump. All the experiments were performed under controlled environmental conditions

with 10 % of humidity at 25 °C. The obtained olfactory biosensor showed a good sensitivity and selectivity to diacetyl with a dose-dependent response in the concentration range between 10^{-13} and 10^{-7} M.

In their second study [99], they intended to improve the immobilization efficiency for ORs to improve the performance of the olfactory biosensor. Here, ORs in membrane fractions were immobilized on the biosensor surface via covalent bond but without precise control over the orientation of ORs, see Fig. 1.5c. For this, initially, the gold surface was functionalized by the formation of SAMs of 16-mercaptohexadecanoic acid thanks to the strong affinity between gold and thiols. Then, terminal carboxylic groups on SAMs were activated by treatment with 1-ethyl-3-[3-dimethylaminopropyl] carbodiimidehydrochloride/sulfo-N-hydroxysuccinimide (EDC/NHS). As a result, SAMs with active esters were obtained, which allowed for attaching primary amines of ODR-10 via the amide bonds. Similar to their previous study, SAW was used as transduction technique. Three odorants having similar structures, including diacetyl, butanone and 2,3-pentanedione, were used to test the performance of the obtained olfactory biosensor. Odorants were prepared in DMSO at 0.5 M. Saturated vapor of odorants were used as stimuli after they were diluted to the desire concentrations with nitrogen by a liquid organic gas blender. The olfactory biosensor showed good sensitivity and selectivity to the specific analyte (diacetyl) with a linear response in the same concentration range as obtained in their first study. In addition, compared to the olfactory biosensor developed in their first study, the sensitivity of the system was two times higher and a much lower detection limit was obtained. The stability was also greatly improved from 2 days to 7 days (stored at 4 °C).

In their third study [100], to further improve the performance of the olfactory biosensors, they developed an original aptamer-assisted specific immobilization technique with better control over the orientation of ORs (c.f. Fig. 1.5d). Here, ODR-10 was expressed heterologously in HEK-293 cells with a 6×His-tag on the N terminus. Western blot and RT-PCR confirmed the expression of His_6-tagged ODR-10 at the protein level and mRNA level, respectively. For the immobilization, initially, the gold surface was functionalized with mixed SAMs composed of thiol-modified anti-His_6 aptamers and 11-mercaptoundecanoic acid. The second thiol had dual functions of blocking free sites on the gold surface and reducing steric hindrance. Then, the membrane fractions carrying the His_6-tagged ODR-10 were

added. As a result, ODR-10 was captured specifically by the anti-His_6 aptamers with precise control over its orientation. QCM was used as the transduction technique. Moreover, in this study, physical adsorption method was also used to illustrate the influences of immobilization methods on the performances of OR-based biosensors. To test the sensitivity and selectivity of the obtained olfactory biosensor, various odorants were analyzed, including specific diacetyl and some other non-specific odorants such as isoamyl acetate, anisole, lavender, butanone, and 2,3-pentanedione. The odorants were freshly prepared in Tedlar bags by a liquid organic gas blender and then injected into the analysis chamber at a constant flow rate using a syringe pump. The olfactory biosensor prepared by aptamer-assisted specific immobilization showed improved sensitivity and selectivity, compared to that prepared by physical adsorption. Its detection limit was as low as 1.5 ppm (v/v). Moreover, it had good stability for 7 days, in contrast to 2 days for the biosensor prepared by physical adsorption.

In Table 1.1, we list all the presented olfactory biosensors based on membrane fractions carrying ORs for comparison.

1.3.2.2. Nanovesicles

Another strategy developed to provide a natural lipidic environment to maintain the stability and biological function of ORs consists in using nanovesicles (NVs). They are spherical structures that encompass a lipid bilayer displaying membrane proteins and encapsulating cytoplasmic compounds. NVs are usually secreted by a cell via a process called exocytosis. Thanks to their ability to entrap molecules, nanovesicles are very attractive candidates for drug delivery and nanomedicine [108, 109]. Another potential application involves using such structures as a miniature cell-like prototype to study cellular signalling process [110]. Through which, Pick *et al.* [110] showed that nanovesicles are able to perform the same signalling process as the "mother" cell. Furthermore, nanovesicles are also very attractive as biomaterials for the development of olfactory biosensors and bioelectronic noses [84, 111-113]. Firstly, they retain the original, natural environment of ORs. Secondly, they can be prepared in large quantities and can be frozen and stored for many weeks without the loss of biological activity. Thirdly, they can serve as miniaturized artificial cells to replace natural ones since their nanometric size are more suitable for their incorporation into nanoscale olfactory biosensors.

Table 1.1. Summary of the olfactory biosensors based on membrane fractions carrying ORs.

Reference	**Hou *et al.* [92]**	**Vidic *et al.* [96]**	**Sung *et al.* [97]**	**Wu *et al.* [98]**	**Wu *et al.* [99]**	**Du *et al.* [100]**
Olfactory receptor	Rat OR I7	Human OR1740	C. elegans ODR-10	C. elegans ODR-10	C. elegans ODR-10	C. elegans ODR-10
Expression system	Saccharomyces cerevisiae yeast cell	Saccharomyces cerevisiae yeast cell	E. coli	Human breast cancer cells MCF-7	Human breast cancer cells MCF-7	Human embryonic kidney cells HEK-293
Structure stabilization	Membrane fractions	Nanosome	Membrane fractions	Membrane fractions	Membrane fractions	Membrane fractions
Immobiliza-tion	Antibody-directed specific immobilization	Antibody-directed specific immobilization	Physical adsorption	Physical adsorption	Covalent binding	Aptamer-assisted specific immobilization
Transduc-tion technique	EIS	SPR	QCM	SAW	SAW	QCM
Odorants tested	Specific: Octanal Heptanal Control: Helional	Specific: Helional Control: Octanal	Specific: Diacetyl Control: Hexanal Heptanal Octanal Decanal	Specific: Diacetyl Control: Ethanol Butanol Pentane-dione Hexanal Isoamyl acetate	Butanone 2,3-pentane-dione	Specific: Diacetyl Control: Butanone Pentane-dione Isoamyl acetate Anisole Lavender
Analysis milieu	Aqueous solution	Aqueous solution	Vapor	Vapor	Vapor	Vapor
Detection limit	10^{-12} M	–	10^{-12} M	10^{-13} M	1.2 10^{-14} M	1.5 ppm
Long term stability	7 days	–	–	2 days	7 days	7 days

Finally, they can be used for signal amplification thanks to the conserved cell signalling pathways. Below we present some interesting examples of nanovesicle-based olfactory biosensors.

T. H. Park's group has greatly contributed to the development of this type of olfactory biosensors. In the first example [112], they expressed the human olfactory receptor 2AG1 (hOR2AG1) fused with a *flag tag* and a *rho-tag* import sequence in HEK-293 (Fig. 1.6a). After transfecting the cells with the expression vector, the production of nanovesicles containing hOR2AG1 was induced by a cytochalasin B treatment under agitation (Fig. 1.6b). The nanovesicles were separated from the cells and collected via multiple centrifugations. The expression of hOR2AG1 in both cells and nanovesicles was confirmed by Western blot. According to the analysis by field emission scanning electron microscope (FE-SEM), the obtained nanovesicles had a well-defined sphere-like shape with a uniform diameter of ~200 nm. To assess the activity of the nanovesicles carrying hOR2AG1, a Ca^{2+} signalling assay was carried out using the fluorescent Ca^{2+} indicator. It was found that such nanovesicles retained most of the activities for cellular signal transduction (Fig. 1.6c). Then, they were combined with a single-walled carbon nanotube-based field effect transistor (swCNT-FET), see Fig. 1.6d. For their immobilization, nanovesicles were attached to the surface of carbon nanotube covered with poly-D-lysine by electrostatic interactions. To evaluate the performance of the obtained olfactory biosensor, specific odorant amyl butyrate and some non-specific odorants with similar structures such as propyl butyrate, pentyl valerate, and butyl butyrate were used in aqueous solution. Thanks to the advantages of nanovesicles with cell signalling pathways for signal amplification, the obtained system exhibited a human-like selectivity with single-carbon resolution and a very high sensitivity with a detection limit of 1 fM. However, unlike the olfactory neurons, nanovesicles lack the restoration functionality. Indeed, in live cells Ca^{2+} pumps enable the restoration of the intracellular ion level at the end of the interaction. Therefore, this absence of restoration could highly affect the reusability of the system and make it less suitable for high throughput measurements.

In the second example, this group explored the application of this kind of system for medical diagnostics [84]. The idea was to make lung cancer diagnosis based on the detection of a VOC biomarker such as heptanal. For this study, an important effort was made on the selection of ORs that have a high sensitivity and specificity to this VOC molecule by building a library of HEK-293 cells expressing 30 types of human ORs. Among

the tested ORs, hOR1J2, having not only good sensitivity but also very good selectivity for heptanal, was selected and used for olfactory biosensor development. The nanovesicles carrying hOR1J2 were produced by transfecting HEK-293 cells using cytochalasin B.

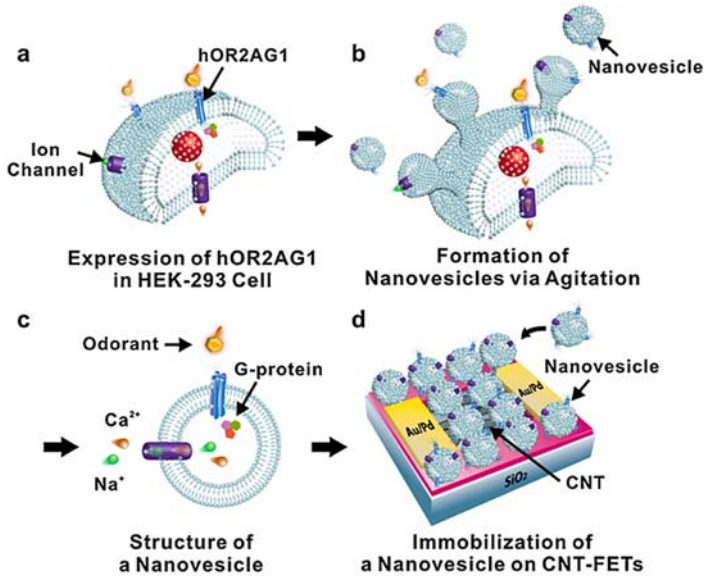

Fig. 1.6. Schematic illustration for the preparation of nanovesicles carrying ORs and their combination with a carbon nanotube-based FET transducer to build an olfactory biosensor [112].

To increase the expression of ORs, the receptor-transporting protein 1S (RTP1S) was also expressed in the cells since it was known to facilitate the traffic of the ORs in mammalian cells [114]. Moreover, the cells were also transfected with the $G\alpha_{olf}$ gene to enhance the intracellular signalling process. Afterwards, nanovesicles were immobilized on swCNT-FET covered with poly-D-lysine by electrostatic interactions. Initially, the efficiency of the obtained olfactory biosensor for heptanal detection was validated in standard buffer solution. Then, to verify its capability for practical diagnosis, the detection of heptanal contained in human blood plasma was examined. It was proven that the system was able to selectively detect heptanal at a concentration as low as 1×10^{-14} M, a sufficient level to distinguish the blood of a lung cancer patient from the blood of a healthy person.

Besides nanovesicles with natural lipid bilayer, Khadka *et al.* [113] reconstituted insect odorant receptors into artificial lipid bilayers such as liposomes for the development of an ultrasensitive olfactory biosensor. In their previous works [115], the production of such liposomes was optimized. Therein, three odorant receptors OR10a, OR22a, and OR71a from fruit fly *Drosophila melanogaster* were recombinantly expressed, purified and integrated into liposomes (100-200 nm). Then, the liposomes were covalently attached to SAMs-modified gold surface, as illustrated in Fig. 1.7. Both quartz crystal microbalance with dissipation (QCM-D) and EIS were used as transduction system. To evaluate the performances of the obtained olfactory biosensors, various odorants were tested, including methyl salicylate (specific odorant of OR10a), methyl hexanoate (specific odorant of OR22a), 4-ethyl guaiacol (specific odorant of OR71a), and E2-hexanal as negative control. Odorant solutions were prepared in phosphate buffer solution (PBS) containing 1 % DMSO for better solubility. The authors showed that the olfactory biosensors based on EIS were much more sensitive. These biosensors were able to sensitively and selectively detect their corresponding specific odorant at femtomolar concentrations. Nevertheless, liposomes are large, unstable, and difficult to prepare with precisely controlled size and stoichiometry. To overcome it, novel technology based on nanodiscs has emerged.

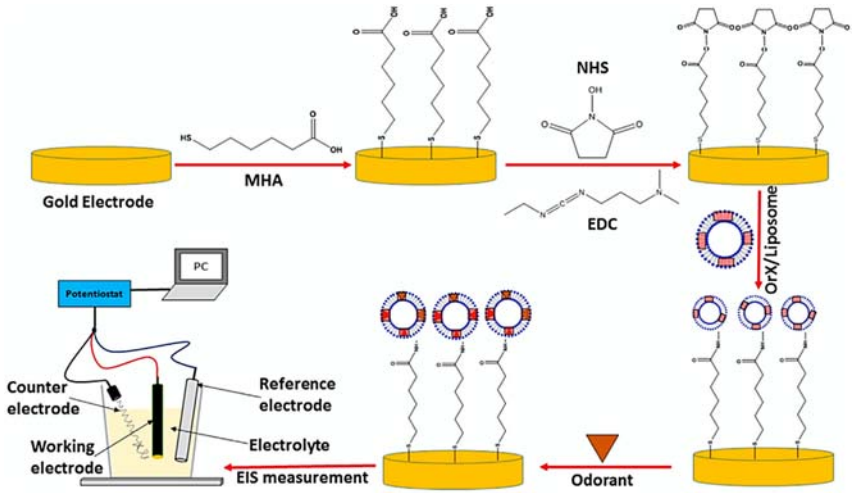

Fig. 1.7. Schematic description of covalent immobilization of liposomes onto gold electrodes [113].

In Table 1.2, we list all the presented olfactory biosensors based on nanovesicles carrying ORs for comparison.

Table 1.2. Summary of the olfactory biosensors based on nanovesicles carrying ORs.

Reference	**Jin et al. [112]**	**Lim et al. [84]**	**Khadka et al. [113]**
Olfactory receptor	Human OR2AG1	Human OR1J2	OR10a, OR22a and OR71a from Drosophila melanogaster
Expression system	Human embryonic kidney cells HEK-293	Human embryonic kidney cells HEK-293	Sf9 insect cells
Structure stabilization	Nanovesicles	Nanovesicles	Liposomes
Immobilization	Electrostatic interaction	Electrostatic interaction	Covalent binding
Transduction technique	CNT-FET	CNT-FET	QCM-D EIS
Odorants tested	Specific: Amyl butyrate Control: Propyl butyrate Pentyl valerate Butyl butyrate	Specific: Heptanal Control: Hexanal Octanal Nonanal	Specific: Methyl salicylate (OR10a) Methyl hexanoate (OR22a) 4-ethylguaiacol (OR71a) Control: Methyl salicylate (OR22a) Methyl hexanoate (OR10a) E2 hexenal (OR71a)
Analysis milieu	Aqueous solution containing Ca^{2+}	Aqueous solution containing Ca^{2+}	Aqueous solution
Detection limit	10^{-15} M	10^{-14} M	10^{-12} M (OR10a) 10^{-15} M (OR22a) 10^{-16} M (OR71a)

1.3.2.3. Nanodiscs

Nanodiscs are soluble artificial self-assembling phospholipid bilayer containing transmembrane proteins. They are able to maintain the native membrane environment of olfactory receptors. Recently, this technology

has become an important tool to functionally reconstitute membrane proteins. To do so, the membrane protein is solubilized transiently with a detergent in the presence of phospholipids and an encircling amphipathic helical protein belt such as a membrane scaffold protein (MSP). Upon removal of the detergent, typically via adsorption to hydrophobic beads, the target membrane protein simultaneously assembles with phospholipids into a discoidal bilayer. Nanodiscs have several advantages. Firstly, ORs embedded in nanodiscs are stable since they are in a native membrane environment. Secondly, the encircling MSP belt renders the entire assembly soluble. Finally, it is possible to control the size of nanodiscs depending on MSP length. For example, the diameter of bare nanodiscs can be tuned between 9.5 to 17 nm. Therefore, nanodiscs are very promising for the development of olfactory biosensors and bioelectronic noses, [116-119] as illustrated by three examples in the following part.

In a first example, A. T. C. Johnson's group combined ORs-embedded nanodiscs with CNT-FET to develop olfactory biosensors [116]. In this study, three recombinant mouse olfactory receptors mOR174-9, mOR203-1 and mOR256-17 were expressed in Sf9 insect cells with an N-terminal His-tag to simplify the purification and to ensure their oriented immobilization on the Ni-coated CNTs. Moreover, the ORs were prepared in two distinct nanoscale constructs: digitonin micelles and nanodiscs for comparison. Then, they were immobilized via a polyhistidine tag onto Ni-coated CNTs as described previously, which was efficient in controlling the orientation of the ORs (Fig. 1.8a). To test the performances of the obtained olfactory biosensors, eight odorants were used: eugenol, 2-heptanone, heptanal, acetophenone, dinitrotoluene, n-amyl acetate, methyl benzoate, and cyclohexanone. For odorant sampling, a system with three flows (humidity, sampling, background) was used, allowing the control of humidity and odorant concentrations in vapor. The results showed that nanodiscs carrying ORs were extremely stable in solution. In contrast, the digitonin micelles aggregated rapidly and thus needed to be used immediately after production. Moreover, after fabrication, nanodiscs based devices were much more stable with reproducible responses for longer than one month, while micelle-based devices remained active with stable responses for only ~5 days. Finally, the obtained olfactory biosensors had good sensitivity and selectivity with rapid responses and full recovery to baseline on seconds time scales.

Murugathas *et al.* developed olfactory biosensors based on insect ORs-embedded nanodiscs and CNT-FET with very high sensitivity [117]. In their study, four olfactory receptors from *Drosophila melanogaster*: OR10a, OR22a, OR35a, and OR71a were recombinantly expressed using a baculovirus-mediated Sf9 insect cells. Then, they were incorporated into nanodiscs. For their immobilization on CNTs, first, the 1-pyrenebutanoic acid succinimidyl ester (PBASE) molecules were attached noncovalently onto the CNT sidewalls via π–π interaction. Then, the amine groups on ORs were anchored onto the NHS ester group on the PBASE molecule via a nucleophilic substitution reaction, see Fig. 1.8b. It is important to note that this immobilization strategy cannot control the orientation of the ORs. To test the performances of these olfactory biosensors, four odorants including methyl salicylate, methyl hexanoate, trans-2-hexen-1-al and 4-ethylguaiacol were used. They were dissolved in PBS with 1 % DMSO to obtain concentrations ranging between 1 fM to 10 pM. It was demonstrated that the four olfactory biosensors selectively responded to their respective positive odorant with limits of detection in the low femtomolar range.

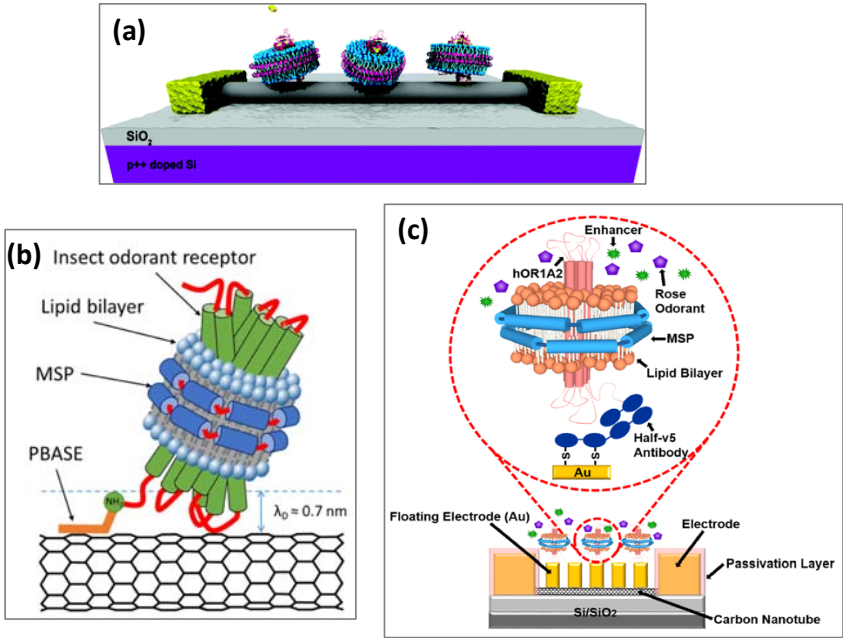

Fig. 1.8. Schematic illustration of nanodiscs carrying ORs immobilized on CNT [116-118].

T. H. Park's group developed an olfactory biosensor capable of quantitatively assessing rose scent components in real samples such as rose oil [118]. Here, human olfactory receptor 1A2 (hOR1A2) was overexpressed in *E. Coli* and purified via affinity chromatography. Then, the purified hOR1A2 were embedded into nanodiscs (15-20 nm) and immobilized on a floating gold electrode-based CNT-FET. For the immobilization, first, a cysteine monolayer was formed on the gold electrode surface using N-acetyl-L-cysteine, on which half-v5 antibody (Ab) fragments were anchored via disulfide bonding. Subsequently, the hOR1A2 was incorporated into the system which specifically bound to the antibody, as shown in Fig. 1.8c. To assess the performance of the olfactory biosensor, specific odorants geraniol and citronellol and non-specific odorants trimethylamine and amyl butyrate were used, additionally, with benzyl salicylate used as an enhancer. These odorants and rose oil solutions were prepared in HEPES buffer solution. The obtained system was able to quantitatively recognize geraniol and citronellol down to 1 fM and 10 fM, respectively, and with very good selectivity. Interestingly, for the first time, this work demonstrated that the sensitivity of olfactory biosensors can be greatly improved in the presence of an enhancer like benzyl salicylate. Where, ORs in the presence of 1 nM benzyl salicylate responded to a rose scent with $\sim 10^3$ times lower concentrations. Finally, it was also proven that the olfactory biosensor could recognize geraniol in complex environments such as rose oil.

Furthermore, based on the same principle, T. H. Park's group also developed olfactory biosensors by using trace-amine-associated receptors (TAARs) [119, 120]. TAARs belong to the G-protein coupled receptor family which were identified in many animal species (mouse, rat, humans) and were attributed to different functions associated with binding trace amines. Since amines such as diamines (putrescine and cadaverine) are often responsible for bad odors i.e. coming from bacterial decomposition of proteins, olfactory biosensors and bioelectronic noses incorporating TAARs may be promising for assessing food quality and olfactory pollution, etc.

Finally, with all these progresses made on olfactory biosensors, it becomes possible to design multiplexed system for the development of bioelectronic noses. For instance, T. H. Park's group initiated studies in this direction [102, 121]. Moving even further, they reported a portable and multiplexed bioelectronic sensor that combines human olfactory and

taste receptor with a multichannel CNT-FET for food freshness assessment (Fig. 1.9) [121].

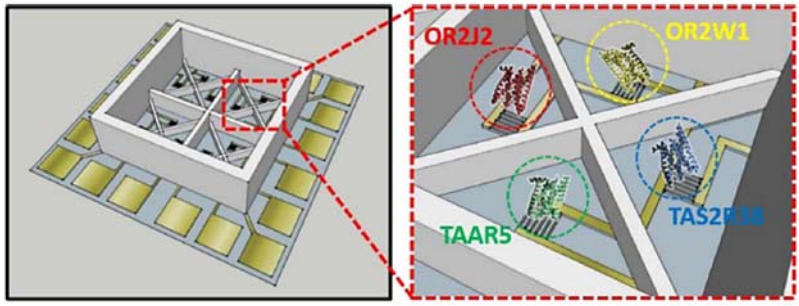

Fig. 1.9. Schematic illustration of the bioelectronic sensor that combined human olfactory and taste receptor with a multichannel carbon nanotube FET [121].

For this, three olfactory receptors (human OR2J2, OR2W1 and trace amine-associated receptor TAAR5) and one taste receptor (TAS2R38) were produced in *Escherichia coli*. A 6×His-tag was fused to the C-terminus of the receptor proteins for purification and oriented immobilization on the Ni-coated CNTs. Notably, these receptor proteins were reconstituted using a detergent micelle method to maintain their original structure. To immobilize the receptor proteins, initially, CNTs were incubated in 4-carboxybenzene diazonium tetrafluoroborate solution. Subsequently, the carboxylic acid of the 4-carboxybenzene was activated by EDC/sulfo-NHS in an appropriate buffer. Then, CNTs were immersed in Nα,Nα-bis(carboxymethyl)-L-lysine hydrate (NTA-NH_2) solution. Afterwards, they were washed with deionized water and immersed in a solution of $NiCl_2$ for coating CNTs with Ni^{2+}. Finally, thanks to the 6×His-tag fused to the C-terminus, olfactory receptors and taste receptor were immobilized on the Ni-coated CNTs with controlled orientation via the formation of coordination bonds. In this study, a customized portable and multiplexed bioelectronic sensor was constructed for the analysis of odorant and taste molecules, including octanol (specific ligand of OR2J2 and OR2W1), hexanal (specific ligand of OR2W1), trimethylamine (specific ligand of TAAR5), and goitrin (specific ligand of TAS2R38). They are known indicators of food contamination. It was demonstrated that the obtained device selectively distinguished mixtures of these molecules as well as individual odor and

taste molecules with high sensitivity. Thus, such a system was suitable for efficient monitoring of food freshness as well as for other applications requiring on-site analysis.

In Table 1.3, we list all the presented olfactory biosensors based on nanodiscs carrying ORs for comparison.

Table 1.3. Summary of the olfactory biosensors based on nanodiscs carrying ORs.

Reference	**Goldsmith *et al.* [116]**	**Murugathas *et al.* [117]**	**Lee *et al.* [118]**	**Son *et al.* [121]**
Olfactory receptor	Mouse OR174-9, OR203-1 and OR256-17	OR10a, OR22a, OR35a, and OR71a from *Drosophila melanogaster*	human olfactory receptor 1A2	(human OR2J2, OR2W1 and trace amine-associated receptor TAAR5 TAS2R38
Expression system	Sf9 insect cells	Sf9 insect cells	*E. coli*	*E. coli*
Structure stabilization	Digitonin micelles and Nanodiscs	Nanodiscs	Nanodiscs	Micelle
Immobiliza-tion	Covalent binding	Non covalent interactions using PBASE	Antibody-directed specific immobilization	Covalent binding
Transduction technique	CNT-FET	CNT-FET	CNT-FET	CNT-FET
Odorants tested	Eugenol 2-heptanone Heptanal Acetophenone Dinitrotoluene N-amyl acetate Methyl benzoate Cyclohexanone	Methyl salicylate Methyl hexanoate Trans-2-hexen-1-al 4-ethylguaiacol	Geraniol Citronellol Trimethylamine Amyl butyrate Rose oil	Octanol Hexanal Trimethylami ne Goitrin
Analysis milieu	Vapor	Aqueous solution	Aqueous solution	Aqueous solution
Detection limit	~7 ppb for dinitrotoluene	1 fM	1 fM	pM range
Long term stability	> 1 month (in humid environment)	Not mentioned	Not mentioned	~7 days

To summarize, all these examples have proven that ORs are very promising sensing materials for the development of olfactory biosensors and bioelectronic noses. In particular, their use makes it possible to attain

a high sensitivity and selectivity, even at the concentration level occurring in the human nose. Today, their production in large quantities are possible based on various expression methods. By keeping ORs in a lipidic environment using membrane fractions, nanovesicles or nanodics, their biological activities are conserved with good stability even in suboptimal environmental conditions after being incorporated into bioelectronic noses. With ingenious design of immobilization technique to control the OR orientation on the biosensor surface, the performances of the olfactory biosensors in terms of sensitivity and stability can be highly improved. Nevertheless, the wide application of this type of device remains limited by their short lifespan and their poor repeatability.

1.3.3. Odorant Binding Proteins Based Olfactory Biosensors and Bioelectronic Noses

Other attractive biomimetic receptors for olfactory biosensors are the odorant binding proteins. These relatively small proteins are suitable elements for several reasons. Firstly, they present a remarkable stability to high temperature and pH variations, and have low susceptibility to proteolytic degradation [5, 58]. Secondly, as mentioned previously, OBPs have broad specificity and can reversibly bind a large spectrum of odorants with a micromolar range dissociation constant. Thirdly, their hydrophilic nature considerably facilitates their expression, purification and thus allows a large-scale production in bacterial systems. Fourthly, site-directed mutagenesis enables to tune the binding properties of OBPs and the introduction of special tags to control their immobilization on biosensors and bioelectronic noses [122, 123]. Finally, it is possible to couple these proteins to an electrical, optical or acoustic transduction technique to build olfactory biosensors and bioelectronic noses. In the last decade, different groups from around the world have contributed to their development [122-136]. Nevertheless, despite the great stability of OBPs, the most challenging task is to maintain their three-dimensional structure and biological activity over time when immobilized onto the biosensor and exposed to odorants. Indeed, being naturally present in an aqueous environment (the olfactory mucus), the humidity level of the working milieu is a very important factor. Therefore, many OBP-based biosensors were designed to analyze and detect odorants in the liquid phase and were proven to be highly sensitive. Moreover, several studies showed that OBP-based biosensors were also efficient in detecting odorants in the gas phase. In this part, we will present the development

of diverse olfactory biosensors and bioelectronic noses based on OBPs for the analysis of odorants in both aqueous and gaseous phase.

1.3.3.1. Odorant Analysis in the Liquid Phase

Thanks to the good solubility and stability of OBPs, they can be used directly without the lipidic environment. Q. Liu's group developed several OBP-based olfactory biosensors using different transduction systems such as EIS [125, 126] and localized surface plasmon resonance (LSPR) [127]. In one of these studies [126], they used a human odorant binding protein to develop an olfactory biosensor with potential applications for medical diagnosis. Recombinant hOBP was expressed with a polyhistidine tag at the C-terminus in the host human cells. Then, the cell extracts were analyzed and the expression of the proteins was confirmed by SDS-PAGE. The obtained hOBPs were immobilized on aluminum oxide surface of nanopores, as schematically illustrated in Fig. 1.10.

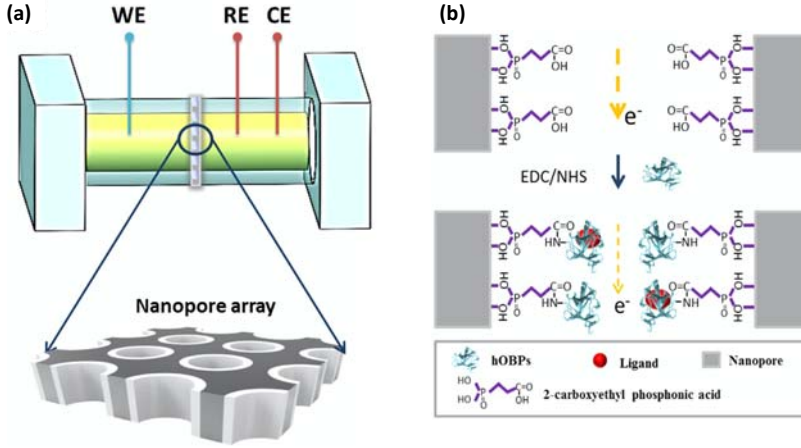

Fig. 1.10. Olfactory biosensor based on nanopore array functionalized with hOBP [126] (a) EIS experimental setup (WE: working electrode; RE: reference electrode; CE: counter electrode) (b) hOBP immobilization process.

First, the nanopore surface was functionalized with 2-carboxyethyl phosphonic acid by the formation of SAMs. Then, carboxylic groups were activated by EDC/NHS, which generated active esters that allowed for the anchoring of the primary amines of hOBPs via

the formation of amide bonds. In this study, EIS was used as the transduction technique. Benzaldehyde and two fatty acids: lauric acid and docosahexaenoic acid, considered as potential biomarkers for cancers and other serious diseases, were chosen as targets to test the efficiency of the device. The three compounds were dissolved in methanol at different concentrations ranging between 10^{-8} and 10^{-4} mg/mL. The obtained system showed dose-response for the three odorants with good sensitivity.

For the incorporation of OBPs into the biosensors, an efficient immobilization is crucial and can highly affect the sensitivity of the device. To highlight this, Manai *et al.* [124] compared the performances of OBP-based olfactory biosensors functionalized by two different chemical grafting strategies. In this study, a wild type OBP from pig (wtOBPpig) and its mutant with 6×His-tag at the N-terminus (m6hisOBPpig) were used as sensing material. They were attached to the surface of poly-crystalline diamond micro-cantilevers used as signal transducers. In the first immobilization method (Fig. 1.11a), hexanoic acid was covalently attached to hydrogen-terminated diamond surfaces then the carboxylic groups were activated by EDC/NHS, to allow the anchoring of wtOBPspig via amide bonds. In the second method (Fig. 1.11b), the hydrogenated diamond surface was first functionalized with Nα,Nα-Bis-(carboxy- methyl)-L-lysine hydrate (NTA), followed by the addition of nickel(II) chloride hexahydrate, which led to the formation of Ni-NTA complex. This complex showed a high affinity with 6×His-tag at the N-terminus of the mutant m6hisOBPpig. The first immobilization strategy resulted in random orientation of the proteins on the sensor surface whereas the latter approach enabled control over the orientation of the proteins. The sensing performances of the obtained olfactory biosensors based on diamond microelectromechanical systems (MEMS) were evaluated and compared for the analysis of 2,4-dinitrotoluene (2,4-DNT) and 2-isobutyl-3-methoxypyrazine (IBMP). The odorants were prepared in aqueous buffer solution. The olfactory biosensor based on the second immobilization method showed 20 % higher sensitivity for the two odorants. This could be explained by a greater immobilization yield and better odorants accessibility to the proteins binding sites. Furthermore, a better repeatability of the sensor response was also observed. As previously mentioned, with the first immobilization method, OBPs were randomly oriented on the sensor surface. Thereby, resulting in the number of available active sites varying from one biosensor to another. In contrast, with the second immobilization method, all the receptors were well oriented, thus,

providing a similar number of binding sites for a more reproducible sensors response.

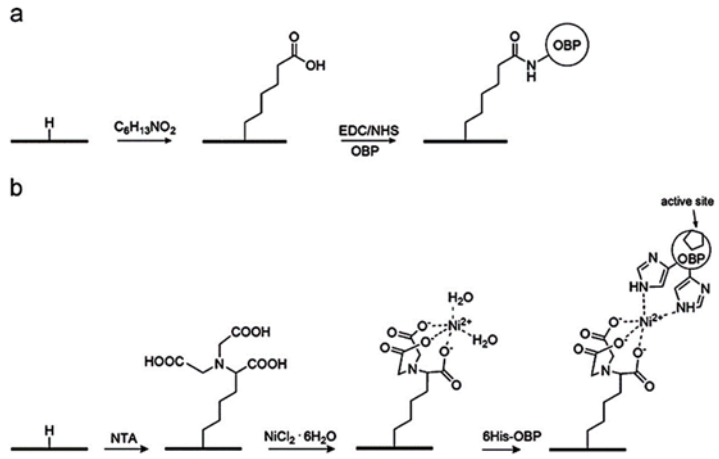

Fig. 1.11. Two strategies for OBP immobilization on diamond surface (a) with random orientation (b) with controlled orientation [124].

As mentioned before, it is possible to tune binding properties of OBPs based on site-directed mutagenesis. In such a way, a set of OBPs with differential affinity to target odorants can be designed and produced, which paves the way for the development of multiplexed bioelectronic noses [122, 123]. Recently, our team carried out a preliminary proof-of-concept study on the development of an OBP-based bioelectronic nose [122]. Three derivatives of the third rat odorant binding protein (OBP3) were used as sensing material, including a "wild type" protein (OBP3-w), and two modified proteins named OBP3-a and OBP3-c. The binding properties of these proteins were customized by modifying the amino acid sequence of their binding pockets. A lysyl residue was introduced into the OBP3-a binding pocket to improve the affinity of the protein for aldehydes. For OBP3-c derivative, bulky amino acids were introduced in its binding pocket. Consequently, resulting in the binding site being cluttered and rendering the receptor incapable of binding with any odorants. Thus, it was used as the negative control. The three recombinant His-tagged proteins were expressed in *Escherichia coli* then purified using immobilized metal affinity chromatography (IMAC). Moreover, a cysteine was added at the N-terminus of the OBPs to enable their immobilization by direct self-assembly on the gold surface of a prism. Importantly, the N-terminus was located on the opposite side of

the binding pocket entrance, ensuring the promotion of correct protein orientation by anchoring at this point.

In this study, great effort was made to optimize the density and orientation of OBPs grafted on the microarray since it may influence the binding properties of the proteins as well as the signal intensity of the obtained bioelectronic nose. Indeed, in an ideal case, the proteins would form a well-organized monolayer with their binding pockets pointing upwards to facilitate the access of odorants. If the OBP layer on the biosensor was not dense enough to ensure steric and electrostatic repulsion between the proteins, this will result in a random orientation of the proteins with less accessible binding sites. On the contrary, if the density of OBPs was too high, the formation of additional disordered layers could be favored. Resulting in the proteins on the top layer to have random orientation which may block access to the binding sites of the proteins in the underlayer. Moreover, it would be difficult to prepare reproducible biosensors under such conditions.

Surface plasmon resonance imaging (SPRi) was used to detect odorant binding. SPRi is a real-time, highly sensitive, label-free, and noninvasive optical transduction technique. It is particularly interesting for the development of bioelectronic noses. Thanks to the imaging mode, the interactions between the analytes and multiplexed biosensors can be simultaneously monitored with the access to real-time kinetic information. The performance of the obtained bioelectronic nose was investigated by the analysis of three odorant molecules: β-ionone, hexanal, and hexanoic acid. β-ionone can bind to both OBP-w and OBP-a with a higher affinity for OBP-w. Hexanal strongly binds to OBP-a. Hexanoic acid was used as a negative control. The odorant samples were prepared by diluting pure products in filtered running buffer. The obtained bioelectronic nose exhibited a detection limit of 200 pM for β-ionone that is among the lowest values reported in literature. Moreover, very remarkably, the system was able to detect odorants having a molecular weight of 100 g/mol (hexanal). This value is lower than the limit of detection in mass commonly admitted for commercial SPRi systems (200 g/mol) without amplification. This result suggested that the SPR signal was not solely due to the binding of odorants but was further amplified by the potential conformational change of the protein which resulted from the binding event. Moreover, the distinct binding properties of the OBP derivatives enabled very high selectivity particularly at low concentrations of odorants. Finally, with appropriate regeneration procedures, the biosensor showed a good

measurement-to-measurement and chip-to-chip repeatability, as well as good stability with a lifespan of up to nearly two months.

1.3.3.2. Odorant Analysis in the Gas Phase

Some other groups have challenged the development of OBP-based olfactory biosensors and bioelectronic nose for the analysis of odorants in gas phase [128-134]. Di Pietrantonio and collaborators [128-130] published several studies on such bioelectronic noses based on SAW biosensor array. In one of these studies [128], they used three different OBPs: wild-type OBP from cow (wtbOBP), a double mutant of the cow OBP (dmbOBP) and a wild-type pig OBP (wtpOBP). The DNA sequence of cow OBPs was combined with a 6xHis-tag, expressed in *E. coli,* then purified using Ni-NTA coated agarose beads and followed by a second chromatography step on fast performance liquid chromatography (FPLC). Pig OBPs were extracted and purified from fresh nasal tissues of the animal. To immobilize the sensing materials, the electrodes of the sensor were coated with a thin gold film to allow the formation of self-assembled monolayer thanks to the high affinity between the gold and the thiol group of the proteins. In this study, each of the three OBPs was deposited on a resonator by a simple droplet deposition method. The response of the bioelectronic nose was monitored upon the injection of R-(–)-1-Octen-3-ol (13-61 ppm) and R-(–)-carvone (9-80 ppm) at different concentrations carried by N_2 flow. It was demonstrated that the three OBPs preserved their full functionality when exposed to the air environment. The obtained bioelectronic nose showed good selectivity and sensitivity with the capacity of detecting low concentrations of octenol and carvone. Despite being fast and simple, the conventional droplet deposition technique did not allow a good reproducibility of surface densities of the OBP coating. Therefore, it is not suitable for large-scale sensor production. For this purpose, Di Pietrantonio and collaborators investigated more sophisticated but precise deposition methods such as matrix assisted pulsed laser evaporation and laser-induced forward transfer [129, 130]. They showed that these new deposition processes did not affect the activity of OBPs and the fabricated olfactory biosensors showed similar performances.

In a second example, Gao *et al.* [132] developed a bioelectronic nose for efficient human body odor detection to meet the needs of many related fields (disease diagnosis, cosmetic, forensic science, etc.). For this, OBPs from the anthropophilic mosquito, *Anopheles gambiae* (AgOBPs) were

used. A poly-histidine tag was fused to the N-terminal of three different AgOBPs: AgOBP5, AgOBP6 and AgOBP7 and the receptors were expressed in *E. coli*. After purification, AgOBPs were immobilized on the surface of CMOS-compatible silicon nanowires (SiNW) array using 3-Aminopropyltriethoxysilane (APTES) and cross-linker glutaraldehyde. As presented in Fig. 1.12, the SiNW surface, possessing hydroxyl groups, was first functionalized with SAMs of APTES possessing primary amino groups. Then, the cross-linker glutaraldehyde was used to covalently anchor AgOBPs onto the surface of SiNW. This functionalization technique is commonly used for protein immobilization in biosensor development [137]. However, it does not allow to control the protein orientation.

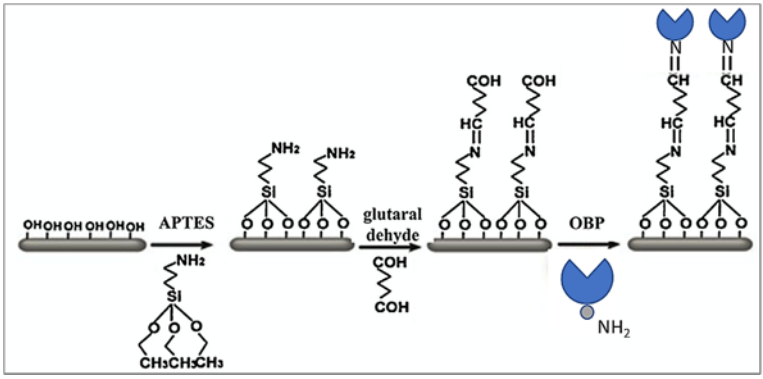

Fig. 1.12. The immobilization of OBPs on silicon nanowire array [132].

The performances of the obtained bioelectronic nose were evaluated using odorants related to human body odor. For evaluating the sensitivity and particularly the selectivity of the obtained system, two sets of odorants were used. The first panel of odorants had the same functional group but different chain lengths, including hexanoic acid, heptanoic acid, octanoic acid, nonanoic acid, decanoic acid, undecanoic acid and dodecanoic acid. The second panel of odorants had a similar single chain scaffold and distinct functional groups, including nonanoic acid, hexanoic acid, geranylacetone, linalool, methyl dodecanoate. Very satisfyingly, the bioelectronic nose had high sensitivity to some of these odorants down to several ppb, and outstanding size and functional group selectivity. Moreover, the responses of devices from different batches were highly reproducible. Finally, when stored at -20 °C, the device

conserved a stable activity for 30 days with a decrease in the signal speed and intensity only observed after the first day of storage.

In Table 1.4, we list all the examples of OBP-based olfactory biosensors given above. To summarize, all these examples showed clearly that OBPs are very promising for the development of olfactory biosensors and bioelectronic noses, in particular, thanks to their good stability and tunable biological properties. When coupled to an appropriate transduction system, the obtained sensors can not only be used to analyze odorants in the liquid phase but also in the gas phase. Therefore, these tools have promising applications in diverse fields.

1.4. Conclusions and Perspectives

This chapter has presented the basic mechanism of olfaction and the important biological elements in the olfactory system. It has given an overview of significant progress made for the development of biomimetic olfactory biosensors and bioelectronic noses based on sensing materials from the olfactory system (i.e. olfactory cells and tissues, ORs, OBPs). In particular, ingenious strategies are highlighted, which have been developed to solve some key technical issues for building robust, sensitive and selective devices. Such olfactory biosensors and bioelectronic noses have improved performances compared to classical eNs. They present great potential for applications in diverse fields, including environmental monitoring, food safety, disease diagnosis, as well as quality control for food, beverages, perfume and cosmetics.

Nevertheless, for these applications, in most cases, the analysis of odorants in the gas phase is required. Unfortunately, olfactory biosensors and bioelectronic noses are limited for gas sensing by their short lifespan and their poor repeatability. For this, the new tendency is to design novel sensing materials that are analogues of proteins but with much better stability, such as peptides. Indeed, peptides are particularly attractive thanks to their chemical robustness, diverse physicochemical properties, and easy synthesis and production. Moreover, most importantly, they can reach similar affinity to that of olfactory proteins either by rational computational design (molecular modeling and molecular docking, virtual screening, and molecular dynamics simulation, etc.) or by high-throughput selection such as phage display.

Table 1.4. Summary of the OBP-based olfactory biosensors.

Reference	**Lu *et al.* [126]**	**Manai *et al.* [124]**	**Hurot *et al.* [122]**	**Di Pietrantonio *et al.* [128]**	**Gao *et al.* [132]**
Odorant binding protein	Human OBP	Pig wtOBP + mutant m6hisOBPpig	OBP3 from rat + 2 mutants	wtbOBP from cow + double mutant (dmbOBP) and wtpOBP from pig	OBP5, OBP6 and OBP7 from *Anopheles gambiae* mosquito
Expression system	Human host cell	*E. coli*	*E. coli*	*E. coli* and pig nasal tissues	*E. coli*
Immobilization	Covalent binding	Covalent binding Random using EDC/NHS Oriented using Ni-NTA	Au-S bond	Au-S bond	Cross-linking
Transduction technique	EIS	MEMS	SPRi	SAW	Silicon nanowire array (SiNW)
Odorants tested	Benzaldehyde Lauric acid Docosahexaenoic acid	2,4-dinitrotoluene (2,4-DNT) 2-isobutyl-3-methoxypyrazine (IBMP)	Specific: β-ionone Hexanal Control: Hexanoic acid	Octenol Carvone	Hexanoic → dodecanoic acid Geranylacetone Methyl dodecanoate Linalool
Analysis milieu	Aqueous solution	Aqueous solution	Aqueous solution	Vapor	Vapor
Detection limit	10^{-9},10^{-12},10^{-8} mg/mL respectively	–	200 pM for β-ionone	0.39-2.8 ppm for octenol 1.4-1.8 ppm for carvone	2 ppb for nonanoic acid
Long term stability	–	2 months (in air at room temperature)	2 months at 4 °C	–	30 days at -20 °C

In order to get closer to the performance of the human nose, many other elements must be taken into account for the development of bioelectronic noses. Firstly, concerning the sensing materials, their diversity must be greatly increased. The human nose possesses about 400 different types of ORs, while so far all reported bioelectronic noses based on ORs and OBPs contain less than five sensing probes. The utilization of peptides can provide an efficient solution. Secondly, the human nose uses the combination of two types of recognition principles. Indeed, some ORs are "narrowly tuned" and thus specific to few odorants while some others are "broadly tuned" and cross-reactive to many odorants. It is such a combination that gives the human nose the extraordinary capacity of discriminating over 10,000 of different odors. Therefore, it is important to take inspiration from this and combine cross-reactive and specific sensing materials on the same multiplexed sensor system for better discrimination capacity. Thirdly, a hydrated sensing environment will be important to conserve the function and stability of sensing materials. In the human nose, mucus provides a hydrated environment thanks to the presence of large glycoproteins (mucins). In bioelectronic nose, the integration of its analogue will be very beneficial for considerably improving the lifespan and repeatability of the device. Fourthly, the transduction system should enable multiplexed format and temporal response with supplementary odorant recognition information. Fifthly, appropriate data processing with the rise of artificial intelligence and by taking inspiration from the unique functioning of olfactory neurons will also help in improving the performances of the bioelectronic noses. Finally, for their wide industrial applications, there is an urgent need to standardize the bioelectronic noses for odor analysis.

Acknowledgments

The authors thank greatly the following organizations for supporting the PhD scholarship of M.E.K (Labex LANEF and the French National Research Agency (ANR)), of C.H. (CEA), and of J.S.W. (Fondation Nanosciences). The authors also thank ANR and AID/DGA for the financial support (ANR-18-CE42-0012). This work has been partially supported by Labex ARCANE and CBH-EUR-GS (ANR-17-EURE-0003).

References

[1]. A. Wilson, M. Baietto, Applications and advances in electronic-nose technologies, *Sensors,* Vol. 9, Issue 7, 2009, pp. 5099-5148.

[2]. A. Loutfi, S. Coradeschi, G. K. Mani, P. Shankar, J. B. B. Rayappan, Electronic noses for food quality: A review, *Journal of Food Engineering,* Vol. 144, 2015, pp. 103-111.

[3]. M. V. Farraia, J. Cavaleiro Rufo, I. Paciência, F. Mendes, L. Delgado, A. Moreira, The electronic nose technology in clinical diagnosis: A systematic review, *Porto Biomedical Journal,* Vol. 4, Issue 4, 2019, e42.

[4]. D. Cipriano, L. Capelli, Evolution of electronic noses from research objects to engineered environmental odour monitoring systems: A review of standardization approaches, *Biosensors,* Vol. 9, Issue 2, 2019, 75.

[5]. T. Wasilewski, J. Gębicki, W. Kamysz, Advances in olfaction-inspired biomaterials applied to bioelectronic noses, *Sensors and Actuators B: Chemical,* Vol. 257, 2018, pp. 511-537.

[6]. T. Wasilewski, J. Gębicki, W. Kamysz, Bioelectronic nose: Current status and perspectives, *Biosensors and Bioelectronics,* Vol. 87, 2017, pp. 480-494.

[7]. T. Dung, Y. Oh, S.-J. Choi, I.-D. Kim, M.-K. Oh, M. Kim, Applications and advances in bioelectronic noses for odour sensing, *Sensors,* Vol. 18, Issue 2, 2018, 103.

[8]. M. Son, J. Y. Lee, H. J. Ko, T. H. Park, Bioelectronic nose: An emerging tool for odor standardization, *Trends in Biotechnology,* Vol. 35, Issue 4, 2017, pp. 301-307.

[9]. J. W. Cave, J. K. Wickiser, A. N. Mitropoulos, Progress in the development of olfactory-based bioelectronic chemosensors, *Biosensors and Bioelectronics,* Vol. 123, 2019, pp. 211-222.

[10]. U. J. Meierhenrich, J. Golebiowski, X. Fernandez, D. Cabrol-Bass, The molecular basis of olfactory chemoreception, *Angew. Chem. Int. Ed.,* Vol. 43, Issue 47, 2004, pp. 6410-6412.

[11]. The Nobel Prize, https://www.nobelprize.org/prizes/medicine/2004/press-release/

[12]. L. Buck, R. Axel, A novel multigene family may encode odorant receptors: A molecular basis for odor recognition, *Cell,* Vol. 65, Issue 1, 1991, pp. 175-187.

[13]. S. Firestein, How the olfactory system makes sense of scents, *Nature,* Vol. 413, Issue 6852, 2001, pp. 211-218.

[14]. K. Mori, The olfactory bulb: Coding and processing of odor molecule information, *Science,* Vol. 286, Issue 5440, 1999, pp. 711-715.

[15]. U. J. Meierhenrich, J. Golebiowski, X. Fernandez, D. Cabrol-Bass, De la molécule à l'odeur Les bases moléculaires des premières étapes de l'olfaction, *L'actualité Chimique,* Issue 289, 2005, pp. 29-39.

[16]. P. Pelosi, Odorant-binding proteins, *Critical Reviews in Biochemistry and Molecular Biology,* Vol. 29, Issue 3, 1994, pp. 199-228.

[17]. C. Bushdid, M. O. Magnasco, L. B. Vosshall, A. Keller, Humans can discriminate more than 1 trillion olfactory stimuli, *Science,* Vol. 343, Issue 6177, 2014, pp. 1370-1372.
[18]. J. E. Amoore, Stereochemical theory of olfaction, *Nature,* Vol. 199, Issue 4896, 1963, pp. 912-913.
[19]. G. M. Dyson, The scientific basis of odour, *J. Chem. Technol. Biotechnol.,* Vol. 57, Issue 28, 1938, pp. 647-651.
[20]. S. Firestein, C. Picco, A. Menini, The relation between stimulus and response in olfactory receptor cells of the tiger salamander, *The Journal of Physiology,* Vol. 468, Issue 1, 1993, pp. 1-10.
[21]. D. Krautwurst, K.-W. Yau, R. R. Reed, Identification of ligands for olfactory receptors by functional expression of a receptor library, *Cell,* Vol. 95, Issue 7, 1998, pp. 917-926.
[22]. B. Malnic, J. Hirono, T. Sato, L. B. Buck, Combinatorial receptor codes for odors, *Cell,* Vol. 96, Issue 5, 1999, pp. 713-723.
[23]. K. Touhara, Functional cloning and reconstitution of vertebrate odorant receptors, *Life Sciences,* Vol. 68, Issues 19-20, 2001, pp. 2199-2206.
[24]. P. Mombaerts, Seven-transmembrane proteins as odorant and chemosensory receptors, *Science,* Vol. 286, Issue 5440, 1999, pp. 707-711.
[25]. P. Mombaerts, Molecular biology of odorant receptors in vertebrates, *Annu. Rev. Neurosci.,* Vol. 22, Issue 1, 1999, pp. 487-509.
[26]. K. Raming *et al.*, Cloning and expression of odorant receptors, *Nature,* Vol. 361, Issue 6410, 1993, pp. 353-356.
[27]. R. Glatz, K. Bailey-Hill, Mimicking nature's noses: From receptor deorphaning to olfactory biosensing, *Progress in Neurobiology,* Vol. 93, Issue 2, 2011, pp. 270-296.
[28]. D. Lancet, N. Ben-Arie, Olfactory receptors, *Current Biology,* Vol. 3, Issue 10, 1993, pp. 668-674.
[29]. J. Bockaert, Molecular tinkering of G protein-coupled receptors: An evolutionary success, *The EMBO Journal,* Vol. 18, Issue 7, 1999, pp. 1723-1729.
[30]. H. Breer, Olfactory receptors: molecular basis for recognition and discrimination of odors, *Analytical and Bioanalytical Chemistry,* Vol. 377, Issue 3, 2003, pp. 427-433.
[31]. Y. Niimura, A. Matsui, K. Touhara, Extreme expansion of the olfactory receptor gene repertoire in African elephants and evolutionary dynamics of orthologous gene groups in 13 placental mammals, *Genome Res.,* Vol. 24, Issue 9, 2014, pp. 1485-1496.
[32]. T. Nakamura, G. H. Gold, A cyclic nucleotide-gated conductance in olfactory receptor cilia, *Nature,* Vol. 325, Issue 6103, 1987, pp. 442-444.
[33]. L. B. Buck, Information coding in the vertebrate olfactory system, *Annu. Rev. Neurosci.,* Vol. 19, Issue 1, 1996, pp. 517-544.
[34]. L. B. Buck, Unraveling the sense of smell (Nobel lecture), *Angew. Chem. Int. Ed.,* Vol. 44, Issue 38, 2005, pp. 6128-6140.

[35]. C. S. Silva Teixeira, N. M. F. S. A. Cerqueira, A. C. Silva Ferreira, Unravelling the olfactory sense: From the gene to odor perception, *Chemical Senses*, Vol. 41, Issue 2*,* 2015, bjv075.

[36]. M. Dibattista, S. Pifferi, A. Boccaccio, A. Menini, J. Reisert, The long tale of the calcium activated Cl^- channels in olfactory transduction, *Channels,* Vol. 11, Issue 5, 2017, pp. 399-414.

[37]. D. M. Rosenbaum, S. G. F. Rasmussen, B. K. Kobilka, The structure and function of G-protein-coupled receptors, *Nature,* Vol. 459, Issue 7245, 2009, pp. 356-363.

[38]. W. M. Oldham, H. E. Hamm, Heterotrimeric G protein activation by G-protein-coupled receptors, *Nat. Rev. Mol. Cell Biol.,* Vol. 9, Issue 1, 2008, pp. 60-71.

[39]. G. Gomila *et al.*, Advances in the production, immobilization, and electrical characterization of olfactory receptors for olfactory nanobiosensor development, *Sensors and Actuators B: Chemical,* Vol. 116, Issues 1-2, 2006, pp. 66-71.

[40]. P. Pelosi, N. E. Baldaccini, A. M. Pisanelli, Identification of a specific olfactory receptor for 2-isobutyl-3-methoxypyrazine, *Biochemical Journal,* Vol. 201, Issue 1, 1982, pp. 245-248.

[41]. E. Bignetti, A. Cavaggioni, P. Pelosi, K. C. Persaud, R. T. Sorbi, R. Tirindelli, Purification and characterisation of an odorant-binding protein from cow nasal tissue, *Eur. J. Biochem.,* Vol. 149, Issue 2, 1985, pp. 227-231.

[42]. J. Pevsner, R. Reed, P. Feinstein, S. Snyder, Molecular cloning of odorant-binding protein: member of a ligand carrier family, *Science,* Vol. 241, Issue 4863, 1988, pp. 336-339.

[43]. L. Briand, C. Nespoulous, V. Perez, J.-J. Rémy, J.-C. Huet, J.-C. Pernollet, Ligand-binding properties and structural characterization of a novel rat odorant-binding protein variant: Ligand binding and characterization of rat OBP-1F, *European Journal of Biochemistry,* Vol. 267, Issue 10, 2000, pp. 3079-3089.

[44]. M. Garibotti, A. Navarrini, A. M. Pisanelli, P. Pelosi, Three odorant-binding proteins from rabbit nasal mucosa, *Chem. Senses,* Vol. 22, Issue 4, 1997, pp. 383-390.

[45]. D. Pes, P. Pelosi, Odorant-binding proteins of the mouse, *Comparative Biochemistry and Physiology Part B: Biochemistry and Molecular Biology,* Vol. 112, Issue 3, 1995, pp. 471-479.

[46]. D. Pes *et al.*, Cloning and expression of odorant-binding proteins Ia and Ib from mouse nasal tissue, *Gene,* Vol. 212, Issue 1, 1998, pp. 49-55.

[47]. L. Briand *et al.*, Evidence of an odorant-binding protein in the human olfactory mucus: Location, structural characterization, and odorant-binding properties, *Biochemistry,* Vol. 41, Issue 23, 2002, pp. 7241-7252.

[48]. L. Briand, C. Nespoulous, J.-C. Huet, M. Takahashi, J.-C. Pernollet, Ligand binding and physico-chemical properties of ASP2, a recombinant odorant-binding protein from honeybee (*Apis mellifera* L.): Odorant

binding by a honeybee OBP, *European Journal of Biochemistry,* Vol. 268, Issue 3, 2001, pp. 752-760.
[49]. J.-J. Zhou *et al.*, Revisiting the odorant-binding protein LUSH of *Drosophila melanogaster*: Evidence for odour recognition and discrimination, *FEBS Letters,* Vol. 558, Issues 1-3, 2004, pp. 23-26.
[50]. J.-J. Zhou, X.-L. He, J. A. Pickett, L. M. Field, Identification of odorant-binding proteins of the yellow fever mosquito *Aedes aegypti*: Genome annotation and comparative analyses, *Insect. Mol. Biol.,* Vol. 17, Issue 2, 2008, pp. 147-163.
[51]. R. Vogt, R. Rybczynski, M. Lerner, Molecular cloning and sequencing of general odorant-binding proteins GOBP1 and GOBP2 from the tobacco hawk moth Manduca sexta: Comparisons with other insect OBPs and their signal peptides, *J. Neurosci.,* Vol. 11, Issue 10, 1991, pp. 2972-2984.
[52]. M. Tegoni *et al.*, Mammalian odorant binding proteins, *Biochimica et Biophysica Acta (BBA) – Protein Structure and Molecular Enzymology,* Vol. 1482, Issues 1-2, 2000, pp. 229-240.
[53]. P. Pelosi, Perireceptor events in olfaction, *Journal of neurobiology,* Vol. 30, Issue 1, 1996, pp. 3-19.
[54]. P. Pelosi, Odorant-binding proteins: Structural aspects, *Annals NY Acad. Sci.,* Vol. 855, Issue 1, 1998, pp. 281-293.
[55]. N. F. Brito, M. F. Moreira, A. C. A. Melo, A look inside odorant-binding proteins in insect chemoreception, *Journal of Insect Physiology,* Vol. 95, 2016, pp. 51-65.
[56]. J.-J. Zhou, Vitamins & Hormones, *Elsevier*, 2010.
[57]. W. S. Leal, Odorant Reception in insects: Roles of receptors, binding proteins, and degrading enzymes, *Annu. Rev. Entomol.,* Vol. 58, Issue 1, 2013, pp. 373-391.
[58]. P. Pelosi, R. Mastrogiacomo, I. Iovinella, E. Tuccori, K. C. Persaud, Structure and biotechnological applications of odorant-binding proteins, *Appl. Microbiol. Biotechnol.,* Vol. 98, Issue 1, 2014, pp. 61-70.
[59]. D. R. Flower, The lipocalin protein family: Structure and function, *Biochemical Journal,* Vol. 318, Issue 1, 1996, pp. 1-14.
[60]. M. Tegoni, R. Ramoni, E. Bignetti, S. Spinelli, C. Cambillau, Domain swapping creates a third putative combining site in bovine odorant binding protein dimer, *Nat. Struct. Mol. Biol.,* Vol. 3, Issue 10, 1996, pp. 863-867.
[61]. M. A. Bianchet *et al.*, The three-dimensional structure of bovine odorant binding protein and its mechanism of odor recognition, *Nat. Struct. Mol. Biol.,* Vol. 3, Issue 11, 1996, pp. 934-939.
[62]. J. Pevsner, S. H. Snyder, Odorant-binding protein: Odorant transport function in the vertebrate nasal epithelium, *Chem. Senses,* Vol. 15, Issue 2, 1990, pp. 217-222.
[63]. R. G. Vogt, L. M. Riddiford, Pheromone binding and inactivation by moth antennae, *Nature,* Vol. 293, Issue 5828, 1981, pp. 161-163.

[64]. B. Burchell, Turning on and turning off the sense of smell, *Nature,* Vol. 350, Issue 6313, 1991, pp. 16-17.
[65]. A. R. Dahl, Molecular Neurobiology of the Olfactory System (F. L. Margolis, T. V. Getchell, Eds.), *Springer*, US, 1988.
[66]. S. Sankaran, L. R. Khot, S. Panigrahi, Biology and applications of olfactory sensing system: A review, *Sensors and Actuators B: Chemical,* Vols. 171-172, 2012, pp. 1-17.
[67]. A. J. M. Barbosa, A. R. Oliveira, A. C. A. Roque, Protein- and peptide-based biosensors in artificial olfaction, *Trends in Biotechnology,* Vol. 36, Issue 12, 2018, pp. 1244-1258.
[68]. L. Du, C. Wu, Q. Liu, L. Huang, P. Wang, Recent advances in olfactory receptor-based biosensors, *Biosensors and Bioelectronics,* Vol. 42, 2013, pp. 570-580.
[69]. K. C. Persaud, Biomimetic olfactory sensors, *IEEE Sensors J.,* Vol. 12, Issue 11, 2012, pp. 3108-3112.
[70]. H. Mitsuno, T. Sakurai, R. Kanzaki, Chemical, Gas, and Biosensors for Internet of Things and Related Applications, *Elsevier*, 2019.
[71]. S. H. Lee, T. H. Park, Recent advances in the development of bioelectronic nose, *Biotechnol. Bioproc. E,* Vol. 15, Issue 1, 2010, pp. 22-29.
[72]. J. D. Bohbot, S. Vernick, The emergence of insect odorant receptor-based biosensors, *Biosensors,* Vol. 10, Issue 3, 2020, 26.
[73]. C. Wu, P. B. Lillehoj, P. Wang, Bioanalytical and chemical sensors using living taste, olfactory, and neural cells and tissues: A short review, *Analyst,* Vol. 140, Issue 21, 2015, pp. 7048-7061.
[74]. P. Wang, G. Xu, L. Qin, Y. Xu, Y. Li, R. Li, Cell-based biosensors and its application in biomedicine, *Sensors and Actuators B: Chemical,* Vol. 108, Issues 1-2, 2005, pp. 576-584.
[75]. E. H. Oh, S. H. Lee, S. H. Lee, H. J. Ko, T. H. Park, Cell-based high-throughput odorant screening system through visualization on a microwell array, *Biosensors and Bioelectronics,* Vol. 53, 2014, pp. 18-25.
[76]. S. H. Lee, S. B. Jun, H. J. Ko, S. J. Kim, T. H. Park, Cell-based olfactory biosensor using microfabricated planar electrode, *Biosensors and Bioelectronics,* Vol. 24, Issue 8, 2009, pp. 2659-2664.
[77]. Q. Liu, H. Cai, Y. Xu, Y. Li, R. Li, P. Wang, Olfactory cell-based biosensor: A first step towards a neurochip of bioelectronic nose, *Biosensors and Bioelectronics,* Vol. 22, Issue 2, 2006, pp. 318-322.
[78]. Q. Liu *et al.*, Olfactory mucosa tissue-based biosensor: A bioelectronic nose with receptor cells in intact olfactory epithelium, *Sensors and Actuators B: Chemical,* Vol. 146, Issue 2, 2010, pp. 527-533.
[79]. S. H. Lee, H. J. Ko, T. H. Park, Real-time monitoring of odorant-induced cellular reactions using surface plasmon resonance, *Biosensors and Bioelectronics,* Vol. 25, Issue 1, 2009, pp. 55-60.

[80]. H. J. Ko, T. Hyun Park, Dual signal transduction mediated by a single type of olfactory receptor expressed in a heterologous system, *Biological Chemistry,* Vol. 387, Issue 1, 2006, pp. 59-68.

[81]. A. A. Gimelbrant, S. L. Haley, T. S. McClintock, Olfactory receptor trafficking involves conserved regulatory steps, *J. Biol. Chem.,* Vol. 276, Issue 10, 2001, pp. 7285-7290.

[82]. N. D. Dwyer, E. R. Troemel, P. Sengupta, C. I. Bargmann, Odorant receptor localization to olfactory cilia is mediated by ODR-4, a novel membrane-associated protein, *Cell,* Vol. 93, Issue 3, 1998, pp. 455-466.

[83]. C. H. Wetzel, M. Oles, C. Wellerdieck, M. Kuczkowiak, G. Gisselmann, H. Hatt, Specificity and sensitivity of a human olfactory receptor functionally expressed in human embryonic kidney 293 cells and Xenopus Laevis oocytes, *J. Neurosci.,* Vol. 19, Issue 17, 1999, pp. 7426-7433.

[84]. J. H. Lim, J. Park, E. H. Oh, H. J. Ko, S. Hong, T. H. Park, Nanovesicle-based bioelectronic nose for the diagnosis of lung cancer from human blood, *Adv. Healthcare Mater.,* Vol. 3, Issue 3, 2014, pp. 360-366.

[85]. C. Hurot, N. Scaramozzino, A. Buhot, Y. Hou, Bio-inspired strategies for improving the selectivity and sensitivity of artificial noses: A review, *Sensors,* Vol. 20, Issue 6, 2020, 1803.

[86]. H. S. Song, S. H. Lee, E. H. Oh, T. H. Park, Expression, solubilization and purification of a human olfactory receptor from Escherichia coli, *Curr. Microbiol.,* Vol. 59, Issue 3, 2009, pp. 309-314.

[87]. K. Michalke *et al.*, Mammalian G-protein-coupled receptor expression in Escherichia coli: I. High-throughput large-scale production as inclusion bodies, *Analytical Biochemistry,* Vol. 386, Issue 2, 2009, pp. 147-155.

[88]. K. Michalke *et al.*, Mammalian G protein-coupled receptor expression in Escherichia coli: II. Refolding and biophysical characterization of mouse cannabinoid receptor 1 and human parathyroid hormone receptor 1, *Analytical Biochemistry,* Vol. 401, Issue 1, 2010, pp. 74-80.

[89]. H. Hamana, L. Shou-xin, L. Breuils, J. Hirono, T. Sato, Heterologous functional expression system for odorant receptors, *Journal of Neuroscience Methods,* Vol. 185, Issue 2, 2010, pp. 213-220.

[90]. L. Kaiser, J. Graveland-Bikker, D. Steuerwald, M. Vanberghem, K. Herlihy, S. Zhang, Efficient cell-free production of olfactory receptors: Detergent optimization, structure, and ligand binding analyses, *Proceedings of the National Academy of Sciences,* Vol. 105, Issue 41, 2008, pp. 15726-15731.

[91]. F. Chen *et al.*, Functional expression of olfactory receptors using cell-free expression system for biomimetic sensors towards odorant detection, *Biosensors and Bioelectronics,* Vol. 130, 2019, pp. 382-388.

[92]. Y. Hou *et al.*, A novel detection strategy for odorant molecules based on controlled bioengineering of rat olfactory receptor I7, *Biosensors and Bioelectronics,* Vol. 22, Issue 7, 2007, pp. 1550-1555.

[93]. J. M. Vidic, J. Grosclaude, M.-A. Persuy, J. Aioun, R. Salesse, E. Pajot-Augy, Quantitative assessment of olfactory receptors activity in immobilized nanosomes: A novel concept for bioelectronic nose, *Lab Chip,* Vol. 6, Issue 8, 2006, 1026.

[94]. I. Benilova *et al.*, Stimulation of human olfactory receptor 17-40 with odorants probed by surface plasmon resonance, *Eur. Biophys. J.,* Vol. 37, Issue 6, 2008, pp. 807-814.

[95]. I. V. Benilova, J. Minic Vidic, E. Pajot-Augy, A. P. Soldatkin, C. Martelet, N. Jaffrezic-Renault, Electrochemical study of human olfactory receptor OR 17-40 stimulation by odorants in solution, *Materials Science and Engineering: C,* Vol. 28, Issues 5-6, 2008, pp. 633-639.

[96]. J. Vidic *et al.*, Gold surface functionalization and patterning for specific immobilization of olfactory receptors carried by nanosomes, *Anal. Chem.,* Vol. 79, Issue 9, 2007, pp. 3280-3290.

[97]. J. H. Sung, H. J. Ko, T. H. Park, Piezoelectric biosensor using olfactory receptor protein expressed in Escherichia coli, *Biosensors and Bioelectronics,* Vol. 21, Issue 10, 2006, pp. 1981-1986.

[98]. C. Wu, L. Du, D. Wang, L. Wang, L. Zhao, P. Wang, A novel surface acoustic wave-based biosensor for highly sensitive functional assays of olfactory receptors, *Biochemical and Biophysical Research Communications,* Vol. 407, Issue 1, 2011, pp. 18-22.

[99]. C. Wu, L. Du, D. Wang, L. Zhao, P. Wang, A biomimetic olfactory-based biosensor with high efficiency immobilization of molecular detectors, *Biosensors and Bioelectronics,* Vol. 31, Issue 1, 2012, pp. 44-48.

[100]. L. Du *et al.*, Piezoelectric olfactory receptor biosensor prepared by aptamer-assisted immobilization, *Sensors and Actuators B: Chemical,* Vol. 187, 2013, pp. 481-487.

[101]. T. H. Kim *et al.*, Single-carbon-atomic-resolution detection of odorant molecules using a human olfactory receptor-based bioelectronic nose, *Adv. Mater.,* Vol. 21, Issue 1, 2009, pp. 91-94.

[102]. O. S. Kwon *et al.*, An ultrasensitive, selective, multiplexed superbioelectronic nose that mimics the human sense of smell, *Nano Lett.,* Vol. 15, Issue 10, 2015, pp. 6559-6567.

[103]. J. Minic *et al.*, Functional expression of olfactory receptors in yeast and development of a bioassay for odorant screening: Expression of olfactory receptors in yeast for screening, *FEBS Journal,* Vol. 272, Issue 2, 2005, pp. 524-537.

[104]. Y. Hou *et al.*, Immobilization of rhodopsin on a self-assembled multilayer and its specific detection by electrochemical impedance spectroscopy, *Biosensors and Bioelectronics,* Vol. 21, Issue 7, 2006, pp. 1393-1402.

[105]. H. J. Ko, T. H. Park, Piezoelectric olfactory biosensor: ligand specificity and dose-dependence of an olfactory receptor expressed in a

heterologous cell system, *Biosensors and Bioelectronics,* Vol. 20, Issue 7, 2005, pp. 1327-1332.
[106]. P. Sengupta, J. H. Chou, C. I. Bargmann, ODR-10 encodes a seven transmembrane domain olfactory receptor required for responses to the odorant diacetyl, *Cell,* Vol. 84, Issue 6, 1996, pp. 899-909.
[107]. T.-Z. Wu, A piezoelectric biosensor as an olfactory receptor for odour detection: electronic nose, *Biosensors and Bioelectronics,* Vol. 14, Issue 1, 1999, pp. 9-18.
[108]. S. Wadhwa, V. Garg, M. Gulati, B. Kapoor, S. K. Singh, N. Mittal, Pharmaceutical Nanotechnology (V. Weissig, T. Elbayoumi, Eds.), *Springer*, New York, 2019.
[109]. M. M. A. Elsayed, O. Y. Abdallah, V. F. Naggar, N. M. Khalafallah, Lipid vesicles for skin delivery of drugs: Reviewing three decades of research, *International Journal of Pharmaceutics,* Vol. 332, Issues 1-2, 2007, pp. 1-16.
[110]. H. Pick, E. L. Schmid, A.-P. Tairi, E. Ilegems, R. Hovius, H. Vogel, Investigating cellular signalling reactions in single attoliter vesicles, *J. Am. Chem. Soc.,* Vol. 127, Issue 9, 2005, pp. 2908-2912.
[111]. E. H. Oh, S. H. Lee, H. J. Ko, T. H. Park, Odorant detection using liposome containing olfactory receptor in the SPR system, *Sensors and Actuators B: Chemical,* Vol. 198, 2014, pp. 188-193.
[112]. H. J. Jin *et al.*, Nanovesicle-based bioelectronic nose platform mimicking human olfactory signal transduction, *Biosensors and Bioelectronics,* Vol. 35, Issue 1, 2012, pp. 335-341.
[113]. R. Khadka *et al.*, An ultrasensitive electrochemical impedance-based biosensor using insect odorant receptors to detect odorants, *Biosensors and Bioelectronics,* Vol. 126, 2019, pp. 207-213.
[114]. L. Wu, Y. Pan, G.-Q. Chen, H. Matsunami, H. Zhuang, Receptor-transporting protein 1 short (RTP1S) mediates translocation and activation of odorant receptors by acting through multiple steps, *J. Biol. Chem.,* Vol. 287, Issue 26, 2012, pp. 22287-22294.
[115]. C. Carraher, A. R. Nazmi, R. D. Newcomb, A. Kralicek, Recombinant expression, detergent solubilisation and purification of insect odorant receptor subunits, *Protein Expression and Purification,* Vol. 90, Issue 2, 2013, pp. 160-169.
[116]. B. R. Goldsmith *et al.*, Biomimetic chemical sensors using nanoelectronic readout of olfactory receptor proteins, *ACS Nano,* Vol. 5, Issue 7, 2011, pp. 5408-5416.
[117]. T. Murugathas, H. Y. Zheng, D. Colbert, A. V. Kralicek, C. Carraher, N. O. V. Plank, Biosensing with insect odorant receptor nanodiscs and carbon nanotube field-effect transistors, *ACS Appl. Mater. Interfaces,* Vol. 11, Issue 9, 2019, pp. 9530-9538.
[118]. M. Lee, H. Yang, D. Kim, M. Yang, T. H. Park, S. Hong, Human-like smelling of a rose scent using an olfactory receptor nanodisc-based bioelectronic nose, *Sci. Rep.,* Vol. 8, Issue 1, 2018, 13945.

[119]. H. Yang *et al.*, Nanodisc-based bioelectronic nose using olfactory receptor produced in *Escherichia coli* for the assessment of the death-associated odor cadaverine, *ACS Nano,* Vol. 11, Issue 12, 2017, pp. 11847-11855.
[120]. J. Oh *et al.*, Ultrasensitive, selective, and highly stable bioelectronic nose that detects the liquid and gaseous cadaverine, *Anal. Chem.,* Vol. 91, Issue 19, 2019, pp. 12181-12190.
[121]. M. Son, D. Kim, H. J. Ko, S. Hong, T. H. Park, A portable and multiplexed bioelectronic sensor using human olfactory and taste receptors, *Biosensors and Bioelectronics,* Vol. 87, 2017, pp. 901-907.
[122]. C. Hurot *et al.*, Highly sensitive olfactory biosensors for the detection of volatile organic compounds by surface plasmon resonance imaging, *Biosensors and Bioelectronics,* Vol. 123, 2019, pp. 230-236.
[123]. C. Kotlowski *et al.*, Fine discrimination of volatile compounds by graphene-immobilized odorant-binding proteins, *Sensors and Actuators B: Chemical,* Vol. 256, 2018, pp. 564-572.
[124]. R. Manai *et al.*, Grafting odorant binding proteins on diamond bio-MEMS, *Biosensors and Bioelectronics,* Vol. 60, 2014, pp. 311-317.
[125]. Y. Lu *et al.*, Olfactory biosensor for insect semiochemicals analysis by impedance sensing of odorant-binding proteins on interdigitated electrodes, *Biosensors and Bioelectronics,* Vol. 67, 2015, pp. 662-669.
[126]. Y. Lu *et al.*, Impedance spectroscopy analysis of human odorant binding proteins immobilized on nanopore arrays for biochemical detection, *Biosensors and Bioelectronics,* Vol. 79, 2016, pp. 251-257.
[127]. D. Zhang *et al.*, Nanoplasmonic monitoring of odorants binding to olfactory proteins from honeybee as biosensor for chemical detection, *Sensors and Actuators B: Chemical,* Vol. 221, 2015, pp. 341-349.
[128]. F. Di Pietrantonio *et al.*, Detection of odorant molecules via surface acoustic wave biosensor array based on odorant-binding proteins, *Biosensors and Bioelectronics,* Vol. 41, 2013, pp. 328-334.
[129]. F. Di Pietrantonio *et al.*, Tailoring odorant-binding protein coatings characteristics for surface acoustic wave biosensor development, *Applied Surface Science,* Vol. 302, 2014, pp. 250-255.
[130]. F. Di Pietrantonio *et al.*, A surface acoustic wave bio-electronic nose for detection of volatile odorant molecules, *Biosensors and Bioelectronics,* Vol. 67, 2015, pp. 516-523.
[131]. H. Zhao, L. Ivic, J. M. Otaki, M. Hashimoto, K. Mikoshiba, S. Firestein, Functional expression of a mammalian odorant receptor, *Science,* Vol. 279, Issue 5348, 1998, pp. 237-242.
[132]. A. Gao *et al.*, Highly sensitive and selective detection of human-derived volatile organic compounds based on odorant binding proteins functionalized silicon nanowire array, *Sensors and Actuators B: Chemical,* Vol. 309, 2020, 127762.
[133]. K. Bonnot *et al.*, Biophotonic ring resonator for ultrasensitive detection of DMMP as a simulant for organophosphorus agents, *Anal. Chem.,* Vol. 86, Issue 10, 2014, pp. 5125-5130.

[134]. S. Capone, C. De Pascali, L. Francioso, P. Siciliano, K. C. Persaud, A. M. Pisanelli, Electrical characterization of a pig odorant binding protein by Impedance Spectroscopy, in *Proceedings of the IEEE SENSORS Conference,* Christchurch, New Zealand, October 2009, pp. 1758-1762.

[135]. Y. Hou *et al.*, Study of langmuir and langmuir-blodgett films of odorant-binding protein/amphiphile for odorant biosensors, *Langmuir,* Vol. 21, Issue 9, 2005, pp. 4058-4065.

[136]. M. Larisika *et al.*, Electronic olfactory sensor based on *a. mellifera* odorant-binding protein 14 on a reduced graphene oxide field-effect transistor, *Angew. Chem.,* Vol. 127, Issue 45, 2015, pp. 13443-13446.

[137]. N. S. K. Gunda, M. Singh, L. Norman, K. Kaur, S. K. Mitra, Optimization and characterization of biomolecule immobilization on silicon substrates using (3-aminopropyl)triethoxysilane (APTES) and glutaraldehyde linker, *Applied Surface Science,* Vol. 305, 2014, pp. 522-530.

Chapter 2

Multifunctional Flexible Nanocomposite Sensors for Biomedical Applications

Ashok K. Batra, Aschalew Kassu, Sharvare Palwai, Mohan Aggarwal and Kunal Grover

2.1. Introduction

Multifunctional materials possess multiple characteristics concurrently, such as enhanced mechanical, electrical, thermal, and chemical properties, etc. Smart materials respond to external stimuli. These are known as piezoelectric, pyroelectric, ferroelectric, and piezoresistive materials, to name the few. Thus, they are being utilized in numerous applications as sensors, actuators, structural materials, and energy harvesting elements, etc. Several research investigations have highlighted the benefits of using nanoparticles, including carbon, dispersed in the polymer matrix to design and fabricate multifunctional materials with higher strength, including with above-cited properties in hybrid sensors or devices for medical and industrial applications. Tactile sensors, most commonly are referred to as train, and pressure sensors can obtain mechanical property data of the human body and local environment. It is recognized where contact, pressure, or traction exerted on the skin as well as in some internal organs. The tactile sense is one of the five traditional senses of the body. The tactile sense is received through millions of nerve ending on the skin, detecting even the slightest touch sensations and reporting it to the brain [1].

For brevity, we define three crucial attributes of smart materials [2-3]. *Piezoresistivity:* Tactile sensors based on piezoresistivity mechanisms

Ashok K. Batra
College of Engineering, Technology and Physical Sciences, Alabama A&M University, Normal (Huntsville), Alabama, USA

change electrical resistance when the mechanical stimulus is applied. Piezoresistivity is the widely utilized technology to implement a tactile sensor due to its simple structure and cost-effective fabrication techniques. Based on the simple principle of operation of the sensor, few prototypes have been fully designed and developed. *Piezoelectricity*: It is the development of voltage, which is caused by electric dipole moments observed in some anisotropic crystalline materials, in response to mechanical stimuli and vice versa; and *Pyroelectricity:* It refers to electric polarization of certain smart materials to generate a transient voltage in response to applied temperature change. Thus, by converting thermal energy to electricity, the pyroelectric effect can be applied to build a self-powered temperature sensor that automatically detects temperature change without the need of extra power supply or battery.

In the recent past, scientists all over the globe have been engaged in the development of tactile technology that can mimic the properties of human skin [4]. Thus, tactile sensors have to be wearable and should be able to incorporate into surfaces of satisfactory shapes with compatible, durable, and abrasion-resistant. It should be capable of multiple environment stimuli such as normal pressure, lateral strain, vibration, and shear, etc. Efficient candidate smart materials capable of reacting to these stimuli simultaneously are based on the principles of piezoelectricity, pyroelectricity, and piezoresistivity are: lead zirconate titanate (PZT), lead magnesium niobate-lead titanate (PMN-PT), zinc oxide (ZnO), gallium nitrate (GaN) and others. However, most of them are brittle, fragile, and non-flexible, including incompatible with the human body due to their toxicity. One promising candidate is the flexible and high strength polyvinylidene fluoride or polyvinylidene difluoride (PVDF) with comparative piezo- and pyro-efficiency, simple processing technology, dimensional stability, and chemical inertness, including compatibility with the human body. One of the issues with PVDF is to separate the piezoelectric effect from the pyroelectric effect, needs protection from thermal interference. It also needs high voltage or mechanical force to pole it to make it functional with a higher amount of β-phase. Furthermore, many efforts have made to embed a variety of nanoparticles and others in the PVDF matrix to enhance its functional properties. However, no deep efforts have been made, especially in PVDF copolymer, P(VDF-TrFE), and their nanocomposites with ultra-sensitivity and high deformability, which can meet the requirements of dynamic tactile sensing in wearable electronics. It also requires comparatively low-voltage to pole. It has all desired features to fabricate flexible tactile sensors such as the ultrahigh stretchability,

bending, wearability, which can be easily integrated into artificial and electronic skins. Thus, it was thought interesting and worthy of exploring P(VDF-TrFE) and its composite films, in particular their suitability in tactile sensors for biomedical sensors. With this train of thought, we investigated piezoelectric- piezoresistive-pyroelectric relevant sensing characteristics, including energy harvesting.

2.2. Fabrication of Polymer Composite Films

The polymer-composite films were fabricated via the solution-cast technique. Firstly, the P(VDF-TrFE) is dissolved in a suitable amount of methyl-ethyl-ketone (MEK) or dimethylformamide (DMF) at around 60 ºC. A requisite amount of composite materials carbon NPs (with diameter ~50 nm) is added to form the polymer-composite matrix. This mixture is ultrasonically agitated for several hours to break-up the agglomerates and then mechanically stirred to disperse the guest concentrations uniformly. The obtained solution is poured into Petri dishes for the solvent to evaporate. The films are annealed for 4-5 hours in air at room temperature. To form a parallel plate capacitor, silver conducting electrodes are deposited on opposite faces of the composite film sample and are cut into `~10 mm × 10 mm sized element for testing. The electrode samples are poled at room temperature with 4 kV voltages for 1/2 an hour via corona poling. After the poling process, the samples are short-circuited and annealed at 50 ºC for 2 hours to remove any extrinsic charges injected during poling [5]. A detailed fabrication process of the composite films is schematically described in Fig. 2.1. Samples of P(VDF-TrFE) embedded with increasing concentration of GRO nanoparticles are named as K1, K2, K3, and K4.

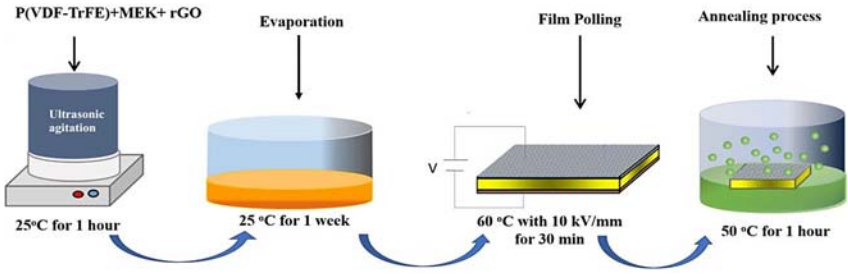

Fig. 2.1. Flow chart describing fabrication process of the composite films.

LabVIEW interfaced Quadtech LCR Bridge network can be used to conduct the dielectric study, and FTIR study provides the normal vibrational modes of PVDF and nanocomposites. The real and imaginary parts of the dielectric permittivity (ε' and ε") can be obtained by measuring terminal parallel capacitance C_P and loss tangent at a fixed measurement frequency of 1 KHz using LCR meter, and measurements were taken during heating run with temperature controller. A thermocouple installed near the sample, and the temperature can be measured with the help of a digital multi-meter. The details of the setup are described elsewhere [5]. The relevant parameters required or infrared sensing and energy harvesting, which include the dielectric constant (ε') and pyroelectric coefficient (p) were calculated. A real part (ε'), imaginary part (ε'') of the dielectric constant and A-C conductivity (σ_{ac}) were determined as:

$$\varepsilon' = \frac{C_p d}{\varepsilon_0 A}, \tag{2.1}$$

$$\varepsilon'' = tan\delta \cdot \varepsilon', \tag{2.2}$$

$$\sigma_{ac} = \omega\, \varepsilon_o tan\delta \cdot \varepsilon', \tag{2.3}$$

where C_p is the parallel capacitance of the sample at a signal frequency of 1 kHz, $tan\delta$ is the dielectric loss; A is the electrode area of the silver electrode, d is the thickness of the sample, $\varepsilon_0 = 8.854\times10^{-12}$ F/m is the permittivity of vacuum. σ_{ac} is the ac conductivity, and ω is the frequency of ac signal.

To record the dynamic relative pyroelectric current $I_{p,}$ the direct method is used. The pyroelectric current I_p was measured at various temperatures at constant heating rate, and the relative pyroelectric coefficient (p) was calculated using the relationship:

$$p = \left(\frac{I_p}{A}\right) / \left(\frac{dT}{dt}\right), \tag{2.4}$$

where dT/dt is the rate of change of temperature, which was kept constant throughout the measurement. The change in the pyroelectric coefficient indicates the change in dipole orientation inside the material; higher the coefficient, the better the material is for converting temperature change in electrical charge. The details of the measurements are described in our earlier publications [6]. Using forgoing parameters, the following

materials *figure-of-merits (F)* for respective performances of the devices can be calculated in order to predict their use in various applications [7, 8].

$F_I = p/c'$, for high current detectivity,

$F_V = p/\varepsilon' c'$, for high voltage responsivity,

$F_D = p/c' \sqrt{\varepsilon''}$, for high detectivity,

where p is the pyroelectric coefficient, c' is the volume-specific heat (it is ignored in the calculations of figure-of-merits), ε' is the dielectric constant and ε'' is the imaginary part of dielectric constant (dielectric loss constant). In the calculations, it is assumed that the specific heat is the same in composite films so it is not used in calculations. Broadly, tactile sensors based on the piezoresistivity mechanism undergo a change in the electrical resistance when the mechanical stimulus is applied. For comparison of the sensitivity of composite sensors fabricated, Gauge Factor (GF) is determined via calculations of $(\Delta R/Ro)/\varepsilon$ for strain sensors and $(\Delta R/Ro)/P$ for pressure sensors, where R, ε and P are the resistance, strain, and intensity of pressure, respectively. In other words, if the dependence of resistance of strain or pressure is linear, the calculated GF is strongly correlative with the tested deformation range. Custom-made setups shown in Fig. 2.2 are designed and fabricated for testing these nanocomposite pressure/strain sensors.

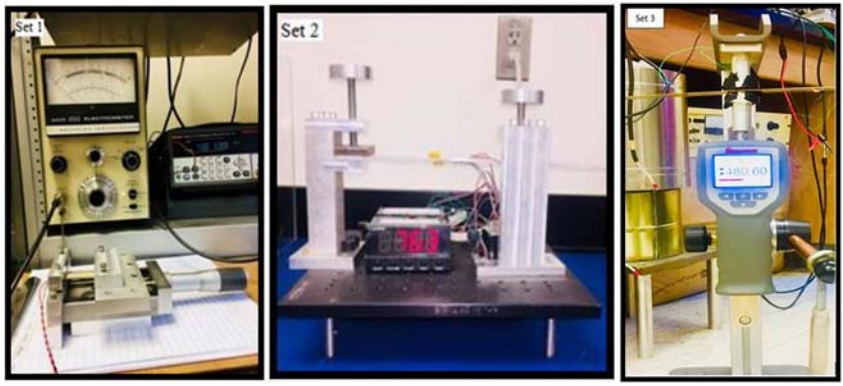

Fig. 2.2. Custom-made sensor performance determination setups: Set 1 (sheer), Set 2 (lateral) and Set 3(transverse pressure).

With the above-cited procedure and setups, electrical, piezoelectric, and pyroelectric properties are investigated to determine their functionality for use in infrared sensing and energy harvesting devices based on pyroelectricity and strain/pressure sensitivity via piezoresistivity. The films are found to be functional and, besides being flexible, can be used in piezoelectric touch/tactile sensors and infrared detectors, including in numerous scientific and medical instruments.

2.3. Characterization of Nanocomposite Films

2.3.1. Dielectric, Conductivity and Pyroelectric Characterization

Fig. 2.3 (a-d) shows the dielectric constants ε', the dielectric loss constant ε'', ac conductivity, pyroelectric coefficient and figure-of-merit of pyroelectric energy conversion of P(VDF-TrFE)-nanocomposite films, respectively. As expected in ferroelectrics, these parameters increase with the increase in temperature and weight fraction of nanocomposite films.

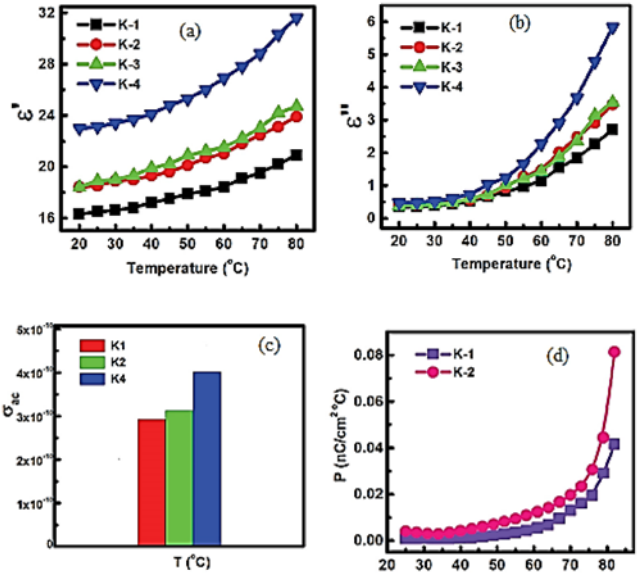

Fig. 2.3. (a) The variation of dielectric constants ε'; (b) the dielectric loss constant ε''; (c) ac conductivity, and (d) the pyroelectric coefficients of P(VDF-TrFE)-nC composite films.

Furthermore, the expansion of the co-polymer matrix due to heat treatment results in an enhancement in interfacial polarization and leads to an increase in dielectric constants. It can be observed from Figs. 2.3(a-d) that the dielectric constant, dielectric loss and ac conductivity increases with an increase in nano-C loading. Its content in the composites increases the interfacial area between the copolymer phase and the nano-C phase, resulting in the interfacial polarization of the dipoles.

2.3.2. Figures-of-merits of Nanocomposites

The figure-of-merit (FOM) is an important parameter for pyroelectric materials for current detective, voltage responsivity, detective, heat sensing and energy-harvesting applications. The maximum performance of the device can be achieved when pyroelectric materials have a high pyroelectric coefficient and a minimum dielectric constant and tangent loss. Hence, a pyroelectric device requires high values of FOM. The figure of merits for high current detectivity, high voltage responsivity, high detectivity, and thermal energy conversion need to be calculated.

2.3.3. Piezoresistive Characterizations

The relative D. C. electrical resistance/sensitivity change versus force applied using fixture shown in Set 1, Set 2, and Set 3 for typical PVDF (P2) and GRO embedded P(VDF-TRFE) nanocomposite films (K2) is illustrated in Fig. 2.4. It is worth mentioning that in polymer composite materials, consisting of an insulating polymeric matrix and conductive reinforcing nanoparticles, the total resistance is due to both components present: matrix and reinforcing nanoparticles [9]. Assuming the resistance of the matrix be constant, then the total resistance of the composite will depend on the number of particles and conducting paths. Thus, the characteristics of the conductive network will be the main factors that may determine the total resistance of the composite materials.

Strain is of three types depending upon the change produced in a body and the stress applied. The three types of strain are longitudinal strain; volume strain; and shearing strain. Furthermore, there are five types of stress: tensile, compressive and shear, torsional and bending. Torsional stress is generally a tangentially arranged collection of shear stresses.

Thus, result illustrated in Fig. 2.4 are indirectly related to these parameters as well.

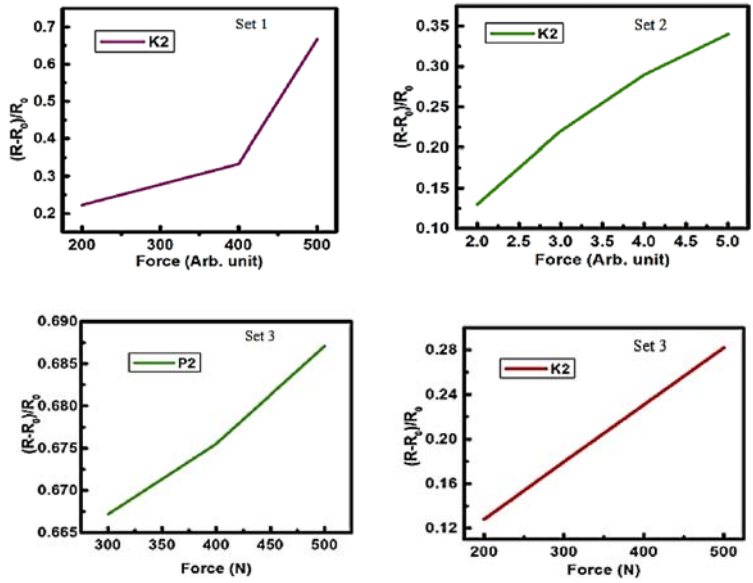

Fig. 2.4. Variation of electrical resistance change with strain applied using 3 sets of machines (Set 1, Set 2, and Set 3).

The investigated flexible composite films could be used in a variety of biomimetic and minimal, medical, invasive diagnostic applications in force and temperature detection via selectively poling active-matrix cells to fabricate a bi-functional device for pressure and temperature sensing, including energy harvesting with improved performance, as briefly described in following paragraph [10]. *Monitoring of respiration*: the respiratory rate could be derived by measuring the pressure applied to a composite-based gauge embedded in a seat or lap belt. *Assessment of the prostate gland disease*: measurement of the prostate gland stiffness is an important diagnostic factor in the detection of prostate disease during a digital rectal exam. However, digital palpation is associated with a large number of physician errors. These films can be used as a more objective sensor of the prostate gland stiffness than other such sensors. Placing the film at the tip of a probe that is driven back and forth via a micro-motor, while touching the prostate gland, would give rise to a voltage signal that is proportional to the prostate gland hardness. Thus, such a device could

be used for the detection of prostate cancer and prostatic hypertrophy. *Quantification and detection of articular cartilage softening*: modified films can be used as stain sensors attached to a stainless steel diaphragm to quantify the softening of articular cartilage during arthroscopy for the early detection of osteoarthritis. *Catheter position sensing*: to observe the position of a catheter in ultrasonography, modified P(VDF-TrFE) composite film can be installed at a certain point in the catheter to detect the position. Piezoresistive pressure sensors are also being used in plantar foot pressure monitoring [11]. Other important applications of piezoresistive sensors are in the areas of rectal manometry which provides a useful method to objectively assess the physiology of defecation. These sensors are used for diagnostic measurement of the dynamic rectal pressure profile which may provide additional information in cases with colorectal disorders.

2.4. Conclusions

In summary, the nanocomposite thick films fabricated by embedding GRO in P(VDF-TFE) displayed better dielectric properties than the pristine specimens did. As expected, the effective dielectric constant of P(VDF-TrFE) increased when it is mixed with reinforcing particles over the entire temperature range investigated.

- Films fabricated using conventional *solution casting method*. This technique is a very useful and inexpensive technique for manufacturing nanocomposite pyroelectric sensors and energy conversion devices because the films can be fabricated with less energy, time, and effort as compared to other fabrication processes.

- The films were characterized for their dielectric, and pyroelectric properties, in order to determine their usefulness in uncooled infrared detector for non-contact body temperature measurement and thermal energy conversion devices applications.

- The calculated pyroelectric *figure-of-merits* (F_1) of the composite films are found to be lower than pristine films.

Based on the results obtained, composite films are attractive for use in uncooled thermal sensing elements, for energy conversion devices and piezoresistive pressure sensors especially in applications where flexible and curved surface based sensors are required.

Wearable sensor technology continues to advance and provide significant opportunities for improving personalized healthcare. In recent years, advances in flexible electronics, smart materials, and low-power computing and networking have reduced barriers to technology accessibility, integration, and cost, unleashing the potential for ubiquitous monitoring.

Possible Applications in Medical Devices

The investigated 0-3 PVDF/MWCNT flexible composite film has enhanced pyroelectric properties as compared with the usual PVDF film. Thus, it could be used in a variety of biomimetic and minimal, medical, invasive diagnostic applications in force and temperature detection via selectively poling active-matrix cells to fabricate a bi-functional device for pressure and temperature sensing with improved performance, as briefly described below [5, 9, 10].

Infant cardiorespiratory monitoring: neonatal intensive care of premature infants is of great importance in their survival and requires the continuous monitoring of their heart and respiration rates, along with other vital signs. Ideally, this could be done without attaching and detaching electrode patches on their extremely delicate skin. A non-invasive sensor array of modified film can be placed on the bed to pick-up voltage signals from the pressure fluctuations on the bed caused by the respiratory movements and heartbeats of a premature infant. Such an array could also possibly monitor body temperature.

Pediatric dynamometer: weight-bearing activity has been demonstrated to benefit childhood bone development via PVDF pressure sensors.

Monitoring of respiration: the respiratory rate could be derived by measuring the pressure applied to a composite-based gauge embedded in a seat or lap belt.

Assessment of the prostate gland disease: measurement of the prostate gland stiffness is an important diagnostic factor in the detection of prostate disease during a digital rectal exam. However, digital palpation is associated with a large number of physician errors. PVDF/MWCNT film can be used as a more objective sensor of the prostate gland stiffness than other such sensors. Placing the film at the tip of a probe that is driven back and forth via a micro-motor, while touching the prostate gland,

would give rise to a voltage signal that is proportional to the prostate gland hardness. Thus, such a device could be used for the detection of prostate cancer and prostatic hypertrophy.

Quantification and detection of articular cartilage softening: modified films can be used as stain sensors attached to a stainless-steel diaphragm to quantify the softening of articular cartilage during arthroscopy for the early detection of osteoarthritis.

Catheter position sensing: to observe the position of a catheter in ultrasonography, modified PVDF composite film can be installed at a certain point in the catheter to detect the position.

Present Status of Candidate Multifunctional Devices: Pressure ulcers are painful sores that arise from prolonged exposure to high-pressure points, which restricts blood flow and lead to tissue necrosis. It is a common occurrence among patients with impaired mobility, diabetics and the elderly.

Disposable pressure monitoring system: A flexible pressure monitoring system for pressure ulcer prevention: has been developed [12]. Due to its low cost, the sensor sheet can be disconnected from the reusable electronics and be disposed of after use, suitable for a clinical setting. Each sensor has a resolution of better than 2-mm Hg and a range of 50-mm Hg and offset is calibrated in software. Real-time pressure data is displayed on a computer. A maximum sampling rate of 12-Hz allows for continuous monitoring of pressure points.

Pressure sensor integrated into a catheter: Sharma et al**.** demonstrated the design of thin, flexible pressure sensors based on piezoelectric PVDF-TrFE (polyvinyledenedifluoride-tetrafluoroethylene) co-polymer film, which can be integrated onto a catheter, where the compact inner lumen space limit the dimensions of the pressure sensors [13]. The authors also demonstrated sensitive pressure sensors that can be directly mounted on the catheter and will allow monitoring the blood pressure inside the organ for effective venous balloon inflation pressures. Besides, the dual-sensor system will be able to determine the blood flow direction downstream of the balloon, which will enable the surgeons to monitor back-flow effectively. On the broader scale, the authors proposed piezoelectric thin-film technology generated from this research can be extended for both implantable sensing and energy harvesting applications, such as implantable self-powered blood pressure sensors

and wireless data transmitters for monitoring real-time patient physiological conditions. A sensor-based on polyvinylidene fluoride (PVDF) piezoelectric thin film was designed and fabricated to detect wrist motion signals [14]. A series of dynamic experiments have been carried out, including the contrast experiments of different materials and force-charge signal characterization. The experimental results show that when the excitation signal exceeds 15 Hz, the sensitivity of the sensor is always stable at 3.10 pC/N. The authors' experimental results show that, with the advantages of small size, excellent flexibility, and high sensitivity, this wrist PVDF sensor can be used to detect the wrist motion signals with weak amplitude, low frequency, substantial interference, and randomness.

Nasal sensor to monitor respiration: A piezoelectric polyvinylidene fluoride (PVDF) thin-film based nasal sensor to monitor human respiration pattern (RP) from each nostril simultaneously has been developed [15]. The thin film-based PVDF nasal sensor is designed in a cantilever beam configuration. Two cantilevers are mounted on a spectacle frame in such a way that the airflow from each nostril impinges on this sensor, causing bending of the cantilever beams—voltage signal produced due to airflow induced dynamic piezoelectric effect to generate a respective RP. The developed sensor is simple in design, non-invasive, patient-friendly, and hence shows promising routine clinical usage. Self-powered operation, flexibility, excellent mechanical properties, and ultra-high sensitivity are highly desired properties for pressure sensors in human health monitoring and anthropomorphic robotic systems. Piezoelectric pressure sensors, with enhanced electromechanical performance to effectively distinguish multiple mechanical stimuli (including pressing, stretching, bending, and twisting), have attracted interest to precisely acquire the weak signals of the human body. Wang et al. prepared a poly(vinylidene fluoride-trifluoroethylene)/ multi-walled carbon nanotube (P(VDF-TrFE)/MWCNT) composite by an electrospinning process and stretched it to achieve alignment of the polymer chains [16]. The composite membrane demonstrated excellent piezoelectricy, favorable mechanical strength, and high sensitivity. The piezoelectric coefficient d33 value was approximately 50 pm/V, the Young's modulus was ~0.986 GPa, and the sensitivity was ~540 mV/N. The resulting composite membrane was employed as a piezoelectric pressure sensor to monitor small physiological signals including pulse, breath, and slight motions of muscle and joints such as swallowing, chewing, and finger and wrist movements. Moderate doping with carbon nanotubes had a positive impact on the formation of the beta-phase of

the piezoelectric device, and the piezoelectric pressure sensor has the potential for application in health care systems and smart wearable devices.

Patch for respiration detection while walking: Lei et al. reported a piezoelectric poly(vinylidene fluoride) (PVDF) polymer-based sensor patch for respiration detections in dynamic walking condition [17]. The working mechanism of respiration signal generation is based on the periodical deformations on a human chest wall during the respiratory movements, which in turn mechanically stretch the piezoelectric PVDF film to generate the corresponding electrical signals. The PVDF sensing film was completely encapsulated within the sensor patch forming a mass-spring-damper mechanical system to prevent the noises generated in a dynamic condition. Their Results demonstrated the respiration signals generated and the respiratory rates measured by the proposed sensor patch were in line with the same measurements based on a commercial respiratory effort transducer both in a static (e.g., sitting) or dynamic (e.g., walking) condition. Other distinctive features include its small size, lightweight, ease of use, low cost, and portability. All these make it a promising sensing device to monitor respirations, particularly in-home care units.

Posture monitoring system: The authors demonstrated a patient posture monitoring system based on a patient cloth with flexible embedded sensors [18]. The patient cloth was fitted loosely and flexible sensors were positioned in the knee and hip parts of the fabric. The sensor generated electrical responses corresponding to the bending and extension of each joint. The sensors outputs were wirelessly transferred to a PC with a custom made program. The data accurately predicted the position of the patient through a rule-based algorithm after processing of electrical signals. The authors tested the monitoring system with six motions between four positions that can happen in or around the bed. The demonstration of an arrangement suggests a patient monitoring system using unobtrusive wearable sensors. The authors used flexible sensors based on PVDF, which is a flexible piezoelectric material. The success rate was 88 %.

Acknowledgments

Work supported through NSF-RISE grant (HRD 1546965) and the Department of Homeland Security-Scientific Leadership Award Grant

No. DHS-SLA 2014-ST-062- 00060-02. Special Thanks to Mr. E. Curtis for fabricating fixtures used in the present work.

References

[1]. S. Stassi, V. Cauda, C. Giancarlo, F. F. Pirri, Flexible tactile sensing based on piezoelectric composites: A review, *Sensors,* Vol. 14, 2014, pp. 5296-5332.

[2]. A. K. Batra, A. Alomari, Power Harvesting via Smart Materials, *SPIE Press*, WA, U.S.A, 2017.

[3]. R. A. Rahim, M. F. A. Waduth, H. I. Jaafar, N. M. N. Ayob, P. L. Leow, Current trend of tactile sensor in advanced applications, *Sensors and Transducers*, Vol. 143, Issue 8, August 2012, pp. 32-43.

[4]. J. S. Lee, K. Shin, O. J. Cheong, J. Kim, J. Jang, Highly sensitive and multifunctional tactile sensors using free-standing ZnO/PVDF thin films with graphene electrodes for pressure and temperature monitoring, *Scientific Reports*, Vol. 7887, Issue 5, 2015, pp. 1-8.

[5]. A. K. Batra, M. D. Aggarwal, Pyroelectric Materials: Infrared Detectors, Particle Accelerators and Energy Harvesters, *SPIE Press*, 2003.

[6]. A. K. Batra, M. E. Edwards, P. Guggilla, M. D. Aggarwal, R. B. Lal, Pyroelectric properties of PVDF: MWCNT nanocomposite film for uncooled infrared detectors and medical applications, *Integrated Ferroelectrics*, Vol. 158, 2014, pp. 98-107.

[7]. A. K. Batra, M. A. Alim, J. R. Currie, M. D. Aggarwal, The electrical response of the modified lead Titanate based thick-films, *Physics B*, Vol. 404, 2009, pp. 1905-1911.

[8]. G. Sebald, L. Seveyat, D. Guyomar, L. Lebrun, B. Guiffard, S. Pruvost, Electrocaloric and pyroelectric properties of $0.75Pb(Mg_{1/3}Nb_{2/3})O_3$-$0.25PbTiO_3$ single crystals, *Journal of Applied Physics*, Vol. 100, 2006, 124112.

[9]. G. Georgousis, E. Kontou, A. Kyritsis, P. Pissis, M. Micusik M. Omastove, Piezo resistivity of conductive polymers nanocomposites: Experiment and modeling, *Journal of Reinforced Plastics and Composites*, Vol. 37, Issue 17, 2018, pp. 1085-1098.

[10]. A. K. Batra, M. E. Edwards, P. Guggilla, M. D. Aggarwal, R. B. Lal, Pyroelectric properties of PVDF: MWCNT nanocomposite film for uncooled infrared detectors and medical applications, *Integrated Ferroelectrics*, Vol. 158, 2014, pp. 98-107.

[11]. A. Razak, A. Zayegh, R. Begg, Y. Wahab, Foot pressure measurement system: A review, *Sensors*, Vol. 12, 2012, pp. 9884-9912.

[12]. M. Yip, E. Winokur, A. G. Balderrama, R. Sheridan, H. Ma, A flexible pressure monitoring system for pressure ulcer prevention, *Conf. Proceedings IEEE Eng. Med. Biol. Soc*., 2009, pp. 1212-1215.

[13]. T. Sharma, A. Kevin, N. Sahil, G. Brijesh, X. J. Zhang, Flexible thin-film PVDF-TrFE based pressure sensor for smart catheter applications, *Annals of Biomedical Engineering*, Vol. 41, Issue 4, 2013, pp. 744-751.

[14]. H. Yaohui, K. Wuwei, F. Yong, X. Lingrui, Q. Longzhen, J. Tao, Piezoelectric poly(vinylidene fluoride) (PVDF) polymer-based sensor for wrist motion signal detection, *Applied Sciences*, Vol. 8, Issue 5, 2018, 836.

[15]. G. R. Manjunath, K. Rajanna, D. R. Mahapatra, M. Nayak, K. U. Maheshwari, R. Srinivasa, Polyvinylidene fluoride film based nasal sensor to monitor human respiration pattern: An initial clinical study, *Journal of Clinical Monitoring and Computing*, Vol. 27, 2013, pp. 647-657.

[16]. W. Aochen, H. Ming, Z. Liwei, Q. Xiaoyong, Self-powered wearable pressure Sensors with enhanced piezoelectric properties of aligned P(VDF-TrFE)/MWCNT composites for monitoring human physiological and muscle motion signs, *Nanomaterials*, Vol. 8, Issue 12, 2018, 1021.

[17]. L. Kin-Fong, H. Yi-Zheng, C. Yi-Yuan, W. Min-Hsien, The structure design of piezoelectric poly(vinylidene Fluoride) (PVDF) polymer-based sensor patch for the respiration monitoring under dynamic walking conditions, *Sensors*, Vol. 15, 2015, pp. 18801-18812.

[18]. Y. Cha, K. Nam, D. Kim, Patient posture monitoring system based on flexible sensors, *Sensors*, Vol. 17, 2017, 584.

Chapter 3

Novel Ni-based Nanostructures for Non-enzymatic Glucose Detection

Mario Urso and Salvo Mirabella

3.1. Introduction

3.1.1. Diabetes and Enzymatic Glucose Sensors

In the last decades there has been an increasing interest towards the quantitative determination of different chemical species, often driven by practical and urgent needs as in the case of glucose detection for the diagnosis and care of diabetes.

Diabetes includes a series of metabolic disorders associated with a persistent hyperglycaemic condition, i.e. an increase of sugars concentration in blood, caused by a pathological reduction of insulin secretion by the pancreas (Type 1 diabetes) or by the body's inability to use the produced insulin (Type 2 diabetes) [1]. Among the complications of diabetes there are ketoacidosis (accumulation of altered metabolism products) and chronic diseases which involve different organs, including eyes, kidneys, heart, blood vessels and peripheral nerves. According to the International Diabetes Federation (IDF), in 2019 there are 463 million people with diabetes in the world, and this number is continuously increasing [2]. It is expected that there will be 700 million people with diabetes by 2045 (51 % increase). Since three in four of them are of working age (20-64 years old), the national productivity and economic growth will be increasingly hindered. In addition, it is unquestionable that the treatment of diabetes and its complications

Mario Urso
Department of Physics and Astronomy 'Ettore Majorana', University of Catania, Italy

heavily influences the finances of national health services. For example, based on the data provided by the American Diabetes Association (ADA), the total cost of diabetes in USA in 2017 was about $327 billion, including $237 billion in direct medical costs and $90 billion in reduced productivity [3].

The costs are significantly high also for people with diabetes, mainly due to glucose self-monitoring. In fact, for a diabetic patient it is of vital importance to constantly monitor the level of glucose in his blood and to regulate it by intermittent insulin injections. The blood glucose measurement is typically done by diabetic patients at home by pricking their fingers to collect the blood sample to be examined, which is then dropped on the test strip of commercial enzymatic sensors [4]. These sensors are composed of an electrode on which the glucose oxidase (GOx), an enzyme specific for glucose oxidation, is immobilized. Upon glucose oxidation, an electrical signal is produced whose intensity is proportional to the concentration of glucose in the blood sample (for healthy people the blood glucose level is 3.9-7.2 mM, i.e. 70-130 mg dl^{-1} [3]). Enzymatic sensors are extremely selective to glucose; however, one main drawback lies in the very invasive blood sample extraction. Moreover, it should be noted that this painful procedure is normally repeated several times during the day and does not allow to catch any anomaly between one measurement and the next one, evidencing the need of continuous glucose monitoring systems [5]. Because of this invasiveness, children and young diabetic patients are particularly reluctant to perform these measurements. Another important drawback of enzymatic sensors is their high cost due to the complex and expensive GOx immobilization and stabilization protocols (25 KU g^{-1} GOx = $383) [6]. Furthermore, GOx activity during sensor fabrication, usage and storage can be affected by temperature, pH, humidity and so on, leading to a limited reproducibility and stability of the measurements [7]. As a result, it is necessary to replace the test strip after one or two weeks of use [8], with consequent higher costs for the diabetic patients. Based on these considerations it is easy to understand the tremendous attention that the scientific community has recently devoted on the development of “user-friendly” enzyme-free glucose sensors that can operate with externally accessible physiological fluids, such as human tears and saliva (Fig. 3.1) [9]. Beyond the stability and selectivity issues, another essential feature is the extremely high sensitivity needed to measure the glucose level out of blood, as it is up to 3 order of magnitude lower. An intense research effort is ongoing to

develop non-enzymatic sensor able to detect down to μM glucose concentration.

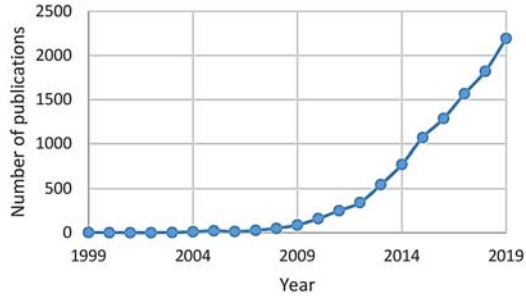

Fig. 3.1. Number of publications on non-enzymatic glucose sensors in the last twenty years (results collected by using the Scopus database and "non-enzymatic glucose sensor" as the search item on 9th April 2020).

3.1.2. Non-enzymatic Glucose Detection

Non-enzymatic glucose sensors are based on the ability of some electrode materials to directly oxidize glucose upon application of a potential. These include noble metals (Au, Pt, Pd, etc.) [10-12], transition metals (Ni, Cu, Fe, etc.) [13], metal oxides (NiO, CuO, ZnO, TiO_2, etc.) [14-16], alloys and bimetallic structures (Pt-Au, Pt-Pb, Cu-Ag, Pd-Cu, etc.) [17-19], complexes (cobalt phthalocyanine tetrasulfonate, nickel hexacyanoferrate, etc.) [20, 21], carbon-based materials (graphene, carbon nanotubes, boron-doped diamond, etc.) [22-25], polymers [26] and metal organic frameworks (MOFs) [27].

For transition metals containing electrode materials, two major theories have been proposed to explain the mechanism of non-enzymatic glucose detection based on experimental observations: the activated chemisorption model and the "Incipient Hydrous Oxide Adatom Mediator" (IHOAM) model [28]. Pletcher's activated chemisorption model, illustrated in Fig. 3.2(a), assumes that the glucose molecule is adsorbed on the electrode surface due to the bond between the glucose hemiacetalic carbon atom and unpaired *d*-electrons and unfilled *d*-orbitals of the transition metal atom, simultaneously with the glucose hemiacetalic hydrogen abstraction [30]. The extracted hydrogen atoms bonds to the adjacent transition metal atom on electrode surface. This process results in a lower strength of the bond between the oxidized

glucose molecule and the transition metal atom, and thus in the desorption of the oxidized glucose molecule. Burke's IHOAM model, shown schematically in Fig. 3.2(b), takes into account for the role of adsorbed OH^- ions (OH_{ads}) on the electrode surface [31]. It assumes that transition metal atoms with low lattice stabilization and enhanced reactivity, for example those in grain boundaries, undergo a pre-monolayer oxidation step, forming an incipient hydrous oxide layer of OH_{ads}. After glucose adsorption, this layer mediates the electro-oxidation of glucose at lower potentials and regenerates the metal surface.

As for any other kind of sensor, the challenge in non-enzymatic glucose detection is the development of a low-cost electrode material which satisfies as many as possible of the fundamental requirements of "5 S", i.e. high Sensitivity, Selectivity, Stability and Speed, and low Signal-to-noise ratio. The absence of GOx in non-enzymatic sensors results in a much lower cost and higher stability, still the selectivity is an issue [32]. Differently from GOx, most non-enzymatic electrode materials can indistinctly oxidize other small molecules with faster kinetics than glucose, interfering with glucose detection [33]. Moreover, chemical species in real samples, such as chloride (Cl^-) ions, can rapidly adsorb on the electrode surface, decreasing the number of active sites for glucose oxidation and thus the sensitivity (poisoning) [34]. The sensitivity of some electrode materials is also significantly reduced when tested at physiological pH [29]. Many efforts have been devoted also in improving the sensitivity and signal-to-noise ratio to enable glucose detection at very low concentrations such as those in human tears (0.05-0.5 mM) and saliva (0.23-0.38 mM) of healthy people [35]. The biocompatibility of the electrode material has been attentioned as well, especially in implantable non-enzymatic glucose sensors for continuous glucose monitoring under the skin [5].

The recent progress of nanotechnology has opened new opportunities in non-enzymatic glucose detection [36-38]. In fact, materials at the nanoscale typically show new and tunable size, shape, and structure-dependent physical and chemical properties, which allow to boost the 5 S for glucose detection with respect to their bulk counterparts. Nanoparticles, nanowires, nanorods, nanotubes and nano/mesoporous thin films have larger surface-to-volume ratio, major electrolyte penetration, unique density of energy states and electronic properties, and higher electrocatalytic activity [39]. High index crystal facets and edges with higher surface reactivity are more prevalent in nanomaterials

[32]. Besides, upon application of a potential as in the case of non-enzymatic glucose detection, unique electric field gradients are generated in nanostructured electrode materials, which strongly influence the redox processes occurring at the electrode/electrolyte interface [40]. Therefore, the rational design of nanostructured electrode materials plays a key role in the development of non-enzymatic glucose sensors with high market value.

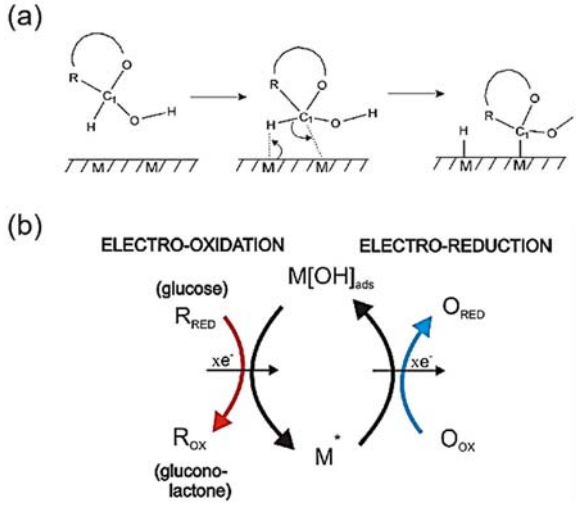

Fig. 3.2. Schematic illustration of (a) Pletcher's activated chemisorption model, and (b) Burke's "Incipient Hydrous Oxide Adatom Mediator" (IHOAM) model for non-enzymatic glucose detection in transition metals containing electrode materials. Adapted from [29].

3.1.3. Ni-based Electrodes

Ni, nickel oxide (NiO) and nickel hydroxide [$Ni(OH)_2$] are the most popular electrode material for non-enzymatic glucose detection due to their low-cost and high sensitivity (mA mM^{-1} cm^{-2}) resulting from the Ni^{2+}/Ni^{3+} redox couple in alkaline solutions [13].

Upon immersion of a Ni electrode in an alkaline solution and application of a potential, Ni^0 on the surface is oxidized to Ni^{2+}, forming a thin layer of $Ni(OH)_2$ [38, 40]:

$$Ni + 2OH^- \rightarrow Ni(OH)_2 \quad (3.1)$$

NiO is also a Ni^{2+} species. Upon application of a certain potential, $Ni(OH)_2$ and NiO electrodes oxidize to nickel oxyhydroxide (NiOOH), a Ni^{3+} species [32]:

$$NiO + OH^- \rightarrow NiOOH + e^-, \quad (3.2)$$

$$Ni(OH)_2 + OH^- \rightarrow NiOOH + e^- + H_2O \quad (3.3)$$

NiOOH oxidizes glucose ($C_6H_{12}O_6$) to gluconolactone ($C_6H_{10}O_6$) through the abstraction of the hemiacetalic hydrogen atom [29]:

$$NiOOH + C_6H_{12}O_6 \rightarrow Ni(OH)_2 + [C_6H_{11}O_6]^-, \quad (3.4)$$

$$[C_6H_{11}O_6]^- + OH^- \rightarrow C_6H_{10}O_6 + 2e^- + H_2O \quad (3.5)$$

Pletcher's model explain the glucose electro-oxidation by NiOOH. IHOAM model is also valid, however in this case the OH_{ads} layer induces a change of Ni oxidation state rather than the oxidation of glucose.

The overall result of glucose oxidation at Ni electrodes is the production of electrons that can be measured by amperometric techniques to detect glucose, and the reversible reduction of NiOOH to $Ni(OH)_2$. Then, the applied potential ensures the oxidation of $Ni(OH)_2$ to NiOOH, sustaining the glucose oxidation process.

Besides their high sensitivity, Ni-based electrodes have good selectivity and resistance to chloride poisoning. These result from their high isoelectric point, which make their surface negatively charged in alkaline solution due to the OH_{ads} layer [41]. Therefore, the effect of negatively charged interferents and Cl^- ions is reduced by the Coulomb repulsion with the negatively charged electrode surface. Ni-based electrodes have also high stability. However, one major drawback is that glucose oxidation by Ni-based electrodes is strongly dependent on the concentration of OH^- ions. Therefore, the high sensitivity which is typically obtained in alkaline solutions (pH 13) is significantly reduced in physiological solutions (pH 7.4).

In the following part of this chapter, the most common experimental procedure to evaluate the 5 S of electrode materials for non-enzymatic glucose detection is first described. Then, the most advanced strategies

for non-enzymatic glucose detection by Ni-based nanostructures are presented and discussed.

3.2. Methodology

3.2.1. Experimental Setup

Electrode materials for non-enzymatic glucose detection are typically tested by using a potentiostat to control a three-electrode electrochemical cell, consisting of a working electrode, i.e. the sensing electrode material, a reference electrode (saturated calomel electrode, Ag/AgCl, etc.) to regulate the bias of the working electrode, and an auxiliary (or counter) electrode (typically an inert material such as Pt) to ensure the current flow in the cell. The three electrodes are connected to the potentiostat and immersed in a supporting electrolyte solution, usually phosphate buffer saline (PBS) at the physiological pH of 7.4, or 0.1 M sodium hydroxide (NaOH) at pH 13 [42-47].

3.2.2. Experimental Procedure

Generally, cyclic voltammetry (CV) experiments are first carried out to investigate and stabilize the electrochemical behaviour of the working electrode. In a typical CV experiment, the potential of the working electrode is ramped linearly versus time between two switching potentials defined by the user. Once the first switching potential is reached (forward scan), the potential is ramped in the opposite direction until the second one is reached (backward scan), defining a cycle. The current density, i.e. current per unit area of the working electrode, is measured during the potential cycling, and plotted as a function of the potential (cyclic voltammogram) [48]. In presence of redox species on the electrode surface and/or in the supporting electrolyte solution, peaks at specific potentials in the forward and backward scan can be observed, attributed to oxidation and reduction processes, respectively (Fig. 3.3). Several CV cycles are normally recorded until a stable cyclic voltammogram is obtained.

Then, a chronoamperometry (CA) experiment is performed under solution stirring by applying a constant potential to the working electrode equal to the oxidation potential obtained by CV. The current density which flows in the cell is measured and plotted as function of the time.

At the beginning of CA, the characteristic current decay described by Cottrell equation is observed [49]. Once as stable current density is reached, known amounts of glucose are added to the supporting electrolyte solution. Each addition induces an increase of the current density as a result of the electrons generated by glucose oxidation at the working electrode surface. After several additions (typically at increasing glucose concentrations), the characteristic step-like behaviour reported in Fig. 3.4 is observed.

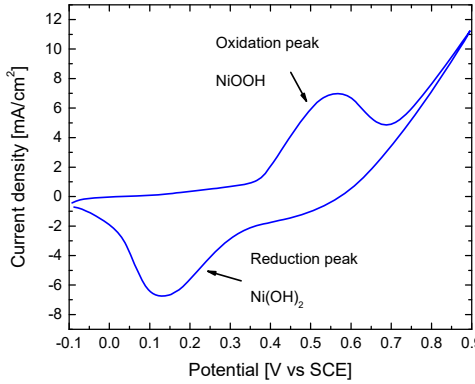

Fig. 3.3. A typical CV curve showing the oxidation and reduction peaks of a Ni-based electrode in 0.1 M NaOH.

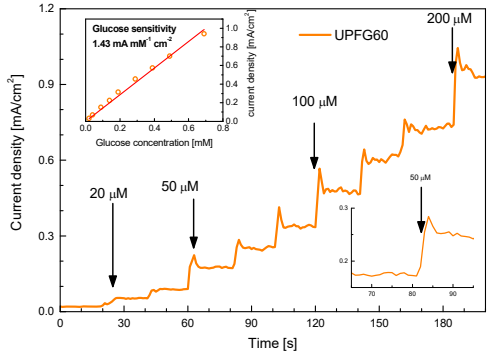

Fig. 3.4. A typical CA curve showing the current density as function of time for successive additions of glucose at 20 s intervals in 0.1 M NaOH. The obtained calibration curve is shown in the top inset, while bottom inset shows one 50 μM glucose addition. Reprinted from [50] with permission from Elsevier.

All the 5S of the sensor can be obtained from CA measurements. The sensitivity is the slope of the linear fit of the calibration curve, i.e. the current density increase as a function of the glucose concentration (top inset in Fig. 3.4), over a linear glucose concentration range. In some cases, two linear ranges, and thus two sensitivities, are reported [51-53]. The selectivity is estimated by an interference test, consisting of a CA measurement carried out by adding glucose and other interfering species (commonly investigated interferents are acetaminophen, uric acid, ascorbic acid, etc.) at concentrations close to those expected in physiological samples. The stability is evaluated by measuring the current increase at a fixed glucose concentration as a function of time (weeks or months). The response time is simply measured as the time interval to reach a stable current density after a glucose addition (bottom inset in Fig. 3.4). The limit of detection (LoD) is defined as the glucose concentration that can be detected at three times the noise level. The resistance to poisoning from chloride ions (Cl^-) can be measured from the response to a fixed glucose concentration in the presence and absence of 0.2 M potassium chloride (KCl) in the supporting electrolyte solution.

This procedure has been used to evaluate the non-enzymatic glucose detection performance of Ni-based nanostructures that are presented and compared in the next part of the chapter.

3.3. Advances in Non-enzymatic Glucose Detection by Ni-based Nanostructures

3.3.1. Porous Structures

The physical and chemical properties of nanostructures are strictly correlated to their morphology. As a result, a large variety of Ni-based nanostructures with peculiar morphologies has been developed and tested for non-enzymatic glucose detection, including nanoparticles [54, 55], nanowires [56, 57], nanoflakes [58, 59], nanowalls [50, 60, 61], etc. Among them, nanowalls, a thin film consisting of a tight network of nanosheets (20 nm thick, 200-1000 nm tall) that are vertically aligned on a substrate, are particularly attractive due to their open porous structure, large surface area and flexibility [61, 62].

Li and co-workers reported the controllable synthesis of NiO nanowalls by hydrothermal method followed by annealing at 400 °C in Ar for 2 h

[60]. NiO nanowalls showed a sensitivity of 2.3 mA mM^{-1} cm^{-2} up to 1 mM glucose, a low LoD of 200 nM, and high selectivity to glucose in presence of galactose, D-fructose, xylose, maltose, and ascorbic acid, in 0.1 M NaOH.

Ni-based nanowalls can be also fabricated by a simpler and cheaper chemical bath deposition (CBD) method [50, 61]. In fact, the only requirements for CBD are a vessel to contain a solution, typically an aqueous solution of $Ni(OH)_2$ precursors, and substrates on which the deposition is carried out. Solution stirring and a thermostat that maintains a specific and constant temperature in the solution are often used. Compared to other methods, CBD offers different advantages. For example, in comparison to the hydrothermal method where pressure vessels and relatively high growth temperatures (55-400 °C) and long growth times (up to 15 h) are used, CBD is performed at very low temperatures (from room temperature up to 80 °C) and for short time (<20 min). Moreover, with respect to the electrodeposition method where the deposition is driven by an electrical power supplied to a conductive substrate, substrates for CBD can be either conductive or not. Furthermore, CBD is considered a suitable method for large-scale production due to the possibility of CBD solution spotting on various substrates. However, particular care is needed with the preparing conditions (reagents and their concentration, temperature, time, stirring, etc.) to ensure CBD effectiveness and reproducibility.

Since the pioneering work of Pramanik and Bhattacharya in 1990 [63], CBD of Ni-based thin films has been extensively investigated with the aim to understand and control the growth process and the properties of the deposited materials for specific applications, among which non-enzymatic glucose detection [50, 61, 64-68].

Recently, the effect of the growth temperature in CBD has been carefully investigated, finding that it significantly influences the thickness, crystalline phase and electrochemical behaviour of the deposited Ni-based nanowalls [61]. In particular, Ni-based nanowalls morphology changes considerably from a disordered structure of random oriented $Ni(OH)_2$·NiOOH nanosheets at room temperature (Fig. 3.5 (a)) to a more ordered one at 50 °C where $Ni(OH)_2$ nanosheets are almost perpendicular to the substrate (Fig. 3.5 (b)). Cyclic voltammetry (CV) proved a higher electro-activity for the ordered nanowalls grown at 50 °C, as indicated by the higher current in the Ni^{2+}/Ni^{3+} oxidation and reduction peaks in the cyclic voltammogram (Fig. 3.5 (c)), showing also a lower charge

transfer resistance by electrochemical impedance spectroscopy (EIS) experiments. The improved catalytic properties of the ordered nanowalls grown at 50 °C were further confirmed by testing their non-enzymatic glucose detection ability in 0.1 M NaOH, where they showed a larger sensitivity (~1 mA mM^{-1} cm^{-2}, 0-1 mM glucose) than the random ones grown at room temperature (~0.5 mA mM^{-1} cm^{-2}, 0-1 mM glucose).

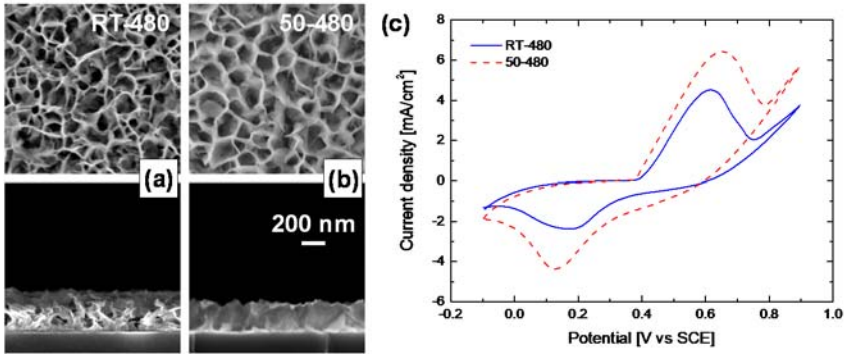

Fig. 3.5. SEM images in plan-view (top panels) and in cross-view (bottom panels) of the Ni-based nanowalls grown by CBD (a) at room temperature for 480 s (RT-480), and (b) at 50 °C for 480 s (50-480). (c) CV curves of RT-480 (blue solid line) and 50-480 (red dashed line) recorded at 50 mV s^{-1} scan rate in the potential range -0.2-0.8 V vs SCE in 0.1 M NaOH. Adapted from [61] with permission from IOP Publishing.

The effect of post-growth annealing processes in reducing atmosphere has been also studied, finding that annealing at 350 °C in forming gas (H_2:Ar 5:95) leads to a chemical transformation from $Ni(OH)_2$ to Ni, and to a morphological transformation since the smooth nanosheets surface is replaced by foam-like clusters of Ni nanoparticles with size of 20 nm [50]. This novel material, called Ni nanofoam, preserves the peculiar porous structure of the nanowalls, and exhibits a high surface area of 25 m^2 g^{-1} measured by BET, and a high conductivity due to its metallic nature. Ni nanofoam was tested for non-enzymatic glucose detection in 0.1 NaOH. Upon immersion and few potential cycles by CV, a thin layer of $Ni(OH)_2$/NiOOH is formed, leading to a core-shell structure [40]. A high sensitivity of 2.37 mA mM^{-1} cm^{-2} was found over the linear range of 0.005-0.7 mM glucose. In addition, the Ni nanofoam showed a fast response (<1 s), high selectivity to glucose with respect to uric acid, ascorbic acid and acetaminophen (Fig. 3.6 (a)), resistance to chloride

poisoning in 0.2 M KCl (Fig. 3.6 (b)), and an impressive long-term stability with only a 4 % loss of the response after 64 days (Fig. 3.6 (c)).

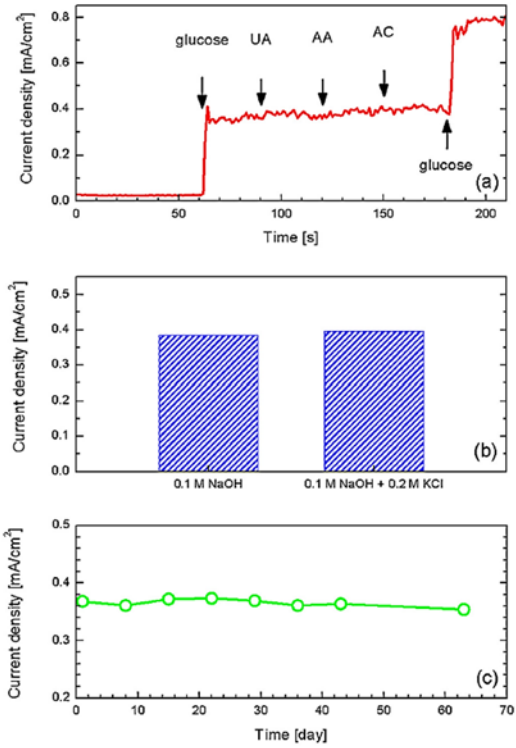

Fig. 3.6. (a) Ni nanofoam interference test showing the current gains upon addition of 200 µM glucose, 20 µM uric acid (UA) and 10 µM ascorbic acid (AA) and acetaminophen (AC); (b) Chloride poisoning test indicating the response of the Ni nanofoam to the addition of 200 µM glucose in the presence and absence of 0.2 M KCl; (c) Long-term stability test of the Ni nanofoam with 200 µM glucose over a 64-day period. Reprinted from [50] with permission from Elsevier.

By combining the improved CBD at 50 °C, leading to ordered $Ni(OH)_2$ nanowalls, and the reducing annealing to Ni nanofoam, and by using a commercial Ni foam substrate as large surface area current collector, an extremely high sensitivity of 31 mA mM^{-1} cm^{-2} was obtained over a liner range of 0.02-0.4 mM glucose. This range matches perfectly those of interest for the detection of glucose in human saliva and tears [35].

Due to its unique non-enzymatic glucose sensing performance, a sensor based on the Ni nanofoam has been also developed. Specifically, Ni-based microspheres, having the same porous structure and morphology of nanowalls, were collected from CBD solution by centrifugation and filtering. The obtained powder was annealed in reducing atmosphere to prepare the Ni nanofoam, and then dropped onto the working electrode of a miniaturized three-electrode system, as shown in Fig. 3.7 [69]. This has been manufactured by using the very-large-scale integration (VLSI) technology on a 6″ Si substrate, and it consists of four integrated electrochemical cells (20 µl volume). Each cell is formed by a planar Pt working electrode (WE) with size 1000×2000 μm^2, and planar Au counter (CE) and reference electrodes (RE) with size 800×500 and 800×1250 μm^2, respectively. The system demonstrated a sensitivity of 80 $\mu A\ mM^{-1}\ cm^{-2}$ up to 5 mM of glucose. Tests with human blood samples were conducted, showing a significant current variation of 100 µA. Based on these results, the proposed system has potential as point-of-care device for non-enzymatic glucose detection.

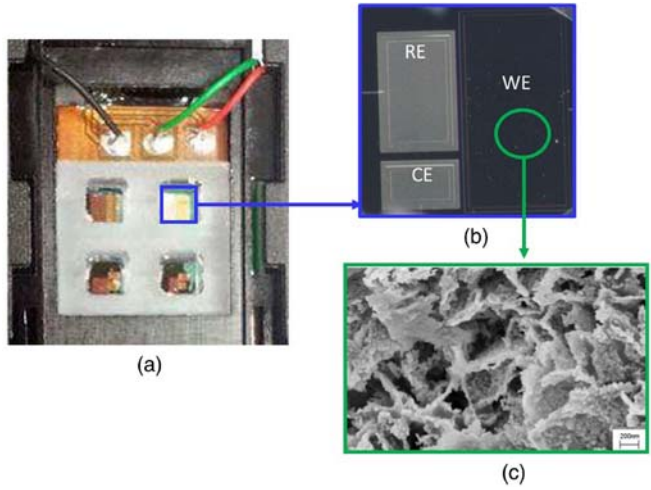

Fig. 3.7. (a) Photo of the miniaturized electrochemical device; (b) Optical micrograph of the integrated three-planar electrode cell; (c) SEM image of the Ni nanofoam. Reprinted from [69] with permission from Springer.

Later on, other microelectrodes geometries have been explored, and tested using a thin layer (7.5 nm) of Ni as sensing element, showing promising results for the detection of glucose in human saliva samples

[70]. Further advances with these systems are expected by replacing the flat Ni layer with high-performing Ni-based nanostructures compatible with the Si technology, such as the Ni nanofoam.

3.3.2. Hierarchical Structures

Hierarchical structures have drawn a great attention due to their characteristic multifunctionality and new properties which result from the combination of different nanomaterials, leading to a higher reactivity to the surrounding environment [71]. Because of their high sensitivity to glucose, Ni-based nanostructures have been often combined with other nanomaterials to design hierarchical structures with improved performance, such as 3D Ni-Fe nanosheet arrays [72], hierarchical Cu-Co-Ni nanostructures [73], ZnO nanorods/$Ni(OH)_2$ nanoflakes [74, 75]. Among them, ZnO nanorods are an advantageous high surface area support for further deposition of Ni-based nanostructures thanks to their good electrical conductivity, low toxicity and low-cost. In fact, similarly to Ni-based nanowalls, ZnO nanorods can be synthesized on various substrate by CBD method [76].

Strano and Mirabella reported a fully-chemical, simple and cost-effective synthetic method for the fabrication of hierarchical ZnO/$Ni(OH)_2$ nanostructures for non-enzymatic glucose detection [74]. ZnO nanorods were grown onto ITO substrates by CBD, and employed as working electrode for further decoration with $Ni(OH)_2$ nanoflakes by pulsed electrodeposition method at constant current density of 1 mA cm^{-2} (inset in Fig. 3.8 (g)), which was carried out in a three-electrode electrochemical cell containing an aqueous solution of a Ni^{2+} salt as supporting electrolyte. The effects of the HMTA concentration (25-50 mM), a reagent used in ZnO nanorods CBD, and the number of electrodeposition cycles (20, 40, 60) on the morphology and electrochemical properties of the resulting nanostructures were examined by SEM and CV (Fig. 3.8). The sample obtained under 25 mM HMTA and 20 cycles (labelled 25-20) is characterized by a ruffled morphology consisting of overlapping thin $Ni(OH)_2$ sheets (Fig. 3.8 (c)), while the sample 50-20 shows a smoother feature (Fig. 3.8 (d)). By increasing the number of electrodepositions cycles up to 60, a higher surface roughness is attained due to the aggregation of the $Ni(OH)_2$ sheets, forming a sort of porous shell as in the case of the sample 50-60 (Fig. 3.8 (e)). The higher amount of $Ni(OH)_2$ obtained in the sample 50-60 induced higher Ni^{2+}/Ni^{3+} oxidation and reduction peaks in the

cyclic voltammogram (Fig. 3.8 (f)). On these bases, a higher glucose sensitivity in 0.1 M NaOH was expected for this sample. However, the highest sensitivity was observed for the sample 50-20 (1.85 mA mM^{-1} cm^{-2} over 0.04-2.10 mM glucose) rather than the sample 50-60 (1.16 mA mM^{-1} cm^{-2} over 0.04-2.60 mM glucose). Typically, better the electrochemical feature is, the more efficient the glucose detection performance results. Nevertheless, in this case the higher number of deposition cycles led to the formation of a higher amount with $Ni(OH)_2$, increasing porosity to such an extent that it may slow down the electrode kinetics in terms of easy diffusion and migration of glucose and its oxidation products.

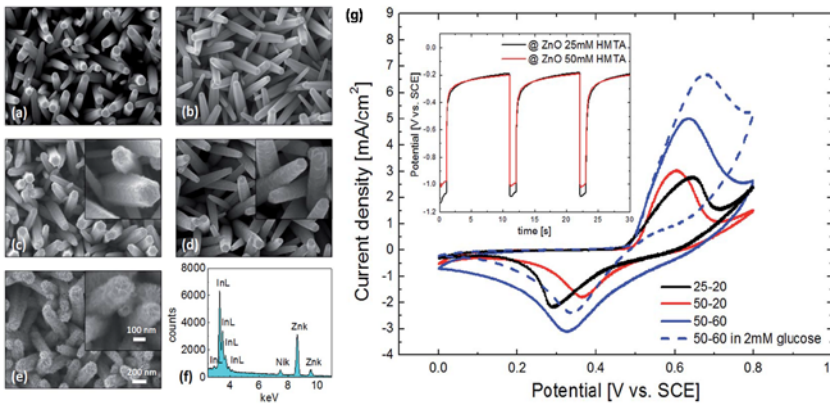

Fig. 3.8. SEM images of ZnO nanorods grown by CBD with (a) 25 mM and (b) 50 mM HMTA in solution; (c) SEM images of ZnO nanorods/$Ni(OH)_2$ nanoflakes grown by CBD with (c) 25 mM HMTA in solution and 20 pulsed electrodeposition cycles (sample 25-20); (d) and (e) SEM images of samples 50-20 and 50-60, respectively. (f) Portion of the EDX spectrum of the sample 50-60. (g) CV curves of 25-20 (black solid line), 50-20 (red solid line), 50-60 (blue solid line) and 50-60 in presence of 2 mM glucose (blue dashed line) recorded at 50 mV s^{-1} scan rate in the potential range 0-0.8 V vs SCE in 0.1 M NaOH. The inset reports the potential as function of time during a few pulsed electrodeposition cycles on ZnO nanorods grown by CBD with 25 mM (black solid line) and 50 mM HMTA in solution (red solid line). Reprinted from [74] with permission from The Royal Society of Chemistry.

Driven by the increasing interest on urban mining, Strano demonstrated also the versatility of the proposed ZnO/$Ni(OH)_2$ nanostructure by growing ZnO nanorods on waste Cu wires, obtained from SATA cables

[75]. ZnO nanorods were further decorated with $Ni(OH)_2$ nanoflakes by pulsed electrodeposition at constant potential. The effects of the applied potential (-0.8, -1.1 and -1.5 V) on the morphology, electrochemical properties and non-enzymatic glucose detection in 0.1 M NaoH were investigated and presented. Again, the larger potential of -1.5 V resulted in a better coverage of ZnO nanorods by $Ni(OH)_2$, higher peaks in the cyclic voltammogram, and a lower sensitivity (2.6 mA mM^{-1} cm^{-2} over 0.18-2.04 mM glucose) than sample -1.1 V (2.6 mA mM^{-1} cm^{-2} over 0.04-1.8 mM glucose), due to the slower electrode kinetics as the amount of the loaded $Ni(OH)_2$ is too high.

3.3.3. Other Approaches

Wang and co-workers recently reported a simple strategy to enhance the electrochemical activity of Ni-based nanostructures by regulating the number of Ni atoms with high valence states in the electrode material [77]. Precisely, ammonium nickel phosphate/nickel foam electrodes were prepared by a chemical method, and the Ni^{3+}/Ni^{2+} ratio was increased after H_2O_2 solution treatment. The Ni^{3+}-rich surface electrode showed a larger catalytic rate constant (K_{cat}) than the original electrode (4.028×10^6 vs 4.928×10^5 cm^3 mol^{-1} s^{-1}), resulting in a high sensitivity (11.361 mA mM^{-1} cm^{-2}) over the linear range 0.001-1 mM glucose in 0.3 M NaOH, which is much higher than that of the original electrode (6.135 mA mM^{-1} cm^{-2}). This approach is particularly promising to improve the sensitivity of other Ni-based nanostructures.

Graphene has been often used as substrate for the deposition of various Ni-based nanostructures for non-enzymatic glucose detection due to its larger active surface area and improved electron transport [78-80]. Subramanian et al. reported a sensitive and stable electrode for non-enzymatic glucose detection based on a reduced graphene oxide (rGO) matrix modified with $Ni(OH)_2$ nanostructures grown by electrophoretic deposition. The $rGO/Ni(OH)_2$ electrodes exhibited the excellent sensitivity of 11.4 mA mM^{-1} cm^{-2} over the linear range 0.015-30 mM glucose in 0.1 M NaOH. An interference test was successfully conducted in presence of ascorbic acid, uric acid and dopamine, and a loss of the response of only 2% was found after 1 month, suggesting a good selectivity and stability of the proposed electrode. The LoD was 15 μM. Still, the cost of graphene-based electrodes remains high and limits their applicability.

Metal organic frameworks (MOFs) are microporous materials formed via self-assembly of metal ions and organic ligands in appropriate solvents [81]. MOFs have crystalline structures and are characterized by large surface areas, uniform and adjustable cavities on the nanometer scale, and adsorption affinities. Thanks to their unique properties, MOFs emerged also in non-enzymatic glucose detection. Xiao and co-workers reported ultrathin Ni-based MOF nanobelts synthesized by a one-pot solution process and tested them for non-enzymatic glucose detection in 0.1 M NaOH [82]. A sensitivity of 1.542 mA mM^{-1} cm^{-2} was observed over the linear range 1-500 μM glucose, and a low LoD of 25 mM was estimated, finding also high selectivity against uric acid, dopamine and ascorbic acid, and resistance to chloride poisoning. The electrode was successfully applied for glucose detection in human blood samples with 6.79 mM glucose, showing almost no decrease in the response to glucose due to interfering species.

The performances of the above-mentioned Ni-based nanostructures for non-enzymatic glucose detection are reported and compared in Table 3.1.

Table 3.1. Comparison of the performances of Ni-based nanostructures for non-enzymatic glucose detection.

Ni-based nanostructure	**Sensitivity [mA mM^{-1} cm^{-2}]**	**Linear range [mM]**	**LoD [μM]**	**Stability**	**Ref.**
Ni nanoparticle-loaded carbon nanofiber	0.42	0.002-2.5	1	N/A	[54]
NiO and Pt nanoparticles on electrochemically rGO	0.69	0.05-5.66	0.2	10 days (10% loss)	[55]
$Ni(OH)_2$ nanowires/CNT	0.06	0.02-0.5	5	N/A	[56]
$Ni(OH)_2$ nanowires on Ni foam	1.6	0.1-6	1	65 days	[57]
NiO nanoflakes arrays	8.5	0.01-0.8	1.2	N/A	[58]
Over-oxidized polypyrrole nanowires modified with $Ni(OH)_2$ nanoflakes	1.05	0.001-4.863	0.3	N/A	[59]
NiO nanowalls	2.3	0.0002-1	0.2	N/A	[60]
Ni nanofoam	2.37	0.01-0.7	5	64 days (4% loss)	[50]
Improved Ni nanofoam on Ni foam	31	0.02-0.4	5	N/A	[61]

Ni-based nanostructure	Sensitivity [mA mM^{-1} cm^{-2}]	Linear range [mM]	LoD [µM]	Stability	Ref.
Miniaturized three-planar electrode device integrating Ni nanofoam	0.08	0-5	N/A	N/A	[69]
Miniaturized sensing device based on a thin Ni oxides	0.04	0.3-6	10	N/A	[70]
3-D/Ni-Fe nanostructures	0.008	0.00005-0.2	0.031	N/A	[72]
Hierarchical Cu-Co-Ni nanostructures	0.10	0.01-4.30	3.05	30 days (4.5% loss)	[73]
Hierarchical ZnO nanorods/$Ni(OH)_2$ nanoflakes	1.85	0.04-2.10	N/A	40 days (5% loss)	[74]
$Ni(OH)_2$/ZnO nanostructures	3	0.04-1.8	N/A	60 days	[75]
Ammonium nickel phosphate on nickel foam with a Ni^{3+}-rich surface	11.36	0.001-1	0.009	N/A	[77]
Reduced graphene oxide-$Ni(OH)_2$ composite	11.4	0.015-30	15	30 days (2% loss)	[78]
NiO mesoporous nanowalls grown on RGO coated Ni foam	3.23	0.01-0.2	0.1	N/A	[79]
NiO nanoparticles decorating graphene nanosheets	0.67	0.005-4.2	5	18 days (12% loss)	[80]
Ultrathin Ni-MOF nanobelts	0.0015	0.001-0.5	0.25	N/A	[82]

3.4. Conclusions

In recent years, novel Ni-based nanostructures have been increasingly developed and tested for non-enzymatic glucose detection. In fact, compared to the other materials, Ni, NiO and $Ni(OH)_2$ ensure low-cost, higher sensitivity, long-term stability and resistance to chloride poisoning. Moreover, Ni-based nanostructures with large surface area and porous structure have shown improved electrochemical properties, which allow to boost the sensitivity. Solution-based synthesis methods, among which chemical bath deposition (CBD), hydrothermal synthesis

and electrodeposition, have attracted great attentions since they do not require complex and expensive apparatus (vacuum, high temperature, etc.) and can be integrated with Si technology. Among the different Ni-based nanostructures developed so far, Ni nanofoam, a porous structure formed by Ni nanoparticles (20 nm) obtained by CBD and reducing annealing, showed an impressive sensitivity of 31 mA mM^{-1} cm^{-2} in the linear range 0.02-0.4 mM glucose, high selectivity against common interferents, 64 days long stability, and a low LoD of 5 μM. Ni nanofoam has been already introduced in miniaturized systems which can be reproduced on large scale, demonstrating a great potential as Point-of-Care devices for the detection of glucose in human blood and saliva. Several hierarchical structures have been also investigated, and among them a combination of ZnO nanorods and $Ni(OH)_2$ nanoflakes obtained by CBD and electrodeposition showed remarkable sensing performances, and also the possibility to be fabricate on cheap substrates as waste Cu wires. Other interesting strategies to enhance the sensitivity are to regulate the density of Ni^{3+} in the electrode material, and the use of graphene as substrate for Ni-based nanostructures deposition due to its improved electron transport. Further improvements can be obtained by combining two or more of these strategies. The major obstacle that prevents the realization of real prototypes able to work with real samples is that Ni-based nanostructures are not able to efficiently catalyse the glucose oxidation in physiological pH. Ni-based materials biocompatibility is also an issue, especially for continuous glucose monitoring application. Nevertheless, with the new possibilities offered by bimetallic nanostructures and hybrid organic-inorganic materials, and new concepts for miniaturized sensors design, it is reasonable to expect significant advances in the near future.

References

[1]. K. M. Shaw, M. H. Cummings, Diabetes: Chronic Complications, *John Wiley & Sons*, 2002.
[2]. International Diabetes Federation, https://idf.org/
[3]. American Diabetes Association, https://www.diabetes.org/
[4]. J. Wang, Electrochemical glucose biosensors, *Chemical Reviews*, Vol. 108, Issue 2, 2008, pp. 814-825.
[5]. S. P. Nichols, A. Koh, W. L. Storm, J. H. Shin, M. H. Schoenfisch, Biocompatible materials for continuous glucose monitoring devices, *Chemical Reviews*, Vol. 113, Issue 4, 2013, pp. 2528-2549.
[6]. Merck, https://www.sigmaaldrich.com/catalog/product/sigma/g7141?lang=en&region=US

[7]. X. Chen, G. Wu, Z. Cai, M. Oyama, X. Chen, Advances in enzyme-free electrochemical sensors for hydrogen peroxide, glucose, and uric acid, *Microchimica Acta*, Vol. 181, Issue 7-8, 2013, pp. 689-705.
[8]. X. Strakosas, J. Selberg, P. Pansodtee, N. Yonas, P. Manapongpun, M. Teodorescu, M. Rolandi, A non-enzymatic glucose sensor enabled by bioelectronic pH control, *Scientific Reports*, Vol. 9, Issue 1, 2019, pp. 1-7.
[9]. M. Senior, Novartis signs up for Google smart lens, *Nat. Biotechnol*., Vol. 32, Issue 9, 2014, 856.
[10]. S. Cherevko, C. H. Chung, Gold nanowire array electrode for non-enzymatic voltammetric and amperometric glucose detection, *Sensors and Actuators B: Chemical*, Vol. 142, Issue 1, 2009, pp. 216-223.
[11]. L. T. Hoa, K. G. Sun, S. H. Hur, Highly sensitive non-enzymatic glucose sensor based on Pt nanoparticle decorated graphene oxide hydrogel, *Sensors and Actuators B: Chemical*, Vol. 210, 2015, pp. 618-623.
[12]. Q. Wang, X. Cui, J. Chen, X. Zheng, C. Liu, T. Xue, H. Wang, Z. Jin, L. Qiao, W. Zheng, Well-dispersed palladium nanoparticles on graphene oxide as a non-enzymatic glucose sensor, *RSC Advances*, Vol. 2, Issue 15, 2012, pp. 6245-6249.
[13]. X. Niu, X. Li, J. Pan, Y. He, F. Qiu, Y. Yan, Recent advances in non-enzymatic electrochemical glucose sensors based on non-precious transition metal materials: opportunities and challenges, *RSC Advances*, Vol. 6, Issue 88, 2016, pp. 84893-84905.
[14]. M. Rahman, A. J. Ahammad, J. H. Jin, S. J. Ahn, J. J. Lee, A comprehensive review of glucose biosensors based on nanostructured metal-oxides, *Sensors*, Vol 10, Issue 5, 2010, pp. 4855-4886.
[15]. N. Izyumskaya, A.Tahira, Z. H. Ibupoto, N. Lewinski, V. Avrutin, Ü. Özgür, E. Topsakal, M. Willander, H. Morkoç, Electrochemical biosensors based on ZnO nanostructures, *ECS Journal of Solid State Science and Technology*, Vol. 6, Issue 8, 2017, pp. Q84-Q100.
[16]. H. Zhu, L. Li, W. Zhou, Z. Shao, X. Chen, Advances in non-enzymatic glucose sensors based on metal oxides, *Journal of Materials Chemistry B*, Vol. 4, Issue 46, 2016, pp. 7333-7349.
[17]. S. A. Zaidi, J. H. Shin, Recent developments in nanostructure based electrochemical glucose sensors, *Talanta*, Vol. 149, 2015, pp. 30-42.
[18]. H. Li, C. Y. Guo, C. L. Xu A highly sensitive non-enzymatic glucose sensor based on bimetallic Cu-Ag superstructures, *Biosensors and Bioelectronics*, Vol. 63, 2015, pp. 339-346.
[19]. M. Yuan, A. Liu, M. Zhao, W. Dong, T. Zhao, J. Wang, W. Tang, Bimetallic PdCu nanoparticle decorated three-dimensional graphene hydrogel for non-enzymatic amperometric glucose sensor, *Sensors and Actuators B: Chemical*, Vol. 190, 2014, pp. 707-714.
[20]. L. Özcan, Y. Şahin, H. Türk, Non-enzymatic glucose biosensor based on overoxidized polypyrrole nanofiber electrode modified with cobalt (II) phthalocyanine tetrasulfonate, *Biosensors and Bioelectronics*, Vol. 24, Issue 4, 2008, pp. 512-517.

[21]. Y. Kong, Y. Sha, Y. Tao, Y. Qin, H. Xue, M. Lu, Non-enzymatic glucose sensor based on nickel hexacyanoferrate/polyaniline hybrids on graphene prepared by a one-step process, *Journal of the Electrochemical Society*, Vol. 161, Issue 12, 2014, pp. B269-B274.
[22]. G. Gnana Kumar, G. Amala, S. M. Gowtham, Recent advancements, key challenges and solutions in non-enzymatic electrochemical glucose sensors based on graphene platforms, *RSC Advances*, Vol. 7, Issue 59, 2017, pp. 36949-36976.
[23]. C. Zhang, Z. Zhang, Q. Yang, W. Chen, Graphene-based electrochemical glucose sensors: Fabrication and sensing properties, *Electroanalysis*, Vol. 30, Issue 11, 2018, pp. 2504-2524.
[24]. Z. Zhu, L. Garcia-Gancedo, A. J. Flewitt, H. Xie, F. Moussy, W. I. Milne, A critical review of glucose biosensors based on carbon nanomaterials: Carbon nanotubes and graphene, *Sensors*, Vol. 12, Issue 5, pp. 5996-6022.
[25]. J. Lee, S. M. Park, Direct electrochemical assay of glucose using boron-doped diamond electrodes, *Analytica Chimica Acta*, Vol. 545, Issue 1, 2012, pp. 27-32.
[26]. S. Prakash, T. Chakrabarty, A. K. Singh, V. K. Shahi, Polymer thin films embedded with metal nanoparticles for electrochemical biosensors applications, *Biosensors and Bioelectronics*, Vol. 41, 2013, pp. 43-53.
[27]. L. Zhang, Y. Ding, R. Li, C. Ye, G. Zhao, Y. Wang, Ni-Based metal-organic framework derived Ni@C nanosheets on a Ni foam substrate as a supersensitive non-enzymatic glucose sensor, *Journal of Materials Chemistry B*, Vol. 5, Issue 28, 2017, pp. 5549-5555.
[28]. K. Tian, M. Prestgard, A. Tiwari, A review of recent advances in nonenzymatic glucose sensors, *Materials Science and Engineering: C*, Vol. 41, 2014, pp. 100-118.
[29]. K. E. Toghill, R. G. Compton, Electrochemical non-enzymatic glucose sensors: a perspective and an evaluation, *International Journal of Electrochemical Science*, Vol. 5, Issue 9, 2010, pp. 1246-1301.
[30]. D. Pletcher, Electrocatalysis: Present and future, *Journal of Applied Electrochemistry*, Vol. 14, Issue 4, 1984, pp. 403-415.
[31]. L. D. Burke, Premonolayer oxidation and its role in electrocatalysis, *Electrochimica Acta*, Vol. 39, Issue 11-12, 1994, pp. 1841-1848.
[32]. P. Si, Y. Huang, T. Wang, J. Ma, Nanomaterials for electrochemical non-enzymatic glucose biosensors, *RSC Advances*, Vol. 3, Issue 11, 2013, pp. 3487-3502.
[33]. J. Wang, D. F. Thomas, A. Chen, Nonenzymatic electrochemical glucose sensor based on nanoporous PtPb networks, *Analytical Chemistry*, Vol. 80, Issue 4, 2008, pp. 997-1004.
[34]. S. Park, H. Boo, T. D. Chung, Electrochemical non-enzymatic glucose sensors, *Analytica Chimica Acta*, Vol. 556, Issue 1, 2006, pp. 46-57.
[35]. D. Bruen, C. Delaney, L. Florea, D. Diamond, Glucose sensing for diabetes monitoring: recent developments, *Sensors*, Vol. 17, Issue 8, 2017, 1866.

[36]. A. A. Saei, J. E. N. Dolatabadi, P. Najafi-Marandi, A. Abhari, M. de la Guardia, M. Electrochemical biosensors for glucose based on metal nanoparticles, *Trends in Analytical Chemistry*, Vol. 42, 2013, pp. 216-227.
[37]. G. Wang, X. He, L. Wang, A. Gu, Y. Huang, B. Fang, B. Geng, X. Zhang, Non-enzymatic electrochemical sensing of glucose, *Microchimica Acta*, Vol. 180, Issues 3-4, 2013, pp. 161-186.
[38]. J. Hovancová, I. Šišoláková, R. Oriňaková, A. Oriňak, Nanomaterial-based electrochemical sensors for detection of glucose and insulin, *Journal of Solid State Electrochemistry*, Vol. 21, Issue 8, 2017, pp. 2147-2166.
[39]. D. W. Hwang, S. Lee, M. Seo, T. D. Chung, Recent advances in electrochemical non-enzymatic glucose sensors – A review, *Analytica Chimica Acta*, Vol. 1033, 2018, pp. 1-34.
[40]. M. Urso, G. Torrisi, S. Boninelli, C. Bongiorno, F. Priolo, S. Mirabella, $Ni(OH)_2$@Ni core-shell nanochains as low-cost high-rate performance electrode for energy storage applications, *Scientific Reports*, Vol. 9, Issue 1, 2019, pp. 1-11.
[41]. C. Guo, Y. Wang, Y. Zhao, C. Xu, Non-enzymatic glucose sensor based on three dimensional nickel oxide for enhanced sensitivity, *Analytical Methods*, Vol. 5, Issue 7, 2013, pp. 1644-1647.
[42]. Y. Xia, W. Huang, J. Zheng, Z. Niu, Z. Li, Nonenzymatic amperometric response of glucose on a nanoporous gold film electrode fabricated by a rapid and simple electrochemical method, *Biosensors and Bioelectronics*, Vol. 26, Issue 8, 2011, pp. 3555-3561.
[43]. G. Chang, H. Shu, Q. Huang, M. Oyama, K. Ji, X. Liu, Y. He, Synthesis of highly dispersed Pt nanoclusters anchored graphene composites and their application for non-enzymatic glucose sensing, *Electrochimica Acta*, Vol. 157, 2015, pp. 149-157.
[44]. H. Shu, G. Chang, J. Su, L. Cao, Q. Huang, Y. Zhang, T. Xia, Y. He, Single-step electrochemical deposition of high performance Au-graphene nanocomposites for nonenzymatic glucose sensing, *Sensors and Actuators B: Chemical*, Vol. 220, 2015, pp. 331-339.
[45]. W. Wang, L. Zhang, S. Tong, X. Li, W. Song, Three-dimensional network films of electrospun copper oxide nanofibers for glucose determination, *Biosensors and Bioelectronics*, Vol. 25, Issue 4, 2009, pp. 708-714.
[46]. S. A. Kumar, H. W. Cheng, S. M. Chen, S. F. Wang, Preparation and characterization of copper nanoparticles/zinc oxide composite modified electrode and its application to glucose sensing, *Materials Science and Engineering: C*, Vol. 30, Issue 1, 2010, pp. 86-91.
[47]. S. Liu, B. Yu, T. Zhang, A novel non-enzymatic glucose sensor based on NiO hollow spheres, *Electrochimica Acta*, Vol. 102, 2013, pp. 104-107.
[48]. N. Elgrishi, K. J. Rountree, B. D. McCarthy, E. S. Rountree, T. T. Eisenhart, J. L. Dempsey, A practical beginner's guide to cyclic voltammetry, *Journal of Chemical Education*, Vol. 95, Issue 2, 2018, pp. 197-206.
[49]. A. J. Bard, L. R. Faulkner, J. Leddy, C. G. Zoski, Electrochemical Methods: Fundamentals and Applications, *Wiley*, 1990.

[50]. K. O. Iwu, A. Lombardo, R. Sanz, S. Scirè, S. Mirabella, Facile synthesis of Ni nanofoam for flexible and low-cost non-enzymatic glucose sensing, *Sensors and Actuators B: Chemical*, Vol. 224, 2016, pp. 764-771.
[51]. A. A. Ensafi, M. M. Abarghoui, B. Rezaei, A new non-enzymatic glucose sensor based on copper/porous silicon nanocomposite, *Electrochimica Acta*, Vol 123, 2014, pp. 219-226.
[52]. L. Han, D. P. Yang, A. Liu, Leaf-templated synthesis of 3D hierarchical porous cobalt oxide nanostructure as direct electrochemical biosensing interface with enhanced electrocatalysis, *Biosensors and Bioelectronics*, Vol. 63, 2015, pp. 145-152.
[53]. N. Shen, H. Xu, W. Zhao, Y. Zhao, X. Zhang, Highly responsive and ultrasensitive non-enzymatic electrochemical glucose sensor based on Au foam, *Sensors*, Vol. 19, Issue 5, 2019, 1203.
[54]. Y. Liu, H. Teng, H. Hou, T. You, Nonenzymatic glucose sensor based on renewable electrospun Ni nanoparticle-loaded carbon nanofiber paste electrode, *Biosensors and Bioelectronics*, Vol. 24, Issue 11, 2009, pp. 3329-3334.
[55]. M. Li, X. Bo, Z. Mu, Y. Zhang, L. Guo, Electrodeposition of nickel oxide and platinum nanoparticles on electrochemically reduced graphene oxide film as a nonenzymatic glucose sensor, *Sensors and Actuators B: Chemical*, Vol. 192, 2014, pp. 261-268.
[56]. Z. Luo, S. Yin, K. Wang, H. Li, L. Wang, H. Xu, J. Xia, Synthesis of one-dimensional β-$Ni(OH)_2$ nanostructure and their application as nonenzymatic glucose sensors, *Materials Chemistry and Physics*, Vol. 132, Issue 2-3, 2012, pp. 387-394.
[57]. Q. Xiao, X. Wang, S. Huang, Facile synthesis of $Ni(OH)_2$ nanowires on nickel foam via one step low-temperature hydrothermal route for non-enzymatic glucose sensor, *Materials Letters*, Vol. 198, 2017, pp. 19-22.
[58]. G. Wang, X. Lu, T. Zhai, Y. Ling, H. Wang, Y. Tong, Y. Li, Free-standing nickel oxide nanoflake arrays: Synthesis and application for highly sensitive non-enzymatic glucose sensors, *Nanoscale*, Vol. 4, Issue 10, 2012, pp. 3123-3127.
[59]. J. Yang, M. Cho, C. Pang, Y. Lee, Highly sensitive non-enzymatic glucose sensor based on over-oxidized polypyrrole nanowires modified with $Ni(OH)_2$ nanoflakes, *Sensors and Actuators B: Chemical*, Vol. 211, 2015, pp. 93-101.
[60]. G. Li, X. Wang, L. Liu, R. Liu, F. Shen, Z. Cui, W. Chen, T. Zhang, Controllable synthesis of 3D $Ni(OH)_2$ and NiO nanowalls on various substrates for high-performance nanosensors, *Small*, Vol. 11, Issue 6, 2015, pp. 731-739.
[61]. M. Urso, G. Pellegrino, V. Strano, E. Bruno, F. Priolo, S. Mirabella, Enhanced sensitivity in non-enzymatic glucose detection by improved growth kinetics of Ni-based nanostructures, *Nanotechnology*, Vol. 29, Issue 16, 2018, 165601.

[62]. Z. Lu, Z. Chang, W. Zhu, X. Sun, Beta-phased $Ni(OH)_2$ nanowall film with reversible capacitance higher than theoretical Faradic capacitance, *Chemical Communications*, Vol. 47, Issue 34, 2011, pp. 9651-9653.

[63]. P. Pramanik, S. Bhattacharya, A chemical method for the deposition of nickel oxide thin films, *Journal of the Electrochemical Society*, Vol. 137, Issue 12, 1990, pp. 3869-3870.

[64]. P. Bukovec, N. Bukovec, B. Orel, K. S. Wissiak, Thermal analysis of nickel oxide films, *Journal of Thermal Analysis*, Vol. 40, Issue 3, 1993, pp. 1193-1196.

[65]. S. Y. Han, D. H. Lee, Y. J. Chang, S. O. Ryu, T. J. Lee, C. H. Chang, The growth mechanism of nickel oxide thin films by room-temperature chemical bath deposition, *Journal of the Electrochemical Society*, Vol. 153, Issue 6, 2006, pp. C382-C386.

[66]. X. H. Xia, J. P. Tu, J. Zhang, X. L. Wang, W. K. Zhang, H. Huang, Electrochromic properties of porous NiO thin films prepared by a chemical bath deposition, *Solar Energy Materials and Solar Cells*, Vol. 92, Issue 6, 2008, pp. 628-633.

[67]. G. Hu, C. Li, H. Gong, Capacitance decay of nanoporous nickel hydroxide, *Journal of Power Sources*, Vol. 195, Issue 19, 2010, pp. 6977-6981.

[68]. Q. Ke, M. Zheng, H. Liu, C. Guan, L. Mao, J. Wang, 3D TiO_2@$Ni(OH)_2$ core-shell arrays with tunable nanostructure for hybrid supercapacitor application, *Scientific Reports*, Vol. 5, Issue 1, 2015, pp. 1-11.

[69]. S. Petralia, S. Mirabella, V. Strano, S. Conoci, A miniaturized electrochemical system based on nickel oxide species for glucose sensing applications, *Bionanoscience*, Vol. 7, Issue 1, 2017, pp. 58-63.

[70]. S. Petralia, E. L. Sciuto, M. A. Messina, A. Scandurra, S. Mirabella, F. Priolo, S. Conoci, Miniaturized and multi-purpose electrochemical sensing device based on thin Ni oxides, *Sensors and Actuators B: Chemical*, Vol. 263, 2018, pp. 10-19.

[71]. Z. Ren, Y. Guo, C. H. Liu, P. X. Gao, Hierarchically nanostructured materials for sustainable environmental applications, *Frontiers in Chemistry*, Vol. 1, 2013, 18.

[72]. P. Kannan, T. Maiyalagan, E. Marsili, S. Ghosh, J. Niedziolka-Jönsson, M. Jönsson-Niedziolka, Hierarchical 3-dimensional nickel-iron nanosheet arrays on carbon fiber paper as a novel electrode for non-enzymatic glucose sensing, *Nanoscale*, Vol. 8, Issue 2, 2016, pp. 843-855.

[73]. H. Liu, X. Lu, D. Xiao, M. Zhou, D. Xu, L. Sun, Y. Song, Hierarchical Cu-Co-Ni nanostructures electrodeposited on carbon nanofiber modified glassy carbon electrode: Application to glucose detection, *Analytical Methods*, Vol. 5, Issue 22, 2013, pp. 6360-6367.

[74]. V. Strano, S. Mirabella, Hierarchical ZnO nanorods/$Ni(OH)_2$ nanoflakes for room-temperature, cheap fabrication of non-enzymatic glucose sensors, *RSC Advances*, Vol. 6, Issue 112, 2016, pp. 111374-111379.

[75]. V. Strano, S. Mirabella, Low-cost and facile synthesis of $Ni(OH)_2$/ZnO nanostructures for high-sensitivity glucose detection, *Nanotechnology*, Vol. 29, Issue 1, 2017, 015502.

[76]. V. Strano, R. G. Urso, M. Scuderi, K. O. Iwu, F. Simone, E. Ciliberto, C. Spinella, S. Mirabella, Double role of HMTA in ZnO nanorods grown by chemical bath deposition, *The Journal of Physical Chemistry C*, Vol. 118, Issue 48, 2014, pp. 28189-28195.

[77]. X. Wang, H. Jian, Q. Xiao, S. Huang, Ammonium nickel phosphate on nickel foam with a Ni^{3+}-rich surface for ultrasensitive nonenzymatic glucose sensors, *Applied Surface Science*, Vol. 459, 2018, pp. 40-47.

[78]. P. Subramanian, J. Niedziolka-Jonsson, A. Lesniewski, Q. Wang, M. Li, R. Boukherroub, S. Szunerits, Preparation of reduced graphene oxide-$Ni(OH)_2$ composites by electrophoretic deposition: Application for non-enzymatic glucose sensing, *Journal of Materials Chemistry A*, Vol. 2, Issue 15, 2014, pp. 5525-5533.

[79]. B. Zhao, T. Wang, L. Jiang, K. Zhang, M. M. Yuen, J. B. Xu, X. Z. Fu, R. Sun, C. P. Wong, NiO mesoporous nanowalls grown on RGO coated nickel foam as high performance electrodes for supercapacitors and biosensors, *Electrochimica Acta*, Vol. 192, 2016, pp. 205-215.

[80]. G. Zeng, W. Li, S. Ci, J. Jia, Z. Wen, Highly dispersed NiO nanoparticles decorating graphene nanosheets for non-enzymatic glucose sensor and biofuel cell, *Scientific Reports*, Vol. 6, 2016, 36454.

[81]. J. Yang, P. Xiong, C. Zheng, H. Qiu, M. Wei, Metal-organic frameworks: A new promising class of materials for a high performance supercapacitor electrode, *Journal of Materials Chemistry A*, Vol. 2, Issue 39, 2014, pp. 16640-16644.

[82]. X. Xiao, S. Zheng, X. Li, G. Zhang, X. Guo, H. Xue, H. Pang, Facile synthesis of ultrathin Ni-MOF nanobelts for high-efficiency determination of glucose in human serum, *Journal of Materials Chemistry B*, Vol. 5, Issue 26, 2017, pp. 5234-5239.

Chapter 4

Wearable Sensors for Individual Grip Force Profiling

Birgitta Dresp-Langley

4.1. Introduction

Biosensors and wearable sensor systems with transmitting capabilities are currently developed and used for the monitoring of health data, exercise activities, and other performance data [1]. Unlike conventional approaches, these devices enable convenient, continuous, and/or unobtrusive monitoring of a user's behavioral signals in real time. Examples include signals relative to body motion, body temperature, blood flow parameters and a variety of biological or biochemical markers and, as will be shown in this chapter here, individual grip force data that directly translate into spatiotemporal grip force profiles for different locations on the fingers and/or palm of the hand. Wearable sensor systems combine innovation in sensor design, electronics, data transmission, power management, and signal processing for statistical analysis, as will be further shown herein. The first section of this chapter will provide an overview of the current state of the art in grip force profiling to highlight important functional aspects to be considered. In the next section, the contribution of wearable sensor technology in the form of sensor glove systems for the real-time monitoring of surgical task skill evolution in novices training in a simulator task will be described on the basis of recent examples. In the discussion, advantages and limitations will be weighed against each other. Finally, although a lot of research is currently devoted to this area, many technological aspects still remain to be optimized, and new methods for data analysis

Birgitta Dresp-Langley
Centre National de la Recherche Scientifique (CNRS), UMR 7357 ICube Lab, CNRS and University of Strasbourg, France

and knowledge representation are urgently needed. These aspects represent an open challenge for the scientific community in the field of wearable sensor technology, as explained in the conclusions of this chapter.

4.2. Functional Characteristics of Human Grip Force

Human grip force is controlled at several hierarchical stages, from sensory receptors to the brain and back to the hand, and its functional aspects have been relatively well studied. For example, the relationship between individual finger positions and external grip forces of men and women was investigated [2] in studies where subjects held cylindrical objects from above, using circular precision grips in the 5-finger grip mode. Effects of 4-, 3- and 2-finger grip modes in circular grip mode were also investigated. Individual finger position was nearly constant for all weights and for diameters of 5.0 and 7.5 cm. The mean angular positions for the index, middle, ring and little fingers relative to the thumb were 98 degrees, 145 degrees, 181 degrees, and 236 degrees, respectively. At the 10-cm diameter, the index and middle finger positions increased, while the ring and little finger positions decreased. There were no differences in individual finger position with regard to gender, hand dimension, or hand strength. Total grip force increased with weight, and at diameters greater or lesser than 7.5 cm. Total grip force also increased as the number of fingers used for grasping decreased. Although the contribution of the individual fingers to the total grip force changes with object weight and diameter, the thumb contribution always exceeded 38 % followed by the ring finger and the little finger (pinky), which contributed approximately 18-23 %, for all weights and diameters. The contribution of the index finger was always smallest, and there was no gender difference for any of the grip force variables. Effects of hand dimension and hand strength on the individual finger grip forces were subtle and minor [2].

The contributions and co-ordination of external finger grip forces during a lifting task with a precision grip using multiple fingers were also investigated [3]. Ten subjects lifted a force transducer-equipped grip apparatus, and grip force from each of the five fingers was continuously measured with different object weights and surface structures. Effects of five-, four-, and three-finger grip modes were also examined [3]. It was found that variation of object weight or surface friction resulted in a change of the total grip force magnitude. The largest change in finger

force was recorded for the index finger, followed by the middle, ring, and little fingers. Percentage contributions of static grip force to total grip force for the index, middle, ring, and little fingers was 42.0 %, 27.4 %, 17.6 % and 12.9 %, respectively, and values were roughly constant across object weights and surface friction conditions. These results suggest that all individual finger force adjustments for lighter loads (<800 g) are controlled by using a single common scaling value [3]. Higher surface friction provided faster lifting initiation and required lesser grip force, indicating the beneficial effects of a non-slippery surface. Nearly 40 % force reduction was obtained with the non-slippery surface. Variation in grip mode changes the total grip force: the fewer the number of fingers used, the greater is the total grip force [3]. The static grip force for the index, middle, and ring fingers in the four-finger grip mode was 42.7 %, 32.5 %, and 24.7 %, respectively. Static grip force for the index and middle fingers in the three-finger grip mode was 43.0 % and 56.9 %, respectively, suggesting that the grip mode, i.e. whether all five or only three fingers are used, influences the force contributions of the middle and ring fingers, but not that of the index finger [3].

Other studies have shown a phenomenon of motor redundancy [4] in human prehensile behavior [4]. The partly redundant design of the hand allows performing a variety of tasks in a reliable and flexible way following the principle of abundance, as shown in robotics with respect to the control of artificial grippers, for example. Multi-digit synergies appear to operate at two levels of hierarchy to control prehensile action [4]. Forces and moments produced by the thumb and the "virtual finger" (an imagined finger with a mechanical action equal to the combined mechanical action of all other four fingers of the hand) co-vary at a higher level only to stabilize the grip action in respect to the orientation of the hand-held object. Analysis of grip force adjustments during motion of hand-held objects suggests that the central nervous system adjusts to gravitational and inertial loads differently, at an even higher level of control. Object manipulation by efficient control of finger and grip force is therefore not only a motor skill but also a cognitive skill [5] exploited in surgery, craft making, and musical performance. Sequences of relatively straightforward cause-effect links directly related to mechanical constraints lead on to a non-trivial co-variation between low-level and high-level control variables [3-5], as in playing a musical instrument, which requires independent control of the magnitude and rate of force production, which typically vary in relation to loudness and tempo [5].

The expert performance of a highly skilled pianist, for example, is characterized by a rapid reduction of finger forces, allowing for considerably fast performance of repetitive piano keystrokes [5]. Skilled grasping behavior (multi-finger grasping) has three essential components: 1) Manipulation force, or resultant force and moment of force exerted on the object and the digits' contribution to force production; 2) Internal forces, which are defined as forces that cancel each other out to maintain object stability, to ensure slip prevention, tilt prevention, and robustness against perturbation, and 3) Motor control (or grasp control), which involves prehensile synergies, chain effects, inter-finger connection [2-4] and the high-level brain command of simultaneous digit adjustments to several, mutually reinforcing or conflicting demands. Prehensile synergies are reflected by characteristics of digit action and their co-variation patterns during task execution or during static holding of an object while the external torque force changes slowly and smoothly.

Conditions of torque forces changing slowly, requiring smooth adjustments of grip efforts from either non-zero pronation to zero, or from non-zero supination to zero were investigated [7]. With the handle kept vertical at all times, indices of variance and co-variation of forces and moments of force produced by individual digits to stabilize performance were measured in terms of total normal force, total tangential force, and total moment of force. Measurements were computed at two levels of an assumed control hierarchy: 1) an upper level, where the task is shared between the thumb and the “virtual finger”, i.e. an imagined digit with mechanical action equal to that of all other four fingers and 2) a lower level, where the action of the “virtual finger” is shared by the true four fingers. When total moment of force is expressed in terms of the sum of the moments of force produced by the thumb and the “virtual finger”, or the sum of the moments of force produced by normal forces and tangential forces, it was found that adjustments in total moment of force were produced primarily by changes in the moment produced by the “virtual finger” and by changes in the moment produced by the normal forces. The normal force of the thumb at the final state was the same across conditions, and solely determined by changes in the external torque force [7]. The co-contraction index reflecting the moment of force production by true four fingers acting against the total moment produced by the “virtual finger” was higher in the “from non-zero supination to zero” condition. Variance indices dropped with the decrease in external torque force while co-variation indices remained unchanged over the task time [7].

These results suggest a trade-off between the two levels of hierarchy assumed, with larger indices at the higher level corresponding to smaller indices at the lower level as characteristic features of prehensile tasks. Functional properties of digit action and interaction do not only depend on the magnitudes of external constraints (i.e. external torque forces), but also on temporal changes in such constraints and their history. Static grasping/holding of a horizontally oriented object was also explored to address issues relative to the sharing patterns of the total moment of force across the digits, the presence of mechanically unnecessary digit forces, and the trade-off between multi-digit synergies at the two levels of assumed control hierarchy [8]. Measurement conditions consisted of holding statically a horizontally oriented handle instrumented with six-component force/torque sensors with different loads and torques acting about the longer axis of the handle. The thumb acted from above, while the other four fingers supported the weight of the object. When the external torque force is zero, the thumb produces a mechanically unnecessary force which does not depend on the external load magnitude [8]. When the external torque force is non-zero, the tangential forces produced over 80 % of the total force. The normal forces by the middle and ring fingers produce consistent moments against the external torque force, while the normal forces of the index and little fingers do not [8]. Overall, results have shown that task mechanics are only one of the many factors that determine the grip forces produced by individual digits. Sensory receptor processing may lead to mechanically unnecessary forces [7, 8], and there seems to be no single rule that describes the sharing of normal and tangential forces across tasks. Fingers such as the ring finger are traditionally viewed as “less accurate” [1-3], yet they may perform more consistently in specific tasks [8].

The trade-offs between variables produced at the two hierarchical control levels assumed suggest that a degree of “functional redundancy” at the higher control level represents an important characteristic of grip force control. Other studies measured grip strength using several methods serially excluding one or two phalanges [9] to shed further light on clinical and/or functional outcomes relating to the contribution of each finger to overall grip force. Two hundred healthy young men were included in this survey, and demographic variables as well as anthropometric parameters of forearms and hands were recorded. Grip strength was measured using all fingers, all fingers except the thumb, all fingers except the index finger, all fingers except the middle finger, all fingers except the ring and little fingers, and all fingers except the little finger. The contribution of each finger to total grip strength was

estimated [9]. Grip strength using all five fingers was, as would be expected, greatest, closely followed by grip strength without the thumb. Grip strengths without the middle, the ring and the little finger were the smallest. Contributions of the index, middle, ring and little fingers to the grip strength were 17 %, 22 %, 31 %, and 29 %, respectively. The middle finger was the most important contributor to grip strength, followed by the combination of ring and little fingers. Positive correlations between each grip method and anthropometric parameters such as hand size were found [9]. Grip force and its distribution across different fingers of the hand are important parameters for evaluating functional aspects of grip forces during task execution. Identifying differences between non-dominant and dominant hands in bimanual grip tasks as a function of anthropometric parameters is another potentially important source of variation.

Some authors [10] compared grip force and load distributions of dominant and non-dominant hands in right-handed healthy subjects, assigned to either a small or a large cylindrical object with respect to their hand size. Maximum and mean grip forces well as the contribution (in percent) of each digit, *thenar,* and *hypothenar* in relation to the total load applied were measured and compared across the dominant and non-dominant hands. The contribution to mean grip strength differed significantly between the thumb and the ring finger, the thumb and the little finger, and between thumb and measurements taken from the palm of the hand. The dominant hand showed a smaller force contribution of the thumb and ring finger, and a greater contribution of the palm of the hand in comparison with the non-dominant hand [10].The contribution of the small fingers to maximum grip force was equal between the dominant and non-dominant hands; no differences were found between the index finger, middle finger, *thenar*, and *hypothenar* when analyzing their cumulated % force contribution to both mean and maximum force. In right-handed subjects, the thumb and the ring finger are functionally the most important contributors to grip force.

4.3. Wearable Grip Force Sensors for Individual Grip Force Profiling in Real Time during Bimanual Task Execution

The example of surgical task training and, in particular, robot assisted minimally invasive surgical training, is evoked here to bring forward clinical, ergonomic, and general functional advantages of individual grip force profiling using wearable (gloves or glove-like assemblies) sensor

systems for the monitoring of task parameters relating to manual skill evolution in real time. In studies on robotic surgery platforms [11, 12], for example, the bi-manual performance skill learning curves of experienced urological robotic surgeons, surgeons with experience as robotic platform tableside assistants, urological surgeons with laparoscopic experience, urological surgeons without laparoscopic experience, and complete novices, either aged 25 and younger, or 40 and older were compared. The results showed that all experienced robotic surgeons reached expert performance level (>90 %, as defined previously in the literature) within the first three trial repeats, and consistently maintained a high level of performance. All other groups performed significantly worse. Platform tableside assistants, laparoscopy experienced surgeons, and younger novices showed better performance in all exercises than surgeons without laparoscopic experience and older novices. In summary, performance in robotic surgery measured by performance scores in virtual simulator modules is significantly dependent on age, and on prior experience with robotic and laparoscopic surgery [12]. Minimally invasive robotic surgery has many advantages over traditional surgical procedures, but the loss of force feedback yields potential for stronger grip forces during task execution, which can result in excessive tissue damage [13].

Grip force monitoring is therefore a highly useful means of tracking the evolution of the surgeon's individual force profile during task execution [14]. While current multi-modal feed-back systems may represent a slight advantage over the not very effective traditional single modality feedback solutions by achieving average grip forces closer to those normally possible with the human hand [13], the monitoring of individual grip forces of the surgeon (or trainee) during task execution by wearable multisensory systems is by far the superior solution. Real-time grip force sensing by wearable systems can directly help prevent incidents, because it includes the possibility of sending a signal (sound or light) to the surgeon whenever his/her grip force exceeds a critical limit before the damage is done. Proficiency, or expertise, in the control of a robotic master/slave system designed for minimally invasive surgery is reflected by a lesser grip force during task execution as well as by a shorter task execution times [14, 15]. Benchmark measures permitting to establish objective criteria for expertise in using such surgical systems, which have a limited degrees of freedom, need to be found to ensure effective training of future surgeons. As shown in the introduction here above, the state of the art in experimental studies on grip force strength and control for lifting and manipulating objects strategically has

provided limited insight into the contributions of each finger to overall grip strength and fine grip force control, with a general conclusion in terms of complex prehensile synergies governed by interactions between at least two hierarchical processes of sensory (low-level) and central (high-level) information processing and control. However, what generally has emerged from that research is that: 1) The middle finger is the most important contributor to the gross total grip force and, therefore, most important for getting a good grip of heavy objects to lift or carry, while, 2) The ring finger and the small (pinky) finger appear most important for the fine control of subtle grip force modulations [16, 17], which is important in surgical tasks, and even more critically important when manipulating the handles of a surgical robot with limited degrees of freedom for hand and finger movements. Also, grip force may be stronger in the dominant hand compared with the non-dominant hand. In two recent studies [14, 15] the grip force profiles corresponding to measurements collected from specific sensor positions on anatomically relevant parts of the finger and hand regions of the dominant and non-dominant hands of an expert in controlling a robotic surgery system were compared to those of a beginner, who manipulated the device for the first time.

A wireless sensor glove hardware-software system, described in detail in [14, 15], was specially designed for these studies. Before the sensor glove system was employed to study expert and novice grip force profiles during manipulation of the robotic system, individual grip force data from the right and left hands of several young individuals were recorded in preliminary test sessions using weighted handles, which had to be lifted up and down to the sound of different types of music [18]. These systematic tests produced relevant data relative to the characteristics of individual grip force profiles in time as a function of the sensor location on the fingers and palms of either of the two hands (Fig. 4.1, left), the hand considered (dominant *versus* non-dominant), and the type of music played during two-handed manipulation (soft music *versus* hard rock music) of the weighted handles. Results from these preliminary tests are described in the next section here below to illustrate how statistical analyses of the individual grip force profiles shed light on specific aspects of individual task performance.

The wireless gloves (Fig. 4.1, right) that produced the data shown here below were specifically designed for individual grip force profiling [14, 15, 18]. They contain 12 small force sensitive resistors FSR, in

contact with specific locations on the inner surface of the hand as given in Fig. 4.2.

Fig. 4.1. Signals relative to grip force were sampled from 12 anatomically relevant force sensitive sensor (FSR) locations on the fingers and in the palm (left) of both hands. The FSRS were sewn into a soft glove (top right) wireless wearable sensor system design [14, 15, 18] for grip force monitoring in bimanually executed tasks such as robotic surgery (bottom right).

Two layers of cloth were used and the FSRs were inserted between the layers. The FSRs did not interact, neither directly with the skin of the subject, nor with the master handles, which provided a comfortable feel when manipulating the system. FSRs were sewn into the glove with a needle and thread. Each FSR was sewn to the cloth around the conducting surfaces (active areas). The electrical connections of the sensors were individually routed to the dorsal side of the hand and brought to a soft ribbon cable, connected to a small and very light electrical casing that was strapped onto the upper part of the forearm and equipped with an Arduino microcontroller. Eight of the FSR positioned in the palm of the hand and on the finger tips had a 10 mm diameter, while the remaining four located on the middle phalanxes on the fingers had a 5 mm diameter. Each FSR was soldered to 10 kΩ pull-down resistors to create a voltage divider. The voltage (V) read by the analog input of the Arduino is given by (4.1)

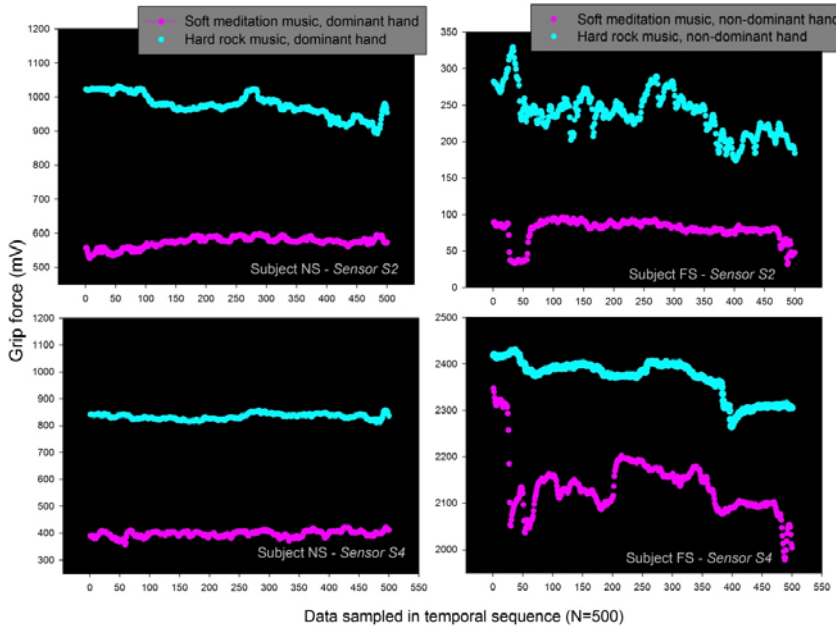

Fig. 4.2. Effects of sound (music) in sensor locations S2 and S4 recorded in the temporal task sequences of two individuals (NS, left; FS, right).

$$Voutput = RPDV3.3/(RPD+RFSR), \quad (4.1)$$

where RPD is the pull-down resistance, RFSR the FSR resistance, and 3.3 the V supply voltage. FSR resistances can vary from 250 **Ω** when subject to 20 Newton (N) to more than 10 M**Ω** when no force is applied at all. Voltages generated in the experiments from which data were drawn [14, 15, 18] varied monotonically between 0 and 3.22 V as a function of grip force applied, which is assumed uniform on the sensor surface. In the experiments, grip forces did not exceed 10 Newton, and voltages varied within the range of [0; 1500] mV. The relation between force and voltage is almost linear within this range. All sensors provided similar calibration curves and comparisons could be made directly between voltages at the millivolt scale. Regulated 3.3 V was provided to the sensors through the Arduino. Power was provided by a 4.2 V Li-Po battery enabling wireless use of the glove system. The battery voltage level is directly controlled by the Arduino, and displayed continuously on the screen of the user interface. The glove system was connected to a computer for data storage via Bluetooth enabled wireless communication

running 115,200 bits-per-second (bps). The software of the glove system has two parts: One running on the gloves, and one running on the computer algorithm for data collection. Each of the two gloves is sending data to the computer separately, and the software reads the input values, and stores them on the computer according to header values indicating their origin. The software running on the Arduino was designed to acquire analog voltages provided by the FSR every 20 milliseconds (50 Hz). Input voltages are merged with their time stamps and sensor identification. The data package is sent to the computer via Bluetooth, which is decoded by the computer software. The voltages are saved in a text file for each sensor, with their time stamps and identifications. The computer software monitors the voltage values received from the gloves via a user interface displaying battery levels. Detailed descriptions and images of the wireless sensor glove in action on a robotic surgery system, system specifications, and the general design chart of the hard-to-software wireless wearable sensor system have been published in [14], accessible online at https://www.mdpi.com/1424-8220/19/20/ 4575/ htm (Licence CC BY 4.0).

4.4. Data Analysis and Visualization

The individual grip force profiles and the group profiles, analyzed and visualized herein, correspond to unpublished data from the preliminary testing phase of the wireless sensor gloves [18] recorded from young volunteers while moving two weighted handles up and down to the sound of different pieces of music. The handles subjects were commercially available cylindrical weights of identical shape and size weighing one kilogram each. Different pieces of music were selected for the different sound exposure conditions. Exposure duration was 10 seconds for each of them. One piece consisted of extremely soft tones designed for meditation, another of highly aggressive hard metal rock performed by the group *Rammstein* (*"Zerstören"* from their album *"Rosenrot"*). Sound intensities were maintained the same for the different pieces of music, on the computer and on the two loudspeakers. Nine healthy men and two healthy women, aged between 20 and 30, all of them right-handed, participated in this study. Handedness was confirmed individually using the Edinburgh inventory for handedness. The subjects were all volunteers and naive to the purpose of the experiment. The study trials were conducted in full conformity with the Helsinki Declaration relative to scientific experiments on human individuals and approved by the ethics board of the lead investigator's host institution (CNRS). All

participants were young volunteers and provided written informed consent. Their identity is not revealed. Hand grip forces were recorded from the twelve sensor *loci* on the dominant and non-dominant hands of eleven subjects in different experimental conditions [18]. All subjects were tested in all the conditions of exposure to different types of music. The order of these different conditions was carefully counterbalanced between subjects. During the tests, subjects were standing upright facing a table on which the two handles they had to grip were placed in alignment with the forearm motor axis. Subjects were instructed to grab the handles with their two hands and to start moving them up and down as soon as the music started. The duration of the music and the handgrip force recordings was ten seconds per subject and experimental condition. Raw data (voltages) from each sensor were recorded every 20 milliseconds in a temporal sequence, for each subject and experimental condition, committed to *Excel* files with labeled columns. Grouped data were imported into *Matlab 7.14* for transformation of the voltage output (*Voutput*) data into Newton (*N*) by (4.2)

$$N = Voutput/(RPDV3.3\text{-}Voutput), \tag{4.2}$$

where RPD is the pull-down resistance, RFSR the FSR resistance, and 3.3 the V supply voltage. The individual force profiles here below show grip force data in millivolt (mV), the grouped force profiles show population grip force data in Newton. Either parameter is valid, given that for the range of variations recorded in the different experiment, the relation between force and voltage is almost linear.

The analyses here below concern individual grip force profiles from two sensor locations (S2 and S4) of two individuals from a subject pool of eleven. Grip forces recorded in task time were plotted as a function of two different music conditions, and the hand they were recorded from. In the grip force profiles of the two individuals, we see that S2 and S4 data produces a clear effect of music (sound), with stronger grip forces for hard rock music. These profiles (Fig. 4.2) also show that the two individuals apply different total forces at the two sensor locations.

The sensors S2 and S4, among others, also showed differences in forces applied by the dominant and the non-dominant of some individuals. Individual grip force profiles of the dominant and the non-dominant hands recorded from these two sensor locations are shown here below for subject FS in the hard rock music condition. The individual grip force profiles reveal systematically stronger grip forces applied by the

dominant hand in sensor locations S2 (Fig. 4.3, top) and S4 (Fig. 4.3, bottom), and systematically and considerably stronger total grip forces in sensor S4, when comparing the range of variations shown (top graph *versus* bottom graph).

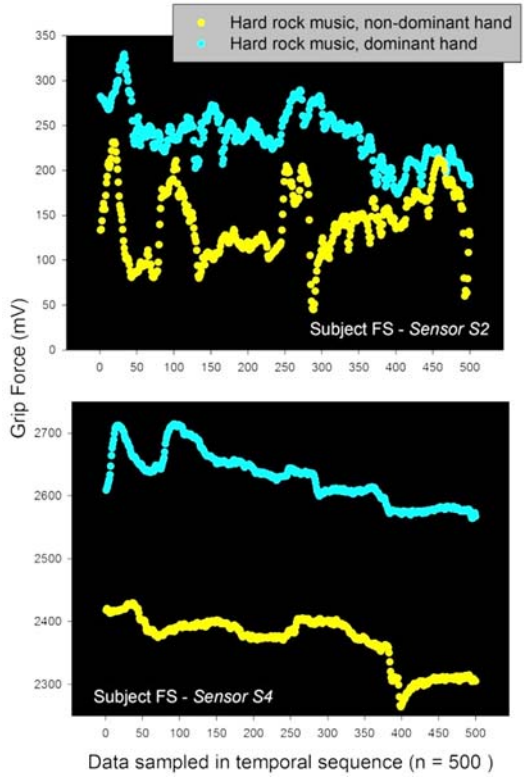

Fig. 4.3. Effects of hand on grip forces recorded from sensor locations S2 and S4 recorded in the temporal task sequence of individual FS in the hard rock music condition.

Average grip force data of a whole population of individuals in a given condition, or factorial combination thereof, may also be computed. This allows to assess how individual grip force profiles compare with the average profile of a whole population under the same conditions. Examples of average population grip force data for the dominant and the non-dominant hands from different sensor locations and across music conditions are shown as examples (Fig. 4.4) here below.

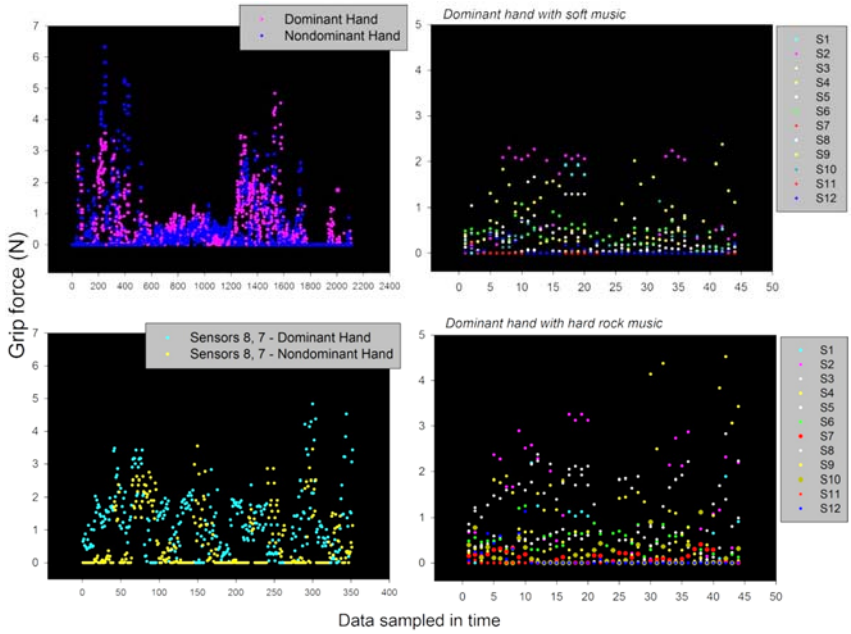

Fig. 4.4. Effects of hand, sensor location, and sound (music) on average population grip forces computed on data sampled in time from the whole study population.

The examples here above show that combining wireless wearable multisensory technology with an appropriate experimental design produces meaningful individual and general (population) grip force profiles that can be compared for the selection of conditions for task performance benchmarking recorded using. The pretesting data (not all are shown here) from these preliminary experiments here have enabled the design of the study on the robotic surgery system [14] referred here above. That study produced highly significant differences in expert and novice grip force profiles, as revealed by a series of robust statistical analysis (ANOVA) across surgical task sessions in time and sensor locations [14]. The characteristic individual grip force profile of an expert surgeon during bimanual manipulation of the robotic surgery device (Fig. 4.1) across repeated task sessions for a four-step pick-and-place task [14] displays higher values for subtle grip control by the small finger, and lesser values for gross grip force by the middle finger when compared with the grip force profiles of the novice (Fig. 4.5). Grip force profiling has thereby permitted to benchmark fine grip force control by

the small finger and minimal gross force deployment by the middle finger, in combination with shorter task execution times [14], as a typical functional characteristic of surgical expertise on the specific robotic system.

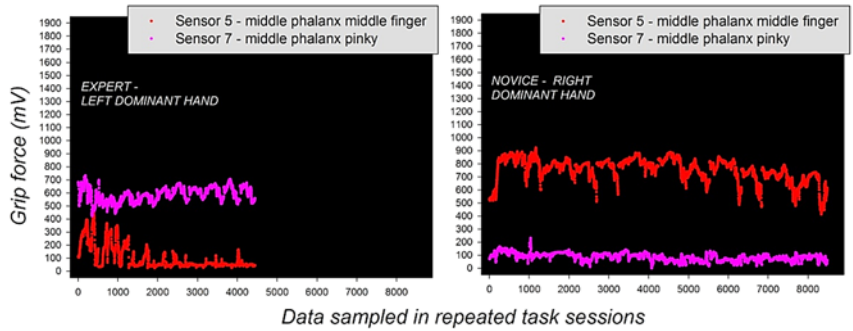

Fig. 4.5. Individual grip force profiles of the dominant hand distinguishing an expert's (left) from a novice's (right) performance during bimanual use of a robotic surgery system in four-step-pick-and-drop task [14]. The shorter task execution times per session of the expert (left) are reflected here by the smaller number of data sampled in task time across sessions (x-axis of the graph on left).

These insights, combined with the effects of sound on individual grip force profiles shown from the pretest study here suggest that it should be possible to effectively use individual grip force profiling with sound feed-back in robotic surgery for modulating excessive grip forces during interventions well before they may cause potentially dangerous tissue damage.

4.5. Conclusions

Prehensile synergies of the human hand are under the command of multiple levels of sensorial integration, cognitive control, and interactions between the two, as summarized here in the introduction. Using wireless wearable sensor technology, possibly in combination with sensory feed-back systems [19-23], for the effective monitoring of manual and bimanual tasks where grip force matters critically represents a promising way towards performance quality benchmarking in training, and in risk prevention, especially for critical tasks such as robot assisted

surgery [14, 15]. The human hand has evolved [24] as a function of active constraints [25-29], and in harmony with other sensory systems such as the auditory system [18, 23, 30] Grip force profiles are a direct reflection of the complex low-level, cognitive, and behavioral synergies this evolution has produced.

References

[1]. M. Di Rienzo, R. Mukkamala, Special issue on wearable and nearable biosensors and systems for healthcare, *Sensors (Basel)*, 2019, https://www.mdpi.com/journal/sensors/special_issues/Nearable#

[2]. H. Kinoshita, T. Murase, T. Bandou, Grip posture and forces during holding cylindrical objects with circular grips, *Ergonomics*, Vol. 39, Issue 9, 1996, pp. 1163-1176.

[3]. H. Kinoshita, S. Kawai, K. Ikuta, Contributions and co-ordination of individual fingers in multiple finger prehension, *Ergonomics*, Vol. 38, Issue 6, 1995, pp. 1212-1230.

[4]. M. L. Latash, V. M. Zatsiorsky. Multi-finger prehension: Control of a redundant mechanical system, *Adv. Exp. Med. Biol*., Vol. 629, 2009, pp. 597-618.

[5]. T. Oku, S. Furuya, Skilful force control in expert pianists, *Exp. Brain Res.*, Vol. 235, Issue 5, 2017, pp. 1603-1615.

[6]. V. M. Zatsiorsky, M. L. Latash, Multifinger prehension: An overview, *J. Mot. Behav.*, Vol. 40, Issue 5, 2008, pp. 446-476.

[7]. Y. Sun, J. Park, V. M. Zatsiorsky, M. L. Latash, Prehension synergies during smooth changes of the external torque, *Exp. Brain Res.*, Vol. 213, Issue 4, 2011, pp. 493-506.

[8]. Y. H. Wu, V. M. Zatsiorsky, M. L. Latash, Static prehension of a horizontally oriented object in three dimensions, *Exp. Brain Res.*, Vol. 216, Issue 2, pp. 249-261.

[9]. S. M. Cha, H. D. Shin, K. C. Kim, J. W. Park, Comparison of grip strength among 6 grip methods, *J. Hand. Surg. Am.,* Vol. 39, Issue 11, 2014, pp. 2277-2284.

[10]. A. Cai, I. Pingel, D. Lorz, J. P. Beier, R. E. Horch, A. Arkudas, Force distribution of a cylindrical grip differs between dominant and nondominant hand in healthy subjects, *Arch. Orthop. Trauma Surg.*, Vol. 138, Issue 9, 2018, pp. 1323-1331.

[11]. I. Sorokin, J. A. Cadeddu, A query on da Vinci robot console preferences: Insights for the novice surgeon, *J. Robot. Surg.*, Vol. 11, Issue 2, 2017, pp. 231-233.

[12]. M. Meier, K. Horton, H. John, Da Vinci© Skills Simulator™: Is an early selection of talented console surgeons possible?, *J. Robot. Surg.*, Vol. 10, Issue 4, 2016, pp. 289-296.

[13]. A. Abiri, J. Pensa, A. Tao, J. Ma, Y. Y. Juo, S. J. Askari, J. Bisley, J. Rosen, E. P. Dutson, W. S. Grundfest, Multi-modal haptic feedback for grip force reduction in robotic surgery, *Scientific Reports*, Vol. 9, Issue 1, 2019, 5016.

[14]. M. de Mathelin, F. Nageotte, P. Zanne, B. Dresp-Langley, Sensors for expert grip force profiling: towards benchmarking manual control of a robotic device for surgical tool movements, *Sensors (Basel)*, Vol. 19, Issue 20, 2019, 4575.

[15]. A. U. Batmaz, A. M. Falek, L. Zorn, F. Nageotte, P. Zanne, M. de Mathelin, B. Dresp-Langley, Novice and expert behavior while using a robot controlled surgery system, in *Proceedings of the 13th IASTED International Conference on Biomedical Engineering (BioMed'17)*, Innsbruck, Austria, 20-21 February 2017, pp. 94-99.

[16]. S. M. Cha, H. D. Shin, K. C. Kim, J. W. Park, Comparison of grip strength among six grip methods, *J. Hand. Surg.,* Vol. 39, 2014, pp. 2277-2284.

[17]. R. W. Bohannon, Grip strength: A summary of studies comparing dominant and non-dominant limb measurements, *Percept. Mot. Skills,* Vol. 96, 2003, pp. 728-730.

[18]. A. U. Batmaz, M. A. Falek, M. de Mathelin, B. Dresp-Langley, Tactile sensors for measuring effects of sight, movement, and sound on handgrip forces during hand-tool interaction, Preprint, *Preprints.org*, 2017.

[19]. R. S. Johansson, K. J. Cole, Sensory-motor coordination during grasping and manipulative actions, *Curr. Opin. Neurobiol.,* Vol. 2, 1992, pp. 815-823.

[20]. A. C. Eliasson, H. Forssberg, K. Ikuta, I. Apel, G. Westling, R. Johansson, Development of human precision grip V. Anticipatory and triggered grip actions during sudden loading, *Exp. Brain Res.,* Vol. 106, 1995, pp. 425-433.

[21]. P. Jenmalm, R. S. Johansson, Visual and somatosensory information about object shape control manipulative fingertip forces, *J. Neurosci.,* Vol. 17, 1997, pp. 4486-4499.

[22]. K. W. Li, R. Yu, Assessment of grip force and subjective hand force exertion under handedness and postural conditions, *App. Ergonomics,* Vol. 42, 2011, pp. 929-933.

[23]. P. Aravena, Y. Delevoye-Turrell, V. Deprez, A. Cheylus, Y. Paulignan, V. Frak, T. Nazir, Grip force reveals the context sensitivity of language-induced motor activity during «action words» processing: Evidence from sentential negation, *PLoS ONE,* Vol. 7, 2012, e50287.

[24]. R. W. Young, Evolution of the human hand: The role of throwing and clubbing, *J. Anat.,* Vol. 202, 2003, pp. 165-174.

[25]. A. G. González, D. R. Rodríguez, J. G. Sanz-Calcedo, Ergonomic analysis of the dimension of a precision tool handle: A case study, *Procedia Manuf.,* Vol. 13, 2017, pp. 1336-1343.

[26]. A. U. Batmaz, M. de Mathelin, B. Dresp-Langley, Seeing virtual while acting real: Visual display and strategy effects on the time and precision of eye-hand coordination, *PLoS ONE,* Vol. 12, 2017, e0183789.

[27]. B. Dresp-Langley, Principles of perceptual grouping: Implications for image-guided surgery, *Front. Psychol.,* Vol. 6, 2015, 1565.
[28]. B. Dresp-Langley, Towards expert-based speed-precision control in early simulator training for novice surgeons, *Information*, Vol. 9, Issue 12, 2018, 316.
[29]. B. Dresp-Langley, M. Monfouga, Combining visual contrast information with sound can produce faster decisions, *Information*, Vol. 10, Issue, 2019, 346.
[30]. C. I. Karageorghis, P. Cheek, S. D. Simpson, M. Bigliassi, Interactive effects of music tempi and intensities on grip strength and subjective affect, *Scand. J. Med. Sci. Sports*, Vol. 28, Issue 3, 2018, pp. 1166-1175.

Chapter 5

Microfluidic Technologies for Clinical Biology and Biomedical Applications

Mohamed Yousuff Caffiyar, A. Jabeena and Ismail Hussain Kamal Basha

5.1. Introduction

Microfluidics is the technology of fluid manipulation in channels with dimensions of tens of micrometers [1]. It has gained popular attention in the recent years since its inception in thirty years. With the rising interest in the various area of research such as chemistry, biology, medicine and physical sciences, microfluidics has shown significant developments in these areas. Microfluidics, a branch of MEMS (Micro-Electro-Mechanical Systems) is key enabling factor in the miniaturization of a system in handheld microdevices and deal with the fluid flow control and manipulation in diminutive amounts, typically a few microlitres (μL). With micrometre dimensions of channel, the device has the ability to possess large surface to volume ratios and enable fast reaction times whereby consuming less sample volumes and reagents. This makes the microfluidic devices ideal candidate for applications in biomedical systems and healthcare industry. The sample manipulation and control inside the microchannel can be liquid or gaseous in nature, or a mixture of both and it is controlled using pumps, valves and filters integrated inside the channel. The governing principles of microfluidics are identical to the equations described at the macroscale systems. However, at microscale level, the dominant forces are different from those we experience at the macroscale, and flows typically exhibit properties that can be exploited in microfluidic devices, for example, microfluidic flows

Mohamed Yousuff Caffiyar
C. Abdul Hakeem College of Engineering and Technology, India

are usually strictly laminar with Reynolds number operated at very low number (1<Re< 100) [2]. Laminar flow is rare in macroscopic systems. Microfluidic research has brought a significant revolution in the field of chemistry and biology with its potential development to fabricate lab on chip (LOC) and organ on chip (OOC) devices as similar to what integrated electronic circuits does in computational capabilities. LOCs are microsystems capable of integrating entire biological or chemical laboratories in a single chip, the high level of integration required in LOCs creates a demand for advanced fabrication technologies that are capable of miniaturizing several key fluidic components with the aim of improving the compactness of these devices and their functionalities [3].

5.2. The Impact of Microfluidics on Biomedical Research

Having its distinct features to perform several analytical functions on the same device (lab-on-a-chip), and possibility of automation of labour-intensive steps by integrating other systems to the device, microfluidics has cater to address solutions for various domains of biology such as drug discovery, cell biology, cell separations, genomics and proteomics studies, tissue engineering and developmental biology. With dynamic efforts being made over the last three years, the technology is getting rapidly matured with growing trends in the inventions and fabrications of customized devices which are helpful to address the solutions in clinical, pharmaceutical, or biotechnological needs. One of the most promising developments of microfluidics is point-of-care (POC) devices for various diagnostic applications [4]. POC diagnostic test devices provides rapid results over range of medical tests and promotes a shift away from lab based traditional diagnostic tests to near-patient settings, providing physicians with timely diagnostic information so as to make informed decisions regarding diagnosis and treatment. With growing developments of microfluidics in applications to biomedical research, cell culture and medical diagnostics, microfluidic systems has the ability to offer better representation of the physiological and pathological condition of complex biological systems in a simple handheld device and provides economically cheaper solutions [5]. For downstream analysis of biological samples (such as in stem cell research, cancer research, fertility research and other similar area), it is important in sample preparation stage that targeted biological cells need to be separated from other substances in the sample. Many microfluidic studies describe methods that aim to replace traditional macro scale assays, and usually perform proof-of-concept (PoC)

experiments that attempt to demonstrate the efficacy of the new approach [6]. With rising interest of portable medical diagnostic tools in to for rapid diagnosis of infectious diseases microfluidics enables a more patient-centric and home-testing approach with its lab-on-a-chip technology. Alongside their continual development, vigorous research is in process to replace the animal model by developing the microengineered models to mimic in vivo environments and thereby develop organs and tissue on chip to the patient. This advancements has paved the way to develop key functional units of human organs, known as organs on chips (OOC) [7]. By mimicking natural architecture, this technology has great potential to advance the study of tissue development, to modal organ physiology, drug discovery and development, to replace animal models for efficacy, toxicity testing and biomarker identification [1]. In this chapter, we have attempted to discuss the advancements of microfluidics technologies in the above field of research.

5.3. Microfluidic Technology for Stem Cell Research

In recent years stem cell research has gained considerable interest with recent developments in microfluidics technology. Stem cells are described as being capable of both self-renewal and generating descendants capable of engaging themselves in a number of distinct directions [4]. Stem cells are generally classified into two types. First type being embryonic stem cell (ESC), have pluripotency to differentiate into nearly all cell lineages in the body and the second type is non-embryonic adult stem cell, which are found in various tissues and are multipotent with ability to differentiate to a limited number of cell types. Stem cells have developed promising applications in fields such as tissue engineering and cell therapy, through their ability to genetically transform into a particular type of cell. Globally, comprehensive research is taking place on the development of pluripotent stem cells for cell-based therapies. Pluripotent cells can be isolated and then cultured on a layer of "feeder" cells that provide new indications for several proliferation rounds while preserving their pluripotence [8]. The field of microfluidics has a lot to contribute to stem cell research and in fact, has several reasons why it is best suited to be adopted. By developing perfusion based culture system and its potential to precisely control flow and continuous exchange of nutrients and waste, the microfluidics offers more in-vivo like microenvironments than conventional culture dishes which further enables the control of stem cell fate, affected by various

soluble factors supplied by the culture medium [9]. Stem cells has the properties of unlimited self-renewal in vitro and to differentiate into exactly the same as the originating cell. However identification of cloned cells and performing analysis at single cell level is cumbersome. Sensitive discrimination of gene expression and/or protein levels at single cell level can be performed effectively using microfluidics approach and thus, they have shown increasing attentions in stem cell biology to understand the heterogeneity of stem-cell populations [10]. Further, separation of rare stem cells from heterogeneous populations is often difficult using flow cytometer as it requires tedious process and the cells are exposed to harsh conditions may lead cell damage which eventually results in low recovery rate. Microfluidics-based systems allows separation of stem cells with an advantage of less damaging to cells than traditional cell sorters. For both analysis and separation, microfluidics offers the means of controlling the cells' environment rigorously. Several groups have also reported that stem cells can be separated from mixed cell populations using their dielectric properties, sizes and density or by tagging the cells with magnetic beads coated antibody and thereby generating magnetic force inside micro channel for separation [11-13].

5.4. Microfluidic Technology for Cancer Research

Recent advances in the development of microfluidic devices has made promising avenues for both basic and applied research in cancer. Microfluidics platforms has enabled characterization of cancer cells such as their physical and structural properties, study cancer cell migration to during metastasis and develop systems to enable separation and isolation of circulating tumor cells (CTCs) from blood for various downstream analysis. These CTCs present both a diagnostic marker of metastatic cancer as well as a potential way to sample a cancer genotype without a tumor biopsy [14]. Numerous research has been reported to separate CTCs using microfluidics. The challenges to isolate CTC is its low concentration in most samples. Compare to conventional benchtop flowcytometry sorter, microfluidics based system provides high purity and recovery of CTC from spiked blood samples. Microfluidics device can be fabricated by employing EpCAM antibodies dependent immunomagnetic separation for CTC enrichments however, CTCs from cancers of non-epithelial origin are not detectable with EpCAM-based enrichment [15]. In addition, the binding of antibodies to EpCAM may induce cytotoxicity, thus altering the original state of CTCs and reducing

the reliability of further biological research. The use of antibodies coated labelling is expensive and laborious process as well. To overcome this limitations, researchers have developed numerous label free isolation of CTCs. The microfluidics approach such as acoustic based, density based, hydrodynamic based, dielectrophoresis based techniques does not requires labelling of cells rather, it utilizes the specific properties of cells (such as size, electrical, shape, permittivity, deformability properties etc. of the cell) to debulk them from whole blood samples. Dielectrophoresis based approach uses electrical properties and size of the CTCs to isolate them while inertial microfluidics techniques uses size and hydrodynamic forces of the microchannel to separate. In Acoustic approach, using size and density together with acoustic radiation force generated inside the microchannel can be utilized to isolate the CTC. Other microfluidics approach such as DLD (deterministic lateral displacements), membrane filtrations are also used to separate based on their sizes. This collective approaches were able to produce recovery and purity efficiency of over 95 %. Using microfluidics, it is possible to integrate multiple processes in a single chip and helps to carry out further analysis and diagnosis of cancer easily. Researchers have developed a chip with cell capture arrays that combine cell separations, culture, and drug testing via fluorescence in a single device. It is also important to understand the cancer invasion and immune responses, by analyzing the interaction between cancer cells and other cell types [16]. Microfluidic chip developed by Businaro and co-workers have investigated the cross talk between cultured B16 melanoma cells and spleen cells in separation chambers connected by narrow microchannels [17].

Microfluidic device was also demonstrated to study the cancer metastasis or migration of cancers which are understood by spatiotemporally regulation of signalling gradients [15]. During cancer metastasis, there is a disruption to the healthy physiological gradient that guides cell migration which eventually leads to abnormal cell motility and metastasis. Microfluidic systems has been developed to control spatiotemporal gradients involved in cell migration in vitro. Two types of gradients to regulate cancel cell migration was reported: (i) chemical gradients, and (ii) electrical gradients [15]. Research has shown direction that, both of these gradients can be effectively generated using microfluidics technologies. Alongside the above mentioned applications of microfluidics in cancer research, it also finds applications in single cell analysis and developing tumor microenvironment using microfluidics for cancer research will be discussed briefly in Section 5.6 and Section 5.7.

5.5. Microfluidic Technology for Fertility Research

One in six couples of reproductive age worldwide are affected at least once by some form of infertility. At least 50 million couples are suffering from infertility worldwide. The sperm quality and sperm concentration reduction due to environmental and genetic reasons have also given rise to concerns in many European and American countries facing high infertility rates that in turn prevents population sustainability. In vitro fertilization (IVF) and intracytoplasmic sperm injection (ICSI) are widely-available assisted reproductive technologies (ART) [15]. Sperm sorting, oocyte manipulation, insemination, embryo culturing, and for assessing sperm and embryo quality, can be done using ART which ultimately affecting treatment consequences and the health of offspring [15]. By relying on the advantages of microfluidics technology, several developments and benefits were achieved towards sorting, selection of gamete (sperm or egg). In recent years, a number of microfluidic devices have been developed for sperm quantification, sperm quality analysis, and sperm manipulation and isolation with subsequent use of the purified sperm population for treatment of male infertility. Numerous attempts have been made for sperm isolation and manipulation using microfluidics in the past years. Samuel et.al, developed multiple straight microchannels with collection reservoir, where mobile sperm swims to target outlets while non-motile sperm and debris remain at the inlet behind [18]. Using electrophoresis method, target motile sperm were isolated from a mixture of sperm samples using porous membrane filters which further enables to study the quality of isolated sperms [19]. In another research recently, Jiyoung et.al demonstrated that, motile sperm cells were separated from blood utilizing inertial forces generated inside a micro channel, this techniques has provided high throughput separation of sperm cells using precisely designed spiral channel [20]. Xie et.al have shown that, utilizing chemotaxis of sperm in addition to sperm mobility. They developed bibranch channel mimicking mammalian female reproductive tract and sperms cells are swim-up towards the chemo attractants gradients generated at the outlet reservoirs, thereby allowing there device for both motility screening and chemotaxis testing simultaneously [21].

One area where microfluidic tools have succeeded notably is, the separation of sperm cells from samples with low sperm cell concentrations compared to existing approaches, including the separation of sperm from epithelial cells for forensic examination, from white blood cells in infected semen, and from testicular cells after a

testicular biopsy [18]. As opposed to conventional methods, these passive and active approaches are centrifuge-free. Thus, the sperms undergo the least damage during the selection process. The throughput is higher and a lower amount of reagents is needed. There is a significant potential for microfluidic products enabling sperm selection to emerge on the market and be used as powerful tools in fertility clinics.

5.6. Microfluidic Technology for Single Cell Analysis

It is difficult to examine the causes of human disease due to the variation of gene expression and the physiological condition of the cells in a given population. Compared to bulk cell measurements, single-cell analysis techniques may provide a clearer understanding of the interactions between molecules, organelles, cells and the microenvironment, which can lead through a development of devices and systems for various therapy and diagnosis. Single-cell technologies have become much more powerful and accessible in recent years, although there are limitations. In terms of cell sizes and concentrations of cell elements, the single-cell analysis is theoretically more complicated than the bulk-cell analysis [22]. Most of cells, for example, mammalian and bacteria cells, have micron-scale sizes. Therefore, by using conventional biological devices, such as petri-dishes and well-plates, manipulation of certain cells at the single-cell level is difficult. Furthermore, high-throughput assays are technically difficult on single cells (such as cancer cells). In this context, microfluidic devices have emerged as an exciting prospect for tackling these challenges by providing high-performance data with minimal reagent consumption and assay complexity, and keeps on advancing with technology for single-cell manipulation and analysis for about two decades. Single-cell studies generally involves isolation and capture of single cell to perform analysis, and to address these problem, different microfluidic methods have been developed, such as hydrodynamic [23], electrical [24], optical [25], magnetic [26], and acoustic [27].

Droplet-based microfluidic systems are useful single-cell handling instruments because of their ability to separate cells for further study. As a branch of microfluidics, droplet microfluidics has emerged as a promising method for single-cell encapsulation and control of single-cell enzymatic activities [28]. Single cells are compartmentalize within a picolitre droplets in the continuous phase of oil and with enzymatic chemical reaction inside the droplets isolate each cells thus facilitating the analysis of cells without cross contamination or loss of genetic

materials. Another creative method of high-throughput analysis of single cells is to enclose them within microwells or traps [10]. The potential benefit of microwell methods is that large numbers of living cells can be studied simultaneously on a single chip. A fairly straightforward method for trapping cells using microwell arrays where cells are seeded and permitted to settle into individual compartments that can hold a single cell at each location. Earlier, microfluidic device were developed using micro magnets for manipulating cells in a microfluidic chamber/channel [29]. This method allows the cells to be tagged with immunomagnetic beads by which each cells are captured in chamber embed with micromagnets. The beads are adhere onto the cell surface through specific interactions between the antibody and the antigen.

Shields IV et al. demonstrated that, cancer cells can be effectively separated from blood with high throughput by comprising three modules in single device, which perform acoustic based focusing in the first stage followed by magnetic based separation of labelled cells and finally a periodic array to capture individual cancer cells for on-chip analysis [30]. However, magnetic bead based separation and bonding may damage cell membrane proteins and structures thus damaged making cells in conducive for subsequent cell culture. Further, several research were undergo to understand the cellular behaviour (such as cell morphology, migration, proliferation, differentiation, and apoptosis) using microfluidics that has general scientific and practical value for biology and medicine. Several microfluidics platforms have been developed for the real-time monitoring of cellular behaviour [31]. Microfluidics was also shown potential to perform genetic analysis. Cytogenetic analysis such as chromosomes abnormalities, chromosomes enumeration and chromosomes spreads, were all studied using microfluidics device in the recent years. Molecular genetic analysis to study the functions of genes at molecular level were also studied using microfluidics by developing on-chip reverse-transcription PCR (RT-PCR) for DNA and RNA quantifications and amplifications. Various aspects, including protein species, amounts, activity, as well as protein interaction with other biomolecules, can be analysed using microfluidic devices, with tremendous advantages over conventional method [31].

5.7. Microfluidic Technology for Tissue Engineering

Tissue engineering has now emerged as a potential choice to tissue or organ transplantation. Cells are a crucial factor in tissue regeneration and

repair due to their proliferation and differentiation, cell-cell signalling, biomolecule production and formation of extracellular matrix. In the past the field of tissue engineering has succeeded in creating viable skin, bone, cartilage, bladders and blood vessels. The ultimate aim is to create large pieces of tissue and entire organs, in order to solve the problem of organ scarcity that leaves many people to wait for donor organs due to unavailability. Conventional tissue engineering methods suffer from limitations including limited distribution of biomolecules by diffusion, and lack of natural interactions between the cells themselves and building artificial organs is a challenge; it requires detailed understanding of fundamental biology [32]. Under suitable conditions, the development of tissues involving cell-cell interactions can take in vitro systems closer to living systems. Here is microfluidic lab-on-a-chip platform that provides unique advantages to mimic complex physiological microenvironments in vivo and has been increasingly exploited to cell research. It allows precise microenvironment manipulation to deliver cell soluble factors, create well-defined gradients, incorporate various biocompatible scaffolds and functional components, as well as dynamically alter the application of mechanical signals to cultured cells [33].

Cells must be placed on a scaffold, which gives them structures before they can be coaxed into tissues that form. Microfluidic systems maintain a constant blood supply throughout the growth of Complex Tissue, thereby circumventing the well-known problem of supplying larger tissue structures with a continuous oxygen and nutrient flow, and removal of waste products [34]. For their potential use as replacements for full animal models in basic biological studies and pharmacological and toxicological screens, and as replacement tissues for clinical applications, the creation of realistic tissues in vitro is desirable. Furthermore, in vitro microfluidic technology may be integrated into tissue engineering processes to mimic the cancer cells in-vivo responses to different drugs [35]. Researchers have been investigating the creation of three dimensional (3D) tissue structures that can be used to establish regulated conditions that can guide cells to shape functional tissue [36]. Such tissue generation requires tools to monitor the biological, chemical, and mechanical environment encountered by the cultured cells. Microfluidic systems have been used in recent years to regulate surrounding soluble factor-cell interactions to study phenomena such as gradient presentation or regulated shear stress on cells. In addition, microfluidic systems can be used to investigate factors that control the nature of stem cells to generate a sustainable sources of cells for different

regenerative medicine applications [37]. In addition, using the ability to design and fabricate structured microchannels, artificial blood vessel-like structures can be produced which eventually be used for generating vascularized tissues or disease models to carry out drug screening. Microfluidic systems for the purpose of neural tissue engineering have been designed and developed to understand the behavior of neural migration and differentiation in various microenvironments. Thus microfluidic reveals the promising advantages in the field of tissue engineering with the ability to accurately monitor biochemical gradients and provide the most suitable physical microenvironment for replicating the cell niche.

5.8. Microfluidic Technology for Pathogen Detections (Diagnostic Applications)

Infectious diseases are a major threat to human health and is the leading cause of deaths worldwide. In 2010, an estimated 15 million people died from infectious diseases. Scientist's project that infectious diseases will continue to cause between 13 to 15 million deaths annually until 2030 from contagious diseases such as measles, cholera, and meningococcal disease. The recent and unanticipated epidemics due to the Corona, Zika, and Ebola virus have raised renewed concern over the readiness of health systems worldwide to contain and treat infectious outbreaks. These outbreaks also highlighted vulnerabilities and new transmission modes through global travel. In endemic infections, treatment to cure the patient begins with the correct identification of the infectious agent. For infectious agents that are more virulent, early identification is critical to maximize the patient's chance of survival. The time pressure is more severe in an epidemic situation because a large and increasing number of people need to be accurately screened and treated in order to contain the spread of the infection. Infectious diseases are caused by microbiological organisms like bacteria, fungi, protozoa, worms and prions, commonly termed as pathogens. A dataset from 1980 to 2013 shows that bacteria and viruses represent 70 % of the human infectious diseases and caused 88 % of outbreaks over time [38]. Moreover, these pathogens may cause similar symptoms for most of the infectious diseases, possessing a great challenge for the physicians towards the treatment. For example, the symptoms of fever, weights loss and respiratory problems are commonly caused by bacteria and virus. The drugs used to treat bacterial infections are ineffective towards virus infections.

To identify the infectious agent, a biological sample (saliva, blood, etc.) from the patient is sent to a laboratory for diagnosis. In laboratories, diagnosis procedure are categorized as conventional and molecular methods. The conventional methods include identification of pathogens based on their morphology using electron microscopy, pathogenic antigenor human antibody detection using enzyme-linked immunosorbent assay (ELISA) method [39]. These conventional methods have much lower sensitivity and specificity compared to molecular methods because morphology, antigen and antibodies are common among the family of bacteria, virus and their serotypes. Pathogenic isolation in cell culture is a non-routine and research based method in which the pathogen is detected with its induced characteristic changes in inoculated cells. The molecular methods are highly sensitive and specific methods because these techniques rely on the unique cellular identity of the pathogen either by amplifying specific regions of viral genome or by hybridization with target specific probes. In time-critical and epidemic situations, lab-based diagnosis cannot meet the demands for timely identification of pathogens. The processing capacity of labs are limited because highly trained personnel still perform the processing steps manually. Processing is also slow because the biological sample must be transported from the patient at the point of care (POC) to the lab and results are usually obtained only after 24 hours or more. In resource limited settings, none of this infrastructure exists and frequently, the need for timely action against infectious outbreaks is more severe because of the limited intervention and medication options. Collectively, these issues point to a crucial need for point-of-care tests to identify infectious agents rapidly and accurately [40]. The World Health Organization (WHO) recommends the following criteria for such devices: (i) Affordable; (ii) Sensitive; (iii) Specific; (iv) User-friendly; (v) Rapid and robust; (vi) Equipment-free, and (vii) Deliverable to end-users. Commercial POC tests in the form of diagnostic strips are widely available and frequently use [41] today, like NS1 Bioeasy™, Anigen Rapid Rabies Ag Test kit (Bionote, Korea; LOT NO: 1801088). These test strips use antigen and antibody detection methods but are limited in diagnostic accuracy. Due to this lack of specificity, their utility is limited [40].

Microfluidic technology offers promising techniques to automate genome detection on a chip which has the advantages of requiring reduced sample and reagent volume and of improving processing speed and contamination avoidance on a disposable low-cost device. In addition to this, microfluidic lab-on-a-chip has provided a platform to

conduct chemical and biochemical analysis in a miniaturized format. Miniaturized analysis has various advantage such as fast analysis time, small reagent consumption, high-throughput potentialities, and less waste generation. Moreover, it has the capability of integration, coupling to sample preparation and further analysis. Recently, microfluidic technologies have made a substantial impact on the development of diagnostic tools by providing a cost-effective platform for the implementation of immunoassay techniques. The first microfluidic device was developed by Terry and his research team in 1970 at Stanford University. Since then, many miniaturized microfluidic device are developed for infectious disease detection. Some of the examples are Wang et al. (2012) developed an integrated microfluidic system for HIV detection. They considered nucleotide probes to precisely bind the HIV particles and then attached them to magnetic beads. Later, an on-chip PCR amplification was performed. The whole process is completed within 95 min. Similarly, Zhang et al. (2010) developed another microfluidic device to detect HBV virus. In this microfluidic chip, modified micro-bead array conjugated with Q-dots are used to detect HBV via DNA segments [42]. In recent decade, many research works have been published on microfluidic systems used for the detection of microorganisms. Furthermore, recent developments in the technology and application of microfluidic systems can benefit human health in under-developed countries with limited health infrastructure and with reduced costs.

5.9. Microfluidic Technology for Protein Detection (Diagnostic Applications)

Detection of human diseases at an early stage increases the possibility of successful therapies. Recent research on human disease have shown that the molecular mechanism linked to the disease are more complex in mechanism and are associated with the genetic incidents converting a normal cell into a diseased cell. Monitoring the genetic expressions of one or more proteins and correlating the concentration changes of these proteins can be taken as signature of existing disease and for the prediction of upcoming disease. Diagnosis based on proteins detection have been successful for more than 150 years. Historically, in 1827, Bright et.al used urinary albumin as a diagnostic marker for kidney disease and in 1845 and Bence jones *et.al.* used immunoglobulin light chains for tumor identification [43]. At present, more than 200 different proteins in plasma and serum are used as diagnostic markers for various

diseases including the detection for variety of cancers, heart, renal, and Alzheimer's diseases. The potential benefits of protein as a biomarker for human disease detection has motivated many industrial and academic researchers towards proteomic technologies and to develop rapid and sensitive biomarker detection. Most of the protein biomarker are found in serum-, plasma and urine-based samples and some in saliva, tears, breath condensates, cerebrospinal fluid and tissue lysates extracted from biopsy samples. Though, concentration of these protein biomarkers exists in saliva or blood are at picomolar concentrations, these concentrations are five to seven orders of magnitude lower than the most abundant plasma proteins. Therefore, protein detection with high specificity and sensitivity is still challenging. Traditional laboratory-based protein detection methods make use of Mass-sensing Bi oCD protein array, enzyme-linked immunosorbent assay (ELISA), gel electrophoresis, surface enhanced Raman spectroscopy (SERS), surface plasmon resonance (SPR), colorimetric assay, electrochemical assay, and fluorescence detection [44]. Most of these methods operate on the principle of immunoassays in which a capture antibody is functionalized on a solid support for target capture and a reporter antibody for assay is read-out [45]. However, these methods are operated in stand-alone units thus hampering the need of point-of care testing.

Microfluidics technology possesses remarkable features for simple, low-cost, and rapid disease diagnosis, such as low volumes of reagent consumption, rapid, high portability along with integrated sample processing. An enormous number of microfluidic devices have been developed for protein biomarker detection which includes ovarian and prostate cancer detection, colorectal carcinoma and hepatocellular carcinoma detection, and Alzheimer’s diseases detection. Most of these devices perform heterogeneous (solid phase) sandwich immunoassays. Microfluidic immunoassays have been established from different surfaces for passive antibody adsorption, such as silicon, PDMS, glass, and plastic. Plastics with their hydrophobic nature are typically preferred as surfaces for antibody adsorption. The most common example of antibody adsorption in immunoassays is the immobilisation of antibodies onto a polystyrene microtiter plate (MTP), which is also referred to as gold standard for laboratory immunoassays. Protein adsorption onto glass appears to occur mainly due to electrostatic interactions, which does not favor quantitative immunoassays [46]. Therefore, covalent immobilization procedures are employed in glass based microfluidic devices. Widely, PDMS is used in the manufacturing of microfluidic prototypes. Although hydrophobic, PDMS possess non-specific

adsorption, Nevertheless, the sensitive quantitation of TNF-α with a LLoD of 0.38 pM has been reported based on antibody adsorption to PDMS surfaces.

Commercialization of microfluidic devices are restricted because of the need of sample pre-processing and integration of complex readout system. The performance of microfluidic immunoassay devices should be validated with biological samples; however, only a very few reported studies quantify the protein biomarkers using undiluted whole blood samples. This includes Microcapillary Film (MCF) with a novel fluoropolymer microfluidic material for the quantitation of PSA in whole blood samples eliminating the need of sample [47]. Sample preparation remains one of the main challenges for immunoassay miniaturization; however, fluoropolymer microfluidic strips was developed recently which eliminates the need of sample preparation that. Moreover 90 % of the microfluidic immunoassays integrate expensive, complex, and non-portable readout systems. This is certainly the main reason why microfluidics immunoassays are still research based and prototypically available. To enable microfluidic based earlier diagnostics, a better understating of protein-based immunoassays is important in designing the microfluidic devices for sensitive POC diagnosis. This will curb the number of deaths related to chronic diseases around the world [48].

5.10. Microfluidic Technology for Organ on Chip

Academic and industrial scientists rely heavily on in vivo animal models and platforms for in vitro cell culture to examine biological processes and establish therapeutic strategies. In general, cell lines cultured in vitro have been largely inactivated and lack physiological functions, and preserving cellular functions for extended periods is extremely difficult, even if these functions are natural immediately after harvest. Much of the time, in vivo models produces integrated multi-organ responses which are impossible to achieve using conventional in vitro models. However, the problems associated with ethical consideration with use of the in vivo model raise significant concerns regarding their biological significance to humans. These will finally end up to lose or deactivate cellular functions in cultures. Since, the organs in our body are of a 3D nature and the complex behavior of cells cannot be adequately modeled in 2D cultures, the technology needs upgradation to develop complex microenvironments at high throughput for various analysis and study [49]. Organ-on-a-Chip (OOC) is a new paradigm shift in the field of

microfluidics and lab on chip and has gain popular interest with the highest demand on the market that have been able to revolutionize current approaches to drug screening and toxicology studies and enables to develop in vitro organ model. Since the in vitro environment can be physically and chemically imitated by the use of microfluidic device technology, the maintenance of cellular function and morphology and replication of organ interactions can be accomplished using organ-on-a-chip devices. OOC is useful for studying organ physiological and disease models. It is appropriate for the investigating biological pathways based on tissue architecture and perfusion [50]. OOC can be introduced as an alternative to other cell cultures and animal models for different diseases or drug trials. Organ-on-a-Chips are devices designed to establish a more dynamic physiological environment for culture and control of the cells inside a body's 2D or 3D structure of a specific organ. These chips allow accurate control of the micro-environment to mimic the natural physiological conditions of the cell. Organ-on-a-Chip has gained considerable attention in recent years for the development of drugs and for modeling diseases. Microfluidic technology has allowed researchers and the pharmaceutical industry to study the drugs even more accurately in preclinical environments compared to traditional 2D cell cultures and animal models.

Lung on chip: A layer of alveolar epithelial and endothelial cells is seeded at opposite sides of a porous ECM-coated membrane to create a genuinely 'lung-like' environment with the required fluid and strong mechanical powers [49]. The arrangement of two layers of channels is vertically divided by a microporous membrane. They cultured alveolar epithelial cells on the top surface of the membrane, vascular endothelial cells on the bottom side, and used flowing air and culture media to reproduce the lung structure on a microfluidic system. They reproduced inflammatory reactions. In addition, neutrophils that circulated through the vascular side channel attached to the vascular endothelial cells following the expression of ICAM-1, then migrated through the vascular endothelial cells and pores of the membrane to the alveolar epithelial cell surface and phagocytized the bacteria. Airway Lung-Chip and Alveolus Lung-Chip have been used to study viral infection and accelerate the development of new therapeutics.

Liver on chip: Human Liver-Chip can be configured into different configurations using our approved protocols, depending on the study requirements – including co-culture, tri-culture and quad culture. Human Liver-Chip incorporates relevant extracellular matrix (ECM)

interactions, a hepatocyte and liver sinusoidal endothelial cell interface, together with relevant cyto-architecture and physiological flow. Most liver-on-chip scaffolds use biophysically, preconfigured, or 3D bioprinted scaffolds to allow for architectural 3D reconstruction [32, 36, 51]. But these kinds of scaffolds often have their drawbacks, and ideally, making this architectural restoration without the need for a scaffold would be easier. The key challenge for on-chip liver tissue models is to retain the metabolic function and morphology of the poorly viable cryopreserved human primary hepatocytes. Few groups co-cultured primary hepatocytes with other key liver cells, such as stellate-containing sinusoidal endothelial cells and Kupffer cells or fibroblasts. On-chip liver models involves intact tissues extracted from humans or animals and integrated on-chip for the in vitro assessment of metabolism and toxicity. Y. S. Weng and others; designed and developed non-scaffold liver-on-chip devices by biomimicking tissue hierarchy reconstruction with the introduction of primary hepatic stellate cells (HSCs), to integrate physiologically relevant ECM. Nonetheless, scaffold-based systems have significant drawbacks, such as a scaffold's intrinsic stability and its unpredictable effects on signalling pathways. Despite a lack of scaffold, they managed to create a liver-on-chip that seemed to recapitulate the key features of the liver architecture needed for the hepatic zonation phenomenon. This allowed to overcome the limitations mentioned earlier that come with a scaffold [34].

Heart on a chip can connect to a liver on a chip for cardiotoxicity testing of a new drug via their specific vascular channels. The combination of the cell culturing microchambers and the assisting microfluidic side channels create near-human environments that are biologically relevant for cell growth, toxicity testing, and personalized medicine. Microfluidic platforms for probing the structure and function of actual blood vessels under physiological conditions was also developed. 3D tumor tissue models were developed with multicellular spheroid, hollow fiber and multicellular layer models [49]. Microfluidics perfusion delivers potential therapeutic agents to such 3D tumor cell models, which emulates the heterogeneous blood supply delivered to tumors in vivo. Two groups recently demonstrated by exposing human lung cancer cells to different concentrations of the anticancer drug verapamil (VP-16) [52].

5.11. Microfluidics for Drug Delivery System

Before a drug becomes available for public use, it takes on average 15 years for it to become approved by regulatory agencies, from when it first starts its life at the drug discovery stage. In addition, a significant number of drug candidates fail during clinical trials, largely due to human toxicity that cannot accurately be addressed via current preclinical standards (e.g., in vivo tests). Consequently, developing an effective drug delivery system is key in bringing safe and effective drugs to market. With promising advancement in microfluidic technologies, it has found incredible need in the field of drug delivery and discovery. In the past, microfluidic exosome analysis for drug delivery blueprints; and cancer therapy were reported. Particularly noteworthy is that the use of biomimetics alongside exosome study could be the solution that drug developers have been seeking over the last decade [53]. Usually, Conventional drug delivery methods usually involve animal models, as well as two-dimensional (2D) monolayer cell cultures with intensive bench work.

Microfluidics enables for precise control of fluid delivery in microenvironments. Drug and delivery environments must be studied in order to fully understand the effects of certain drugs within physiological micro-environments which will further provides avenues for studying cell-based drug response and testing. Particularly, the gradient generating microfluidic platforms has been devised for testing drug response in time-evolving and steady-state [54]. In vivo and in vitro organ-on-chips can help speed up the drug delivery process in a safe manner by precisely mimicking human physiological conditions. In terms of the lung-on-a-chip, the respiratory system is one of the most significant entry points of infection in the human body1 and such an entrance can serve as a good microenvironment for studying drug delivery processes; it has been shown that aerosol nanocomplexes are able to diffuse through the alveoli-capillary barrier efficiently. However, nanoparticles behave differently when they are in static and flow conditions [53].

Exosomes are also being used to target cancerous cells for drug delivery. Exosomes that originate from tumour cells possess a different set of characteristics than exosomes from normal cells. Such unique characteristics can be used to increase the effectiveness of exosome-based drug delivery to cancer sites. Microfluidic platforms integrate exosome isolation with downstream molecular marker

profiling, allowing on-line measurement of exosomal markers on surface and inside. The specific circulating exosomes from the blood of patients can be directly detected and shows the high potential of exosomes for tracking and monitoring disease status and therapy [55]. Generation of artificial nanovesicles and exosomes continuously in microfluidic devices is attractive, either through mechanical force breaking down cells or passing cells through hydrophilic microchannels. This engineered nanovesicle is expected to be used in developing safer drug delivery systems. Using microfluidics, cells can be stimulated with spatiotemporal resolution to study, for example, the effect of drug levels on chemotaxis of living cells in vitro. It is even possible to deliver reagents to defined domains of the cell surface or cell interior rather than to expose them to the whole cell. One simple approach to partial treatment of cells was demonstrated by Takayama et al. in mammalian cell [54]. Studies show that there is a close relationship between the concentration of cytokines and the invasion and metastasis of cancer cells. Such characteristics are also used to develop anticancer drugs. The creation of microfluidic concentration gradients is useful for studying cellular response to chemical stimuli. Cells can be stimulated in order to study the effects of drug concentration on chemotaxis and gradients can be applied to cell behavioral studies on stem cell differentiation [21]. Drug screening requires the use of in vivo animal models, but due to its high cost, low throughput, and long analysis time, microfluidic systems are increasingly used to simulate in vivo conditions, such as chip tissue and chip organs. Researchers have developed various gradient generators for investigating cell response to drugs over the long term. Due to the flexibility in creating various gradient shapes upon time, microfluidics provides pathways for studying drug toxicity and monitoring [7]. Using microfluidics devices, it is also made possible to manipulate nanoparticles and provides avenues to understand how nanoparticles interact in vivo which is another important area to be considered whilst designing nanoparticles for drug delivery systems [56]. Nanoparticles are transported through the bloodstream, distributed at the target site and taken up by cells, so all aspects of them need to be well understood to enable the design a successful drug delivery system1. Currently, the least toxic nanoparticle used for in vivo applications is lipid-based. There are two types of drug targeting systems in microfluidics that can be classified as either active or passive. Passive targeting aims to improve blood circulation time of the targeted drug delivery system; active targeting depends on the interactions between the drug and the intended target. Organs-on-chips discussed in above sections are able to control complex interactions between different cell types such as cytokines, nutrients,

growth factors, hormones, extracellular matrix and intracellular junctions [4]. Having its capabilities to understand the real-time analysis of biological processes, the organ-on-a-chip is currently employed for discovering new drugs and studying drug delivery process, though it is still in the early stages of development. Ideally, connecting all of the 'organ-on-a-chip' organ models would create the ultimate drug delivery test system for mimicking the human body. One of the major concern when manufacturing a new drug is the potential for hepatotoxicity [57]. Microfluidics based system has been established that mimicks the liver model for studying drug metabolism and hepatoxicity. Integrating liver on chip with other drug toxicity studies will provide avenues to assess the cytotoxicity of the drug delivery systems [58].

A microfluidics device with hydrogel layer in controllable matrix stiffness mimicks the physiology of the heart in vitro and developed for cardiomycet cultures. Such a platform can control the calcium dynamics of the cardiomyctes and monitor in real time. There has been a huge need for microfluidics in the field of drug discovery, and this exciting technology has been found even to outperform conventional bench work. The development of a full 'human-on-a-chip' would defiantly revolutionise this process [58, 59]. More research into exosomes as blueprints for drug delivery also opens a new avenue for seeking safer, more effective and targeted drug delivery systems. Developing novel drug delivery systems will potentially lead to more drugs being available on the market and microfluidic technology will play an important role as the next-generation tool in facilitating future drug discovery.

5.12. Conclusion and Future Perspective

Microfluidics has seen a tremendous growth in the last three decades in various pharmaceutical and medical fields and an impactful research in the field towards its applications to various diagnosis, treatments, high throughput screening and an attempt for development artificial organs was made. The application of microfluidics in various field of biomedical research and medicines continues to demonstrate stunning results. The potential to integrate various lab based component into miniaturized single device has made microfluidics systems to be key enabling technology for point of care diagnosis and therapeutic applications. In more remote parts of the globe, these on-site diagnostic possibilities can substantially increase treatment rates and the health of local populations. Microfluidics have also had an impact on drug

delivery on the tissue and organ level. It has the ability to effectively and precisely perform drug synthesis and targeted delivery in various ways which eventually avoids unhealthy areas of interest. Another focused area of research, viz. organ-on-chip discussed in the literature, has a big concerns to mimic exact replica of human organs. Due to these reasons, researchers are still hedging their bets and are working on making their devices more and more accurate, before introducing them to a mass-marketing strategy and commercialization. It is evident that, microfluidics provided ground-breaking solutions in almost every possible area of biomedical and clinical biology and has led to transform the way biological research is conducted. Nevertheless, microfluidics research is still considered to be young, as there are several problems that still need to be addressed. The microfluidics devices are just tested in the laboratories so far and are not introduce into the market for commercialization except few tested devices. This may due to their ability to replace certain 'gold standards', for example, biomolecule detection and analysis, that still remains questionable, since their reliability is yet to be satisfactorily demonstrated. Secondly, the technology for fabricating such devices is not widespread [60]. Industry partnered with academia together can able to solve these problems so that, the prototypes and proof of concepts devices developed by laboratories are not restricted within there but realizes its potential to be commercialized.

References

[1]. C. M. Yousuff, E. T. W. Ho, K. Ismail Hussain, N. H. B. Hamid, Microfluidic platform for cell isolation and manipulation based on cell properties, *Micromachines*, Vol. 8, Issue 1, 2017, 15.

[2]. H. Andersson, A. Van Den Berg, Microfluidic devices for cellomics: A review, *Sensors and Actuators*, Vol. 92, 2003, pp. 315-325.

[3]. F. Bragheri, R. M. Vázquez, R. Osellame, Microfluidics, 2nd Ed., *Elsevier Inc.*, 2020.

[4]. D. Lombardi, P. S. Dittrich, Advances in microfluidics for drug discovery, *Expert Opin. Drug Discov.*, Vol. 5, Issue 11, 2010, pp. 1081-1094.

[5]. J. Mairhofer, K. Roppert, P. Ertl, Microfluidic systems for pathogen sensing: A review, *Sensors (Switzerland)*, Vol. 9, Issue 6, 2009, pp. 4804-4823.

[6]. A. Webster, J. Greenman, S. J. Haswell, Development of microfluidic devices for biomedical and clinical application, *J. Chem. Technol. Biotechnol.*, Vol. 86, Issue 1, 2011, pp. 10-17.

[7]. D. Liu, H. Zhang, F. Fontana, J. T. Hirvonen, H. A. Santos, Current developments and applications of microfluidic technology toward clinical translation of nanomedicines, *Adv. Drug Deliv. Rev.*, Vol. 128, 2018, pp. 54-83.
[8]. Q. Zhang, R. H. Austin, Applications of microfluidics in stem cell biology, *Bionanoscience*, Vol. 2, Issue 4, 2012, pp. 277-286.
[9]. H. W. Wu, C. C. Lin, G. Bin Lee, Stem cells in microfluidics, *Biomicrofluidics*, Vol. 5, Issue 1, 2011, pp. 1-26.
[10]. S. Sugiura, K. Nakazawa, T. Kanamori, K. Ohnuma, Application of microfluidics in stem cell culture, in Advances in Microfluidics – New Applications in Biology, Energy, and Materials Sciences, *IntechOpen*, 2016.
[11]. A. A. S. Bhagat, H. Bow, H. W. Hou, S. J. Tan, J. Han, C. T. Lim, Microfluidics for cell separation, *Med. Biol. Eng. Comput.*, Vol. 48, Issue 10, 2010, pp. 999-1014.
[12]. A. Willasch *et al.*, Enrichment of cell subpopulations applying automated MACS technique: Purity, recovery and applicability for PCR-based chimerism analysis, *Bone Marrow Transplant.*, Vol. 45, Issue 1, 2010, pp. 181-189.
[13]. M. J. Mitchell, C. A. Castellanos, M. R. King, Immobilized surfactant-nanotube complexes support selectin-mediated capture of viable circulating tumor cells in the absence of capture antibodies, *J. Biomed. Mater. Res. – Part A*, Vol. 103, Issue 10, 2015, pp. 3407-3418.
[14]. A. Kulasinghe, H. Wu, C. Punyadeera, M. E. Warkiani, The use of microfluidic technology for cancer applications and liquid biopsy, *Micromachines*, Vol. 9, Issue 8, 2018, pp. 1-22.
[15]. P. K. Chaudhuri, M. Ebrahimi Warkiani, T. Jing, Kenry, C. T. Lim, Microfluidics for research and applications in oncology, *Analyst*, Vol. 141, Issue 2, 2016, pp. 504-524.
[16]. D. Pappas, Microfluidics and cancer analysis: Cell separation, cell/tissue culture, cell mechanics, and integrated analysis systems, *Analyst*, Vol. 141, Issue 2, 2016, pp. 525-535.
[17]. L. Businaro *et al.*, Cross talk between cancer and immune cells: Exploring complex dynamics in a microfluidic environment, *Lab Chip*, Vol. 13, Issue 2, 2013, pp. 229-239.
[18]. R. Samuel, H. Feng, A. Jafek, D. Despain, T. Jenkins, B. Gale, Microfluidic-based sperm sorting & analysis for treatment of male infertility, *Transl. Androl. Urol.*, Vol. 7, Issue I, 2018, pp. S336-S347.
[19]. D. P. Patel, T. G. Jenkins, J. M. Hotaling, Microfluidics: A way to interrogate a single sperm?, *Fertil. Steril.*, Vol. 112, Issue 5, 2019, 808.
[20]. J. Son, K. Murphy, R. Samuel, B. K. Gale, D. T. Carrell, J. M. Hotaling, Non-motile sperm cell separation using a spiral channel, *Anal. Methods*, Vol. 7, Issue 19, 2015, pp. 8041-8047.
[21]. L. Xie *et al.*, Integration of sperm motility and chemotaxis screening with a microchannel-based device, *Clin. Chem.*, Vol. 56, Issue 8, 2010, pp. 1270-1278.

[22]. P. Shinde *et al.*, Current trends of microfluidic single-cell technologies, *Int. J. Mol. Sci.*, Vol. 19, Issue 10, 2018, 3143.
[23]. R. Wang, Hydrodynamic trapping of particles in an expansion-contraction microfluidic device, *Abstr. Appl. Anal.*, Vol. 2013, 2013, 496243.
[24]. B. H. Lapizco-Encinas, B. A. Simmons, E. B. Cummings, Y. Fintschenko, Dielectrophoretic concentration and separation of live and dead bacteria in an array of insulators, *Anal. Chem.*, Vol. 25, 2004, pp. 1695-1704.
[25]. T. Ashkin, A. Dziedzic, J. M. Yamane, Optical trapping and manipulation of single cells using infrared laser beams, *Nature*, Vol. 330, 1987, pp. 769-771.
[26]. G. R. Souza *et al.*, Three-dimensional tissue culture based on magnetic cell levitation, *Nat. Nanotechnol.*, Vol. 5, Issue 4, 2010, pp. 291-296.
[27]. X. Ding *et al.*, Cell separation using tilted-angle standing surface acoustic waves, *PNAS*, Vol. 111, Issue 36, 2014, pp. 12992-12997.
[28]. F. L. Battye, A. Light, D. M. Tarlinton, Single cell sorting and cloning, *J. Immunol. Methods*, Vol. 243, Issues 1-2, Sep. 2000, pp. 25-32.
[29]. Y. Zhou, Y. Wang, Q. Lin, A microfluidic device for continuous-flow magnetically controlled capture and isolation of microparticles, *J. Microelectromechanical Syst.*, Vol. 19, Issue 4, 2010, pp. 743-751.
[30]. C. W. Shields IV *et al.*, Magnetographic array for the capture and enumeration of single cells and cell pairs, *Biomicrofluidics*, Vol. 041101, Issue 8, 2014, pp. 14-18.
[31]. T. Luo, L. Fan, R. Zhu, D. Sun, Microfluidic single-cell manipulation and analysis: Methods and applications, *Micromachines*, Vol. 10, Issue 2, 2019, pp. 1-31.
[32]. Q. Zhong, H. Ding, B. Gao, Z. He, Z. Gu, Advances of microfluidics in biomedical engineering, *Adv. Mater. Technol.*, Vol. 4, Issue 6, 2019, pp. 1-27.
[33]. Y. Torisawa, Microfluidic organs-on-chips to reconstitute cellular microenvironments, in Applications of Microfluidic Systems in Biology and Medicine, 2019, *Springer*, Singapore, pp. 227-246.
[34]. J. Zhang, X. Wei, R. Zeng, F. Xu, X. J. Li, Stem cell culture and differentiation in microfluidic devices toward organ-on-a-chip, *Futur. Sci. OA*, Vol. 3, Issue 2, 2017, FSO187.
[35]. C. Beck, M. Goksör, Microfluidics in single cell analysis, in Advances in Microfluidics, *IntechOpen*, 2012.
[36]. N. W. Choi, M. Cabodi, B. Held, J. P. Gleghorn, L. J. Bonassar, A. D. Stroock, Microfluidic scaffolds for tissue engineering, *Nat. Mater.*, Vol. 6, Issue 11, 2007, pp. 908-915.
[37]. H. Andersson, A. Van Den Berg, Microfabrication and microfluidics for tissue engineering: State of the art and future opportunities, *Lab Chip*, Vol. 4, Issue 2, 2004, pp. 98-103.
[38]. K. F. Smith *et al.*, Global rise in human infectious disease outbreaks, *J. R. Soc. Interface*, Vol. 11, Issue 101, 2014, pp. 1-6.

[39]. M. Karle, S. Kumar, R. Zengerle, F. Von Stetten, Micro fluidic solutions enabling continuous processing and monitoring of biological samples: A review, *Anal. Chim. Acta*, Vol. 929, 2016, pp. 1-22.
[40]. I. H. K. Basha, E. T. W. Ho, C. M. Yousuff, N. H. Bin Hamid, Towards multiplex molecular diagnosis – A review of microfluidic genomics technologies, *Micromachines*, Vol. 8, Issue 9, 2017, 266.
[41]. M. Fessler *et al.*, Development of a microfluidic system for measuring HIV-1 viral load, *Bone*, Vol. 23, Issue 1, 2008, pp. 1-7.
[42]. B. T. T. Chirag, M. Lakhani, A. K. Manrai, J. Yang, P. M. Visscher, C. J. Patel, Point-of-care microfluidic devices for pathogen detection, *Physiol. Behav.*, Vol. 176, Issue 3, 2019, pp. 139-148.
[43]. M. A. Ferguson, S. S. Waikar, Established and emerging markers of kidney function, *Clin. Chem.*, Vol. 58, Issue 4, 2012, pp. 680-689.
[44]. E. A. Schilling, A. E. Kamholz, P. Yager, Cell lysis and protein extraction in a microfluidic device with detection by a fluorogenic enzyme assay, Vol. 74, Issue 8, 2002, pp. 1798-1804.
[45]. Y. Wu *et al.*, A neutralizing antibody assay based on a reporter of antibody-dependent cell-mediated cytotoxicity, *AAPS J.*, Vol. 17, Issue 6, 2015, pp. 1417-1426.
[46]. M. Herrmann, T. Veres, M. Tabrizian, Surface modification and characterization of a cyclic olefin copolymer for magnetic bead-based stop-flow microfluidic ELISA, in *Proceedings of the NSTI Nanotechnology Conference and Trade Show (NSTI-Nanotech'06)*, Vol. 2, 2006, pp. 244-247.
[47]. N. Lion, F. Reymond, H. H. Girault, J. S. Rossier, Why the move to microfluidics for protein analysis?, *Curr. Opin. Biotechnol.*, Vol. 15, Issue 1, 2004, pp. 31-37.
[48]. A. H. Diercks, A. Ozinsky, C. L. Hansen, J. M. Spotts, D. J. Rodriguez, A. Aderem, A microfluidic device for multiplexed protein detection in nano-liter volumes, *Anal. Biochem.*, Vol. 386, Issue 1, 2009, pp. 30-35.
[49]. H. Kimura, Y. Sakai, T. Fujii, Organ/body-on-a-chip based on microfluidic technology for drug discovery, *Drug Metab. Pharmacokinet.*, Vol. 33, Issue 1, 2018, pp. 43-48.
[50]. A. U. R. Aziz, C. Geng, M. Fu, X. Yu, K. Qin, B. Liu, The role of microfluidics for organ on chip simulations, *Bioengineering*, Vol. 4, Issue 2, 2017, 39.
[51]. X. J. Li, Y. Zhou, Microfluidic Devices for Biomedical Applications, *Woodhead Publishing*, 2013.
[52]. A. M. Ghaemmaghami, M. J. Hancock, H. Harrington, H. Kaji, A. Khademhosseini, Biomimetic tissues on a chip for drug discovery, *Drug Discov. Today*, Vol. 17, Issues 3-4, 2012, pp. 173-181.
[53]. J. Sun, A. R. Warden, X. Ding, Recent advances in microfluidics for drug screening, *Biomicrofluidics*, Vol. 13, Issue 6, 2019, 061503.
[54]. P. S. Dittrich, A. Manz, Lab-on-a-chip: Microfluidics in drug discovery, *Nat. Rev. Drug Discov.*, Vol. 5, Issue 3, 2006, pp. 210-218.

[55]. M. He, Microfluidic technologies: Lifting the veil of exosomes, *MOJ Proteomics Bioinforma.*, Vol. 1, Issue 3, 2014, pp. 54-55.
[56]. I. U. Khan, C. A. Serra, N. Anton, T. F. Vandamme, Production of nanoparticle drug delivery systems with microfluidics tools, *Expert Opin. Drug Deliv.*, Vol. 12, Issue 4, 2015, pp. 547-562.
[57]. E. S. Björnsson, Hepatotoxicity by drugs: The most common implicated agents, *Int. J. Mol. Sci.*, Vol. 17, Issue 2, 2016, 224.
[58]. J. Deng *et al.*, Engineered liver-on-a-chip platform to mimic liver functions and its biomedical applications: A review, *Micromachines*, Vol. 10, Issue 10, 2019, pp. 1-26.
[59]. S. Damiati, U. B. Kompella, S. A. Damiati, R. Kodzius, Microfluidic devices for drug delivery systems and drug screening, *Genes (Basel).*, Vol. 9, Issue 2, 2018, 103.
[60]. K. Mahesh, S. Vaidya, Microfluidics: A boon for biological research, *Curr. Sci.*, Vol. 112, Issue 10, 2017, pp. 2021-2028.

Chapter 6

A Simple and Accurate Method to Assess Autonomic Nervous System through Sudomotor Function

Kamel Khalfallah, Jean-Henri Calvet, Philippe Brunswick, Marie-Laure Névoret, Hanna Ayoub and Michel Cassir

6.1. Introduction

Peripheral neuropathies are assessed mostly by large fiber tests like vibration perception, pinprick and electromyography. Unfortunately, large myelinated fibers are damaged later in the progression of peripheral neuropathies than small fibers, except in diseases specific to myelin.

The autonomic nervous system, mostly managed by small fiber nerves, is very important for many vital functions like heart rate, blood pressure, digestion, temperature control and grip, but it is not easily assessed today.

The current small fiber tests evaluate temperature (hot and cold sensation) but are subjective and operator dependent, which impacts the reliability of the results. An interesting paper from Peter Dyck shows that even world renowned neuropathy experts could arrive at different diagnoses in the same patients when using the existing sensory tests [1].

The gold standard test for small fiber neuropathies is Epidermal Nerve Fiber Density (ENFD) measured from punch skin biopsies. This invasive

Kamel Khalfallah
Impeto Medical, Paris, France

and lengthy process is not appropriate for recurrent assessments and not recommended for diabetic patients with known impaired healing.

Therefore, starting in the 1990s the Mayo Clinic in Rochester, Minnesota, developed an interesting concept of testing sudomotor function to evaluate autonomic neuropathies and small fiber neuropathies simultaneously and objectively.

First, this chapter will present key information about the physiology of sweat glands and their control *via* small C fibers releasing Cholinergic and Adrenergic neurotransmitters. Then a full physical model of sweat gland behavior in the presence of low direct voltage applied to the skin will be developed and its physico-electrochemical properties demonstrated. This will be followed by a description of the Sudoscan patented technology. Finally, the main results of the principal clinical development programs performed over the last 10 years using this very easy to use technology will be summarized.

6.2. Foundations: The Eccrine Sweat Glands

Two types of sweat glands have been identified: apocrine and eccrine. All mammals have eccrine sweat glands on their paws (palms and soles in apes and humans). In addition, humans are unique in that they have millions of bodily eccrine sweat glands distributed throughout their hair-bearing skin. Although structurally alike and producing a similar water-based sweat, these two types of eccrine sweat glands form two distinct subcategories based on their function and characteristics. Sweat is made on the palms and soles to increase adherence and grip. In contrast, bodily sweat glands produce sweat to regulate body temperature. They are both controlled by the hypothalamus and primarily respond to cholinergic effectors (as for salivation and digestion) [2, 3]. Indicative of their different phylogenic origin, paws and body eccrine sweat glands appear at different times during development (16^{th} vs. 22^{nd} week in humans, respectively) [4, 2, 5].

Eccrine sweat glands are independent from pilosebaceous units. They are made of a coiled tubular epithelium associated in its coiled secretory portion with myoepithelial cells that allow sweat excretion. Eccrine sweat glands are solitary and evenly distributed throughout the skin, although their density varies by skin site [6, 7] with the highest densities on the palms and soles. Their coil is closely associated in the deep dermis with nerve endings, adipose pockets, and vasculature.

6.2.1. Physiological Behavior

Sudomotor function is the only component of the Autonomic Nervous System that is managed only by the sympathetic arm. As shown in Fig. 6.1, sympathetic nervous system physiology is comprised of ganglions near the spine connected to very long thin C fibers innervating the glands. Fibers to the sweat glands on the soles of the feet are the longest small nerves in the body, stretching along the entire leg. These nerves are most often the very first to be damaged in case of metabolic insult, for instance. Consequently, evaluating sudomotor function on the soles of the feet could be the earliest way to detect the first signs of small fiber neuropathies.

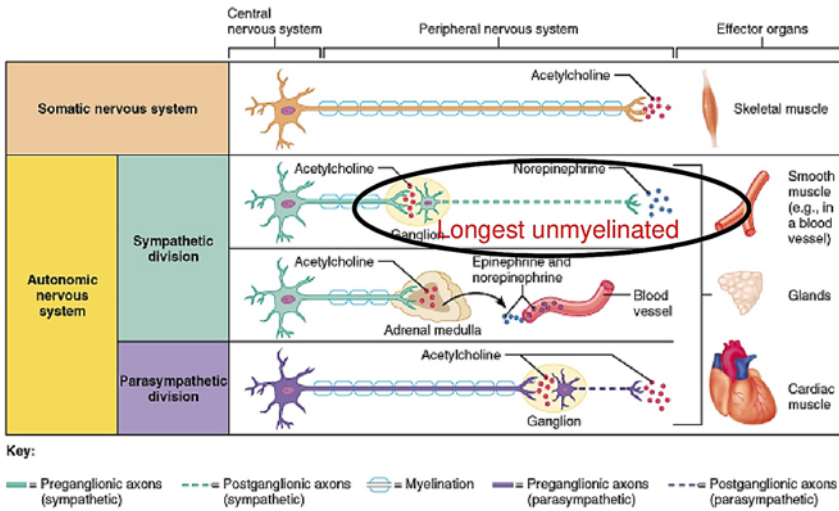

Fig. 6.1. Human nervous system.

One important point to note is that these small nerves can regenerate, as shown by Christopher Gibbons et al. [8], and do so quite faster than other small nerves of the sensory nervous system, making them the best tool to assess treatment efficacy.

In addition, Laure Rittié [9] published some interesting articles demonstrating that sweat glands initiate the healing process of scar formation on the palms of human hands.

During normal physiological function, activation of the eccrine sweat glands starts with a "chemical" stimulus. For instance, in the cholinergic pathway (the most important), this leads to the following sequence, or activation cascade, see Fig. 6.2:

(i) The neurotransmitter acetylcholine binds to its corresponding muscarinic acetylcholine receptor on the membrane cells of the sweat gland wall;

(ii) This activates the G proteins coupled to the neuroreceptor;

(iii) The G proteins, or their intracellular messengers, then modulate ion channels, creating an ion flux through the luminal membrane;

(iv) This polarizes the gland to voltages around 10 mV.

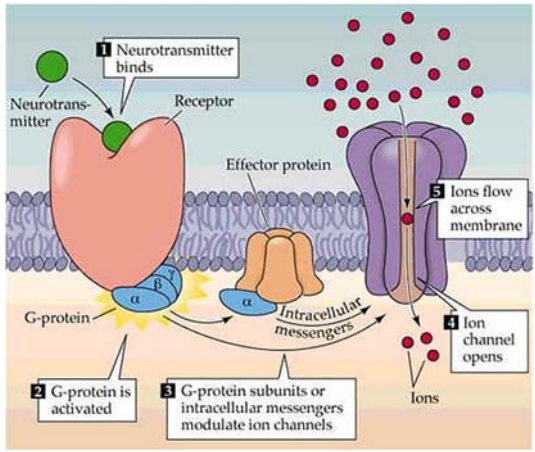

Fig. 6.2. Cholinergic sequence activation.

6.2.2. Agonist and Antagonist Neurotransmitter Activations

The small C nerves of sweat glands involve mainly cholinergic neurotransmitters, but some adrenergic fibers can be found in low percentage. The cholinergic fibers are principally responsible for activation of chloride ion channels *via* Muscarinic M3 receptors, while Adrenergic fibers target the Cystic Fibrosis Transmembrane Conductance Regulator (CFTR) chloride channels, which are well known and have been thoroughly studied in Cystic Fibrosis (CF), (see [10] and Fig. 6.3).

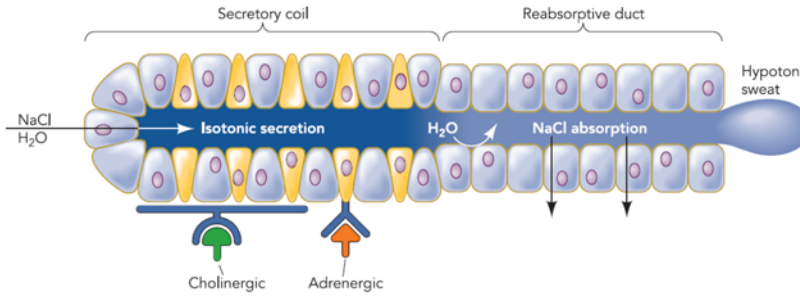

Fig. 6.3. A diagram of the two components and two steps required in the Schwartz-Thaysen mode of exocrine gland secretion to explain the final composition of excreted gland fluid.

Due to defective chloride CFTR channels (the only ones on the duct which should recycle chloride ions), the concentration of chlorides in sweat is elevated in individuals with CF. This unique characteristic is exploited in the diagnosis of CF: the sweat test measures the concentration of chloride ions that are excreted in sweat. Sweating is induced on the skin by pilocarpine iontophoresis. At the test site, an electrode is placed over gauze containing pilocarpine and an electrolyte solution that will not interfere with sodium and chloride measurements. A second electrode (without pilocarpine) is placed at another site and a mild electric current draws the pilocarpine into the skin where it stimulates the sweat glands chemically.

Philip Low at Mayo Clinic proposed to use the same pharmacological stimulation to measure and quantify sweat excretion, leading to the development of the Quantitative Sudomotor Action Reflex Test (QSART). Using this approach, he proved that sudomotor function testing had clinical utility to assess autonomic neuropathies in different diseases like diabetes. However, this pharmacological stimulation is not easy to quantify and to reproduce. In addition, very small quantities of sweat (µl) are difficult to measure and require an environment with very well controlled temperature and hygrometry. QSART measures sweat function at several locations on the body (forearm, proximal & distal leg, and foot) but over an area covering few glands, and normative data depend on gender and age. Finally, chemical iontophoresis will only stimulate cholinergic nerves.

6.2.3. Electrical Stimulations

Sympathetic Skin Response (SSR) has been described as a sudomotor function test but is not defined as a real stimulation of sweat glands. SSR measures a change in the skin electrical potential in response to an arousal stimulus or an electric shock applied to the skin. The test thus assesses a polysynaptic reflex (spinal, bulbar, and suprabulbar); the source of the skin's electrical potential is attributed to sweat glands and the epidermis, but there is no evidence of a direct stimulation being applied to the sweat glands, and any global response to the stimulus applied is not taken into account.

Direct stimulation of the glands

A very important body of scientific work has been published by Vitale et al. [11] on electrical stimulation of recently biopsied eccrine sweat glands from the palms of adult monkeys. An Electrical Field Stimulation (EFS) elicited an immediate secretory response which ceased abruptly upon its termination. This response was inhibited in a dose-dependent manner by atropine (a cholinergic antagonist). Although most glands were inhibited by atropine, a minor component insensitive to atropine was operative in some preparations. Physostigmine (a cholinesterase inhibitor) potentiated the response to a subthreshold EFS. More importantly, lidocaine completely and reversibly blocked EFS secretion but had no effect on methacholine-induced secretion. These experiments prove that the electrical stimulation excites nerves which deliver neurotransmitter to activate secretion.

The conclusion of this article was that "These results confirm that eccrine sweat glands from the palms are activated predominantly *via* cholinergic pathways and that EFS may be used to study the control of secretory function in normal and diseased states".

The details of the electrical stimulation's experimental conditions show that a minimum of 750 mV to 1 V threshold is necessary to activate complete secretion of these eccrine sweat glands.

6.3. Insight into the Sudoscan Measure: Electrochemical Hairless Skin Model at Low Voltages

Sudoscan technology combines reverse iontophoresis, *i.e.,* migration of some ions from the human skin to the electrodes, and steady multiple

chronovoltammetry, which is the application of rectangular direct current (DC) pulses of varying voltage amplitudes.

6.3.1. Global Qualitative Considerations

The measurement relies on the particularities of the outer-most layer of the human skin, called the stratum corneum (SC). It consists of a lipid corneocyte matrix crossed by skin appendages (sweat glands and their follicles). See Fig. 6.4a and [12].

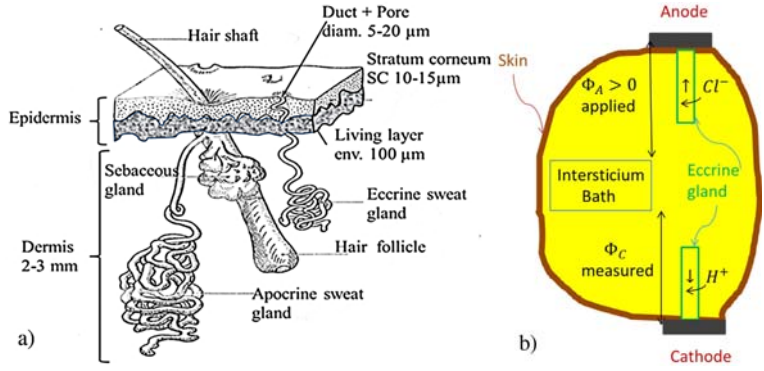

Fig. 6.4. a) Simplified representation of the human skin. b) Electrodes and voltages.

According to [12], at low voltages – less than 10 V- the SC is electrically insulating (essentially capacitive and negligible) and only the appendageal pathway is conductive. In the current application, only eccrine glands on the palms and the soles are concerned. The palms and soles are where these glands are most numerous and present in abundance (~ $500/cm^2$), and therefore, where the electrodes are placed. Their secretory canal extends straight towards the skin where it leads to a pore.

The aim here is to present a new and very complete electrochemical model for the hairless skin at low voltages, previously only partially published [13]. Recall the most complete and well-known model of Chizmazdhev & al [12], which is purely electric (no chemical aspects are considered directly) but remains undoubtedly a starting point and a compulsory passage for more sophisticated and realistic models.

Concretely, an electrode (the anode) applies a low positive direct current (DC) voltage on the skin to the gland, and the current leaves *via* the cathode (see Fig. 6.1b). To simplify and because obviously it is the polarization (*i. e.* the potential difference) that counts, the reference voltage will be the one reached by the body, namely the interstitium in which the gland bathes.

Some minor assumptions are needed and useful: for instance, the electrodes are supposed to behave "perfectly", with no overpotential and the sweat inside the gland (~ salt water) is an incompressible fluid. The interstitium is made up of water and several ions [14-16], mainly (with their concentrations in mmol/L): Cl^- (120), Na^+ (145), H^+ (pH = 7.4), HCO_3^- (20) and lactate (15). So that, as mentioned in 2.3, electro-active species that will migrate and react with electrodes are essentially:

- Chlorides Cl^- at the anode (entering current to the gland);
- The proton H^+ at the cathode (leaving current from the gland), because Na^+ cannot react for considered polarization.

Only these two species will be retained and their reactions and exchanges of electrons with the electrode are assumed kinetically (much) faster than physiological kinetics, which is largely the case with nickel or stainless steel electrodes. Under the electrochemical gradients, the species move (migrate) inside the gland and some exchanges with the interstitium across the wall of the gland will occur. The conservation laws of physics can be applied to eccrine glands in order to understand these physiological kinetics.

6.3.2. General Law of Conservation

It is important to state clearly the origin and hypothesis of the physical laws considered; see [17] for details on the construction of the laws of conservation in classical continuum mechanics. Hence, despite the presence at a microscopic level of species (ions) moving and interacting, the medium will be considered continuous as in classical continuum mechanics, *i.e.*, the geometric parameters of the problem and the infinitesimal volumes, distances needed to proceed some limits are much higher than the size of ions …

A complete exposition on the general law presented in this subsection with concepts necessary to recall, is provided in Appendix 1; we will solely use the main results below.

6.3.3. Geometrical Model of Eccrine Gland, Variables and Currents

6.3.3.1. Geometry and Variables

The eccrine gland is composed of two parts: the secretory portion, a coil where physiologically the sweat is (isotonically) filtered from the interstitium; and the excretory portion where some species can move in both directions (entry or absorption according to their electrochemical gradient) across some ionic channels or not. The excretory portion is a quasi-straight duct that leads to a pore on the skin surface. These two regions have lengths of the same order, with the coil being slightly larger than the duct [14].

The geometrical model consists in unrolling the coil and joining it to the duct to form, as in the Chizmazdhev model [12], a cylindrical tube, but here of a finite and more realistic length. See Fig. 6.5.

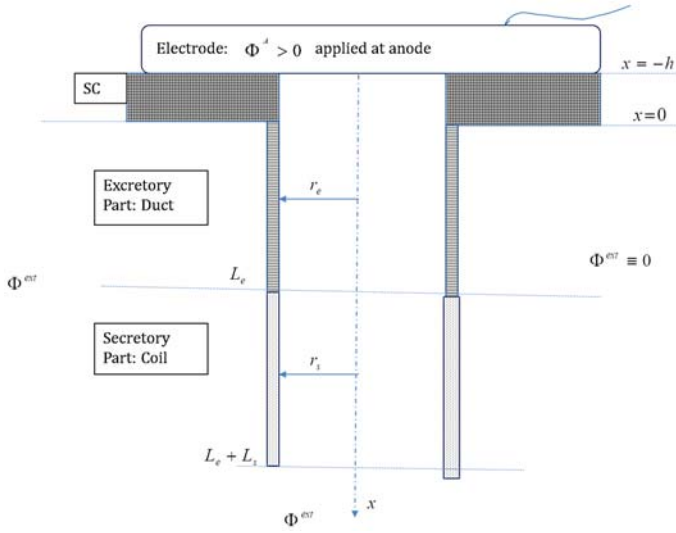

Fig. 6.5. Geometrical model for the eccrine gland.

The principal variables are the concentrations c_k and the velocities u_k of the electro-active ions present in the sweat: $k \in \mathbb{S} = \{Cl^-, H^+\}$. We shall add the electric potential inside the gland Φ. It will be expressed

from the principal variables, see further. They are all functions of (x, t), where x is the abscissa along the axis and t is time.

The geometric parameters are:

h: thickness of the stratum corneum (SC),

r_e: radius of the duct, r_s: radius of the coil,

Lengths L_e, $L_s$of excretory and secretory portions.

The electrical parameters are:

σ: conductivity of the electrolyte (sweat),

Φ^A: potential applied at the anode,

Φ^{ext}: potential reached by the body after the application of the anodic tension. As previously specified, to simplify the analysis and the calculations, the potential $\Phi^{ext} = 0$, will be chosen as reference.

Surfacic conductances of the wall of the two portions, G_k^e, G_k^s, depend on the species k and are generally a function of the potential difference between both sides of the gland wall $(\Phi - \Phi^{ext})$. They may involve the gaping probabilities of some ionic channels and/or electroporation phenomena, see [12].

Surfacic capacitances of the wall of the two portions, C_k^e, C_k^s, may depend on the species k and are almost constants, according to Chizmazdhev [12].

6.3.3.2. The Currents

A. Cross-wall current: is a transverse current due to charges that cross the wall of the gland, and which depends on the ion k. Its density (per unit area on the wall of the gland) depends on the way the crossing occurs, through an ion channel or not.

The ion channel is related here to the Cl^- ion that can go through this epithelial membrane using its own dedicated ion channel [19-21]. This ion channel approach is more fecund than a simple conductance model because it also considers the chemical gradient. The density of this current J_k^{cross} for ion k is given by

$$J_k^{cross} = z_k . G_k . \left(\Phi - \Phi^{ext} - \Phi_k^{Nernst}\right),$$

where z_k is the charge of the ion and G_k the conductance per unit area, Φ_k^{Nernst} is the equilibrium potential of the ion according to Nernst's law (see [22] and Fig. 6.6)

$$\Phi_k^{Nernst} = \frac{R.T}{z_k.F}.ln\left(\frac{c_k}{c_k^{ext}}\right),$$

in which R is the perfect gas constant, T is the absolute temperature and F the Faraday constant (charge of a mole). In physiological polarizations, this channel behaves according to Boltzmann function, voltage dependent.

Here, it is important to mention that the muscarinic channels are driven by cholinergic neurotransmitters, which are supposed to be voltage dependent. The duct, meanwhile, consists essentially of CFTR channels that are minimally voltage dependent and especially sensitive to the chemical (concentration) gradient.

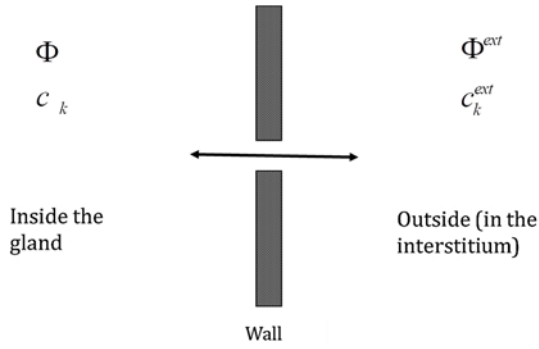

Fig. 6.6. Channel across the gland wall.

B. Capacitive wall current: is a transverse current due to charges that accrue on (or leave) the wall of the gland; it may depend on the ion k and its density (per unit area on the wall of the gland) and is expressed as follows:

$$J_k^{capa} = z_k.C_k^p.\frac{\partial \Phi}{\partial t}, p \in \{s, e\}, \quad (6.1)$$

where C_k^x is the capacitance per unit area, which is almost constant ~0.5 $\mu F/cm^2$ [12].

This current is unsteady (*i.e.,* it vanishes at steady states).

C. Axial current: is a current along the gland axis due to the motion (migration) of ions following this axis inside the gland. The surfacic density of the axial current, as a function of the main variables, for any species k, is by definition:

$$J_k^a = F.z_k.c_k.u_k, \quad (6.2)$$

Then the axial current is given by:

$$I_k^a = \pi.r^2.J_k^a,$$

and the total density and current are:

$$J^a = F.\sum_k z_k.c_k.u_k, I^a = \pi.r^2.F.\sum_k z_k.c_k.u_k$$

6.3.3.3. Ohm's Law and Electrical Field

Ohm's law stipulates that the current = conductance * potential difference; thus conductance = conductivity * surface/length. When applied to the (previous) axial current:

$$I^a = -\sigma.\pi r^2 \frac{\partial \Phi}{\partial x} \quad (6.3)$$

The electric field $\mathbb{E}$ is inferred therefrom, which by definition is:

$$\mathbb{E} \equiv -\frac{\partial \Phi}{\partial x} = \frac{F}{\sigma}\sum_k z_k.c_k.u_k \quad (6.4)$$

6.3.4. Governing Conservation Equations

It is shown in the following that the whole problem can be solved sequentially: first the mass equation will lead to the potential, then the momentum balance gives the constant concentration, and finally the velocity can be deduced from Ohm's law.

6.3.4.1. Mass Conservation

As represented in Appendix 1 equation (6.15) and Table 6.1, the conservation of mass can be written:

$$\frac{\partial}{\partial t}(\rho\,) + \frac{\partial}{\partial x}(\rho\, u) \;=\; \mathcal{A}$$

It remains now to specify the source term $\mathcal{A}$ which represents, per unit volume, the loss or gain due to the transverse (cross-wall and capacitive) current. This is described in Appendix 2.

Finally, with the concentration, the mass balance is given by:

$$\frac{\partial c_k}{\partial t} + \frac{\partial (c_k.u_k)}{\partial x} \;=\; \frac{-2}{r.F}.J_k^t\,, \tag{6.5}$$

where $J_k^t \;=\; J_k^{cross} + J_k^{capa}$.

This is recognized as a classical transport equation with an original source term.

Thus, by multiplying (6.5) with z_k, using (6.3) and (6.4), the (total) axial current is written:

$$\pi.r^2.F\,\frac{\partial\left(\sum_k z_k.c_k\right)}{\partial t} + \frac{\partial I^a}{\partial x} \;=\; -2\pi.r.\sum_k z_k.J_k^t \quad ,$$

which at steady state ($\partial/\partial t$ = 0) shows that the variation of the axial current equalizes the sum of the transverse currents.

Now as $J_k^t \;=\; J_k^{capa} + J_k^{cross}$, by using expression (6.1) of J_k^{capa} and Ohm's law (6.3) with the capacitive currents gathered, we end up with:

$$\frac{2F}{r}\frac{\partial\left(\sum\; z_k.c_k\right)}{\partial t} + \left(\sum_k C_k\;\right)\frac{\partial \Phi}{\partial t} \;=\; \frac{\sigma.r}{2}\frac{\partial^2 \Phi}{\partial x^2} - \sum_k z_k.J_k^{cross}$$

To compare to the purely electric balance equation[7] of Chizmazdhev [12]: eq. (8) page 846, in which the first term does not exist! See the extract in Fig. 6.7.

[7] which is the unique equation of the model of Chizmazdhev.

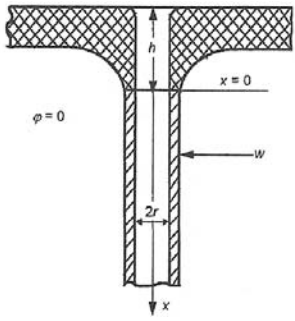

experimental protocol. The potential distribution along x can be found from the balance equation for electric current averaged over the tube cross section

$$C_w \frac{\partial \varphi}{\partial t} = \frac{\sigma r}{2} \frac{\partial^2 \varphi}{\partial x^2} - G_w \varphi \qquad (8)$$

with initial and boundary conditions

$$\varphi|_{t=0} = 0, \quad \varphi|_{x\to\infty} = 0, \quad \text{and} \quad \left(\varphi - h\frac{\partial \varphi}{\partial x}\right)\Big|_{x=0} = U \qquad (9)$$

The last condition is a consequence of zero wall conductance in the upper, SC-lined region ($-h \leq x \leq 0$). We neglect the potential drop across the resistance $R_b + R_c$,

Fig. 6.7. Extract from Chizmazdhev [12].

6.3.4.2. Momentum Conservation

Appendix 1 equation (6.15) and Table 6.1 demonstrate that the momentum conservation is written:

$$\frac{\partial}{\partial t}(\rho\, u) + \frac{\partial}{\partial x}(\rho\, u^2) = \mathcal{F} \qquad (6.6)$$

It remains now to specify the source term $\mathcal{F}$ which represents, per unit volume, the resultant of the present external forces. In the following, and since only one species is involved at each electrode side, the species index i will be dropped.

The ions are supposed to be rigid spheres moving in a continuous incompressible fluid. Recall that when some charged species are in motion, they create an electric field $\mathbb{E}$ (already seen) and a magnetic one $\mathbb{B}$.

Assuming that thermal agitation and interactions between species and with the wall are negligible and that Stokes law [24] is applicable, the species is submitted to the following forces:

Lorentz force:

$$z.e.\mathbb{E} + z.e.u \wedge \mathbb{B},$$

the second term is rigorously null in the 1D model because it is orthogonal to the velocity.

Drag force due to sweat opposition:

$$-\xi.(u-v),$$

where v is the speed of sweat (here $v = 0$, because the application of the electrode firmly against the skin plugs its gland pores and blocks the physiological sweat flow) and ξ is the Stokes coefficient [24] given by

$$\xi = 6\pi.\mu.\mathcal{H},$$

where μ is the dynamic viscosity of the sweat (water) and $\mathcal{H}$ the hydrodynamic radius of the ion.

Stokes law is only approximative because the shape of the ions is certainly not spherical. Moreover, at a microscopic scale, the ions bathe in a medium far from being continuous but rather filled with particles of similar size to one of the ions studied. However, the hydrodynamic radius is the radius of a hypothetical hard sphere that diffuses with the same speed as the ion. And in fact, deduced from the real mobility of the ion in the electrolyte, defined by:

$$\mathcal{M} \equiv lim\, u/\mathbb{E} = (z.e)/\xi,$$

which was tabulated, see for example Atkins & al [25].

Thus, the resultant force is:

$$\mathcal{R} = z.e.\mathbb{E} - \xi.u$$

And per unit volume

$$\mathcal{F} = \mathcal{R}.\frac{\rho}{m} \equiv \mathcal{R}.\frac{c.M}{m}$$

We infer finally the momentum conservation law:

$$\frac{\partial(c.u)}{\partial t} + \frac{\partial(c.u^2)}{\partial x} = \frac{z.e}{m}.c.\mathbb{E} - \frac{\xi}{m}.c.u, \qquad (6.7)$$

6.3.4.3. Momentum Steady Equation: Concentration Constancy

A numerical solution of the whole problem, *i.e.,* the previous partial differential equations augmented with suitable initial and boundary conditions, although it may be delicate, is possible. Here it is conceivable to simplify the problem to obtain analytical results in two ways:

- Considering steady solutions, which allow capacitive aspects and time derivatives to vanish;

- Considering, as assumed in Section 6.3.1, only electroactive ions, *i. e.,* Cl^- at the anode and H^+ at the cathode.

At steady state, the equation for the momentum, for chloride near the anode, reduces to:

$$\frac{d(c.u^2)}{dx} = -\frac{e}{m}.c.\mathbb{E} - \frac{\xi}{m}(c.u)$$

A main result is the theorem of constant concentration:

Assuming that c is constant then:

$$c_* \leq c \leq c_*.(1+\alpha),$$

with

$$\alpha = \frac{8\, m.e.G.\Phi^A}{\xi.\left[r.\xi.\sigma+\sqrt{(r.\xi.\sigma)^2+16\ \sigma.m.e.r.G.\Phi^A}\right]},$$

$$c^* = \frac{\xi.\sigma}{e.F},$$

$$\mathcal{C} = \frac{\sigma^2.m}{F^2.e}$$

Consequence:

$$\boldsymbol{If\ \alpha \ll 1\ then\ c = Cte = c_*}$$

The proof is developed in Appendix 3.

Some numerical applications are necessary to obtain the order of magnitude of the quantities $c^*, \mathcal{C}\ and\ \alpha_{abs}$, see Fig. 6.8.

Thus, in both cases, it appears clearly that the error is absolutely negligible and this leads to a constant distribution of the concentrations along the gland's axis, remarkably almost equal, for chloride ions, to the concentration in the interstitium (bath): ~120 $mmol/L$. Fig. 6.9 illustrates this remarkable result and recalls the shape of the distribution of the concentration of chlorides in the healthy physiological state: isotonic filtration in the secretory coil and reabsorption in the excretory duct.

General Data	
μ [kg/(m.s)]	0,001
σ [S/cm]	0,01
e [C]	1,602176E-19
F [C/mol]	96485
N	6,022415E+23
r [cm]	0,001
Gmax [μS/cm2]	10
Φ_{max} [V]	1

Ions Data Input		
	Cl-	H+
ℵ [m2 /(s .V)]	7,98E-08	3,6230E-07
H [m]	1,00E-10	2,3459E-11
M [kg/mol]	0,035	0,001

Ions Data Output		
	Cl-	H+
m [kg]	5,8116E-26	1,6605E-27
ζ	2,0077E-12	4,4222E-13
ℭ	3,8964E-17	1,1133E-18
c* [mmol/L]	129,88	28,61
α_{abs} [mmol/L]	1,4211E-14	-1,7764E-15
α_{relat} [%]	1,0942E-14	-6,2095E-15

Fig. 6.8. Numerical application for $\boldsymbol{Cl^-}$ near the anode and $\boldsymbol{H^+}$ near the cathode.

Uniqueness of this solution is ensured since $\mathcal{C} \ll 1$ and all the other terms in equation (6.20) of Appendix 3 are bounded and of the order of ~1.

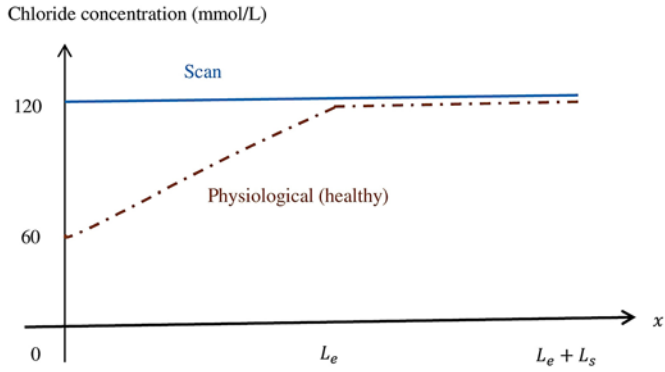

Fig. 6.9. Distribution of the concentration of chlorides inside the eccrine gland, along the axis of the gkand.

This simple result is noticeable and will simplify the mass equation because the equilibrium potential will be null.

6.3.4.4. Mass Steady Equation

For the proton, there is no dedicated channel; it is a "passe-partout".

For chloride ions, the steady state can be expressed as $c(x) = Cte = c^{ext}$, which implies that the equilibrium (Nernst) potential, see 6.3.3.2, is constant and almost null: $\Phi_k = Cte \approx 0$.

So that in all cases, the conservation of mass is reduced to:

$$\frac{d(c.u)}{dx} = \frac{-2.z}{r.F}.G.\Phi \tag{6.8}$$

Taking into account Ohm's law $\left(c.u = \frac{\sigma}{F}.\frac{d\Phi}{dx}\right)$, at steady state, the potential can be depicted using an ordinary (non-linear) differential equation:

$$\frac{d^2\Phi}{dx^2} = \frac{2}{r.\sigma}.G.\Phi, \tag{6.9}$$

with $G = G(\Phi)$.

Hence, a complete decoupling between the equations is observed and the whole problem can be solved sequentially: first, the momentum balance yields the constant concentration, then the mass equation (6.9) will lead (see next subsection) to the potential, and finally the velocity can be deduced from Ohm's law.

6.3.5. Steady State Additional Analytics for the Conservation of Mass Equation

Considering the steady conservation of mass equation just obtained, augmented with suitable boundary conditions, and recalling that no steady contact discontinuity in a medium with moving species, as seen in Appendix A1.4, then the model reduces to the system of differential equations, with notations from Fig. 6.5.

Current continuity at the entry of the duct:

$$\frac{d\Phi_e}{dx}(0) = \frac{\Phi_e(0)-\Phi^A}{h}$$

Balance in the duct:

$$\frac{d^2\Phi_e}{dx^2} = \frac{2}{\sigma.r}G_e(\Phi_e).\Phi_e$$

Combine with the coil (continuity of current and potential):

$$r_e^2\frac{d\Phi_e}{dx}(L_e) = r_s^2\frac{d\Phi_s}{dx}(L_e), \Phi_e(L_e) = \Phi_s(L_e)$$

Balance in the coil:

$$\frac{d^2\Phi_s}{dx^2} = \frac{2}{\sigma.r} G_s(\Phi_s).\Phi_s$$

Current continuity at the end of the coil:

$$\frac{d\Phi_s}{dx}(L_e + L_s) = -\frac{G_s(\Phi_s(L_e+L_s)).\Phi_s(L_e+L_s)}{\sigma}$$

To progress in the exploration for the last equations, a minor but quite obvious assumption is necessary:

$$\forall \Phi > 0, G(\Phi) > 0 \text{ and } G \text{ increasing}^8$$

Then the first lemma can be proven:

$$\forall x, \Phi(\mathrm{x}) \leq \Phi(0) \leq \Phi^A \text{ and } \Phi \text{ decreasing}$$

The proof is demonstrated in Appendix 4.

6.3.5.1. The Voltage inside the Gland is Almost Constant

In fact, because the human skin is electrically weakly conductive, the model solution can be shown to be quite close to the linearized problem. In a first step, we begin by the lemma:

Consider the simplified linearized model (with the same upper boundary condition):

$$\frac{d^2\Phi^{simple}}{dx^2} = \frac{2}{\sigma.r} G_s(\Phi^A).\Phi^A = Cte,$$
$$\frac{d\Phi^{simple}}{dx}(L_e + L_s) = -\frac{G_s(\Phi^A).\Phi^A}{\sigma},$$

Then:

$$\forall x, \Phi^{simple}(x) \leq \Phi^A \text{ and } \Phi^{simple} \text{ decreasing,}$$

$$\forall x, \Phi(\mathrm{x}) \geq \Phi^{simple}(x)$$

Now, the important corollary can be stated:

[8] This hypothesis can be relaxed by assuming it is monotone, which is always observed

We have

$$\forall x, \Phi^A.(1-\varepsilon) \leq \Phi(\mathrm{x}) \leq \Phi^A,$$

with

$$G_e = G_e(\Phi^A) \text{ and } G_s = G_s(\Phi^A),$$

$$\varepsilon = \frac{G_s}{\sigma.r_s.r_e^2}[r_s^3(h+L_e) + r_e^2.L_s^2 + r_s.L_s(r_e^2 + 2r_s[h+L_e])] +$$

$$+\frac{G_e}{\sigma}[L_e(2h+L_e)]$$

The order of magnitude is given in Fig. 6.9 where the parameters of the gland are taken from [12, 14]. No doubt, $\varepsilon < 8\,\% \ll 1$. To illustrate this, see the following Fig. 6.10(a) for realistic simulations corresponding to different patient status.

The proof of the lemma and corollary is demonstrated in Appendix 5.

6.3.5.2. The Axial Current is Almost Piecewise Linear

The important corollary continues as follows:

Let $I^a(\Phi^A, x)$ be the axial current and $I^{a\_simple}(\Phi^A, x)$ be the simplified current, then

$$I^{a\_simple}(\Phi^A, x) =$$
$$= \pi.\Phi^A.\begin{cases} 2G_e(\Phi^A).(-x+L_e)r_e + G_s(\Phi^A).r_s(2L_s+r_s), \text{if } x \leq L_e \\ G_s(\Phi^A).r_s(-2x+2L_e+2L_s+r_s), \text{otherwise} \end{cases}$$

And if $\varepsilon < 1$:

$$\forall x, I^{a\_simple}(\Phi^A.[1-\varepsilon], x) \leq I^a(\Phi^A, x) \leq I^{a\_simple}(\Phi^A, x)$$

Fig. 6.10(b) confirms this result with realistic simulations.

For the proof, see Appendix 6.

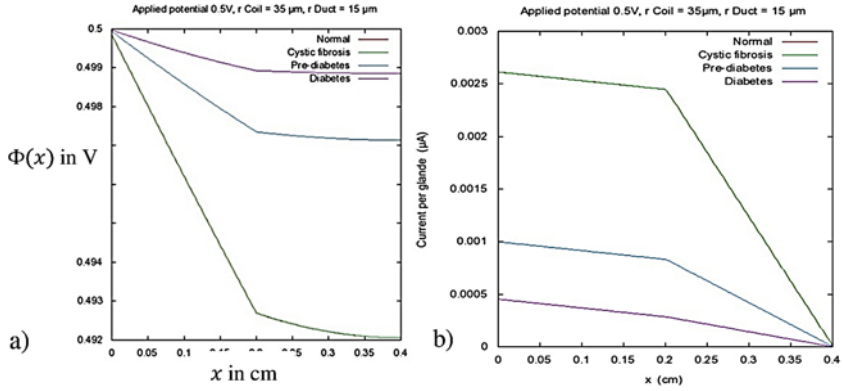

Fig. 6.10. Along the gland axis a) Voltage is almost constant, b) Current is quite piecewise linear, Normal and Cystic fibrosis curves are confused because the voltage imposed here (0.5 V) is before detachment (see Fig. 6.12 below).

6.3.6. Skin Conductance: Gland Wall Ion Permeability

One parameter of the measured signal, among others, see Section 6.4, is the Electrochemical Skin Conductance (ESC). It is deduced from the (axial) current crossing the electrode and the applied voltage Φ^A. Because, from the previous formula

$$I^{a\_simple}(\Phi^A, 0) = \pi.[2G_e(\Phi^A).L_e.r_e + G_s(\Phi^A).r_s(2L_s + r_s)].\Phi^A$$

The main theorem can be proven:

Notations by definition:

$$ESC(\Phi^A) = \frac{I^a(\Phi^A,0)}{\Phi^A}, \tag{6.10}$$

The (total) conductance of the gland wall:

$$GWC(\Phi^A) = 2\pi.r_e.L_e.G_e(\Phi^A) + 2\pi.r_s.L_s.G_s(\Phi^A) + \pi.{r_s}^2.G_s(\Phi^A)$$

Result:

$$(1-\varepsilon)GWC(\Phi^A.[1-\varepsilon]) \leq ESC(\Phi^A) \leq GWC(\Phi^A)$$

To demonstrate this, the previous result with the axial current can be used:

$$\forall x, I^{a\_simple}(\Phi^A.[1-\varepsilon], x) \leq I^a(\Phi^A, x) \leq I^{a\_simple}(\Phi^A, x),$$
$$\Rightarrow I^{a\_simple}(\Phi^A.[1-\varepsilon], 0) \leq I^a(\Phi^A, 0) \leq I^{a\_simple}(\Phi^A, 0),$$

and

$$I^{a\_simple}(\Phi^A, 0) = \pi.[2G_e(\Phi^A).L_e.r_e + G_s(\Phi^A).r_s(2L_s + r_s)].\Phi^A$$

6.3.7. Normalization

To conclude this section, normalization of the conductances is necessary to refine results. The range of skin conductance is from a few µS to several hundred µS. The aim of this normalization is to pack very high and healthy conductances as well as stretch weak and problematic conductances. For a gross conductance Y expressed in µS, the normalization is defined by the increasing dimensionless bijection from $[0, +\infty[$ to $[0, 100[$:

$$Y_{norm} = \frac{100.Y}{X_{ref}+Y},$$

where $X_{ref} = 40\ \mu S$

The theorem is written:

Given:

$$\theta = \frac{\varepsilon.X_{ref}}{X_{ref}+(1-\varepsilon).GWC(\Phi^A.[1-\varepsilon])},$$

where $GWC(\Phi^A)$ in μS. Then:

$$\forall \Phi^A, (1-\theta).GWC_{norm}(\Phi^A.[1-\varepsilon]) \leq ESC_{norm}(\Phi^A) \leq \leq GWC_{norm}(\Phi^A)$$

The order of magnitude is given in Fig. 6.11. No doubt, $\theta < 0.8\,\% < \varepsilon < 8\,\% \ll 1$.

The second inequality is obvious thanks to the increasing bijection. For the first one, we have:

$$ESC_{norm}(\Phi^A) = \frac{100.ESC(\Phi^A)}{X_{ref}+ESC(\Phi^A)} \geq \frac{100.(1-\varepsilon)GWC(\Phi^A.[1-\varepsilon])}{X_{ref}+(1-\varepsilon)GWC(\Phi^A.[1-\varepsilon])} =$$

$$= GWC_{norm}(\Phi^A.[1-\varepsilon]).\frac{(1-\varepsilon)(X_{ref}+GWC(\Phi^A.[1-\varepsilon]))}{X_{ref}+(1-\varepsilon)GWC(\Phi^A.[1-\varepsilon])} =$$
$$= (1-\theta).GWC_{norm}(\Phi^A.[1-\varepsilon])$$

Here, in Fig. 6.12, are displayed realistic simulations corresponding to different patient status and their conductances. An actual measurement will be presented in Section 6.4.

Gland density (/ cm2)	500
Electrode area (cm2)	30
Number of glands	15000
Duct length (cm)	0,2
Coil length (cm)	0,2
Duct radius (cm)	0,0015
Coil radius (cm)	0,0035
SC thickness (cm)	0,004
Sweat conductivity (µS/cm)	10000
Xref Normalisation (µS)	40

Normalize conductance max	90			
Conductance (µS)	360			
Gland conductance (µS)	0,024			
Ratio Ge/Gs	Ge (µS/cm2)	Gs (µS/cm2)	eps ε	teta θ
0,1	0,523249	5,232491	7,38%	0,79%
0,05	0,267113	5,342264	7,47%	0,80%
0,01	0,054335	5,433455	7,53%	0,81%

Fig. 6.11. Numerical application with very high and realistic electrochemical skin conductance.

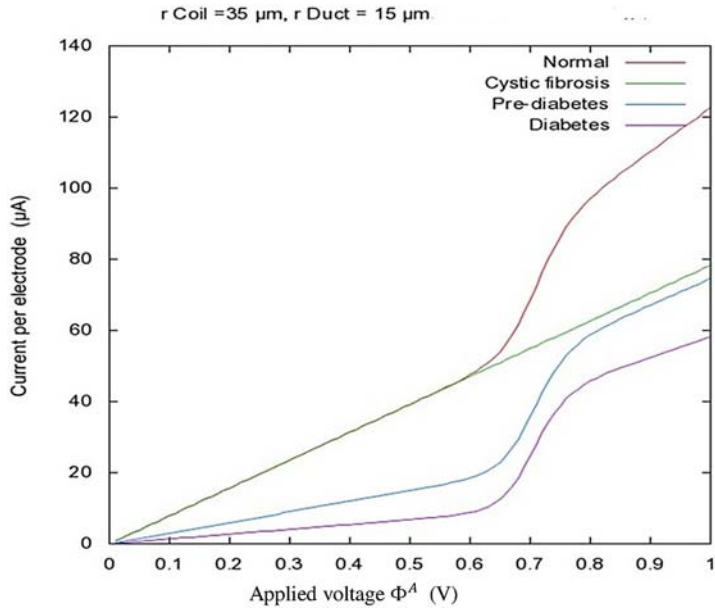

Fig. 6.12. Curve current – Applied anodic voltage.

6.3.8. Section Conclusion

The voltage applied on the anode is nearly the same as the one applied on the nerves on the secretory portion, which confirms that these sympathetic nerves are electrically stimulated and can deliver, if they are present, their neurotransmitters to open the chloride ions channels as seen in Section 6.2.

ESC measurement gives the possibility of strictly determining the conductance of the walls of the eccrine glands, *i.e.*, the capability of the gland to secrete ions. Thus, when these glands are activated and stimulated by electric polarization, sudomotor function is evaluated very precisely. ESC measurement, in addition to other parameters of the signal, (see next section), are measurably impacted in certain pathologies and treatments, as further described in Section 6.5.

Thus, to conclude here, ESC does not depend on concentrations, sweat conductivity or **stratum corneum thickness**. As for prospects, the technology could be used as an *in vivo* and non-invasive tool for the reverse problem: deduce immediately the surfacic conductances of the two portions, the excretory and secretory, and also link the sudomotor function and electrical characteristics of glands: C, G to structure *i.e.,* muscarinic and adrenergic innervation quality and diverse ion channels, pumps, shunts and co-transporters.

6.4. The Sudoscan Technology

Two PhD research projects have been devoted to the electrochemistry of the technology, notably, the electrochemical behavior of different types of electrodes with an electrolyte mimicking sweat, see publications [28] and [31], in collaboration with the Engineering Institute Chimie ParisTech, France (part of PSL Research University). Fig. 6.13 displays the ranges of involved currents.

The first study showed that different types of nickel and/or stainless steel electrodes generate a very high current consumption in NaCL solutions of different Cl^- concentrations and pH as long as the voltage applied is greater than 500 mV for human physiology-mimicking conditions. This work also showed the importance of “cleaning” or regenerating the electrode from cumulative oxyde layers of complex compounds by applying a reverse negative voltage after each test.

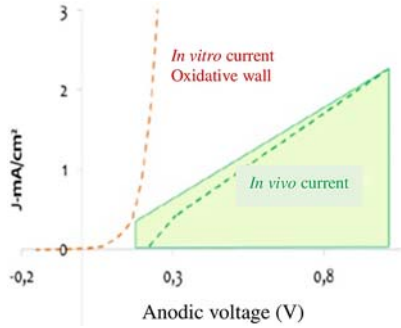

Fig. 6.13. (Surfacic) current ranges of in vitro experiments and in vivo measures.

The second study was able to mimic the condition of an *in vivo* measurement considering the real kinetics of the electrochemical reactions due to the conductance of the sweat glands. A central finding in [27] showed the very poor result of single voltage voltammetry due to the large variability of the layers on the electrodes depending on each patient's pH and HCO_3^- concentrations.

6.4.1. Sudoscan Medical Device Description

The simplified principle of Sudoscan technology consists in imposing on human skin decreasing pulses of low direct current voltages and to collect, once the capacitive and transient effects have stabilized, the electrochemical response of the skin. It is therefore a question of multiple steady chronovoltammetry, possibly thanks to the reverse iontophoresis through the eccrine sweat glands, essentially chlorides at the anode and protons at the cathode.

No specific patient preparation (fasting or other) or medical personnel training is required for Sudoscan testing. The measure is rapid (approximately 2 minutes) and non-invasive.

Measurements are performed on glabrous skin surfaces where the eccrine sweat glands are the most numerous: on the palms of the hands and soles of the feet. The apparatus consists of two sets of two electrodes for the hands and the feet, connected to a computer for recording and data management purposes, see Fig. 6.14. To conduct the test, the patients are required to place their hands and feet on the electrodes. They

must then stand still for the 2-minute duration of the test, in contact only with the electrodes.

Fig. 6.14. Photo of the medical device and its electrodes.

Large area stainless steel electrodes are used alternately as anode or cathode.

The overall measurement scheme, see patent [26], is presented in Fig. 6.15.

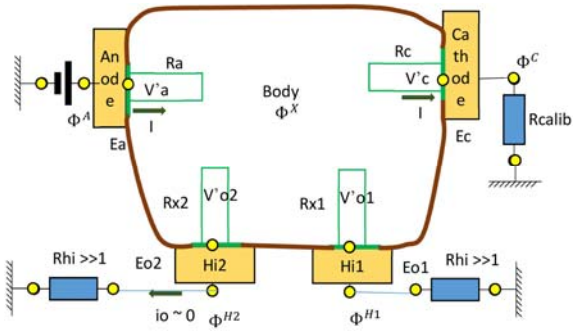

Fig. 6.15. Schematic circuit of the measure.

At the low voltages used, the stratum corneum is purely capacitive; the steady current therefore only passes through the sweat glands. The active electrodes are the anode where the voltage is imposed, and the cathode connected to ground by a calibration resistance making it possible to

close the circuit and deduce the current. The other 2 electrodes, Hi1 and Hi2, are connected to the ground by high impedances, so that no current flows through them and they serve to recover the voltage reached by the body.

The voltages imposed on the active anode for the fifteen steps, as well as their durations, are shown in Fig. 6.16.

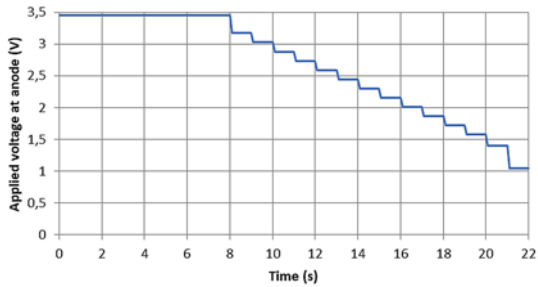

Fig. 6.16. Anode voltage steps.

At the end of the recording, the ESC for all 4 extremities are displayed immediately. The results are expressed in µS (microsiemens). The test also evaluates the percentage of asymmetry between the left and right side, for both hands and feet, indicating whether one side is more impaired than the other. The results can also be displayed in the form of a geometric figure that allows for rapid interpretation (see example in Section 6.5.2.5).

6.4.2. The Signal Measured and Its Main Parameters

For each limb (hand or foot) and on each side (left or right), the raw signal thus collected is a current-voltage curve at the anode and at the cathode. An actual measurement is presented in Fig. 6.17.

Only the various voltages Φ^A, Φ^C, Φ^{H1} and Φ^{H2} are measured; the current in the circuit, between anode, cathode and ground, is expressed as:

$$I = \frac{\Phi^C}{R_{calib}}$$

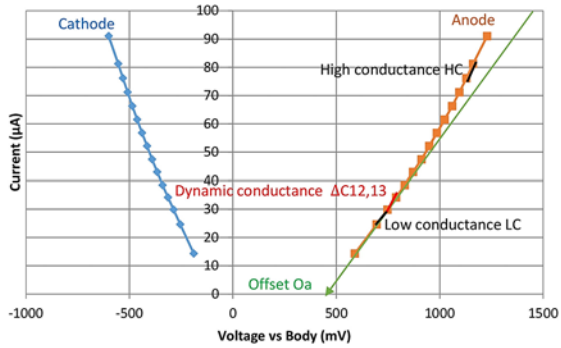

Fig. 6.17. The current-voltage curve measured.

A first important parameter is the **low conductance LC**. It is the ESC at that voltage (see figure), defined previously, in equation (6.10) by the chord. However, here ESC is defined by the dynamic conductance between steps 13 and 14, because of overpotential and offset (see next parameter), and because this low part is linear. It is given by the discrete slope (here at the anode and similar at the cathode):

$$LC \equiv \Delta C13{,}14 \; = \; \frac{I_{13}-I_{14}}{\Phi^{A}_{13}-\Phi^{X}_{13}-\Phi^{A}_{14}+\Phi^{X}_{14}}$$

Below, the main other parameters considered:

The offset, Oa: results from the overpotential (voltage consumption, diode effect) omnipresent at the anode in electrochemistry, due to the electrode surface oxidation and corresponding to the bottom of the oxidation wall. It depends in particular, see [27], on certain concentrations of the electrolytes in sweat (chlorides Cl^{-} and carbonates HCO_3^{-}) and the material composition of the electrode,. It can also be affected by certain pathologies or treatments.

The first voltage step is not used directly, but it stabilizes the overpotential and offset due to its extended duration of eight seconds instead of the usual one second. The last level is also not used; instead, it confirms that the measured signal has not reached the oxidative wall.

Once the offset has stabilized, the entire measured signal is just a simple shift, without distortion, of the purely physiological signal. On the other hand, as the lower part of the signal is generally – and is assumed and

found to be – linear, this offset is obtained by extending the slope of the low conductance towards the abscissa axis, by (see figure):

$$Oa = \Phi_{14}^{A} - \Phi_{14}^{X} - \frac{I_{14}}{LC}$$

By shifting the signal of the offset, the conductance C_s for any step s is then deduced simply by the chord:

$$C_s = \frac{I_s}{\Phi_s^A - \Phi_s^X}$$

The **high conductance** HC is defined by:

$$HC = C_2$$

The **detachment ratio** r:

$$r = \frac{HC}{LC}$$

The **coefficient of non-linearity** ρ, quantifying the non-linearity at the bottom of the curve (~ second derivative):

$$\rho \equiv \frac{\Delta C12,13}{\Delta C13,14}$$

So if $\rho \approx 1$: linear lower part,

If $\rho > 1$: early detachment case,

If $\rho < 1$: case of early landing.

The **hand to foot ratio** R:

$$R = \frac{LChand}{LCfoot}$$

At the cathode, the formulas are analogous. Note that the offset on the cathode side is very low because the first step allows the regeneration [28] of this electrode.

6.4.3. A Much Desired and Important Property of the Measure: Reproducibility

Besides being rapid, non-invasive and quantitative, the technology is able to recognize any movement or tremor during the scan by detecting a break in the monotony of the signal and will alert the technician to the

failure of the measurement. In addition, multiple studies were completed showing that the technology has a good reproducibility [29]. Two test measurements were assessed on the same day in patients with at least one cardiovascular risk and in patients with diabetes; in a second study healthy individuals and patients with diabetes completed 2 tests on each of 3 different devices. Results were compared using a Bland and Altman plot. (see 6.5.2.1)

This very good reproducibility can be explained by several factors:

a) The large number of sweat glands measured on the palms and soles (several thousands) which average the effect of any disease;

b) The application of the electrode firmly against the skin which plugs the pores of the glands and blocks the physiological sweat flow, thus minimizing a possible dependence on test conditions such as stress, temperature, physical effort or exercise [30];

c) The steady measure, *i.e.,* after the stabilization of the transitory capacitive aspects of the SC, the gland and the sweat/electrode interface;

d) The active measure with the same constant polarizations, about ten times higher than physiological ones;

e) The non-dependence of the measure on the stratum corneum thickness, as noted above, which warrants that even calloused feet can be accurately measured;

f) The ESC being computed by the slope of the curve (resulting current over applied voltage), as previously explained and therefore not polluted by any electrochemical overpotential of the electrode [27];

g) The internal electronic circuit of the technology, which measures the voltages precisely with an accurate analog-to-digital converter having a resolution of 10 bits;

h) The high sensitivity of stainless steel electrodes which creates a strong current generator due to Cl^- consumption [31].

6.4.4. Section Conclusion

As a conclusion for this section, the measured Sudoscan signal is very rich: the linear lower part followed by detachment (or landing) make it possible to assess with precision and in a reproducible way the

sudomotor function. Multiple steady chronovoltammetries allow a signal measurement over a wide range of voltages, without electrochemical pollution, contrarily to a single voltammetry [27].

6.5. Clinical Applications for Various Pathologies and Treatments

Sweat glands are innervated by small C fibers that can be affected early in systemic diseases like diabetes or amyloidosis. Impairment of these C fibers portends the progression to a more diffuse neuropathy. Small fibers are often the first to degenerate in diabetic peripheral neuropathy and are responsible for loss of pain, cold, and heat perception, increasing the risk for foot trauma. In addition, impaired sweat function, resulting in dry skin and loss of healing, further accelerates the development of diabetic foot complications.

Usual clinical tests for peripheral neuropathy mainly explore large fibers and are operator dependent and time consuming; more importantly, large fiber deficits – and thus their detection with usual clinical tests – occur late in the evolution of the diabetic neuropathy process. Therefore, a small fiber neuropathy (SFN) test can be helpful for at least three reasons: i) Making the diagnosis of SFN can lead to a focused search early for its etiology; ii) Disease modifying or symptomatic treatments can be started early; and iii) Awareness of the disease can increase patient's compliance, which is critical in the follow-up of a chronic condition like diabetes.

In the context of this widespread need for a rapid, non-invasive, objective, quantitative, accurate and easy to use SFN diagnostic tool, the Sudoscan device, measuring sudomotor function, was developed.

After a brief review of the method as it is explained to clinicians who use the device in daily practice, the clinical development strategy and principal research results will be presented. In this section ESC correspond to Low Conductances (LC) as defined in the previous section.

6.5.1. Principle of the Method as It Is Explained to Clinician Users

"Sudoscan measures the capacity of the sweat glands to release chloride ions in response to an electrical stimulation. The patient is only asked to place the palms of the hands and soles of the feet, areas with the highest sweat gland density, in contact with two large electrodes for 3 minutes. Gradual voltages less than 4 V are applied to the electrodes. There is an observable electrochemical reaction between the Cl^- ions present in sweat and the electrodes. The device records an electrochemical conductance (ESC) related to the amount of chloride ions extracted from the sweat glands and detected by the electrodes. The level of conductance depends on the number of chloride ions that react with the electrodes. In patients with normal sweat function, many chloride ions react with the electrodes when direct current is applied to excite the small nerves on the glands and open chloride ion channels; this results in a high level of conductance. In patients with sweat dysfunction, less chloride ions are attracted and the level of conductance is lower (Fig. 6.18).

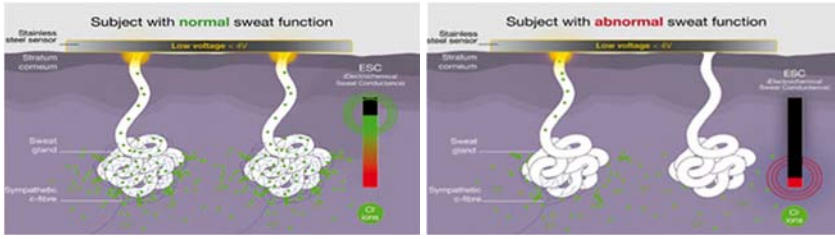

Fig. 6.18. Illustration of the mechanism as presented to clinician users.

6.5.2. Clinical Development

As there was no equivalent device available that had already established the clinical utility of this sudomotor methodology, the Sudoscan technology had to be evaluated in clinical studies. Since the test is rapid and non-invasive – in contrast to the majority of clinical and research tests used in the diagnosis of SFN – the principal clinical studies were performed as add-on assessments during standard of care follow-up of patients.

The aim of the clinical development program was to establish the following properties of the Sudoscan technology to support its diagnostic

clinical utility: i) Normative data and accuracy of the method; ii) Performance in the assessment of sweat function and small fiber neuropathies as compared to usual reference methods; iii) Performance in the detection of peripheral neuropathy in patients with diabetes; iv) Performance in the diagnosis of peripheral neuropathy in patients with neurodegenerative diseases; v) Performance in the follow-up of patients with peripheral neuropathy.

6.5.2.1. Normative Data and Accuracy of the Method

Normative ESC values in adults were defined in a population of over 1350 healthy subjects. Mean ESC for women or men at the hands (75 [57-87] *vs.* 76 [56-89] µS, p = 0.35) or feet (83.5 [71-90] vs. 82.5 [70-91] µS, p = 0.12) [32] were not significantly different. Overall, there was no effect on ESC of body mass index (BMI), or exercise status; a very small (and clinically insignificant) decrease with age, and a significant effect of race/ethnicity. Specific ESC thresholds have thus been defined for patient race/ethnicity and are applied for proper test interpretation (Fig. 6.19).

Sudoscan tests completed among 100 healthy children confirmed that normative values were equivalent to those for adults [33].

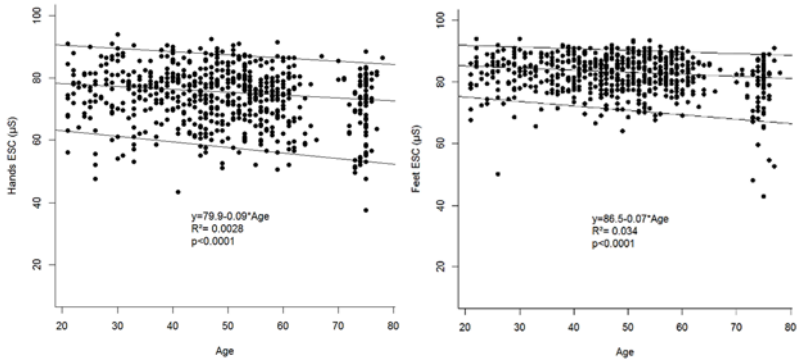

Fig. 6.19. Evolution of Hands ESC and Feet ESC with age on 1350 healthy volunteers from [32].

The accuracy of the method was determined according to FDA guidelines (2 measurements performed on each of 3 devices, for a total of 6 Sudoscan tests per patient), and evidenced a coefficient of variation

of feet / hand ESC of 4 % in healthy subjects and 7 % in patients with diabetes [34].

The results for these studies established that the Sudoscan technology was robust under a variety of clinical circumstances and for a wide range of populations; additionally, if the technology is used to monitor patients over time, the good reproducibility ensures that a change in ESC is a reliable marker of sudomotor function change and should prompt further investigation.

6.5.2.2. Performance in the Assessment of Sweat Function and Small Fiber Neuropathies as Compared to Usual Reference Methods

Established sudomotor function tests have long been recognized as some of the most sensitive and specific means to diagnose distal small fiber neuropathies. However, they are also all affected by ambient temperature, hydration status, medications, age and gender, previous exposure of the skin to alcohol, repeated testing over the same region, and application of moisturizing creams – factors to which Sudoscan, as discussed above, is not necessarily prone [35]. Though restricted to specialized centers, QSART is probably the most widely available sudomotor function test and thus most commonly used clinically.

Sudoscan was compared to the QSART in 3 studies that documented a larger Area Under the Curve (AUC) (0.77 vs 0.57, 0.71 vs 0.53 for Sudoscan compared to QSART, respectively) in the diagnosis of small fiber or diabetic neuropathy [36, 37] (Fig. 6.20, Table extracted from [37]). Though established as a standard, validated test of sudomotor function, QSART appears to have no table diagnostic limitations for small fiber and diabetic neuropathies – in addition to the fact that the technology has significant technical requirements, limited availability, and a high susceptibility to environmental factors.

Two studies established the higher performance of Sudoscan as compared to Neuropad® [38] (poster Ziegler D et al, Neurodiab 2017, publication ongoing).

In a comparison with 4 reference diagnostic methods for small fiber neuropathy, Sudoscan was found to be less sensitive than Laser Evoked Potential (LEP), a highly specialized and time-consuming research method; however, Sudoscan had marginally better diagnostic

performance than Quantitative Sensory Testing (QST) for warm detection and much better performance than cold detection and sympathetic skin response [39].

	Controls	**Diabetes**	**DPN**	**P**
	N = 16	**N = 20**	**N = 27**	**value**
ESC feet (μS)	83.0 (16.3)^{A}	76.3 (15.9)^{AB}	64.4 (15.9)^{B}	0.017
ESC hands (μS)	71.3 (18.0)	70.4 (17.6)	58.2 (18.2)	0.037
Sweat latency, distal leg (B)[a]	87.2 (49.4)	96.4 (49.5)	90.5 (49.7)	0.909
Sweat volume, distal leg (μl)[a]	0.90 (0.60)	0.70 (0.60)	0.60 (0.60)	0.107
Sweat latency, distal foream (B)	80.3 (41.1)	89.1 (40.2)	84.9 (42.3)	0.807
Sweat volume, distal foream (μl)[a]	1.00 (1.40)	1.20 (1.40)	1.30 (1.40)	0.4

Fig. 6.20. Mean values of ESC and QSART parameters in healthy controls, patients with diabetes but no diabetic peripheral neuropathy (DPN), and patients with diabetes and DPN (Data are age- and gender adjusted mean (SD). [a]Log-transformed variable. ESC, Electrochemical Skin Conductance. DPN Diabetic Peripheral Neuropathy. Unequal superscript letters indicate significant group differences, Table extracted from [37].

The authors concluded that LEP, QST for warm detection and Sudoscan provide significant diagnostic sensitivity compared to other tests of small fiber neuropathy evaluated, and that the combination of all three tests provided improved diagnostic accuracy. However, it must also be noted that LEP and QST are limited to research institutions and therefore cannot be considered practical for real world diagnostic evaluation of small fiber neuropathy. Finally, the clinical strategy proposed by this reference center, when a patient presents for small fiber neuropathy assessment is to perform a Sudoscan. If Sudoscan is positive, SFN is established and taken into account for patient follow-up. If Sudoscan is normal, another more specialized test is performed to confirm absence of SFN.

The current gold standard in the diagnosis of distal small fiber neuropathy is intraepidermal nerve fiber density (ENFD). This test requires removal of a small skin punch biopsy at the lower leg, and shipment to a specialized lab for processing and microscopic

examination prior to results being available. Several studies investigated the diagnostic performance of Sudoscan and ENFD in healthy controls and patients referred to specialized centers for small fiber neuropathy evaluation. Smith *et al*. demonstrated that feet ESC and ENFD had similar AUC (0.761 and 0.752, respectively) [40], while Novak *et al.* demonstrated high correlation between ESC and ENFD adjusted for weight ($r = 0.73$, $p = 0.0001$; Fig. 6.21) [41]. These findings suggest that Sudoscan technology is a robust alternative diagnostic test for small fiber neuropathy, providing a non-invasive, painless assessment with results immediately available. In addition, repeated testing for follow-up of treatment or disease progression is markedly simpler and more acceptable with Sudoscan than skin biopsy.

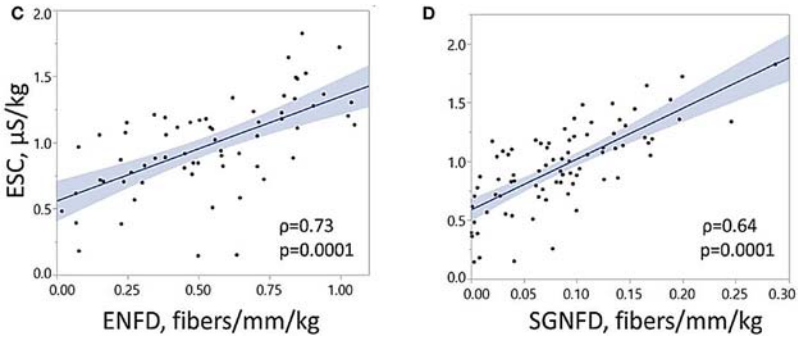

Fig. 6.21. Correlation between FESC and skin biopsy (Epidermal Nerve Fiber Density (ENFD) and Sweat Gland Nerve Fiber Density (SGNFD) from [41].

Finally, a significant correlation between Sudoscan ESC and corneal nerve fiber length (CNFL) assessed using in vivo laser confocal microscopy has been evidenced ($r^2 = 0.8$) [42]. CNFL is considered a surrogate marker of denervation in diabetic sensorimotor and autonomic neuropathy; in this study, the authors evaluated patients with transthyretin familial amyloid polyneuropathy, a genetic disorder in which small fiber neuropathy is a prominent feature. The authors showed that ESC and CNFL – two non-invasive, quantitative tests with immediately available results – were very highly correlated in a small population ($n = 15$) with small fiber neuropathy of varying severity. It must be noted, however, that confocal microscopy requires complex ophthalmological equipment and analytical software, as well as anesthetizing the patient's cornea for examination.

6.5.2.3. Performance in the Detection of Peripheral Neuropathy in Patients with Diabetes

Among patients with diabetes, peripheral neuropathy is the most common complication, affecting up to 70 % of patients during their lifetime; diabetic peripheral neuropathy (DPN) results in significant morbidities such as a chronic pain, loss of sensation, foot ulcers, gangrene, and amputations. Distal sensorimotor peripheral neuropathy is a dying-back disorder, most commonly affecting small nerves on the extremities first. Early detection could allow identification of and aggressive intervention in those at greatest risk for further morbidity. Considering the vast number of patients with diabetes across the world, its unrelenting chronicity, and the complicity of care of each patient, a simple, rapid, but quantitative test for DPN is valuable for the initial triage and ongoing follow-up of this population. Nine studies involving more than 1000 patients with diabetes showed sensitivities from 73 to 97 % to detect peripheral neuropathy with negative predictive values from 83 to 94 % when Sudoscan was compared to reference symptom scores or usual tests for DPN [43]. The high negative predictive value of Sudoscan is particularly important as it can reassure clinicians to the current lack of DPN in patients with normal ESC.

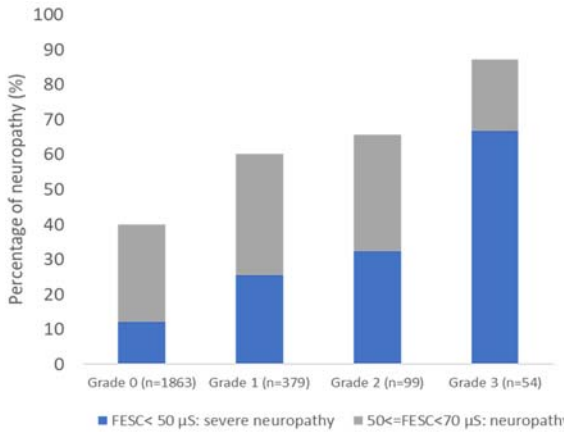

Fig. 6.22. Feet ESC distribution according to grade of diabetic foot risk in 2400 patients from 4 French Hospitals.

Boulton *et al.* [44] initially developed the scale of 4 risk categories based on results of a comprehensive foot examination; it was to be used to

determine how frequently patients with diabetes should undergo foot evaluations and by whom (generalist or specialist). A risk of 0 indicates no loss of protective sensation (LOPS), no peripheral artery disease, and no foot deformity. In contrast, a risk of 3 is reserved for patients with prior ulcer or amputation. Unfortunately, rarely is a comprehensive foot exam performed on every diabetic patient on a yearly basis, as recommended by the American Diabetes Association. In addition, even a risk category of 1 represents relatively advanced DPN, when LOPS – suggesting myelinated nerve fiber damage – has developed. A study is ongoing on more than 2400 patients with diabetes to compare ESC values and gradation of diabetic foot risk (Fig. 6.22, poster presentation in EASD, 2019, publication ongoing). The figure below shows that even among patients rated as risk category 0, 40 % have abnormal Sudoscan results and may be at elevated risk for diabetic foot. Sudoscan may be more sensitive early in the progression of diabetic foot – before clinical signs become apparent – and allow for prompt identification of patients requiring intensified foot care or referral to podiatry.

6.5.2.4. Performance in the Detection of Cardiac Autonomic Neuropathy in Patients with Diabetes

As stated in the introduction, the autonomic nervous system is the primary extrinsic control mechanism regulating heart rate, blood pressure, and myocardial contractility. Cardiac autonomic neuropathy (CAN) describes a dysfunction of the ANS and its regulation of the cardiovascular (CV) system. CAN is an important risk factor for CV morbidity and mortality. In the diabetes population, the prevalence of CAN varies from 2.5 % to 50 %; it is implicated in a five-fold increased risk of CV mortality and in fact is the strongest predictor for mortality in diabetes mellitus [45].

The American Diabetes Association has recommended screening patients with diabetes for autonomic neuropathy, but only by assessing for symptoms and signs in those with microvascular complications. However, early symptoms of CAN tend to be nonspecific and frank clinical manifestations of hypoglycemia unawareness, resting tachycardia, orthostatic hypotension, gastroparesis, constipation, diarrhea, or fecal incontinence occur too late to be reversible. Thus, a diagnosis of CAN is frequently delayed or may never occur before the occurrence of a catastrophic event.

Cardiovascular autonomic reflex tests (CARTs) remain the gold standard for the diagnosis of CAN but are time-consuming and are limited to highly specialized centers. Therefore, universal screening for and diagnosis of CAN are widely disregarded in clinical practice. This dichotomy between the ideal and actual reality highlights the need for diagnostic procedures of sufficient reliability and accuracy that are at the same time accessible and easy, and that might also allow for the selection of persons at higher risk for CAN to be further evaluated with CARTs. Three studies performed on significant groups of patients evidenced the performances of feet ESC (FESC) in the screening of CAN in patients with diabetes. Sensitivities of FESC to detect CAN or confirmed CAN diagnosed according to CARTs were between 80 and 100 % [46-48] (Fig. 6.23).

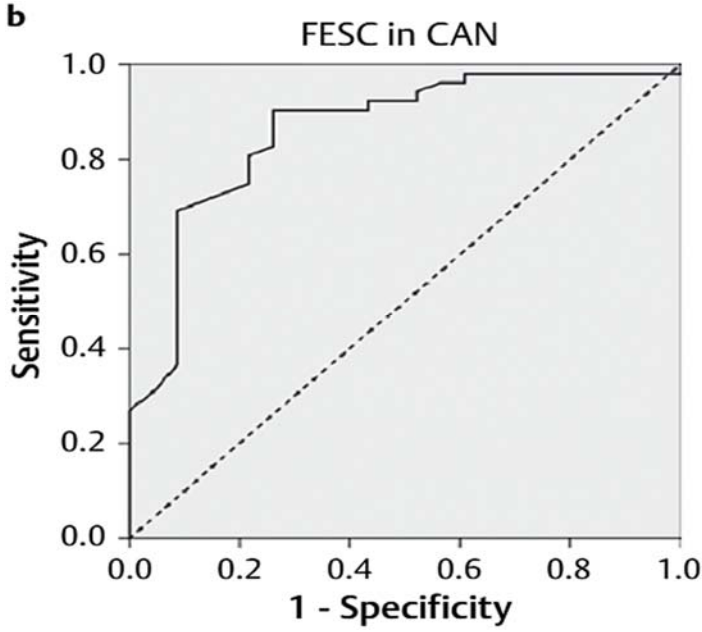

Fig. 6.23. ROC curve of feet electrochemical skin conductance (FESC) to diagnose CAN, AUC = 0.86, from [46].

D'Amato *et al.* studied over 100 patients with diabetes with COMPASS 31 (a simple, self-administered questionnaire), FESC and CARTs; CAN was defined as ≥ 1 abnormal CART and confirmed CAN as ≥ 2 abnormal

CARTs. The authors noted that either an abnormal COMPASS 31 and/ or abnormal FESC score has a 92 % sensitivity to identify CAN and 100 % sensitivity for confirmed CAN [48].

Importantly, CAN was noted to be reversible in a population of severely obese diabetic patients following bariatric surgery: both FESC and cardiac autonomic function improved at 12 and 24 weeks; interestingly, improvements in CAN measures were not correlated with changes in weight, BMI, body fat, or lipid level. These studies demonstrate that sudomotor function testing can detect asymptomatic CAN in the clinical setting, select patients for more advanced testing and/or aggressive treatment, and may allow for easy assessment of treatment efficacy of an often-deadly complication [49].

6.5.2.5. Performance in the Diagnosis of Peripheral Neuropathy in Patients with Neurodegenerative Diseases

Sudoscan was evaluated in several diseases involving small fiber neuropathies.

Hereditary transthyretin amyloidosis is a rare, autosomal dominant, progressive and fatal disease caused by mutations in the TTR gene. Amyloid polyneuropathy (TTR-FAP) is a progressive sensory–motor and autonomic neuropathy, initially affecting small fibers followed by larger fibers. Early identification is critical to prevent permanent tissue damage, in particular cardiac autonomic neuropathy which contributes to premature demise. Unfortunately, most established small fiber and autonomic tests have low sensitivity and specificity in TTR-FAP or are impractical for chronic clinical care. Patients with familial amyloidosis demonstrate a dramatic decrease in ESC, and AUC of feet ESC to detect dysautonomia was 0.76 [50] (Fig. 6.24). Feet ESC were decreased in 40 % of pauci-symptomatic patients; in addition, correlations with clinical symptom scores, Neuropathy Impairment Score (NIS) and Karnofsky performance status, were 0.62 and 0.61, respectively.

Sudoscan was found to be similarly effective in other disorders where autonomic neuropathy or SFN is prominent: in Parkinson's disease the AUC to detect dysautonomia was 0.82 [51]. A decrease in feet ESC was observed in 87 % of patients with Gougerot-Sjögren and SFN [52].

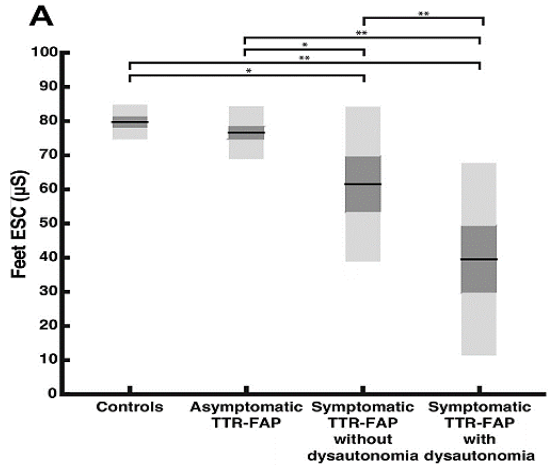

Fig. 6.24. Values of Feet ESC in healthy controls and patients with transthyretin-related familial amyloid polyneuropathy (TTR-FAP) according to presence of symptoms and dysautonomia from [50].

6.5.2.6. Performance in the Follow-up of Patients with Peripheral Neuropathy

As Sudoscan is non-invasive, quantitative and highly reproducible, it can be used for the follow-up of patients to assess treatment efficacy. A significant increase in ESC was demonstrated among subjects with limited cardiorespiratory performance after implementation of lifestyle changes [30]. In diabetic patients, an improvement in ESC has been observed after bariatric surgery [49]. In patients receiving chemotherapy (oxaliplatin or taxanes), a decrease in ESC could be measured in parallel with clinical deterioration [53]. Longitudinal studies have been performed in patients receiving treatment for TTR-FAP [54], Vitamin B12 deficiency [55], or painful small fiber neuropathy (capsaicin patch [56]), all supporting the ability of Sudoscan to quantify changes in nerve function.

Overall, more than 120 papers involving Sudoscan have been published in peer-reviewed journals. These have established the technology's robustness, performance, and normative data, and demonstrated its clinical utility; but most importantly, Sudoscan has been shown to be safe (no adverse event related to Sudoscan reported in > 1,000,000 tests completed) and suitable for use in all clinical settings.

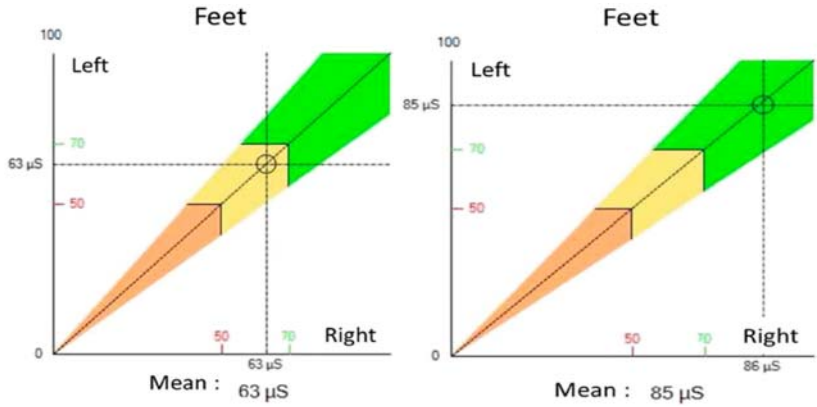

Fig. 6.25. Changes observed in feet ESC 3 months after capsaicin patch application from [56].

6.5.3. New Clinical Developments

As advanced previously in Section 6.4, a Sudoscan test incorporates new parameters not clinically analyzed in the ESC results currently processed and expressed. It is understood that some of these parameters may provide more information on the ratio of adrenergic to cholinergic nerves on the sweat glands, knowing that these nerves can regenerate at different speeds [9]. Characteristics of these new parameters (mean, standard deviation, median, interquartiles) have been calculated on a population of more than 1200 healthy subjects without peripheral neuropathy. In the near future, characteristics of these parameters in well characterized patients including populations with Parkinson's disease, receiving chemotherapy, and with cystic fibrosis will be compared to healthy controls. The next step will be to assess the evolution of these parameters in the progression of the diseases.

Finally, another way of enhancing the detection and work-up of small fiber and autonomic neuropathies is to complete the Sudoscan test along with relevant, internationally recognized questionnaires. Patients can easily answer questions about their symptoms during or just after recording a Sudoscan test. Questionnaires can be selected according to the suspected or known condition: a questionnaire for small fiber neuropathy in patients where Sudoscan is used to explore SFN, or a questionnaire adapted to diabetic foot risk in patients with diabetes. A recent study has evidenced the benefits of combining the COMPASS 31 questionnaire and Sudoscan to assess CAN. In this study

involving 102 patients with diabetes, COMPASS 31 and ESC individually had sensitivities of 75 % and 83 %, respectively, for confirmed CAN, and specificities of 65 % and 67 %, respectively, for DPN. When combining the tests, the sensitivity for CAN rose to 100 % for CAN and the specificity up to 89 % for DPN [48].

6.5.4. Conclusion on Clinical Applications

Assessment of autonomic dysfunction is important in the follow-up of several diseases like Diabetes and Parkinson's disease. Sweat glands are innervated by small C fibers, and thus sweat function measurement is now recognized as a reliable way to assess autonomic function and small fiber neuropathy. Several methods have been developed but many of them are not suitable for daily practice since they are invasive, time consuming, highly specialized or of low reproducibility. Based on the presence of chloride ions in sweat, Sudoscan was developed using the electrochemical reaction between chlorides and stainless-steel electrodes. Clinical development of this simple, rapid and noninvasive method was performed to define normative values, reproducibility and performance compared to established neurophysiologic testing methods. In dozens of clinical studies, Sudoscan has been shown to have diagnostic utility to assess diabetic foot risk, and quantify impairment of autonomic and small fiber nerves in neurologic diseases. As the method is highly reproducible it is well suited to the follow-up of patients to evaluate treatment efficacy or neurotoxicity from chemotherapy. New developments are ongoing to utilize additional test parameters to discern among different disorders, and to add diagnostic value to Sudoscan with the concurrent use of disease-specific questionnaires which can be filled out during the test. The simplicity and performance of Sudoscan technology has the potential to accelerate early detection of autonomic and small fiber neuropathies in routine clinical practice, and provide highly specific data to monitor patients much more precisely and routinely than has been possible up until now. Ultimately, Sudoscan could lessen the burden of costly and morbid neuropathic complications.

6.6. General Conclusion

This chapter shows the importance of measuring sweat function on the palms and soles where the highest concentration of eccrine glands occurs. Sudoscan patented technology benefits from a conjunction of

very interesting physiological and physical phenomena. The physiological one is related to the frailty of these long thin nerves managing sweat glands, resulting in an excellent sensitivity to diagnose early neuropathic complications.

The main physical phenomenon is the fact that the range of DC voltages applied on the skin allows:

– An electrochemical reaction between chloride ions and stainless-steel electrodes;

– A flow of chloride ions passing only through the sweat ducts (as the stratum corneum cannot transfer ions at these voltages);

– The stimulation of small nerves on the glands which deliver neurotransmitters to open muscarinic and CFTR ion channels;

– A flow of chloride ions generating a current related to the density of small nerves on the gland, producing the exact conductance of the total amount of glands.

These voltages surpass physiological voltages usually perceived by the nerves and the ion channels, which leads to a very robust measurement independent of environmental conditions in real life such as temperature, emotion, and exercise as demonstrated in many clinical studies.

Overall, more than 120 papers involving Sudoscan have been published throughout the world in peer-reviewed journals with very consistent results.

New parameters included in the signal processed by Sudoscan as well as the concomitant use of adapted questionnaires seem very interesting to enhance the diagnostic and prognostic qualities of the technology.

Acknowledgements

We would like to thank Abdul Kayoum Moutairou, biostatistician at Impeto Medical, Paris, France for the data mining results.

References

[1]. P. J. Dyck, et al., Signs and symptoms versus nerve conduction studies to diagnose diabetic sensorimotor polyneuropathy: Cl vs. NPhys trial, *Muscle & Nerve*, Vol. 42, Issue 2, 2010, pp. 157-164.

[2]. M. J. Marples, The Ecology of the Human Skin, *Thomas*, 1965.
[3]. C. Y. Cui, S. David, Eccrine sweat gland development and sweat secretion, *Experimental Dermatology*, Vol. 24, Issue 9, 2015, pp. 644-650.
[4]. A. Siver, W. Montagna, I. Karacan, Age and sex differences in spontaneous, adrenergic and cholinergic human sweating, *The Journal of Investigative Dermatology*, Vol. 43, 1964, pp. 255-265.
[5]. W. Montagna, Some particularities of human skin and the skin of nonhuman primates, *Giornale Italiano di Dermatologia e Venereologia: Organo Ufficiale,* Vol. 119, Issue 1, 1984, 1.
[6]. K. Sato, F. Sato, Individual variations in structure and function of human eccrine sweat gland, *American Journal of Physiology-Regulatory, Integrative and Comparative Physiology*, Vol. 245, Issue 2, 1983, pp. R203-R208.
[7]. K. Hwang, S. H. Baik, Distribution of hairs and sweat glands on the bodies of Korean adults: A morphometric study, *Cells Tissues Organs*, Vol. 158, Issue 2, 1997, pp. 112-120.
[8]. C. H. Gibbons, N. Wang, R. Freeman, Capsaicin induces degeneration of cutaneous autonomic nerve fibers, *Annals of Neurology*, Vol. 68, Issue 6, 2010, pp. 888-898.
[9]. L. Rittié, et al., Eccrine sweat glands are major contributors to reepithelialization of human wounds, *The American Journal of Pathology*, Vol. 182, Issue 1, 2013, pp. 163-171.
[10]. K. Wilke, et al., A short history of sweat gland biology. *International journal of cosmetic science* Vol. 29, Issue 3, 2007, pp. 169-179.
[11]. G. I. Vitale, et al., Electrical field stimulation of isolated primate sweat glands, *British Journal of Dermatology*, Vol. 115, Issue 1, 1986, pp. 39-47.
[12]. Y. A. Chizmadzhev, A. V. Indenbom, P. L. Kuzmin, S. V. Galichenko, J. C. Weaver, R. O. Potts, Electrical properties of skin at moderate voltages: Contribution of appendageal macropores, *Biophys. J.*, Vol. 74, 1998, pp. 843-856.
[13]. K. Khalfallah, H. Ayoub, J. H. Calvet, *et al.*, Noninvasive galvanic skin sensor for early diagnosis of sudomotor dysfunction: Application to diabetes, *IEEE Sensors Journal*, Vol. 12, Issue 3, 2012, pp. 456-463.
[14]. K. Sato, W. H. Kang, K. Saga, K. T. Sato, Biology NORMAL of sweat glands and their disorders. I. Normal sweat gland function**,** *Journal of the American Academy of Dermatology*, Vol. 20, Issue 4, April 1989, pp. 537-563.
[15]. P. M. Quinton, M. M. Reddy, Cl-conductance and acid secretion in the human sweat duct, *Annals of the New York Academy of Sciences*, Vol. 574, Issue 1, 1989, pp. 438-446.
[16]. A. B. Stefaniak, C. J. Harvey, Dissolution of materials in artificial skin surface film liquids, *Toxicology in Vitro*, Vol. 20, Issue 8, 2006, pp. 1265-1283.
[17]. J. Salençon, Handbook of Continuum Mechanics, *Springer-Verlag*, Berlin, Heidelberg, 2001.

[18]. C. M. Dafermos, Hyperbolic Conservation Laws in Continuum Physics, *Springer-Verlag*, Berlin, Heidelberg, 2010.
[19]. T. Chen, C. Miller, Nonequilibrium gating and voltage dependence of the clc-0 cl- channel, *J. Gen. Physiol*., Vol. 108, Issue 4, 1996, pp. 237-250.
[20]. N. K. Wills, P. Fong, ClC chloride channels in epithelial: Recent progress and remaining puzzles, *News Physiol. Sci*., Vol. 16, 2001, pp. 161-166.
[21]. D. Granger, M. Marsolais, J. Burry, R. Laprade, Na+/H+ exchangers in the human eccrine sweat duct, *Amer. J. Physiol. Cell. Physiol*., Vol. 285, 2003, pp. 1047-1058.
[22]. J. Cronin, Mathematics of Cell Electrophysiology, Vol. 63, *CRC Press*, 1981.
[23]. P. M. Quinton, Cystic fibrosis: A disease in electrolyte transport, *FASEB J.*, Vol. 4, 1990, pp. 2709-2717.
[24]. J. O. Bockris, A. K. N. Reddy, Chapter 4, in Modern Elechrochemistry 1: Ionics, *Plenum*, New York, 1998.
[25]. P. W. Atkins, J. D. Paula, Elements of Physical Chemistry, *Oxford University Press*, 2005.
[26]. P. Brunswick, N. Bocquet, Electrophysiological Analysis System, *U.S. Patent No 8,918,170,* USA, 2014.
[27]. V. Lair, A. Calmet, V. Albin, et al., Electrolytic cell design to simulate the electrochemical skin response, *Electroanalysis*, Vol. 31, Issue 1, 2019, pp. 22-30.
[28]. H. Ayoub, et al., Electrochemical basis for EZSCAN/SUDOSCAN: A quick, simple, and non-invasive method to evaluate sudomotor dysfunctions, in Developments in Electrochemistry, *IntechOpen*, 2012.
[29]. H. Mayaudon, P. O. Miloche, B. Bauduceau, A new simple method for assessing sudomotor function: Relevance in type 2 diabetes, *Diabetes & Metabolism*, Vol. 36, 2010, pp. 450-454.
[30]. A. Raisanen, J. Eklund, J. H. Calvet, J. Tuomilehto, Sudomotor function as a tool for cardiorespiratory fitness level evaluation: comparison with maximal exercise capacity, *Int. J. Environ. Res. Public Health*, Vol. 11, 2014, pp. 5839-5848.
[31]. H. Ayoub, V. Lair, S. Griveau, P. Brunswick, F. Bedioui, M. Cassir, Electrochemical characterization of stainless steel as a new electrode material in a medical device for the diagnosis of sudomotor dysfunction, *Electroanalysis*, Vol. 24, Issue 6, 2012, pp. 1324-1333.
[32]. A. I. Vinik, A.G. Smith, J. R. Singleton et al., Normative values for electrochemical skin conductances and impact of ethnicity on quantitative assessment of sudomotor function, *Diabetes Technol. Ther.*, Vol. 18, Issue 6, 2016, pp. 391-398.
[33]. L. Leclair-Visonneau, T. Bosquet, A. Magot et al., Electrochemical skin conductance for quantitative assessment of sweat function: Normative values in children, *Clinical Neurophysiology Practice*, Vol. 1, 2016, pp. 43-45.
[34]. L. Bordier, M. Dolz, L. Monteiro et al. Accuracy of a rapid and non-invasive method for the assessment of small fiber neuropathy based

on measurement of electrochemical skin conductances, *Front Endocrinol. (Lausanne)*, Vol. 7, 2016, 18.

[35]. B. M. Illigens, C. H. Gibbons, Sweat testing to evaluate autonomic function, *Clin. Auton Res*., Vol. 19, Issue 2, 2009, pp. 79-87.

[36]. B. C. Callaghan, R. Xia, E. Reynolds et al., Better diagnostic accuracy of neuropathy in obesity: A new challenge for neurologists, *Clin. Neurophysiol.*, Vol. 129, Issue 3, 2018, pp. 654-662.

[37]. S. M. Krieger, M. Reimann, R. Haase, *et al.*, Sudomotor testing of diabetes polyneuropathy, *Front. Neurol.*, Vol. 26, 2018, 803.

[38]. H. G. Zouari, S. Ng Wing Tin, A. Wahab, *et al*., Assessment of autonomic innervation of the foot in familial amyloid polyneuropathy, *European Journal of Neurology*, Vol. 26, Issue 1, 2018, 94-e10.

[39]. J. P. Lefaucheur, A. Wahab, V. Planté-Bordeneuve *et al*., Diagnosis of small fiber neuropathy: A comparative study of five neurophysiological tests, *Neurophysiol. Clin.*, Vol. 45, Issue 6, 2015, pp. 445-455.

[40]. A. G. Smith, M. Lessard, S. Reyna, M. Doudova, *et a*l., The diagnostic utility of Sudoscan for distal symmetrical peripheral neuropathy, *J. Diabetes Complications.,* Vol. 28, Issue 4, 2014, pp. 511-516.

[41]. P. Novak, Electrochemical skin conductance: A systematic review, *Clin. Auton. Res*., Vol. 29, Issue 1, 2019, pp. 17-29.

[42]. A. Rousseau, C. Cauquil, B. Dupas, *et al*., Potential role of in vivo confocal microscopy for imaging corneal nerves in transthyretin familial amyloid polyneuropathy, *JAMA Ophthalmol*., Vol. 134, Issue 9, 2016, pp. 983-989.

[43]. D. Selvarajah, *et al.,* Diabetic peripheral neuropathy: Advances in diagnosis and strategies for screening and early intervention, *Lancet Diabetes Endocrinol*., Vol. 7, Issue 12, 2019, pp. 938-948.

[44]. A. J. Boulton, D. G. Armstrong, S. F. Albert, et al., Comprehensive foot examination and risk assessment: A report of the task force of the foot care interest group of the American Diabetes Association, with endorsement by the American Association of Clinical Endocrinologists, *Diabetes Care*, Vol. 31, Issue 8, 2008, pp. 1679-1685.

[45]. S. Tesfaye, A. J. Boulton, P. J. Dyck, *et al*., Toronto Diabetic Neuropathy Expert Group. Diabetic neuropathies: Update on definitions, diagnostic criteria, estimation of severity, and treatments, *Diabetes Care*, Vol. 33, Issue 10, 2010, pp. 2285-2293.

[46]. J. Jin, W. Wang, T. Gu et al., The application of Sudoscan for screening diabetic peripheral neuropathy in Chinese population screening DPN by Sudoscan, *Exp. Clin. Endocrinol. Diabetes*, Vol. 126, Issue 8, 2018, pp. 472-477.

[47]. T. He, C. Wang, A. Zuo et al., Electrochemical skin conductance may be used to screen for diabetic cardiac autonomic neuropathy in a Chinese population with diabetes, *Journal of Diabetes Research*, Volume 2017, 2017, 8289740.

[48]. C. D'Amato, C. Greco, G. Lombardo et al., The diagnostic usefulness of the combined COMPASS 31 questionnaire and electrochemical skin conductance for diabetic cardiovascular autonomic neuropathy and

diabetic polyneuropathy, *J. Peripher. Nerv. Syst.*, Vol. 25, Issue 1, 2020, pp. 44-53.
[49]. C. M. Casellini, H. K. Parson, K. Hodges et al., Bariatric surgery restores cardiac and sudomotor autonomic c-fiber dysfunction towards normal in obese subjects with type 2 diabetes, *PLoS ONE*, Vol. 11, Issue 5, 2016, e0154211.
[50]. J. Castro, B. Miranda, I. Castro et al., The diagnostic accuracy of Sudoscan in transthyretin familial amyloid polyneuropathy, *Clin. Neurophysiol.*, Vol. 127, Issue 5, 2016, pp. 2222-2227.
[51]. X. Xu, *et al.*, Clinical utility of Sudoscan in predicting autonomic neuropathy in patients with Parkinson's disease, *Parkinsonism Relat. Disord*., Vol. 64, 2019, pp. 60-65.
[52]. S. Ng Wing Tin, H. G. Zouari, A. Wahab et al., Characterization of neuropathic pain in primary Sjögren's syndrome with respect to neurophysiological evidence of small-fiber neuropathy, *Pain Med*., Vol. 20, Issue 5, 2019, pp. 979-987.
[53]. M. Saad, D. Psimaras, C. Tafani, *et al.*, Quick, non-invasive and quantitative assessment of small fiber neuropathy in patients receiving chemotherapy, *J. Neurooncol.*, Vol. 127, Issue 2, 2016, pp. 373-380.
[54]. J. Castro, J. Costa, I. de Castro et al., Electrochemical skin conductance in hereditary amyloidosis related to transthyretin V30M – A promising tool to assess treatment efficacy ?, *Amyloid.*, Vol. 25, Issue 4, 2018, pp. 267-268.
[55]. C. S. Yajnik, *et al*., A physiological dose of oral vitamin B-12 improves hematological, biochemical-metabolic indices and peripheral nerve function in B-12 deficient Indian adolescent women, *PloS ONE*, Vol. 14, Issue 10, 2019, e0223000.
[56]. A. P. Trouvin, S. Perrot, Functional and histological improvements of small nerve neuropathy after high-concentration capsaicin patch application. A case study, *Pain Rep*., Vol. 4, Issue 4, 2019, pp. 1-4.

Appendix 1. General Law of Conservation

A1.1. Integral (Global) Form

Let us consider a continuous medium where ρ is the density or volumic mass and $\underline{U}$ is the velocity, in a material volume $\Omega(t)$ $i.\ e.$: A subdomain of the medium, of arbitrary size, composed of the same particles, dependent of time t, that we will study and follow in his motion, of boundary $\partial\Omega(t)$ with its outward normal $\underline{n}$. We note the spatial coordinate (position) $\underline{x} \in \Omega(t)$.

Let $a(\underline{x}, t)$ be a scalar or vector field enough regular, one can prove the transport theorem:

$$\frac{d}{dt} \int_{\Omega(t)} a(\underline{x}, t) \; d\Omega(t) \; = \; \int_{\Omega(t)} \left[\frac{\partial a}{\partial t} + div\left(a \otimes \underline{U}\right) \right] d\Omega(t), \quad (6.11)$$

$\otimes$ designates the usual vector product, $\frac{d}{dt}$ is the (total or particular) time derivative, and $\frac{\partial}{\partial t}$ is the partial time derivative.

And for a vector field $\underline{f}$ enough regular, the divergence formula:

$$\int_{\partial\Omega(t)} \underline{f}.\underline{n} \, d\Sigma(t) \; = \; \int_{\Omega(t)} div\left(\underline{f}\right) d\Omega(t) \quad (6.12)$$

A balance equation for the quantity ($\rho \, a$) can be written under the general form:

$$\frac{d}{dt} \int_{\Omega(t)} \rho \, a \; \; d\Omega(t) \; = \; \int_{\Omega(t)} \mathcal{A} \, d\Omega(t) + \int_{\partial\Omega(t)} A.\underline{n} \, d\Sigma(t), \quad (6.13)$$

where $\mathcal{A}$ is a (volumic) production-disappearance term and A is a (surfacic) exchange flux across the boundary $\partial\Omega(t)$.

A1.2. Conservative Differential (Local) Form

Using the transport theorem (6.11) and the divergence formula (6.12), we get immediately:

$$\frac{d}{dt} \left(\rho \, a\right) + div\left(\rho \, a \otimes \underline{U}\right) \; = \; \mathcal{A} + div(A) \quad (6.14)$$

And in one space dimension (1D) of interest here because it will be our case:

$$\frac{d}{dt} \left(\rho \, a\right) + \frac{\partial}{\partial x} \left(\rho \, a \, u\right) \; = \; \mathcal{A} + \frac{\partial A}{\partial x} \quad (6.15)$$

A1.3. Mass and Momentum

The classical conserved physical quantities are: Mass, momentum and energy. The last one is of less interest here because it introduces thermic power, heat exchanges and additional variables of whom at least the temperature… Moreover it will not bring any thing here because the measure is isotherm.

For the two others, Table 6.1 summarizes:

Table 6.1. Balance terms.

Balance	a	$\mathcal{A}$	A
Mass	$\mathbf{1}$	See after	$\mathbf{0}$
Momentum	$\underline{\boldsymbol{U}}$	$\boldsymbol{\mathcal{F}}$	$\mathbf{0}$[9]

where $(\mathcal{F})$ is the resultant of the external volumic forces.

A1.4. Case of Discontinuity

Consider a discontinuity surface $\Lambda(t)$ moving with velocity $\underline{S}$. Let us note $[\![z]\!] = z_+ - z_-$ the jump of a variable z across this discontinuity. Then the divergence formula and the transport theorem can be generalized:

$$\int_{\partial\Omega(t)} \underline{f}.\underline{n}\, d\Sigma(t) = \int_{\Omega(t)} div(\underline{f}) d\Omega(t) + \int_{\Lambda(t)} [\![\underline{f}]\!].\underline{n}\, d\Lambda(t)$$

$$\frac{d}{dt}\int_{\Omega(t)} a(\underline{x},t)\, d\Omega(t) = \int_{\Omega(t)} \frac{\partial a}{\partial t}\, d\Omega(t) + \int_{\Omega(t)} (a \otimes \underline{U}).\underline{n}\, d\Sigma(t) - \\ - \int_{\Lambda(t)} [\![a]\!](\underline{S}.\underline{n})\, d\Lambda(t)$$

And besides the previous conservation laws under conservative differential form, one can deduce the Rankine-Hugoniot jump relations that govern the discontinuities:

$$[\![\rho\, a \otimes (\underline{U} - \underline{S}) - A]\!].\underline{n} = 0,$$

which gives in 1D because $A = 0$:

$$[\![\rho\, a\, u]\!] = s[\![\rho\, a]\!],$$

and then precisely for the mass and momentum

$$[\![\rho\, u]\!] = s[\![\rho\,]\!] \; and \; [\![\rho\, u^2]\!] = s[\![\rho\, u]\!]$$

[9] In the absence of shear forces (or viscosity) and pressure gradient…

By eliminating s, we obtain:

$$[\![\rho]\!]\,[\![\rho\,u^2]\!] \;=\; [\![\rho\,u]\!]^2,$$

and after simplification:

$$\rho_-\;\rho_+\,(u_+ - u_-)^2 \;=\; 0 \;\Rightarrow\; u_+ \;=\; u_- \;=\; s \qquad (6.16)$$

Thus the discontinuity propagates at the continuous speed of the medium. It is the so called **contact discontinuity** (the mediums on both sides of the discontinuity do not mix). It is the only possible discontinuity. Hence in this model NO CHOC.

This shows also that there is no steady ($s \;=\; 0$) contact discontinuity in moving medium. What we will use later.

A1.5. Problem Type

We refer to [18] for the definitions and notions used here. To simplify the analysis, we stay with our 1D case. The model under the classical vector form is:

$$\frac{\partial w}{\partial t} + \frac{\partial f(w)}{\partial x} \;=\; \mathcal{S}(w), \qquad (6.17)$$

w is the vector of conservative variables, f is the flux and $\mathcal{S}$ is a source[10] term. They are given by:

$$w \;=\; \begin{pmatrix}\rho\\ \rho\,u\end{pmatrix}, f(w) \;=\; \begin{pmatrix}\rho\,u\\ \rho\,u^2\end{pmatrix} \;=\; \begin{pmatrix}w_2\\ \frac{w_2^2}{w_1}\end{pmatrix}, \mathcal{S} \;=\; \begin{pmatrix}\mathcal{A}\\ \frac{\rho\,F}{m}\end{pmatrix} \qquad (6.18)$$

The Jacobian matrix of the flux writes:

$$A(w) \equiv \frac{df}{dw}(w) \;=\; \begin{pmatrix}0 & 1\\ -\frac{w_2^2}{w_1^2} & \frac{2\,w_2}{w_1}\end{pmatrix} = \begin{pmatrix}0 & 1\\ -u^2 & 2u\end{pmatrix}$$

Its eigenvalues verify $det(A - \lambda\, I) \;=\; 0$, thus:

[10] See the details further. Here let us precise only that $\mathcal{A}$ is proportional to the transverse current, m is the mass of a particle and F is the resultant force submitted by this ion

$$\lambda.(2u-\lambda)+u^2 \;=\; (\lambda-u)^2 \;=\; 0$$

This leads to a double eigenvalue:

$$\lambda_1 \;=\; \lambda_2 \;=\; u,$$

and the (UNIQUE) associated (right) eigenvector is:

$$r \;=\; \begin{pmatrix}1\\ u\end{pmatrix}$$

The matrix A is not diagonalizable. The system[11] is not really hyperbolic!

To close this subsection, we end with the link with the usual fundamental principle of dynamics. For this, we notice the general result: when an eigenvalue is double; the associated characteristic field is "linearly degenerate", that is by definition:

$$\frac{d\lambda}{dw}.r \;=\; 0,$$

which is easily verified and the corresponding discontinuities are exclusively of "contact discontinuity", what we have already noted. In addition, in this case $\mathcal{R} \equiv \lambda \;=\; u$ is a Riemann invariant:

$$\frac{d\mathcal{R}}{dw}.r \;=\; 0$$

By multiplying (at left) the initial system by $\frac{d\mathcal{R}}{dw}$, we obtain the general equation for the invariant:

$$\frac{\partial\mathcal{R}}{\partial t}+\lambda\,\frac{\partial\mathcal{R}}{\partial x} \;=\; \frac{d\mathcal{R}}{dw}.\mathcal{S}$$

Telling that the Riemann invariant verifies an (ODE) ordinary differential equation[12] on the characteristic curve Γ (which here is nothing else than the trajectory because $\lambda \;=\; u$):

$$\Gamma\colon \frac{dx}{dt} \;=\; \lambda, \frac{d\mathcal{R}}{dt}\Big)_{\Gamma} \;=\; \frac{d\mathcal{R}}{dw}.\mathcal{S}$$

[11] We meet such systems in gas dynamics with constant pressure called "pressureless" and used to study the formation of large-scale structures in the universe!
[12] This is the basis of the method of characteristics…

By developing this ODE, we obtain:

$$\underbrace{\frac{\partial u}{\partial t} + u\,\frac{\partial u}{\partial x}}_{\gamma \equiv \frac{du}{dt}} = -\frac{u}{\rho}\mathcal{A} + \frac{1}{\rho}\left(\frac{\rho F}{m}\right)$$

That is:

$$m\,\gamma = F - \frac{m\,u}{\rho}\mathcal{A}, \tag{6.19}$$

This is an elegant way to retrieve the "Lagrangian" fundamental dynamic principle (force = mass × acceleration) with an unobvious corrective term due to the flux of ions of the transverse current, from an "Eulerian" conservation of momentum!

Appendix 2. Mass Equation Source Term

First, recall that for ion k, the density ρ_k is related to our variable: its concentration c_k by the simple relation

$$\rho_k = c_k.M_k,$$

where M_k is the "constant" molar mass.

We will calculate $\mathcal{A}$ on a slice inside the gland with radius r and thickness dx. Its volume is $V = \pi.r^2.dx$ and its lateral area is $S = 2\pi.r.dx$; the total current crossing this lateral surface is

$$-S.J_k^t,$$

where $J_k^t = J_k^{cross} + J_k^{capa}$.

So if we note e the elementary charge and m_i the mass of the ion, the mass transfer is

$$-S.J_k^t.\frac{m_k}{e} \equiv -S.J_k^t.\frac{M_k}{F}$$

Hence, per unit volume

$$\mathcal{A} = -S.J_k^t.\frac{M_k}{F}.\frac{1}{V},$$

$$\mathcal{A} = -\frac{2\,M_k}{r.F}.J_k^t$$

Appendix 3. A Result Proof

At steady state, the equation for the momentum, for chloride near anode, reduces to

$$\frac{d(c.u^2)}{dx} = -\frac{e}{m}.c.\mathbb{E} - \frac{\xi}{m}(c.u),$$

which, by using the expression of the electric field (6.4) $\left(\mathbb{E} = -\frac{\mathrm{d}\Phi}{dx}\right)$ and Ohm's law (6.3) $\left(c.u = \frac{\sigma}{F}.\frac{\mathrm{d}\Phi}{dx}\right)$ gives

$$\frac{\sigma^2}{F^2}\frac{d\left(\left[\frac{d\Phi}{dx}\right]^2.\frac{1}{c}\right)}{dx} = \frac{e}{m}.c.\frac{d\Phi}{dx} - \frac{\xi.\sigma}{m.F}.\frac{\mathrm{d}\Phi}{dx},$$

or else, after developing and simplifying by $\frac{\mathrm{d}\Phi}{dx}$:

$$c = c^* + \mathcal{C}.\left[\frac{d\Phi}{dx}.\frac{d}{dx}\left(\frac{1}{c}\right) + \frac{2}{c}.\frac{d^2\Phi}{dx^2}\right], \tag{6.20}$$

$$c^* = \frac{\xi.\sigma}{e.F},$$

$$\mathcal{C} = \frac{\sigma^2.m}{F^2.e},$$

To prove, begin with equation (6.20) above and suppose c is constant, then we have $c'(x) = 0$ and

$$c = c^* + \frac{2\mathcal{C}.\Phi^{"}}{c} \Leftrightarrow c^2 - c^*.c - 2\mathcal{C}.\Phi^{"} = 0$$

Solving this second order algebraic equation, we get the constant c^* and an absolute error:

$$c = c^* + \varepsilon_{abs},$$

$$\varepsilon_{abs} = \frac{4\mathcal{C}.\Phi^{"}}{c^* + \sqrt{c^{*2} + 8\mathcal{C}.\Phi^{"}}}$$

For the moment, to finish, just assume, see further the mass steady equation:

$$0 < \Phi^{"} = \frac{2G}{r.\sigma}\Phi < \frac{2G}{r.\sigma}\Phi^{A}$$

Appendix 4. A Result Proof

We have $\Phi_s'' \geq 0 \Rightarrow \Phi_s'$ increasing.

But $\Phi_s'(L_e + L_s) \leq 0 \Rightarrow \Phi_s' \leq 0 \Rightarrow \Phi_s$ decreasing.

Current continuity and $\Phi_s' \leq 0 \Rightarrow \Phi_e'(L_e \leq 0 \Rightarrow \Phi_e' \leq 0 \Rightarrow \Phi_e$ decreasing.

As $\Phi_e'(0) \leq 0$ and current continuity $\Rightarrow \Phi_e(0) \leq \Phi^A$.

Appendix 5. A Result Proof

Let us put $D = \Phi^{simple} - \Phi$ then

$\frac{d^2\mathrm{D}}{dx^2} = \frac{2}{\sigma.r}[\mathrm{G}(\Phi^A).\Phi^A - G(\Phi).\Phi] \geq 0 \Rightarrow \frac{d\mathrm{D}}{dx}$ increasing.

But $\frac{d\mathrm{D}}{dx}(L_e + L_s) = -\frac{[\mathrm{G}(\Phi^A).\Phi^A - G(\Phi).\Phi]}{\sigma} \leq 0 \Rightarrow D$ decreasing.

However $D(0) = h\frac{d\mathrm{D}}{dx}(0) \leq 0 \Rightarrow \forall x, D(x) \leq 0: \Phi^{simple}(x) \leq \Phi(\mathrm{x})$.

We can solve exactly the linearized problem, we find:

$$\Phi^{simple}(x) =$$
$$= \begin{cases} \frac{\Phi^A}{\sigma r_e^2}(G_e(x^2 - 2(h+x)L_e)r_e + \sigma r_e^2 - (h+x)G_s r_s(2L_s + r_s)), \text{if } x \leq L_e \\ \frac{\Phi^A}{\sigma r_e^2 r_s}(r_e(-G_e L_e(2h + L_e) + \sigma r_e)r_s \\ +G_s((x - L_e)r_e^2(x - L_e - 2L_s - r_s) - (h + L_e)r_s^2(2L_s + r_s))), \text{otherwise} \end{cases} \quad (6.21)$$

These formula show easily that:

$\forall x, \Phi^{simple}(x) \leq \Phi^A$ and Φ^{simple} decreasing.

We can deduce $\forall x, \Phi(\mathrm{x}) \geq \Phi^{simple}(L_e + L_s)$ because Φ^{simple} decreasing.

It remains just to calculate $\Phi^{simple}(L_e + L_s)$ to get $\varepsilon\ldots$ Because here, simply

$$\varepsilon = \frac{\Phi^A - \Phi^{simple}(L_e + L_s)}{\Phi^A}$$

Appendix 6. A Result Proof

For the proof, we use Ohm's law, see (6.3):

$$I^{a\_simple} = -\sigma.\pi.r^2.\frac{d\Phi^{simple}}{dx},$$

and begin by calculation I^{a_simple} from formula (6.21), we obtain the desired result.

Next, we continue with the Ohm's law:

$$I^a = -\sigma.\pi.r^2.\frac{d\Phi}{dx},$$

and using the balance equation (6.9), we have

$$-\frac{dI^a}{dx} = 2\pi.r.G(\Phi).\Phi,$$

$$\Rightarrow I^a(\Phi^A, x) = I^a(\Phi^A, L_e + L_s) + 2\pi.r.\int_x^{L_e+L_s} G(\Phi).\Phi.\mathrm{dx},$$

or

$$I^a(\Phi^A, L_e + L_s) = \pi.r^2.G\big(\Phi(L_e + L_s)\big).\Phi(L_e + L_s),$$

and

$$G(\Phi^A.[1-\varepsilon]).\Phi^A.[1-\varepsilon] \le G(\Phi).\Phi \le G(\Phi^A).\Phi^A$$

Chapter 7

Zinc Oxide (ZnO) Nano Particles for Anxiolytic Effect

Burcu Ertuğ and Suzi Amado

7.1. Introduction

Anxiety is an uncomfortable state but it can serve a function: It can motivate a person to take action or focus on a certain subject. It can contribute to achievement of a person [1]. To a certain extent anxiety is necessary and useful. However when it reaches a threshold of duration and or intensity it starts to have an effect on a person's functioning and anxiety disorders are more likely to occur beyond that threshold. Everybody experiences anxiety to a certain extent. People are programmed to experience anxiety so that they can anticipate danger and take action [2].

Anxiety and fear co-occur often. The main distinction between fear and anxiety is that people are afraid of a specific stimulus and their fear dissolves when the stimulus disappears. They don't experience fear when the stimulus is absent. However anxiety doesn't dissolve when the stimulus disappears. Actually anxiety can be present although any stimulus is absent. The person experiences worry and believes that something dangerous will happen. In the brain the amygdala is hypersensitive and misinterprets data related to danger. The amygdala codes a neutral situation as dangerous and anxiety starts. When the prefrontal cortex cannot distinguish between a benign stimulus and a threat it doesn't stop the amygdala. So anxiety continues and the person worries and feels anxious about a stimulus that may be absent, or not as dangerous as the amygdala perceives. Of course there are times the

Burcu Ertuğ
Nişantaşı University, Istanbul, Turkey

stimulus is there and dangerous thus anxiety is necessary and useful to survive or take action [3].

Anxiety and stress impose negative effects on the human mental health. These two take place as a result of psychological and physiological effects triggering each other. According to American Institute of Stress, the most common definition of stress is mental or physical tension. Stress is a feeling based on the perception that personal and social resources of the individual are exceeded. In addition, contemporary stress is a common problem and it seems persistent today [4, 5]. During the lifetime a quarter percent of the individuals in the society experiences anxiety. A number of various mental disorders are treated using a drug therapy today. However, most of the time these drug therapies might not prove as effective as expected to be. In addition, many patients express a suffering from some of the side effects of these drug therapies [4]. One of these mental disorders is the anxiety disorder, which is common in the population.

Thus in the present study, we have reviewed some recent researches on the nano-zinc oxide supplements, which are investigated increasingly against anxiety. Anxiolytic effects of zinc are utilized as a reinforcement to the current classical drug therapies. Zinc is regarded to play a role in the neurotransmitter production and also in the regulation of neurotransmitter release. First of all, a brief explanation of the term anxiety has been given. Secondly, the influence of the trace element zinc on the human metabolism has been explained. In the third section, principle methods of the nano-ZnO particle synthesis have been mentioned. Finally, the recent researches for a sufficient anxiety treatment via nano-zinc oxide particles have been examined.

7.2. Nature of Anxiety: A Brief Look

An individual with anxiety disorder might suffer from another mental health disorder sleep disorder, irritable bowel syndrome etc. as comorbidities. The prevalence of anxiety in the population is given in Fig. 7.1. [5].

The serotonin receptor is also under the effect of zinc and the receptors are significant in order to modulate the anxiety. The mood disorders are related to the element of zinc and its function in a great number of proteins. The total weight of zinc is 2-3 mg in the whole body whereas

some parts of the brain (frontal cortex, amygdala) are rich in zinc, which are related to human emotions. It has been proposed that a deficiency in the zinc may result in a negative mood [6]. The higher the special oxygen species, the more damaging will the oxidative stress be. In medicine, nano-ZnO has become popular for future therapy opportunities due to its effect on brain oxidative status and the anxiety behavior [7, 8].

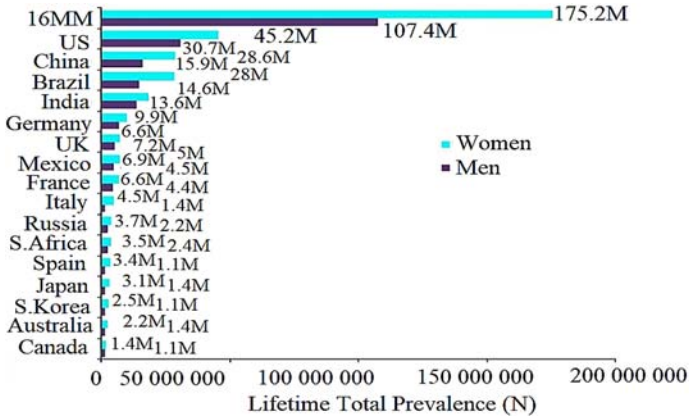

Fig. 7.1. Lifetime prevalence of anxiety [5].

Needless to say, quality of life is the perception of the status of the oneself in life related to his/her purposes, expectations, standards and his/her worries on the basis of his/her cultural and value systems. Anxiety is a wide and complex concept affected by the individual's physical health, psychological state, self-dependence level and the social intercourses. Particularly, some of the individuals experiencing the anxiety are negatively affected in their social life leading to poor quality of life. The results might be job loss due to working performance reduction, problems with the partner, reduction of the social interaction, poor academic success in the adolescents. The relationship between anxiety and life satisfaction has been found to be inversely proportional in many of the researches [9-11].

Anxiety disorders are associated with excessive fear and anxiety. Fear and anxiety overlap in some ways. An important distinction is in the time zone. Fear is responses to a current threat a person experiences or perceives. Anxiety is a response to a threat a person anticipates. When people experience fear they experience autonomic arousal that they

utilize for their fight or flight response. Their cognitions include thoughts of immediate danger and they may display behaviors associated with escape. When people experience anxiety, they can have muscle tension, be vigilant to prepare for a potential danger in future or they can display avoidant behavior. Avoidance can sometimes help to reduce the fear or anxiety. When a person has an anxiety disorder his or her anxiety is either more excessive and/or more persistent than it is expected within norms. People who have anxiety disorders tend to overestimate a danger in a given situation. Thus the clinician assesses if the anxiety is out of proportion for a given situation or not. Different anxiety disorders are diagnosed as a result of different durations of anxiety and different situations and conditions that awaken excessive anxiety and/or fear in the person. Usually if a person has an anxiety disorder as a child and is not treated the disorder continues in one form in adulthood. Women are more vulnerable to anxiety disorders than men [12].

7.3. Zinc and Human Metabolism

Food is the fuel for the human metabolism in order to maintain the physical and psychological well-being. Thus it is related to the cognitive functions and the human mind as a whole. Also, the insufficiency in some of the nutrients in the human body cause negative mood, improper function of the cognitive abilities and aggression [13]. Zinc is effective on human metabolism via hundreds of enzymes in the growth process such as the rapid growth in the infancy period. Total body zinc amount is 2-3 g in the human organism, the highest concentration of zinc is found in hair, nails, bones etc. [14].

A small percentage of the world annual ZnO production is consumed for medical purposes. These medical purposes might be the replacement of the antibiotics as an antibacterial drug or as a drug carrier in the treatment of the cancer. ZnO is considered to be a safe material according to US Food and Drug Administration though the duration of the exposure and the exposure concentration might still be influential on the toxicity [15].

It is estimated that one-third of the World population is affected by zinc deficiency problem. The worldwide diet-caused zinc deficiency prevalence is as high as 40 %. It is reported that in Turkey for 25 % of the adult population serum Zn level is below 76.2 μg/dL [14].

Significant factors reducing the absorption of zinc are frequent coffee and tea consumption. The smoking habit and the regular consumption of the alcoholic drinks also contribute to the reduction of zinc absorption. There is a correlation between the zinc deficiency and the oxidative stress. Since zinc is a biological antioxidant, it protects the cells from the oxidative damage of the free radicals. In the cases of zinc deficiency, the cells via the oxidative stress are damaged more easily and the aging process becomes more rapid. While the zinc deficiency affects the whole body, its effect on the central nervous system is significant and the zinc deficiency is found to be related to the neuropsychiatric disorders. Daily requirements of zinc are 10 and 12 mg for men and women, respectively and 15 mg for both adolescents and the individuals aged over 65 years. The underlying factor behind the zinc deficiency might also be an absorption, which is defective and in fact, inherited. This kind of zinc deficiency is termed as zinc malabsorption syndrome. Another issue related to the absorption of zinc is termed as pyroluria. Pyroluria has got a genetic cause and it is a biochemical problem, which leads to the depleted vitamin B6. This result, in turn, causes the anxiety disorder [14, 16].

Many proteins, such as enzymes which are responsible to regulate various cellular processes are known to contain zinc element. Zinc as a trace element takes part in the nerve repair of the central nervous system. The difficulty in memory-learning capabilities and hyperactivity take place as a result of zinc deficiency. The highest content of zinc element exists in hippocampus, which is related to mood and the memory. In addition, zinc plays a role in the modulating of the human responses under stress conditions. However, the processed food of the modern life generally lacks zinc element. Zinc in the human body is unable to be stored. Thus zinc of a small dose must be taken regularly. In the human body, zinc carries out a reinforcement role to the immune system against the infections. Very low zinc levels prevent the proper functioning of the immune system. During high-level stresses, zinc loss takes place through saliva, sweat and also the urination [16].

The neural activities of the body are able to function only by the presence of zinc. It is probable that zinc supplements have got an effect of decreasing anger, etc. Recently, the medical usages of the inorganic nanoparticles, i.e. zinc oxide- might be utilized to treat the pain perception or anxiety condition. Acute pains can also be treated by injecting nano-ZnO suspensions. There are other studies that show if

high amount of zinc is given by the diet, it can be used to treat the stress induced anxiety [17].

7.4. Synthesis of Nano Zinc Oxide

Despite the fact that the biological processes are under the effect of ZnO, the extend of the effect is a function of some factors such as size of the particles, particle morphology, particle concentration, the duration of the exposure, pH value and biocompatibility characteristics of the particles [15].

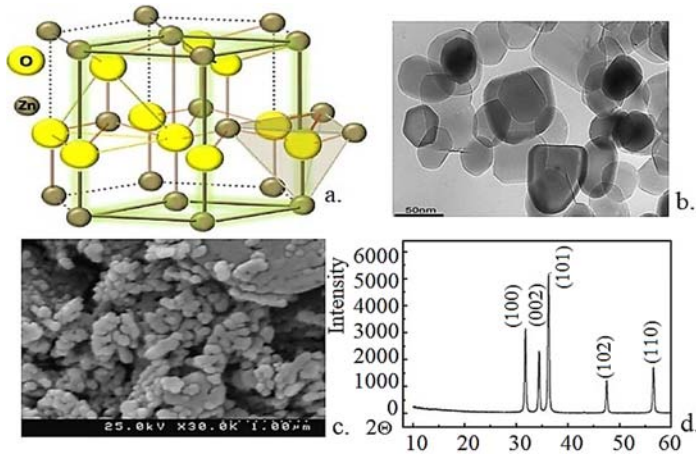

Fig. 7.2. (a). Crystal structure of ZnO (gray Zn^{2+} ions and yellow O^{2-} ions) [18], (b). TEM image [19], (c). SEM image [20] and (d). XRD diagram of nano ZnO particles [19].

The hexagonal wurtzite type is known to be the most common structure of zinc oxide as shown in Fig. 7.2(a) whereas there are two other types as zinc blende and rock salt. In the wurtzite structure, one Zn^{2+} has got a tetrahedral coordination with the four O^{2-} ions. Similarly, one O^{2-} is in coordination with the four Zn^{2+} ions. The lattice parameters of the wurtzite zinc oxide are 3.25 Å and 5.21 Å. for *a* and *c*, respectively [18]. X-ray Diffraction (XRD) pattern of the crystalline zinc oxide is shown in Fig. 7.2(d) and the microstructure of the zinc oxide particles is observed by Scanning Electron Microscopy (SEM) and Transmission Electron Microscopy (TEM).

The optimum requirement of the biomedical applications is the uniformity of the particle size and the particle morphology. The up-to-date synthesis procedures of the nano-size zinc oxide particles are briefly explained below.

7.4.1. Chemical Precipitation

This chemical precipitation synthesis is the most widely-used method. The starting materials are acetates, nitrates or sulphates of Zn. The compounds of ammonium hydroxide ($NH_3.H_2O$) or sodium hydroxide might be preferred as the precipitator. After finishing the process, zinc hydroxide, $Zn(OH)_2$ compound is produced. Finally, the converting of zinc hydroxide to zinc oxide is conducted by the sintering step [21].

One choice is the selection of starting materials to be $Zn(CH_3COO)_2.2H_2O$ (acetate precursor) and NaOH. A calcination step of the intermediate products is carried out in order to produce nano-zinc oxide. In another simpler route, the starting materials might be selected to be $ZnSO_4$ (sulphate precursor) and NaOH as shown in Fig. 7.3. Here a vigorous mixing step is done at ambient temperatures. Following the washing step of the precipitate, drying is carried out [21, 22].

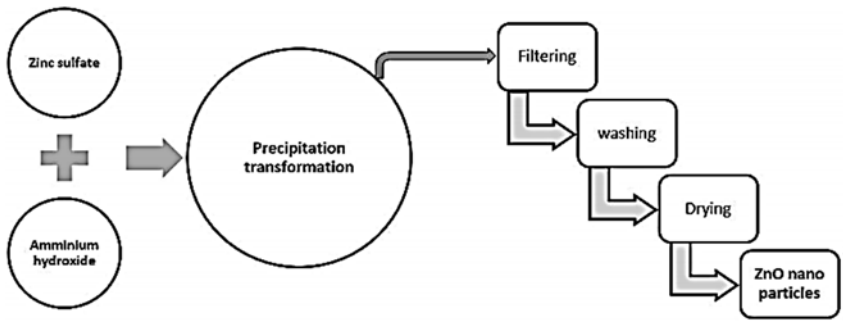

Fig. 7.3. Preparation of nano-ZnO particles by chemical precipitation [22].

In the simple precipitation method, zinc nitrate, zinc acetate or zinc sulphate is used as the raw material. After drying at 100 °C for overnight, a calcination step is carried out at 300-500 °C depending on the type of the precursor. As a result, the particle size of the final product is in the range of 30-60 nm [23].

7.4.2. Sol-gel Method

In the first stage of the sol-gel method, a zinc precursor is prepared by dissolving $Zn(CH_3COO)_2.2H_2O$ in ethanol. The refluxing of the resultant solution is conducted using a distillation apparatus. Following the boiling and stirring of the aqueous solution, a hygroscopic product is obtained. In the second stage, ZnO clusters are prepared. For this purpose, $LiOH.H_2O$ is added into the hygroscopic product of the first stage. An ultrasonic bath is utilized in order to make the product transparent, which accelerates the hydroxide, OH^- ion release. A low temperature reaction is carried out in open air so that the particles do not grow rapidly, leading to zinc oxide sol. The last stage is carried out for the crystal growth at the room temperature with the help of LiOH. The growth rate of the crystals depends on the LiOH content. The sol-gel synthesis route of the nano-particles has been conducted by many researches due to the simplicity of the method and the cost of the method is also low. Another advantage of this method is that the synthesis conditions are not as severe as the other methods [21, 24, 25].

7.4.3. Pyrolysis Methods

The quality of the final nanoparticle is high when a pyrolysis synthesis technique is used. In the pyrolysis method, the first step is a room temperature mixing of $Zn(CH_3COO)_2.2H_2O$ and $NaHCO_3$ and then a pyrolysis process is carried out at the temperature of reaction. Following the cleaning by the deionized water, finally a thermal decomposition step is applied to produce nano-ZnO [21].

In the spray pyrolysis technique, the particle size is precisely controlled and the cost of the method is low. Using this method, the final specific surface area is larger. Nitrate, chloride and acetate solutions are used as the precursors. Acetate solutions are the best choice due to environmental considerations. Starting with the acetates, a product with a small grain size and thus a large specific surface area is obtained. The method termed as the spray pyrolysis is carried out by the starting material of zinc acetate. A tubular reactor as in Fig. 7.4(a) is utilized to synthesize nano zinc oxide. TEM image of nano zinc oxide particles produced by this method is observed in Fig. 7.4(b) [26].

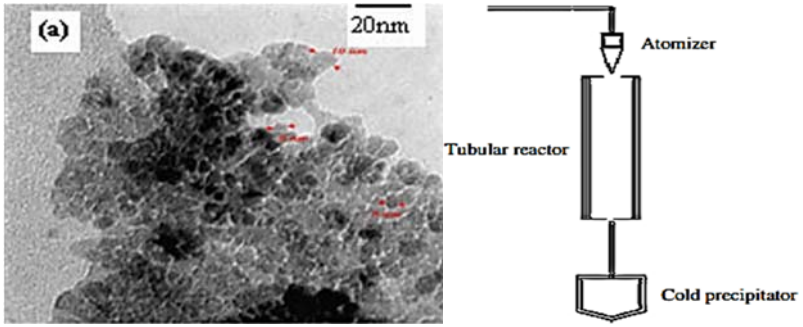

Fig. 7.4. (a) TEM image of nano-ZnO, and **(**b) the apparatus of spray pyrolysis [23].

7.4.4. Mechanochemical Method

This synthesis method is the most advantageous one among the others and it permits the preparation of nano-materials with some superior properties. In this method, the synthesis conditions are not severe since it involves dry milling of a solid phase. The mechanical energy is also utilized for the synthesis of nano-ZnO [27]. The mechanical milling is both an ecological and economical route to produce nano-ZnO particles. Without using any solvent, the milling process can be carried out at low temperatures. The formation of nano-particles and at the same time dispersion enhance the mechanochemistry process [28].

In order to prepare the nano-sized materials, the mechanical milling is preferred because this method is relatively simple, it can be applied for the preparation of many nano-materials and the synthesis cost is low. In fact, the mechanical milling method is a top down approach for the synthesis. In this method, the dimension of a micro-scale material can be reduced to nano-size by grinding. High shear forces are applied to the powder mixture. Planetary ball-mill is one of the frequently used devices [29].

The movement of the balls and the powder can be seen in Fig. 7.5. The bowl and disc rotate oppositely to each other and thus there is an alternate synchronization of the centrifugal forces. The friction occurs between the balls and powder. A high-speed milling is achieved by the planetary ball-mill. Four main steps can be described during the milling process. At the first step, collision of the balls result in the compressive forces

and these forces flatten the powder particles. The particles change their shapes or the milling balls impact the particle clusters. Diffusion distance is reduced by the powder constituents at the intermediate step. The predominant processes are the fracturing and cold welding. The powder composition is not homogeneous. The particle sizes are excessively reduced at the final step. The particle microstructure becomes more homogenous. The deformations in the powder particles are excessive. If the mechanical milling is carried out further, the dispersion will not be physically improved at the completion step [30].

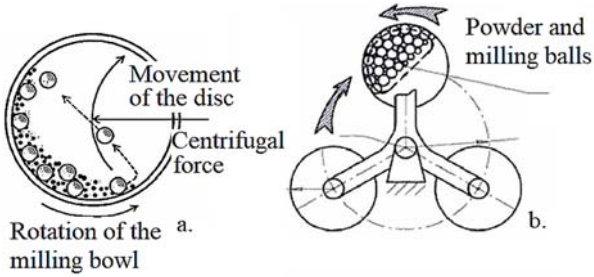

Fig. 7.5. (a) The motion of the ball [30] and powder;
(b) Planetary ball mill [31].

During this high-energy milling carried out in the ball-mill, a low-temperature reaction takes place by the impact effects of the balls on the powder. However, uniform grinding might present a problem during the milling process. Because as the milling duration increases, the grain size reduction might decrease. This effect might be observed in the same way with the milling energy. In addition, more contamination might be observed as the milling duration increases. Despite these drawbacks, this method yields fine particle size, and the particle agglomeration tendency is low. Thus, a highly-homogeneous final mixture can be obtained [32]. In order to eliminate the agglomeration (if any), a salt addition can be done during the reaction. Afterwards, washing can be applied to the final powder for the separation, prior to the calcination step [23].

In a recent study, a mixture of $Zn(CH_3COO)_2$ and $H_2C_2O_4.2H_2O$ has been ground to produce nano-$ZnC_2O_4.2H_2O$ particles. Later on, nano-$ZnC_2O_4.2H_2O$ particles have been thermally decomposed in order to obtain nano-sized particles. The resultant morphology of the nano

particles has been observed to be highly-homogeneous. As the milling time has been increased, finer particle sizes have been produced [21]. In another study, anhydrous $ZnCl_2$ and Na_2CO_3 reactants have been exploited as the starting materials. In order to separate the particles of zinc oxide, the addition of a NaCl medium has been made during the reaction. Final carbonate precursors, $ZnCO_3$ have been subjected to a calcination step at the range of 400-800 °C [32].

7.4.5. Biological Method

Using the biological method to produce nano zinc oxide materials has been the focus of the current researches since this technique is friendly to the environment. Up to now, some different plant extracts have been utilized to synthesize nano ZnO particles as shown in Fig. 7.6. Also, nano ZnO particles produced by this method, have been proved to be non-toxic and highly-biocompatible thus, they are suitable candidates for the biomedical field. Besides, the production cost of these nano particles is low [33].

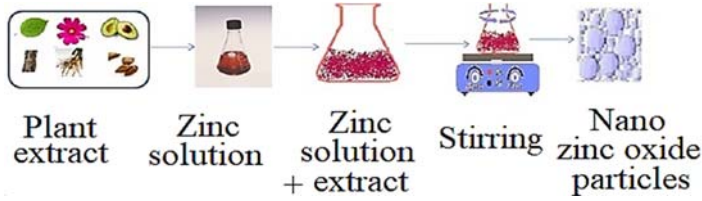

Fig. 7.6. Nano-ZnO particle preparation using plants [33].

In the biological method, *phytoconstituents* are taken advantage for the reduction of oxides to nano-sized particles. The organics and the inorganics are combined to produce the metal oxide nanoparticles. Though, one of the largest amounts of nanoparticle production consists of zinc oxide, there are other nanoparticles produced namely, Ag, Au, SiO_2, TiO_2, CuO, etc. [33].

In a recent study, zinc oxide nano particles have been synthesized using some parts of a plant. The aqueous plant extracts from the leaves, stems, roots and fruits as shown in Fig. 7.7 have been put into reaction with zinc nitrate hexahydrate, ($Zn(NO_3)_2.6H_2O$) in order to obtain nano ZnO particles [34].

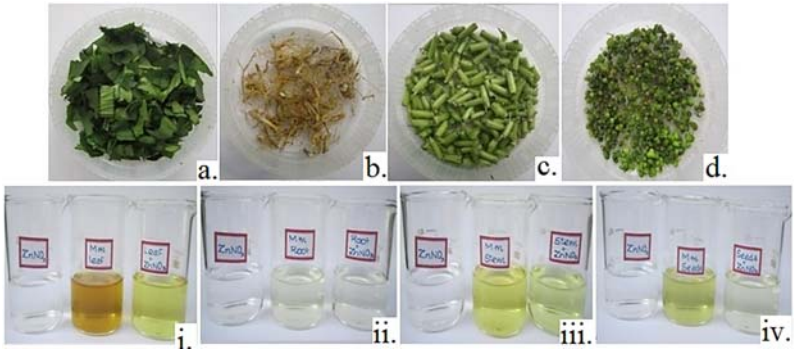

Fig. 7.7. Biological method (a) fresh leaves; (b) stems; (c) roots; (d) fruits, and (i-iv) extract and reaction mixtures [34].

7.5. Nano Zinc Oxide for Anxiety Treatment

As the nanotechnology has improved, moderate-sized particles have been gradually replaced by the nano-sized particles. Among these nano-sized particles, particularly the nano-metal oxides are the most frequently produced types. Today, for the biomedical and cancer applications, there is a growing interest in the use of nano-metal oxides. With the help of the rapid improvement of the nanotechnology field, very fine particles (in the range of 1-100 nm) have been produced, which provides these particles with larger surface areas. Thus these nanoparticles are able to exhibit much more reactivity inside a cell. One of the popular nanoparticles are ZnO based [8]. Oxide compound of zinc is a common pharmaceutical product as well as a good cosmetic product. The stimulation of the enzyme activity or the enzyme growth are carried out by the zinc oxide. Besides, ZnO is a good drug carrier, it is also used to stimulate the growth of the neurons and for the analgesic and the antimicrobial requirements [7].

Recently, nano zinc oxide particles have been the focus of research by providing them with some adequate surface properties for the future therapies of anxiety. Nano-zinc oxide supplements are at the focus of medical researches nowadays due to the fact that the current drug therapies for anxiety have not been proved sufficiently effective. It is known that zinc is a significant factor affecting on the neurotransmitter production and zinc also influences the regulation of the neurotransmitter release. Zinc element induces its anxiolytic effects via serotonin neurotransmitter[16]. The conventional ZnO, Zn methionine or $ZnSO_4$

(zinc sulphate) are the zinc supplements that have got a reduction effect on the anxiety [7].

According to the animal-anxiety test results, zinc sulphate, conventional zinc oxide, zinc methionine supplements have been found to be helpful in the anxiety reduction. There is a higher Zn^{2+} concentration in zinc oxide compound, in comparison to the other two. Despite the less effectivity, zinc oxide and the sulphate forms exhibit a lower toxicity. There are some studies particularly on the toxicity of the nano-sized zinc oxides. The result of these studies indicate that the nano zinc oxide particles exhibit low toxicity and thus they can be used as a supplement in the human body [8]. In order to evaluate the anxiolytic compounds, a test called EPM-elevated plus maze- test has been conducted in the anxiety research. Low doses of nano-sized and high doses of coarser-sized supplements have been injected for therapy in order to induce anxiolytic effects in the EPM test. The anxiety evaluation tests have reported that there is a correlation between the zinc deficiency in the diet and the anxiety level [4].

The influences of nano-ZnO on the central nervous system have been searched for treatment in neurotransmitter system disorders [8]. Also, the impact of the other nano-materials on the central nervous system is the focus of the recent researches. Particularly, in order to examine whether the human emotional behaviours are influenced by the nano-zinc oxide, nano-zinc oxide suspensions have been examined by the animal-anxiety evaluation tests using the injections of 25 mg per body weight. However, the test results indicated that nano-zinc oxide treatment had a slight effect on the emotional behaviour [36]. The central nervous system might be affected by nano-zinc oxide supplements only slightly. The impact of nano-zinc oxide on the behavioral performance has also been studied using the suspensions per body weight. According to the test results, both plasma and brain zinc concentrations moved upwards with the nano-zinc oxide supplements. On the contrast, serotonin neurotransmitter amount in brain remained constant [35].

In another recent study, the stressed state anxiety parameters obtained by the EPM test remained constant with the nano-ZnO. Also, the test results have been compared to the control group. Another behavioural test for the anxiety evaluation is the hole-board test [20]. Torabi_et al. examined the anxiety behaviour with the treatment of the conventional and nano zinc oxide types with several doses. The highest anxiolytic result has been achieved with a treatment of the conventional ZnO using a dose of

10 mg/kg. In this study, nano-ZnO particles with the sizes of 70 nm and 133 nm have been utilized [4].

In order to enhance the treatment of the anxiety, in some of the studies, zinc supplements have been reinforced with vitamin. However, there has been no consistent result in these studies to integrate successfully into clinical practice [16]. A small dose of vitamin C has got an anxiolytic effect along with a stress relieving result. A combined effect of ZnO-vitamin C on the anxiety has been evaluated by the injection of 1.25-5 mg nano-ZnO per unit kg and the results have been compared to those after the injection of 30-120 mg vitamin C per unit kg. Another sample group has been injected only by saline solution. A combined effect of nano-zinc and vitamin C has produced an antioxidant effect on the anxiety [37]. The ascorbic acid (vitamin C) accumulates in the brain mostly. For a healthy mental state, vitamin C is absolutely necessary for the human body. The vitamin C deficiency might result in the fatigue and anxiety because the ascorbic acid is reduced on the case of anxiety. In addition, if the ascorbic acid is absorbed at a low level than necessary, the state of anxiety is a result [7].

Despite the various researches on the anxiolytic effects of nano-ZnO particles, there are several aspects of these particles waiting to be explored. First of all, a comparison of the biological properties of nano-ZnO particles to the other nano-metal oxide particles has not been performed yet. Secondly, toxicity property of the nano-ZnO particles in the biological systems is still controversial [21].

7.6. Conclusions and Future Perspectives

Zinc -as a trace element in the human body- is utilized in many scientific branches involving medicine. The certain amount of zinc content is lost by urination and sweating. Thus daily intake of zinc-based supplements is suggested for the adults.

The oxide compound of zinc is considered to be a multifunctional material owing to a number of attractive properties of it. Two significant properties of zinc oxide are the biocompatibility and biodegradability. Thus, ZnO nano-particles are promising materials for the biomedical field. There are researches on the anticancer or anti-inflammatory properties of these materials. Also, these particles are potential drug carriers to increase the efficiency of the therapy.

A current literature survey has been briefly given in this review related to the evidence on nano-ZnO usage for anxiolytic purposes. There are some certain doses of zinc oxide, which helps the reduction of stress effects. The detailed mechanism of stress and anxiety reduction due to nano-ZnO particles has to be investigated.

Based on the previous researches, it may be inferred that for an effective anxiety treatment, vitamin C can be suggested together with several doses of nano-ZnO.

There are conflicting research results related to the nano-particle usage for the human body. Despite the fact that the element of zinc is absolutely essential for the human body, it may become harmful in case the zinc intake is excessive.

It is possible to produce nano-ZnO particles with different structures. Each of these structures are candidate materials to be used for a number of technologic applications. Thus currently a growing interest is present for developing novel synthesis methods for nano-ZnO particles. One of these methods is the mechanochemical process where nano-sized zinc oxide particles are produced by the high-energy milling and grinding of the precursor powder mixtures. Sol-gel, chemical precipitation, pyrolysis and biological method, which takes advantage of the *phytoconstituents* are among the most frequently used synthesis methods.

There are a number of topics to be explored on ZnO-based nano-particles. First of all, comparison studies on the biological properties of nano-ZnO particles (other nano-metal oxides) are required to be conducted. Also, the toxicity of the nano-sized ZnO is still debatable. The detailed researches focusing on therapeutic function of nano-sized zinc oxide supplements will make contribution to the practical medical use of these particles.

It can be expected that nano-sized ZnO particles could be considered as an attractive alternative for the treatment of anxiety. Therefore, rapid improvements in the nano-particle synthesis technologies will open the way to enhance the *therapeutic* efficiency.

References

[1]. J. Healey, Understanding Anxiety, *Spinney Press*, 2014.

[2]. A. E. Sansone, 10 Things you need to know about anxiety prevention, May 2020, https://www.prevention.com

[3]. Neuroscience in Everyday Life: The Pain Worry The Anxious Brain, https://www.psychologytoday.com
[4]. M. Torabi, M. Kesmati, H. E. Harooni, H. N. Varzi, Different efficacy of nanoparticle and conventional ZnO in an animal model of anxiety, *Neurophysiology*, Vol. 45, 2013, pp. 299-305.
[5]. AIS: The American Institute of Stress 1979-2019, https://www.stress.org/
[6]. Anxiety Disorders on the Rise: Analysis of Lifetime Prevalence in Major Pharma Markets Global Data Healthcare 26 Aprıl 2019, https://www.pharmaceutical-technology.com
[7]. M. Piao, X. Cong, Y. Lu, C. Feng, P. Ge, The role of zinc in mood disorders, *Neuropsychiatry,* Vol. 7, Issue 4, 2017, pp. 378-386.
[8]. M. H. Hafez, S. B. Gad, Zinc oxide nanoparticles effect on oxidative status, brain activity, anxiety-like behavior and memory in adult and aged male rats, *Pak. Vet. J.,* Vol. 38, Issue 3, 2018, pp. 311-315.
[9]. J. J. V. Branca, G. Morucci, M. Maresca, B. Tenci, R. Cascella, F. Paternostro, C. Ghelardini, M. Gulisano, L. Di Cesare Mannelli, A. Pacinia, Selenium and zinc: Two key players against cadmium-induced neuronal toxicity, *Toxicology in Vitro,* Vol. 48, 2018, pp. 159-169.
[10]. H. Sarıçam, S.H. Şahin, E. Soyuçok, The examination of the relationship between nature relatedness, depression, anxiety and stress, *International Journal of Psychiatry and Psychological Researches*, Vol. 4, 2015, pp. 38-57.
[11]. M. Beutel, H. Glaesmer, J. Wiltink, H. Marian, E. Brähler, Life satisfaction, anxiety, depression and resilience across the life span of men, *The Official Journal of the International Society for the Study of the Aging Male,* Vol. 13, 2009, pp. 32-39.
[12]. American Psychiatric Association, Anxiety Disorders DSM 5 ® Selections, *APA Publishing,* 2016.
[13]. A. Özenoğlu, Relationship between mood, food and nutrition, *Nutrition and Dietetics,* Vol. 9, Issue 4, 2018, pp. 357-365.
[14]. Z. Karakaş, Çocuklarda çinko eksikliği, tanı, tedavi, TPHD Türk Pediatrik Hematoloji Derneği, 1999, pp. 1-40, http://tphd.org.tr/
[15]. K. S. Siddiqi, R. T. Husen, A. Husen, Properties of zinc oxide nanoparticles and their activity against microbes, *Nanoscale Research Letters,* Vol. 13, 2018, 141.
[16]. E. Deans, Zinc: An Antidepressant. The essential mineral for resiliency, 2013, https://www.psychologytoday.com/us/blog/evolutionary-psychiatry/201309/zinc-antidepressant
[17]. M. Kesmati, M. Torabi, N. Pourreza, M. Tayebkhah, F. Asadi, Effects of anxiolytic doses of ZnO nanoparticle on ECG parameters in restraint and non-restraint ovariectomized female rats, *Nanomed. Res. J.,* Vol. 4, Issue 4, 2019, pp. 253-260.
[18]. N. H. Alvi, Luminescence properties of ZnO nanostructures and their implementation as white light emitting diodes (LEDs), PhD Thesis, *Linköping University*, June 2011.

[19]. I. B. Slama, I. Mrad, N. Rihane, L. E. Mir, M. Sakly, A. Salem, Sub-acute oral toxicity of zinc oxide nanoparticles in male rats, *Journal of Nanomedicine and Nanotechnology,* Vol. 6, Issue 3, 2015, 284.

[20]. N. Names, Effects of anxiolytic doses of ZnO nanoparticle on ECG parameters in restraint and non-restraint ovariectomized female rats, *Nanomed. Res. J.,* Vol. 4, Issue 4, 2019, pp. 253-260.

[21]. J. Jiang, J. Pi, J. Cai, The advancing of zinc oxide nanoparticles for biomedical applications, *Bioinorganic Chemistry and Applications,* Vol. 2018, 2018, pp. 1-18.

[22]. R. A. Sadraei, Simple method for preparation of nano-sized ZnO, *Research & Reviews: Journal of Chemistry,* Vol. 5, 2016, pp. 45-49.

[23]. A. Ali, A. R. Phull, M. Zia, Elemental zinc to zinc nanoparticles: Is ZnO NPs crucial for life? Synthesis, toxicological, and environmental concerns, *Nanotechnology Reviews,* Vol. 7, Issue 5, 2018, pp. 413-441.

[24]. P. P. Mahamuni, P. M. Patil, M. J. Dhanavade, M. V. Badiger, P. G. Shadija, A. C. Lokhande, R. A. Bohara, Synthesis and characterization of zinc oxide nanoparticles by using polyol chemistry for their antimicrobial and antibiofilm activity, *Biochemistry and Biophysics Reports*, Vol. 17, 2019, pp. 71-80.

[25]. S. Najidha, M. M. Malik, L. Shastri, V. Koutu, Synthesis of nano sized ZnO by chemical method via refluxing, *AIP Conference Proceedings*, Vol. 1849, 020050.

[26]. H. R. Ghaffarian, M. Saiedi, M. A. Sayyadnejad, Synthesis of ZnO nanoparticles by spray pyrolysis method, *Iran. J. Chem. Chem. Eng.,* Vol. 30, Issue 1, 2011, pp. 1-6.

[27]. C. Xu, S. De, A. M. Balu, M. Ojeda, R. Luque, Mechanochemical synthesis of advanced nanomaterials for catalytic applications, *Chem. Commun.,* 2015, Vol. 51, pp. 6698-6713.

[28]. G. Gorrasi, A. Sorrentino, Mechanical milling as a technology to produce structural and functional bio-nanocomposites, *Green Chemistry,* 2015, Vol. 17, pp. 2610-2625.

[29]. Top-down Methods, https://ninithi.wordpress.com

[30]. Synthesis of Nanomaterials by High Energy Ball Milling, 2019, https://www.understandingnano.com

[31]. H. Wu, Q. Li, Application of mechanochemical synthesis of advanced materials, *Journal of Advanced Ceramics,* 2012, Vol. 1, Issue 2, pp. 130-137.

[32]. A. Kołodziejczak-Radzimska, T. Jesionowski, Zinc oxide – From synthesis to application: A review, *Materials*, Vol. 7, 2014, pp. 2833-2881.

[33]. A. Umamaheswari, S. Lakshmana Prabu, A. Puratchikody, Biosynthesis of zinc oxide nanoparticle: A review on greener approach, *MOJ Bioequivalence and Bioavailability,* Vol. 5, Issue 3, 2018, pp. 151-154.

[34]. M. Manokari, C. P. Ravindran, M. S. Shekhawat, Production of zinc oxide nanoparticles using aqueous extracts of a medicinal plant Micrococca mercurialis (L.) Benth, *World Scientific News,* Vol. 30, 2016, pp. 117-128.

[35]. S. Amara, I. B. Slama, K. Omri, J. El Ghoul, L. E. Mir, K. B. Rhouma, H. Abdelmelek, M. Sakly, Effects of nanoparticle zinc oxide on emotional behavior and trace elements homeostasis in rat brain, *Nanotoxicology and Industrial Health,* Vol. 31, Issue 12, 2015, pp. 1202-1209.

[36]. S. Amara, I. B. Slama, I. Mrad, N. Rihane, M. Jeljeli, L. E. Mir, K. B. Rhouma, W. Rachidi, M. Seve, H. Abdelmelek, M. Sakly, Acute exposure to zinc oxide nanoparticles does not affect the cognitive capacity and neurotransmitters levels in adult rats, *Nanotoxicology,* Vol. 8, Issue 1, 2014, pp. 208-215.

[37]. M. Rafieirad, S. Valipour-Chahardah-Charic, Effect of zinc oxide nanoparticles along with vitamin C on motor activity and anxiety in adult male rat, *J. Bas. Res. Med. Sci.,* Vol. 6, Issue 3, 2019, pp. 12-18.

Chapter 8

Enzyme Biosensors

Ashok Saini, Sandeep Yadav and Kavita Vasdev

8.1. Introduction

As discussed in earlier chapters, biosensors are fast, portable, simple-to-use and reliable automated devices which have applications in various fields like biomedical diagnosis, point-of-care monitoring of treatment and disease progression, environmental monitoring, food control, drug discovery, forensics and biomedical research [1].

A wide range of techniques can be used for the development of biosensors using different type of bio-recognition elements like enzymes, whole cells or microorganisms, antibodies, DNA sequences or aptamers to achieve specific and sensitive recognition of target analyte. On the basis of mechanism of monitoring and biorecognition elements, biosensors can be divided into two types- affinity biosensors and catalytic biosensors. In affinity biosensors, biorecognition elements such as antibodies, oligonucleotides, and cellular receptors are used which can specifically bind their target analytes mainly composed of protein or oligonucleotide whereas catalytic biosensors employ enzymes with catalytic activity as a biorecognition element. Generally, the target analytes of catalytic biosensors are non-proteinaceous in nature [2].

In this chapter, we will discuss about the enzyme biosensors. In 1962, Leland C. Clark introduced first enzyme biosensor using immobilized glucose oxidase enzyme and describe the method to make electrochemical sensors using enzyme transducers as membrane enclosed sandwiches as shown in Fig. 8.1 [3]. In 1975, Yellow Springs Instrument Company had launched first commercial biosensor to analyse

Kavita Vasdev
Department of Microbiology, Gargi College, University of Delhi, New Delhi, India

glucose based on the amperometric detection of hydrogen peroxide (H_2O_2). Since then, various research communities come together and developed more sophisticated, reliable and advanced biosensing devices.

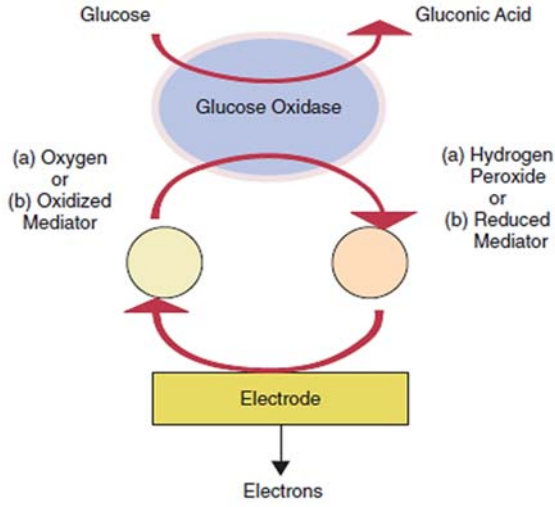

Fig. 8.1. Mechanism of first enzyme biosensor shown by Clark and Lyons (1962).

8.2. Basic Principle of Biosensors

All types of biosensors are mainly composed of two elements: **Bioreceptors** and **Transducers** (Fig. 8.2). Selection of suitable transducers and bioreceptors are crucial for the development of an effective and sensitive biosensor. Moreover, the method used for immobilization of bioreceptor also plays very important role in the efficiency of the biosensors [4].

8.2.1. Bioreceptors

Bioreceptors are the immobilized molecules which recognize or detect specific target analyte (e.g., enzyme substrate, complementary DNA, antigenic). They are also known as biorecognition elements due to their biological origin (Enzyme/DNA/Antibody etc.). These biorecognition elements specifically enzymes can be isolated directly from various living systems or can be synthesized in the laboratory.

Different biomolecules shows different recognition mechanism behavior. The biorecognition elements can be classified into three categories on the basis of their recognition behavior and source (Fig. 8.3): natural, semi-synthetic and synthetic (molecularly imprinted polymer) [6].

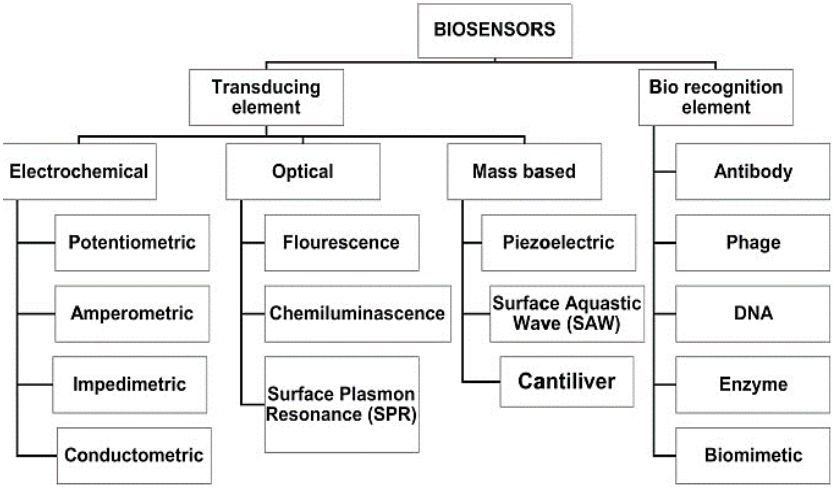

Fig. 8.2. Components of a biosensor [5].

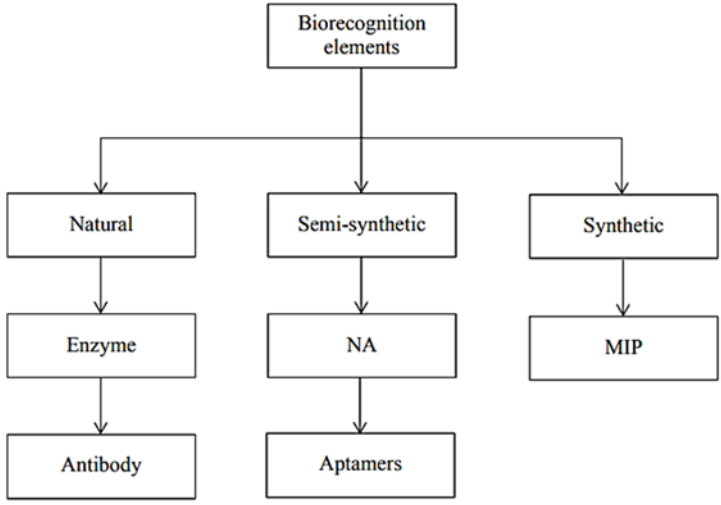

Fig. 8.3. Types of Biorecognition elements [6].

8.2.2. Transducers

Transducers are the components used in biosensors which convert a biochemical signal produced by interaction of bioreceptor (enzyme) and their targets (substrate/inhibitor) into a detectable electrical or other signal. The intensity of signal arising as a result of the biochemical reaction can be directly or inversely proportional to the analyte concentration.

On the basis of the transducing elements, enzyme biosensors can be classified into four types (discussed later):

i) Electrochemical (EC) biosensors;

ii) Optical biosensors;

iii) Piezoelectric biosensors;

iv) Thermal biosensors.

8.3. Enzymes as Biorecognition Elements

Enzymes have been widely used as biosensor recognition elements in various applications due to their properties like specificity, efficiency and wide range of catalytic processes which offers various measurable reaction products (protons, electrons, light and heat) [7].

Enzymes or other recognition elements are immobilized on a surface which has intimate association with transducer layer. The process of immobilization affects activity of biological element. Thus, it is very crucial that the enzyme should exhibit maximum activity in immobilized microenvironment [8, 9]. There are mainly four different methods used for immobilization of enzyme/s as shown in Fig. 8.4 [10, 11].

1) Adsorption;

2) Covalent Linkage;

3) Crosslinking;

4) Entrapment/Encapsulation.

Each method has its advantage and limitations.

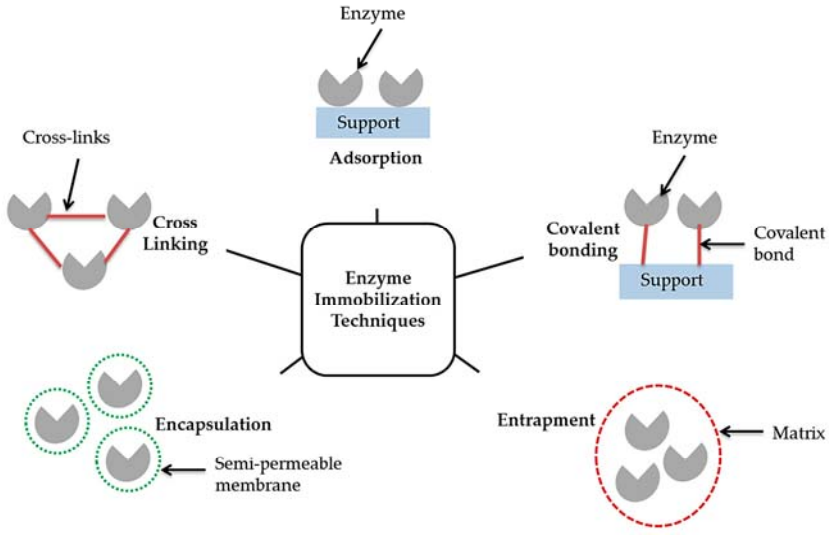

Fig. 8.4. Various methods of enzyme immobilization [16].

a) Adsorption

It is the simplest and widely used method to immobilize bioreceptors. In this method enzyme is bound on the supporting matrix by weak non-covalent interactions like van der Waals forces, ionic etc. Due to these weak interactions the lifetime of an electrode is short [12].

b) Covalent Linkage

In this method, functional group present on the amino acids of an enzyme are covalently bonded to the supporting matrices. Various conditions like temperature, ionic strength and pH affects the binding as well as activity of the biomolecule although the binding is strong and stable [13]. The functional groups that are involved in covalent bonding are $-NH_2$, -COOH, -OH, $-C_6H_4OH$ and -SH.

c) Crosslinking

In crosslinking method of immobilization, two or more molecules of the enzyme are crosslinked with each other by forming covalent linkages between their functional groups using various bifunctional crosslinking agents like glutaraldehyde [14].

d) Entrapment/Encapsulation

In this method, enzymes are entrapped in the solutions (or gels) of polymeric materials. The solution is then coated on the electrode by various methods. The enzyme immobilization can be achieved by any of the following strategies:

(1) Enzyme are added and mixed with a highly cross-linked polymer matrix;

(2) Enzyme can be dissolute in a non-aqueous phase;

(3) Enzyme can be enclosed in a semi-permeable microcapsule which separates it from bulk solution.

There are other methods available for enzymes entrapment like fiber entrapping, gel entrapping, microencapsulation etc. [15, 16]. However, this method faces some limitations like problems in diffusion of the substrate which leads to a delay in the reaction and sometimes a loss of bioactivity may occur. Starch gels, nylon and conductive polymers such as polyaniline (PANI) or nafionare commonly used for entrapment [17].

8.3.1. Effects of Immobilization on Enzyme Biosensor Response

The immobilization techniques described above affects the enzyme activity and its responses. None of the immobilization technique can be considered as a universal method to attain better response. So, decision of immobilization technique to be used during the fabrication of biosensor has been very crucial in terms of attaining higher sensitivity and functional stability. It is also known as immobilization effect which alters the enzyme in the following ways [18]:

- Sometimes during immobilization the conformation of enzyme structure changes which leads to change in its affinity for the substrate.
- Immobilization may also result in variation in the dissociation equilibrium of charged groups of the active center.
- A non-uniform distribution of substrate and/or product between enzyme matrix and the surrounding solution occurs which leads to variation in apparent kinetic constants.

- Reaction rate of an enzymatic reaction is also changed due to a multi-layer immobilization in system which forms a diffusional barrier between enzyme and its substrate.

8.3.2. Working Principle of Recognition

In enzyme-based biosensors, there is a close association of enzyme containing sensing layer with a transducer and the working principle is based mainly on the catalytic action and binding capabilities for specific detection of analyte by the enzymes.

The binding of substrate (analyte) to the active site of an enzyme begins catalytic reactions. The **active site** is a specific region in the structure of an enzyme which specifically binds with its substrate. This binding causes changes in the distribution of electrons in the chemical bonds of the substrate and ultimately causes the reactions that lead to the formation of products. The products are released from the enzyme surface to regenerate the enzyme for another reaction cycle.

The specificity and the binding mechanisms of the interaction between enzyme and substrate has been explained by 'lock and key' and 'induced fit' hypotheses [19].

1) Lock and Key Theory

Enzymes specifically react with only one or a very few similar compounds and this specificity of an enzyme with a single substrate (or similar) had explained by a Lock and Key analogy proposed by Emil Fischer. As per this analogy, the active site of an enzyme has a unique geometric shape which acts as lock hole that is complementary to the geometric shape of a substrate molecule act as key like a lock can be opened by its key only.

2) Induced-Fit Theory

Lock and Key model could not explain the enzyme kinetics during a catalytic reaction as it suggests that substrate as well as enzyme structure are rigid in nature. Then, induced-fit model was proposed by Daniel E. Koshland in 1958. It states that the substrate structure determines the final shape of active site of an enzyme which is partially flexible rather than rigid as described in lock and key hypothesis. This model able to explain the binding of those compounds which binds and distort the

shape of an enzyme without any catalytic reaction. Also, it explains the non reactivity of small molecules which are too small to induce the proper alignment. Finally it proposed that the protein chains in the active site region (or enzyme) are flexible in nature and fit around the substrate after binding.

As compared with other traditional binding assays, the enzyme biosensors detect much lower limits of the catalytic reaction occur between enzyme and analyte (or substrate). The reaction mechanism between the enzyme and analyte has been explained by Michaelis–Menten equation. Furthermore, various components like substrate concentration, pH, temperature and presence of an inhibitor (competitive or non-competitive) affect the catalytic activity of enzyme and its output.

Several approaches, such as the use of permselective membranes (nafion), preliminary oxidation of interferons, or the use of self-referencing electrodes can be used to overcome these barriers [20]. Recently, electrochemical (EC) enzyme biosensors based on various novel electrode materials and immobilization strategies have been used because they provide efficient and stable attachment of the enzyme, biocompatibility and enhance the surface area and EC response [21, 22]. The principle of working of an enzyme electrode is shown in Figure. The analyte firstly diffuses into the enzyme layer and catalytic reaction occurs there as per the equation given below resulting in a product (P or R') or consuming co-reactant (R) which is further measured by transducers.

$$\text{Substrate (S)} + \text{R} \xleftrightarrow{Enzyme} \text{Product (P)} + \text{R'} \quad (1)$$

8.4. Classification of Enzyme Biosensors

Enzyme biosensors can be classified into different classes on the basis of their evolution, transducing mechanism and monitoring principle.

8.4.1. Classification on the Basis of Evolution

Biosensors have evolved rapidly since their discovery in 1962, due to advancement of technologies and their applications. On the basis of evolution and use of technology, the enzyme biosensors can be categorizes into different 'generations' of biosensors.

8.4.1.1. 1st Generation Biosensors

The biosensors which were proposed by Clark and Lyons (1962) are considered as First generation biosensors [3]. In this type of enzyme biosensors, the enzyme was usually immobilized on semi-permeable membrane either by entrapment or adsorption which was then fixed on the surface of the transducer. No mediator has been used in these biosensors thus these are also known as mediator-less biosensors as shown in Fig. 8.5 [23]. Mainly two categories of enzymes have been used in the development of these biosensors- **oxidases** [24-26] and **dehydrogenases** [27-29]. Both enzymes require certain coenzymes during catalytic reaction (for e.g. NAD^+, $NADP^+$, NADH, NADPH, ATP FAD, FADH) which regenerates during the reaction to catalyze subsequent reactions.

Oxidase enzyme based biosensors either monitor the production of hydrogen peroxide (H_2O_2) or oxygen (O_2) consumption [30] using following reactions (2 & 3):

$$S+E\text{-}FAD \rightarrow E\text{-}FAD\text{-}S \rightarrow E\text{-}FADH_2+P \quad (2)$$

$$E\text{-}FADH_2+O_2 \rightarrow E\text{-}FAD+H_2O_2 \quad (3)$$

Usually a highly positive overpotential above 1 V versus Ag/AgCl is applied to detect the analytes directly.

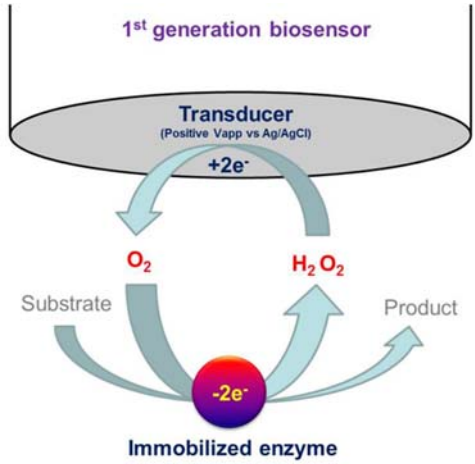

Fig. 8.5. Schematic representation of a first generation biosensor [38].

Dehydrogenase enzyme based biosensors detect NADH concentration is directly proportional to the concentration of the monitored analyte [31] as per following reaction (4 & 5):

$$S + E + NAD^{+} \rightarrow S\text{-}E\text{-}NAD^{+} \rightarrow E + P + NADH + H^{+} \quad (4)$$

$$NADH \rightarrow NAD^{+} + H^{+} + 2e^{-} \quad (5)$$

First generation biosensors have proven to be highly sensitive and are characterized by a very low response-time, typically around one second [32] but it faces some limitations also as oxidase enzymes need O_2 as a second substrate and thus is oxygen dependent. Some of these biosensors use oxygen as an electron acceptor are thus subject to errors arising from changing or low concentration of dissolved oxygen affecting sensor response and reducing linearity [33]. Another limitation is that due to high over-potential used during catalytic reaction many side reactions such as oxidation of ascorbic acid, acetaminophen, uric acid, and lactic acid took place leads to decrease its selectivity toward the target analytes. So, there are various reports in which additional mediators like Platinum [34], Prussian blue [35, 36] have been used to increase the selectivity of the assay by lowering the over-potential and minimizing the oxidation of interfering species. In addition, prolonged use of these biosensors, especially in complex biological matrices or undiluted samples, often results in fouling of the surface of the transducers [37], thus affecting the biosensor response.

8.4.1.2. 2nd Generation Biosensors

In second generation enzyme biosensors, enzymes are mostly covalently linked directly on the transducer's surface which eliminates the use of the semipermeable membrane [39]. Also, various mediators has been added to the sample or immobilized on electrode surface where they act as oxidizing agents and electron carriers [40]. Thus, this type of biosensors is also known as mediator biosensors as shown in Fig. 8.6. Addition of mediators allows carrying out the reaction at very low potentials and without the O_2 dependence. The most common and well-known mediators are ferricyanide and ferrocene, although, methylene blue, phenazines, methyl violet, alizarin yellow, Prussian blue, thionin, azure A and C, toluidine blue and inorganic redox ions are also widely used [41]. In some biosensors oxygen can be replaced with an electron acceptor which is capable of carrying electrons from the redox center of

the enzyme (E) to the electrode. The reaction takes place as follows (6, 7 & 8):

$$S + E(ox) \rightarrow P + E(red) \quad (6)$$

$$E(red) + 2M_{OX} \rightarrow E(ox) + 2M_{RED} + 2H^{+} \quad (7)$$

$$2MRED \rightarrow 2MOX + 2e\text{-}, \quad (8)$$

where M_{RED} and M_{OX} are the reduced and oxidized forms of the mediator and M_{RED} is oxidized at the electrode surface, giving a current signal proportional to the detected analyte concentration [42].

But sometimes the mediator used for the reaction may diffuse freely and leak from the electrode surface which further results in decreasing of long-term operational stability [43].

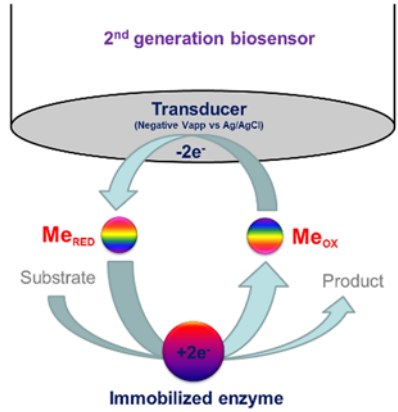

Fig. 8.6. Scheme of a second generation biosensor; MeOX: oxidized mediator; MeRED: reduced mediator [44].

8.4.1.3. 3rd Generation Biosensors

Third generation biosensors are self-contained in nature and are mainly dependent on bio-electrocatalysis [45], where a direct electron transfer takes place between enzyme and electrode as in Fig. 8.7. This type of biosensors consists of mainly three elements: bio-recognition element (enzyme), the redox polymer (or the nano-scale wiring element) to ensure the signal propagation and the electrode as the entrapping surface

[37]. Using a redox polymer to "wire" the redox center of the sensing enzyme to the electrode surface improves performance. Third-generation biosensors have the mediator integrated with the enzyme and the electrode to ensure direct electron transfer. Mediators for this generation include conducting polymers, such as polypyrrole [46], polyaniline [47] etc. Direct electron transfer has been realized with the use of carbon nanotubes [47, 48] or zinc oxide nanoparticles [46, 49] etc. Third-generation biosensors are still being developed and are not commonly used for analysis. These sensors are likely to have very short response times and be relatively independent of oxygen/cofactor concentrations.

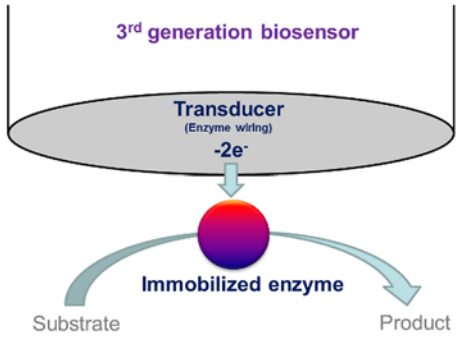

Fig. 8.7. Schematic representation of a third generation biosensor [38].

8.4.2. Classification of Biosensor on the Basis of Transducing Mechanism

8.4.2.1. Electrochemical Enzyme Biosensors

Electrochemical detection is one of the means of transduction mechanism that has been used in enzyme biosensors. During the interaction of enzymes with the analyte (or substrate) various electrochemical species has been either consumed or generated which are further detected by the electrochemical detectors as a signal e.g. zinc oxide/polypyrrole based xanthine biosensor [46] and c-MWCNT/PANI based oxalate biosensor [48] & xanthine biosensor [50].

Based on the electrochemical properties measured by a detector system, electrochemical enzyme biosensors can be further classified into three types:

a) **Conductometric enzymatic biosensors** which measure conductivity changes that occur between a pair of metal electrodes in a bulk solution. These are usually used to study enzymatic reactions producing changes in the concentration of charged species in a solution [51] which further affects conductivity directly or indirectly;

b) **Potentiometric enzymatic biosensors** measure the oxidation or reduction potential difference between the reference electrode and the indicator electrode which changes with the change in activity or concentration of a specific analyte in solution. In these biosensors ion specific electrodes (ISE) can be used which can detect variety of specific ions produced or consumed during the reaction in solution [52, 53]. The sensitivity and selectivity of potentiometric biosensor makes them applicable in environmental monitoring along with clinical applications. However, availability of a highly stable and accurate reference electrode is always required and that limits its application;

c) **Amperometric enzymatic biosensors** detects electro-active species which produces signal in the form of electric current that is linearly dependent upon the concentration of the analyte present in biological test samples [54].In these biosensors, the movements of electrons produced in a redox reaction is measured and response is in amperes e.g. oxalate biosensor [48], xanthine biosensor [46];

d) **Photoelectrochemical (PEC) enzymatic biosensors-** PEC enzymatic biosensors are a new subclass of enzymatic biosensors which combine the selectivity of enzymes and inherent sensitivities of PEC bioanalysis. In typical PEC enzymatic biosensors, the PEC enzymatic systems, upon irradiation, could convert the specific biocatalytic events into electrical signals via the interactions between the semiconductor species and the biocatalyzed reaction chain as shown in Fig. 8.8. Many PEC enzymatic biosensors have now been developed and advancement is going on rapidly in this field [55-59].

In PEC enzymatic biosensor, the biorecognition elements (enzymes) are initially immobilized onto the electrode surfaces, and the subsequent biocatalytic events would then be recorded by the electrical signals prior to and after enzymatic reaction.

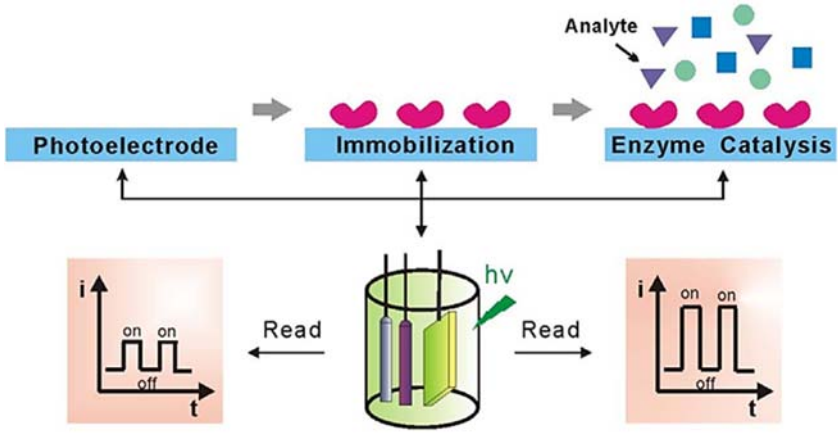

Fig. 8.8. General design of photoelectrochemical (PEC) biosensor. The major process involves immobilization of enzymes on the photoelectrode substrate as bio recognition element for subsequent catalytic transformations [60].

8.4.2.2. Optical-detection Biosensors

Sometimes various biological reactions and other chemical reactions produce an optical signal in the form of luminescence, fluorescence, colorimetric, etc. These optical signals are detected by optical detectors and further correlated with the concentration of target compound/s. The resulting signal could be measured or could be further amplified before measurement for improved sensitivity e.g. optical biosensor for dichlovos using stacked sol–gel films containing acetyl cholinesterase and a lipophilic chromoionophore [61] and electro-chemiluminescence biosensor for uric acid determination [62]. Optical sensing techniques are especially attractive in high throughput screening since they enable biosensors to monitor multiple analytes simultaneously [63]. Fluorescence and chemiluminescence transducers are the most developed within the optical transducer class. Their limits of detection are the lowest that one can obtain using biosensors. Fluorescent biosensors have been widely applied in analytical chemistry due to their easy construction using standard molecular biology techniques [64] whereas chemiluminescence occurs when during photon emission in chemical reaction. The main limitations of these biosensors are relatively long assay time [65, 66]. The bioluminescence biosensors have the longest response time of the biosensors.

8.4.2.3. Piezoelectric Biosensors

In these types of biosensors, the surface is coated with selectively binding biologically active substances [67, 68] and then analyte is applied to bind. The analyte bind to the biologically active substance on the surface and changes the mass. Change in mass was sensed by variations in the frequency of oscillation in a piezoelectric crystal or surface acoustic wave by the detector e.g. Cholesterol oxidase was immobilized covalently onto 11-amino-1-undecanethiol hydrochloride (AUT) self-assembled monolayer (SAM) fabricated on gold (Au) substrates using glutaraldehyde as a crosslinker [69].

8.4.2.4. Thermal-detection Biosensors

Most of biological reactions either absorb or produce heat during catalysis. The heat generated or absorbed changes the temperature of the solution/medium which is detected as signal by the thermal detection biosensors. In these types of biosensors, enzymes are immobilized on temperature sensors e.g. calorimetric glucose biosensor [70] and the heat generated or absorbed during the reaction of enzyme with analyte is measured and calibrated against the analyte concentration. The total heat produced or absorbed is proportional to the molar enthalpy and the total number of molecules in the reaction. The measurement of the temperature is typically accomplished via a thermistor, and such devices are known as enzyme thermistors. The common applications of thermal detector biosensors include the detection of pesticides and pathogenic bacteria.

8.4.3. Classification on the Basis of Monitoring Method

Biosensors may be further classified into two types on the basis of the analyte monitoring principle (Fig. 8.9).

1. **Direct monitoring of analyte**- This type of biosensor mainly detects or analyze the catalytic reactions that they monitor i.e. analyte concentration either by its consumption or production of product formed. The output here is directly related to the analyte (or product) concentration.

2. **Indirect monitoring of analyte**- In this type monitoring of inhibitor or activator of the biological analyte recognition element (biochemical

receptor) has been detected. The output in indirect monitoring is directly related to concentration of inhibitor (or activator) of the enzyme used as biorecognition element [71].

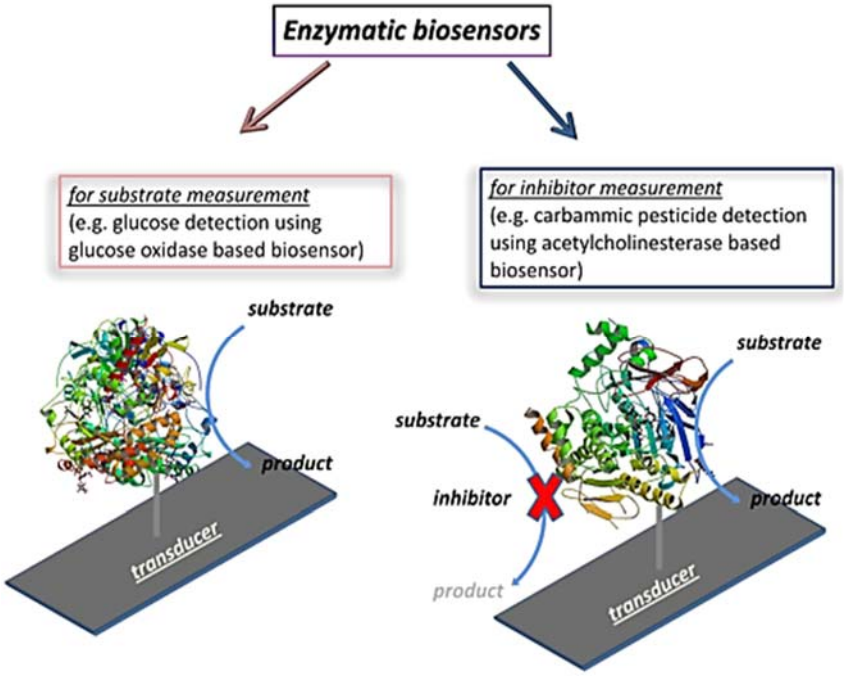

Fig. 8.9. Types of enzyme biosensors on the basis of monitoring-Substrate (Direct) monitoring and inhibitor (indirect) monitoring [72].

In these biosensors inhibition is quantified in terms of "degree of inhibition" which is defined as the ratio of the difference of enzyme activity in absence and in presence of inhibitor divided by the enzyme activity in absence of inhibitor.

Various kinds of inhibition have been reported in literature: the inhibitor may link the free enzyme (competitive inhibition), complex enzyme–substrate (uncompetitive inhibition), both free and complex enzyme–substrate with the same affinity (non-competitive inhibition) or with different affinity (mixed inhibition). Broadly the inhibition can be divided into two different types-irreversible inhibition and reversible inhibition (Table 8.1. below).

Table 8.1. Comparison between irreversible and reversible inhibition.

Character	Biosensor based on Irreversible inhibition	Biosensor based on Reversible inhibition
Binding of inhibitor to enzyme	Irreversibly at enzyme active site	Reversibly at enzyme active site
Effect on enzyme activity after binding	Permanently inactive	Can recovered its original activity
Analysis time	Long time	Less time
Reuse of biosensor	Limited	Can use multiple times
Concentration of substrates required	High	Low
Avoidance of interfering species	Can be eliminated	Cannot be eliminated

8.5. Advantages of Enzyme Biosensors [73-75]

1) Enzymes can increase the rate of a reaction significantly relative to an uncatalyzed reaction;
2) Enzymes have magnificent specificity for their substrates and can easily detect individual substances in a complex mixture, such as urine or blood in a very selective manner;
3) Enzyme biosensors can be used for detection of very small compounds (activator or inhibitors) which cannot be detected by any other methods efficiently;
4) Enzymes are very sensitive and can detect analytes even at their very low levels;
5) Enzyme biosensors are very rapid in analysis, easy to use and less labor-intensive;
6) Enzyme biosensors are easy to regenerate and reusable in most of cases;
7) These are simple and inexpensive to construct.

8.6. Limitations of Enzyme Biosensors [76]

Various types of enzyme biosensors have been discussed above. Different types of biosensors have their unique advantages and limitations. But few are common to all as given below:

1) The catalytic properties and kinetic mechanisms of numerous enzymes are still unknown;
2) Cost-effective mass production is limited due to less enzyme availability;
3) Lack of novel enzyme systems;
4) Lack of identification and isolation procedures of enzymes from other sources like cell membranes, extremophiles etc.;
5) Various enzyme properties like turnover, selectivity, shelf-life, stability etc. are affected by various factors such as pH, temperature, interfering species and immobilization procedures;
6) In most cases enzyme layer in the biosensor has to be replaced periodically since it gradually loses activity;
7) Also, some interfering non-specific reactions also occur during detection process which reduces the efficiency of biosensor.

8.7. Factors Responsible for Enzyme Biosensor Failure

Many times enzyme biosensors or other analytical tools didn't work in the manner they have been designed for. Biosensor failure can be categorized in two categories: **component-based failure** and **biocompatibility-based failure.**

Component based failure includes electrical failure, loss of enzyme activity and lead detachment while biocompatibility-based failure occurs due to the membrane biofouling, membrane degradation and electrode passivation [38].

1) **Membrane biofouling**- It is most common cause for biosensor failure mainly in *in vivo* applications. Various macromolecules such as proteins, living cells or their debris adhere (or adsorb) to the outer surface of the biosensor which obstruct the diffusion of an analyte leading to a decrease in sensor response. This process is known as membrane biofouling.

2) **Electrode passivation**- It is second type of bio-compatibility-based failure in which small molecules like phenolic compounds are transformed to adherent substances at the electrode surface, reducing its active area [77].

Adherence of various macromolecules, small surface active compounds and electrode reaction products such as NAD^+ are responsible for biofouling and passivation. These compounds mainly affect the diffusion and partitioning of the analyte leading to inhibition of catalysis.

3) **Membrane degradation –** In this process, the biosensor losses its activity mainly due to denaturation and deactivation of immobilized enzyme which ultimately reduces the life of the biosensor [78].

8.8. Applications of Enzyme Biosensors

In general, biosensors have varied applications such as for medical diagnostics, detection of toxins in food and water, pharmaceuticals, environmental monitoring, and food and agricultural industries.

8.8.1. Biomedical and Diagnostics

a) Diabetes Mellitus

Diabetes is the most widespread disease in the world which occurs due to glucose metabolism disorders. In this disease, the amount of glucose in blood plasma increases many fold than normal range which induces a hyperglycemic condition leads to multiple complications such as blindness,[79] cardiovascular disorders, [80-82] and kidney failure [83, 84]**.**

Due to severe medical implications of diabetes, there is a critical need for its monitoring and control of the blood glucose level. Therefore, many type of glucose biosensors have been developed to accurately estimate the concentration of blood glucose on commercial basis for labs and personal monitoring of diabetic patients.

Mainly two types of enzymes based glucose biosensors are available in market- 1) enzyme glucose oxidase (GO_x) and 2) enzyme glucose dehydrogenase in various forms like handheld operated or glucose strips etc. [42]. GO_x oxidizes glucose to yield gluconic acid and hydrogen peroxide (H_2O_2) via the following reaction (9).

$$\text{Glucose} + O_2 \xrightarrow{Glucose\ oxidase} \text{Gluconic acid} + H_2O_2 \qquad (9)$$

GO_x based biosensors either monitors the production of H_2O_2 or consumption of O_2 during the reaction to indicate the amount of glucose [85].

In addition to GO*x*, another enzyme glucose dehydrogenases (GDHs) has been also used. The detection of GDH-based biosensors is mainly independent of O_2 rather it depends on various cofactors includes tightly bound FAD or pyrroloquinoline quinone (PQQ) to unbound nicotinamide adenine dinucleotide (phosphate) [NAD(P)] [86, 87]. The commercially sold blood glucose meters typically have a range of 1.1–33.3 mM glucose with a precision of 3–8% and test time of about 30 seconds or less [88, 89].

b) Lactose Intolerance and Lactate Detection

Lactate (an ester of lactic acid) is a product of most of the fermentations and is produced during cellular respiration after glucose breakdown. Its concentration varies in blood from 0.9 mM to 12 mM depending upon physical activity of body [90].

Lactate is usually produced during anaerobic conditions formed in the body due to oxygen deprivation. Thus, the concentration of lactate in the blood is indirect measure of oxygen deprivation which can cause from ischemia, trauma, and hemorrhage which can lead to life-threatening shock [91]. Also, blood lactate levels are used as indicators of other conditions such as acidosis or bacterial meningitis [92]. So, its measurement is also critical in most of medical monitoring mainly sports medicine [91]. Many biosensors have been commercially used to measure lactate monitoring [91, 92]. Lactose intolerance has become very common now a-days. A study has shown that 65% of the world population experiences from various degrees of lactose intolerance [93]. Lactose intolerance can cause diarrhea, nausea, muscular spasm, swelling, borborygmi and chronic flatulence [94]. In body β-Galactosidase enzyme hydrolyzes D-galactosyl residues like lactose into glucose and galactose [94]. β-galactosidase has been also used in many food industries to hydrolyze lactose, enhance digestibility, sweetness, solubility and flavor of dairy products [96, 97]. The lack of β-galactosidase enzyme or reduction in its activity are the main causes of lactose intolerance. The amount of lactose in body as well as in food items should be monitored crucially.

Many enzyme based biosensors has been developed to quantify lactose, glucose, starch and sucrose in the body fluids and food samples [98]. Enzymes like β-galactosidase, mutarotase, invertase and Glucose oxidase has been used in these biosensors. An amperometric biosensor was developed using immobilized β-galactosidase and Galactose oxidase enzymes for the determination of lactose in raw milk [99].

c) Cardiovascular Diseases

Cardiovascular disease (CVD) is the main cause of death in the whole world. The main risk factor for CVD is the presence of excessive amount of cholesterol in body as it leads to blood pressure or chances of diabetes. Also, elevated level of cholesterol in blood is responsible for other health effects as coronary artery disease, hypertension, nephritic syndrome or cirrhosis, atherosclerosis, heart attack and stroke or even death [100, 101].

With increasing incidents of cardiac arrest and stroke more exact and quicker determination of cholesterol in the serum is very crucial in medical field. Many biosensors based on enzymes mainly using cholesterol oxidase (ChO) and cholesterol esterase (ChE) as recognition element has been developed for cholesterol determination. Cholesterol oxidase is a flavoenzyme belongs to oxidoreductase family which uses flavin adenine dinucleotide (FAD) as cofactor and catalyses the oxidation and isomerisation of steroids containing a hydroxyl group at 3' position [102]. While cholesterol esterase (ChE) catalyses the hydrolysis of sterol esters into sterols and fatty acids [103].

These two enzymes work synergistically in a reaction where cholesterol esterase (ChE) first hydrolyses esterified cholesterol and then cholesterol oxidase (ChO) oxidizes cholesterol to produces cholest-4-en-3-one and hydrogen peroxide (H_2O_2) as per given equations (10-12). Various amperometry based biosensors produces current after application of electric potential on H2O2 which get oxidized to produce electrons. The current produced is directly proportional to the concentration of cholesterol present in the sample [104, 105].

Potentiometric biosensors can also be used which measures the concentration of protons.

$$\text{Cholesterol ester} + H_2O \xrightarrow{ChE} \text{Cholesterol} + \text{fatty acids} \qquad (10)$$

$$\text{Cholesterol} + O_2 \xrightarrow{ChO} \text{Cholest-4-en-one} + H_2O_2 \quad (11)$$

$$H_2O_2 \xrightarrow{Electric\ Potential} 2H^+ + O_2 + \text{electrons} \quad (12)$$

Other enzymes like horse radish peroxidase (HRP) have been also used to develop biosensors [106].

d) Detection of Various Disease Biomarkers

For the diagnosis of a disease various disease biomarkers has been used as indicators which directly affect the various physiological process in human tissues. To detect these biomarkers and their linkage with particular diseases various analytical techniques like HPLC, Chromatography, ELISA etc. has been widely used in medical industry. Apart from these tools many sensitive enzyme based biosensors has been also designed discussed later.

(i) Detection of Neurotransmitters

Various neurotransmitters like catecholamine, dopamine, acetylcholine etc. affect almost all physiological process in most of the human tissues and they are act as a biomarker for those processes. The detection of these neurotransmitter biomarkers is very crucial for the early diagnosis of various diseases. Enzyme based biosensors have been developed to detect these molecules in the patient's sample [107, 108].

Dopamine (DA) neurotransmitter is an analytical biomarker for clinical diagnosis of various diseases related to central nervous system like schizophrenia and Parkinson's disease [107]. Cesarino *et al.* (2013) had developed a novel biosensor for detection of DA using electro-co-deposition method which detects DA in a very easy and fast way [108].

Other enzyme based biosensors like laccase enzyme-based were also designed and synthesized. Wang et al (2014) had developed such type of biosensor using phytic acid-functionalized silica nanoparticles for dopamine detection. This biosensor had a good detection performance for DA with a wide linear range (0.99– 103.10 μM) and a low detection limit (0.26 ± 0.003 μM) [109].

An amperometric laccase enzyme based biosensor for the detection of catecholamine neurotransmitters using electro-catalytic substrate recycling was developed by Ferry and Leech in 2005. An osmium complex with the poly (N-vinylimidazole) was introduced and the

constructed sensor had the detection potential of - 0.2 V towards dopamine (DA), and detection limits of 11nM for epinephrine, 8 nM for norepinephrine, and 4nM for DA [110].

(ii) Detection of Triglycerides

Triglycerides (TGs or triacylglycerols) are macromolecules in which one glycerol molecule attached to three fatty acid molecules (Unsaturated/saturated or both) via ester linkages. Triacylglycerols are a major source of energy in metabolism and transport dietary fat throughout the bloodstream in the form of very-low-density lipoprotein (VLDL) and chylomicrons [111].

Lipase enzymes and bile salts broke these TGs inside the body afterwards they are absorbed. But sometimes due to various diseases or decrease in catabolism, these TGs starts accumulating in the body which can results in various diseases like hyperlipidemia, mellitus, liver obstruction, hypertension, atherosclerosis, Alzheimer disease [112] and various cardiovascular diseases [113]. So, the quantification of triglycerides (TGs) in human serum is crucial for health care diagnostics. Biosensing methods are using now a –days for detection of TGs in blood due to their various advantages like rapid sensing, broad detection range, easy operation, low-detection limit, ease of miniaturization and high sensitivity [114].

Mainly three enzymes lipase (LIP), glycerol kinase (GK) and glycerol phosphate oxidase (GPO) has been used in TG biosensors using tributyrin and triolein as substrate. Amperometric TG biosensors have been designed in which collective reaction of enzymes –lipase, glycerol kinase and gycerol-3-phosphate oxidase generates H_2O_2 which is finally decomposed to release electrons at high voltages. The production of H_2O_2 is directly proportional to the flow of electrons, i.e. current which in turn, is directly proportional to the amount of analyte (TG) in the sample [115, 116].

(iii) Detection of Uric Acid

Uric acid (2,4,6-trihydroxypurine) is an end product of metabolism and usually excreted out from the body [117, 118]. But sometimes it starts accumulating in the biological fluids in several disorders such as gout [119, 120], renal disease [121] and Lesch–Nyhan syndrome [122]. Excessive amount of uric acid in serum is known as hyperuricemia and

this has been found to be associated with hypertension [123, 124], metabolic syndrome [125] and cardiovascular disease [126-128]. Thus, its fast and reliable determination in biological fluids is very crucial for diagnosis and treatment of above diseases.

Amperometric enzyme based biosensors has been developed for uric acid determination which uses either uricase (UOX) or horseradish peroxidase (HRP) enzymes. Uricase enzyme (UOX) catalyzes the oxidation of uric acid to allantoin, H_2O_2 and CO_2 as per reaction given (13).

$$\text{Uric acid} + 2H_2O + O_2 \xrightarrow{Uricase\ (UOX)} \text{Allantoin} + H_2O_2 + CO_2 \quad (13)$$

These biosensors measure the amount of enzymatically generated H_2O_2 or the consumption of O_2 during the enzymatic reaction. A biosensor based on uricase and peroxidase enzymes for uric acid determination in urine was reported [129-132].

(iv) Ethanol Detection

Ethanol detection is very crucial task in various areas like forensic science, industries and clinical analysis. It is one of the most common poisonous compounds consumed by human beings and a major causative factor in a variety of road accidents [133]. In excessive amounts it can cause swelling and conjunctiva of the nasal mucous layer and exasperation of the skin which can lead to alcohol poisoning. Quantitation of ethanol is also required in food and beverage industries. Thus, its rapid and reliable quantitative detection is very important for various clinical diagnostics [134], fermentation industry, food and beverage industries [135].

Enzyme biosensors are now frequently used in the analysis of ethanol for clinical diagnostics (e.g. blood, sweat, serum, breath, saliva and urine) and in food and alcoholic beverage industries (wine, brew and spirits).

Mainly two major enzymes has been using for ethanol sensing are alcohol oxidase (AOX) and alcohol dehydrogenase (ADH). AOX enzyme mainly oxidizes the primary low molecular weight alcohols with the consumption of O_2 into corresponding aldehydes and H_2O_2 as per the reaction shown (14) [136].

$$CH_3OH + O_2 \xrightarrow{Alcohol\ oxidase\ (AOX)} HCHO + H_2O_2 \quad (14)$$

Most of the AOX based biosensors detect either O_2 consumption or H_2O_2 formation during the reaction. ADH enzyme also oxidises ethanol utilizing NADP and form acetaldehyde and NADPH. Biosensors based on ADH mainly detect released electron and protons formed during the reaction [135].

Many biosensors has been developed using these enzymes for the quantitative detection of ethanol in various fields [134, 135, 137, 138].

e) Oxidative Stress

Oxidative stress is one of the underlying cause of various diseases including ischemia-reperfusion injury [139], amyotrophic lateral sclerosis (ALS) [140], Parkinson's disease [141], Alzheimer's disease [142], psoriasis [143], cardiovascular diseases etc. [144]. It usually occurs as a result of imbalance between the formation of free oxygen radicals and antioxidant defense system of the body. The high concentration of reactive oxygen species (ROS) and/or a decrease in antioxidant (AO) defense system against ROS is very detrimental for the cells of the body [145].

In cells, superoxide anion (O2•–) radical is the main reactive oxygen species generated from oxidative stress. Enzymes like catalase, peroxidase and superoxide desmutases (SODs) act as antioxidants which prevent cells from the toxic effects of ROS.

The determination of these ROS is very important as they are factors involved in pathogenesis and clinical outcome of human diseases. Various SOD enzyme based biosensors have been developed in which SOD is used as a biomarker to analyze a wide variety of analytes viz., $O_2•^-$, H_2O_2, NO & its metabolites (viz. NO_2^-, NO_3^-), cysteine, etc. [146, 147].

f) Detection of Toxic Substances

In nature, there are many small molecules are present having toxicity or other harmful effects. They mainly act as inhibitors of various enzymes involved in metabolic reactions in the cell. Several drugs, nerve gases (sarin, soman, tabun), pesticides (such as organophosphates and carbamates) are known as enzyme inhibitors (mainly inhibit cholinesterases (ChE) [148-150].

It is desirable to develop a simple warning system, which is reliable and portable and readily available for soldiers and medical personnel. This system should be able to detect the presence of very low amount of these agents like nerve gases in real time.

Biosensors based on presence of acetylcholinesterase AChE (preferred) as a bio-recognition element has been developed which are worked on enzyme inhibition monitoring method [2, 151]. Many other biosensors which used enzymes as biorecognition element has been developed using AChE or ChE enzymes to detect variety of small toxic or harmful substances like Aflatoxin B [152, 153] and Anatoxin-a(s) [154, 155], Glycoalkaloids [156].

g) Drugs Screening

Chemical substances which are not present in nature and artificially produced and found within an organism are known as xenobiotic substances such as various drugs. Within the body their metabolism is mainly done by oxidative reactions called phase I metabolism, which are catalyzed by enzymes of the cytochrome P450 superfamily. Human cytochrome P450 enzymes act on more than 90 % of all drugs available in the market [157].

The Human cytochrome P450 functions in two ways- it either activates chemicals or increase their bioavailability or done detoxification with following excretion of drugs or reactive products. The P450 enzymes are very diverse in nature and very specific for their substrate. In many patients various adverse effects has been observed who had undergone multidrug treatments due overlapping substrate specificities or inhibitory effects of those drugs. Therefore, the measurement of the substrate specificity and distribution of P450 isoenzymes and polymorphic enzymes has greater clinical relevance for drug screening, assessment of toxicity and prediction of drug clearance.

Thus, many P450enzyme-based biosensors (electrodes) have been developed to detect various chemicals, such as chlorophenols, pesticides such as paraoxon, or drugs such as bupropion, bufuralol, warfarin, and cyclophosphamide [158-161].

8.8.2. Agriculture and Environment

Various enzyme based biosensors have been developed for detection of different small molecules (or chemicals) such as pesticides like organophosphate and carbamate; respiratory poisons such as cyanide and azide, as well as toxic heavy metalspresent in environment due to their high use in agriculture and food industry [73].

(i) Detection of Pesticides

Pesticides are majorly used in agricultural fields for crop production enhancement. There are many classes of pesticides have been designed mainly to persist in the environment over a longer duration after their application to achieve maximum effectiveness [162, 163]. But most of these pesticides have acute toxicological effects on various life forms. Moreover, their accumulation in higher concentrations is detrimental (toxic) to the living systems and can act as mutagen, carcinogen, and tumorogen [164]. Majorly of the pesticides are neurotoxic compounds (Organophosphorus pesticides (OP) and irreversibly inhibit various enzymes such as acetylcholine esterase [165], tyrosinase [166], and laccase. Inhibition of acetylcholine esterase leads to the accumulation of the neurotransmitter acetylcholine in nerves which interferes with muscular activities and the functioning of vital organs, produces serious symptoms, and may even lead to death [167, 168].

Thus, their rapid and accurate detection and quantification is very crucial. In addition to various conventional techniques used for detection such as chromatography (HPLC, GC) etc. [169] many types of biosensors has been developed.

Mainly two types of enzyme biosensors have been used in the detection of pesticides. First type are based on measurements of enzyme inhibition, also known as indirect approach and second type are based or on direct measurement of compounds involved in the enzymatic reaction i.e. direct approach.

In the **indirect approach** (inhibition biosensor), pesticide detection is based upon the inhibition of mainly two acetylcholinesterase (AChE) and butyrylcholinesterase (BChE). The acetylcholinesterase (AChE) activity-based biosensors have been developed for detection of organophosphorus (OP) pesticides [170]. AChE belongs to the family of hydrolases and at its active site three amino acids: histidine, serine, and

aspartic acid are present. Positively charged quaternary ammonium group of Ach (acetylcholine) binds to binding site then serine hydroxyl group attacks and hydrolyzes the compound by deprotonation. In the presence of pesticide like OP, the nucleophilic serine present at the active site is covalently bound to the phosphorus atom of the organophosphate, and this blocking of the serine inactivates the enzyme.

Biosensors with AChE-modified amperometric transducers have been developed which measures hydrogen peroxide (H_2O_2) generated as a result of the oxidation of choline produced from acetylcholine hydrolysis in the presence of choline oxidase) have been reported as shown in equation (15) [171-174].

$$\text{Acetylcholine} \xrightarrow[(AchE)]{Acetylcholine\ esterase} \text{Choline} \xrightarrow{Choline\ oxidase} \text{Betain} + H_2O_2 \quad (15)$$

In second approach (**direct approach**) biosensors have been developed in which pesticide to be detected act as substrates are known as catalytic biosensors. In this approach usually of enzyme organophosphorus hydrolase (OPH) which causes the hydrolysis of organophosphorus pesticides, such asparathion, methyl parathion, or paraoxon. OPH catalyzes the hydrolysis of organophosphorus pesticides with p-nitrophenyl substituent such as paraoxon, parathion, and methylparathion to p-nitrophenol [175, 176].

Other enzyme bases like laccase have been also used in various biosensors to detect the toxic pesticide residues like Pirimicarb (a kind of carbamate) which acts as an endocrine disruptor and found in very minute quantity in food material [177, 178].

(ii) Detection of Heavy Metals

Heavy metals are used in various industries like paints, agriculture etc. and have ability to accumulate in environment and living organisms. Heavy metals also act as inhibitors of various enzymes like AChE producing toxicity and other ill health effects. Their monitoring in water, food and environment is a crucial task.

Various enzyme biosensors has been developed which can detect different heavy metals. Stoytcheva et al had developed an AChE based biosensor for the determination of arsenic working on its inhibitory mechanism [179, 180]. It has been reported that glucose oxidase-based

biosensors immobilized by electro-polymerization help to detect heavy metals [181]. Similarly, urease when immobilized in both PVC and cellulose triacetate layers on the surface of pH-sensitive iridium oxide electrodes helps to detect the levels of mercury [182, 183].

Another heavy metal, chromium (or its compounds)is used in various industries for the manufacturing of magnetic tape, colored glass, paints, and pigments as oxidizing agents, catalysis, ceramic coatings, safety matches, glues, and adhesives, enchant for plastics, wood preservatives, and inhibition of water corrosion [184, 185]. But a large amount of chromium has been discharged into soil, air and water bodies in various forms like chromic acid. The chromic acid or Cr(VI) state are highly toxic and non-biodegradable in nature which can enters into the body of living organism through breathing or skin contact or by swallowing. It causes many health issues like irritation in upper respiratory tract, inflammation in the nose, injury in the nasal septum, cancer in respiratory track, skin problems (allergic skin reactions, skin burn), gastrointestinal problems (chronic ulceration, dermatitis, gastrointestinal ulcer), weaken the immune system, kidney, and liver damage may lead to other carcinogenic effects [186]. Biosensor based detection methods have been developed for chromium as well as other heavy metals. Caroline et al. (2003) had developed an amperometry based enzyme biosensor using chromate reductase and cytochrome c3 for chromium detection [187]. Many other enzymes such as nitrate reductase [188], urease [189] ,tyrosinase [156] and enzyme cytochrome c3 [187] based biosensors has been developed for the detection of chromium and other heavy metals such as Cd(II), Cu(II), Ni(II), Pb(II) and Zn(II).

(iii) Detection of Nitrite

Fertilizers, industrial waste water, dyes, detergents and corrosion inhibitors are very rich in various pollutants such as nitrite [190]. Nitrite is frequently used various industries such as textile, pharmaceutical industries, metal and petroleum where it is used as an additive and preservative to enhance the fragrance and taste of the food [191]. Due to its high uses it frequently eutrophicates in water bodies and soil which further comes in food chain at each level even in humans. Elevated levels of nitrite have many health hazards especially in infants and children often known as the blue-baby syndrome. Moreover, excessive ingestion of nitrite can lead to formation of carcinogenic nitrosamines by the interaction of nitrite with amines and methemoglobinemia by the irreversible oxidation of hemoglobin in blood [192]. The evaluation of

nitrite concentration in soil, food, biological fluids and water is very significant for clinical, human health and environment safety.

Apart from other techniques, some enzyme based biosensors has been demonstrated for the estimation of nitrite. Horseradish peroxidase (HRP) enzyme [193-195] and Superoxide dismutase (SOD1) [196] based biosensors has been fabricated.

(iv) Detection of Algal Toxins

Harmful algal blooms (HABs) produced by over growth of various microalgae affects severely the coastal waters and bivalve aquaculture [197, 198]. Some of the species of these microalgae produce toxins, which can affect marine organisms and cause sea food poisoning if consumed [199]. These Microalgae mainly produces three groups of toxins - diarrheic shellfish toxins (DSTs), paralytic shellfish toxins (PSTs) and amnesic shellfish toxins (ASTs).

PSTs usually inhibit voltage-gated sodium channel in excitable cells [200] and can cause severe neurological symptoms with overall mortality ranging between 2–14% [201, 202]. There are various analytical tools to detect these toxins but they are less reproducible, time-consuming, labor-intensive and expensive [203]. Thus, a rapid, cost – effective screening method or tools is required. Some of the biosensors has been developed earlier to quantify these toxins [204].

Raposo et al (2020) developed an enzyme based potentiometric biosensor which is capable of hydrolyzing the carbamate and sulfocarbamoyl groups of PSTs [205]. PST hydrolysis can be done by two enzymes - sulfocarbamoylase and carbamoylase [206, 207]. Carbamoylase converts carbamate (STX) and N-sulfocarbamate toxins (GTX5 and C1+2) into decarbamoylsaxitoxin (dcSTX) and decarbamoylgonyautoxins 2+3 (dcGTX2+3), respectively. The toxins can be detected Enzymatic in the concentration range from 0.43 to 3.30 $\mu molL^{-1}$ using this biosensor.

8.8.3. Food and Other Industries

Food safety is a global challenge now days. Variety of naturally occurring food and feed contaminants and other substances may pose serious health concerns to humans and animals for example mycotoxins, plant secondary metabolites, fish toxins etc. Various kinds of biosensors

have been developed for detection of variety of substances like xanthine, food contaminants, alcohol concentration etc. to be used in food and beverage industries.

(i) Detection of Xanthine/hypoxanthine

Fish is mostly consumed in coastal areas as well as throughout the world. So, due to various treatments and storage of fishes sometimes its quality becomes degraded. The freshness of the fish can be analysed by using some enzyme based biosensors which is a need for maintaining its acceptable quality to the consumers [208]. After the death of a fish, nucleotides such as ATP are usually got degraded and formation of inosine occurs. Ionsine is further converted to hypoxanthine by the action of the enzyme nucleoside phosphorylase. Hypoxanthine causes a bitter taste in the degraded meat [209]. Xanthine oxidase (XO) converts hypoxanthine to xanthine which further converted into uric acid as the given reaction (16) [210]. The quantitation of xanthine or hypoxanthine can therefore be used to determine the freshness of fish.

$$\text{Xanthine} + O_2 \xrightarrow{Xanthine\ oxidase} \text{uric acid} + H_2O_2 \qquad (16)$$

There are many reports in which various biosensors have been developed to detect the xanthine concentration or uric acid concentration used in food industries [211-213].

(ii) Detection of Mycotoxins

Many fungal pathogen species have produced various small compounds (roughly 300-700 Da) as secondary metabolites and most of them are toxic in nature and known as “mycotoxin”. These are mainly produced by various fungi, the genera of which include *Aspergillus*, *Penicillium* and *Fusarium* [214, 215]. The major and significant mycotoxins are areochratoxin, aflatoxin, deoxynivalenol, nivalenol, 3-acetyl-deoxynivalenol, 15-acetyl-deoxynivalenol, zearalenone, trichothecenes, and fumonisin. These mycotoxins have negative impact on both animal and human health in food commodities, more frequently enhancing the risk of chronic diseases [216]. Thus, their detection and further identification is very important for the prevention of their negative effects on animal and human health. The detection of mycotoxins has been ongoing for approximately50 years [217]. Maximum levels at which mycotoxins are permitted in food and animal feed have been set by various regulations worldwide. In addition to other analytical method,

various biosensors also had been developed for detection of these mycotoxins. Goud et al. (2018) summed up the recent developments of electrochemical (EC) biosensors for mycotoxin detection [30].

(iii) Detection of Phenolic Compounds

Tea drinks and juices have various nutritional and antioxidant capacity [218] due to the presence of various small molecules likes catechol and other polyphenols [219]. Also, all kinds of wine contain tannins, and a variety of phenolic compounds like cinnamic acid derivatives, catechins, and anthocyanidins, which are usually measured by the total polyphenol index which is directly related to the quality of wine. According to earlier reports, the content of polyphenolic compounds is 2 to 5 g/L in red wines on average and 100 mg/L in white wines [220]. Polyphenols are also known for their positive effect on human health due to their antioxidant properties, which are associated with reduced risk of cancer, stroke, heart disease, and diabetes [221].

On the contrary, phenols in fruit juice may become a serious human health threat, which can cause diseases in humans. For example, the phenol bisphenol A (BPA) widely used in manufacturing of plastic bottles used for packing food materials mainly juices. BPA can be leached into food and cause serious illness due to their teratogenic property.

Thus, the detection of phenols (or polyphenolic compounds) in food samples (tea, juices, wine etc.) is very crucial for food safety as well as their quality determination. Various biosensors had been developed to detect and quantify these molecules. In recent years, many laccase enzyme based biosensors have been developed for detecting catechols [222] and BPA in the given sample.

Different types of laccase enzyme biosensors have been developed to determine the poly-phenols and tannins in wine samples [221]. A novel type of laccase biosensor has been developed by Zhang et al. in 2018 in which engineered *E. coli* cells having laccase enzyme were directly adsorption on the surface of electrode to detect the catechol in a linear range of 0.5–300.0 μM. This type of laccase enzyme-based biosensors can be used for phenol detection in red wine, with high accuracy and recovery [223, 224]. Ribeiro et al. had also demonstrated a laccase enzyme based biosensor for the detection of for metanate hydrochloride in fruit samples [225]. Laccase enzyme based biosensor has been also

used to detect the toxic pesticide residues which found in very minute quantity in the food samples like Pirimicarb (a kind of carbamate) which acts as an endocrine disruptor and found in very low concentrations in food [177, 178].

Dabhade et al (2020) had developed a paper based enzyme biosensor using immobilized horseradish peroxidase (HRP) enzyme to detect phenolic compounds- catechol and resorcinol. Phenolic compounds are oxidized by HRP into semiquinones, which on reaction with a chromogenic substrate (3-methyl 2-benzothiazolinone hydrazine) gave light pink to red color depending on the concentration of phenolic compound [226].

8.9. Future Prospects

Biosensors have the characteristics of cross disciplinary integration and miniaturization, multifunction, integration, and intelligence are the developing trends of biosensors. Enzyme biosensors have shown tremendous potential in replacing the conventional-high end equipments-based analytical techniques. However, the real-world applications of enzymes are limited due to various factors discussed above. The introduction of some new frontier technology such as, nanotechnology, and is applied to the biomedical sensor Introduction of nanotechnology, microelectronics and microelectromechanical technology (Microelectronic Mechanism) in this field is producing outstanding results in the development of a new generation of biosensor with low cost, low response time high sensitivity, high reliability, high life and bionic function, achieving rapid and accurate test of trace components in the sample. Using enzymes in nano range materials for biosensor doing the same i.e. improvement in properties of sensing. This field is opening its arms from last 5-10 years and a very few work has been done in this field. Recently, improvement in the sensitivity and sensitivity of enzyme biosensors has been studied by researchers by successful use of nanomaterials for the fabrication of enzyme electrode and optimization of enzyme-analyte reactions. The future research on enzyme –based biosensors for their applications in the detection, identification and quantification of emerging contaminants in the real world should focus on to improve the sensitivity, the selectivity, miniaturization (lab-on-chip) of enzyme biosensors and commercialization of enzyme –based biosensors. With the development of computer software and hardware technology, sensor technology will

also develop, and the biological system of closed-loop control will be possible. In the future, biosensors will be widely used in many fields, such as food detection, medical care, disease diagnosis, environmental monitoring, fermentation industry, and so on. These techniques can be utilized to the point of control version of the electrochemical enzyme biosensors, both miniaturizing and improving analytical performance.

References

[1]. N. Bhalla, P. Jolly, N. Formisano, and P. Estrela, Introduction to biosensors Characteristics of a biosensor, *Essays Biochem.*, 60, 2016, pp. 1-8.

[2]. Y. D. Han, Y. H. Jang, and H. C. Yoon, Cascadic multienzyme reaction-based electrochemical biosensors, *Adv. Biochem. Eng. Biotechnol.*, 140, 2014, pp. 221-251.

[3]. L. C. Clark and C. Lyons, Electrode Systems For Continuous Monitoring In Cardiovascular Surgery, *Ann. N. Y. Acad. Sci.*, 102, 1962, pp. 29-45.

[4]. S. GS, A. CV, and B. B. Mathew, Biosensors: A Modern Day Achievement, *J. Instrum. Technol.*, 2, 1, 2014, pp. 26-39.

[5]. M. A. Najeeb, Z. Ahmad, R. A. Shakoor, A. M. A. Mohamed, and R. Kahraman, A novel classification of prostate specific antigen (PSA) biosensors based on transducing elements, *Talanta*, 168, 2017, pp. 52-61.

[6]. M. A. Morales and J. M. Halpern, Guide to Selecting a Biorecognition Element for Biosensors, *Bioconjug. Chem.*, 29, 10, 2018, pp. 3231–3239.

[7]. H. H. Nguyen, S. H. Lee, U. J. Lee, C. D. Fermin, and M. Kim, Immobilized enzymes in biosensor applications, *Materials*, 12, 1, 2019, 121.

[8]. M. Misson, B. Jin, B. Chen, and H. Zhang, Enhancing enzyme stability and metabolic functional ability of β-galactosidase through functionalized polymer nanofiber immobilization, *Bioprocess Biosyst. Eng.*, 38, 2015, pp. 1915-1923.

[9]. A. Koyun, E. Ahlatcolu, and Y. Koca, Biosensors and Their Principles, in *A Roadmap of Biomedical Engineers and Milestones*, 79, 2012, pp. 117-142.

[10]. B. R. Eggins, Immobilisation of Biological Component, in Biosensors: an Introduction (Teubner Studienbücher Chemie), *Vieweg+Teubner Verlag,* Wiesbaden. 1996.

[11]. M. Moyo, J. O. Okonkwo, and N. M. Agyei, Optimization of horseradish peroxidase immobilization on glassy carbon electrode based on maize tassel-multiwalled carbon nanotubes for sensitive copper(ii) ion detection, *Int. J. Electrochem. Sci.*, 9, 2014, pp. 1439-1445.

[12]. V. L. Sirisha, A. Jain, and A. Jain, Enzyme Immobilization: An Overview on Methods, Support Material, and Applications of Immobilized Enzymes, *Adv Food Nutr Res*., 79, 2016, pp. 179-211.
[13]. R. A. Sheldon, Enzyme immobilization: The quest for optimum performance, *Advanced Synthesis and Catalysis*, 349, 2007, pp. 1289-1307.
[14]. J. H. Bowes and C. W. Cater, The reaction of glutaraldehyde with proteins and other biological materials, *J. R. Microsc. Soc.*, 85, 2, 1966, pp. 193-200.
[15]. D. T. Wadiak and R. G. Carbonell, Effectiveness factors for substrate and product inhibition, *Biotechnol. Bioeng.*, 17, 1975, pp. 1761-1773.
[16]. N. F Mokhtar, R. N. Z. R. Abd. Rahman, N. D. Muhd Noor, F. Mohd Shariff and M. S. Mohd Ali, The Immobilization of Lipases on Porous Support by Adsorption and Hydrophobic Interaction Method, *Catalysts,* 10, 7, 2020, p. 744.
[17]. A. Koyun, B. Koksal, E. Ahlatcioglu, and A. B. H. Yoruc, Statistical Evaluation Tensile Properties of High-Density Polyethylenes, *Adv. Mater. Res.*, 2012.
[18]. T. Kobayashi and K. J. Laidler, Theory of the kinetics of reactions catalyzed by enzymes attached to membranes, *Biotechnol. Bioeng.*, 16, 1, 1974, pp. 77-97.
[19]. J. Boyle, Lehninger principles of biochemistry (4th ed.), Nelson, D. and Cox, M., *Biochem. Mol. Biol. Educ.*, 2005.
[20]. J. J. Burmeister, M. Palmer, and G. A. Gerhardt, L-lactate measures in brain tissue with ceramic-based multisite microelectrodes, *Biosens. Bioelectron.*, 20, 2005, pp. 1772-1779.
[21]. W. Putzbach and N. J. Ronkainen, Immobilization techniques in the fabrication of nanomaterial-based electrochemical biosensors: A review, *Sensors (Switzerland)*, 13, 4, 2013, pp. 4811-40.
[22]. M. Samer, Biological and Chemical Wastewater Treatment Processes, in Wastewater Treatment Engineering (Mogens Henze, Ed.), *Springer*, 2015, https://www.intechopen.com/books/wastewater-treatment-engineering/biological-and-chemical-wastewater-treatment-processes.
[23]. N. Jaffrezic-Renault and S. V. Dzyadevych, Conductometric microbiosensors for environmental monitoring, *Sensors*, 8, 2008, pp. 2569-2588.
[24]. S. R. Chinnadayyala, M. Santhosh, N. K. Singh, and P. Goswami, Alcohol oxidase protein mediated in-situ synthesized and stabilized gold nanoparticles for developing amperometric alcohol biosensor, *Biosens. Bioelectron.*, 69, 2015, pp. 155-161.
[25]. L. Kumari and S. S. Kanwar, Purification and Characterization of an Extracellular Cholesterol Oxidase of Bacillus subtilis Isolated from Tiger Excreta, *Appl. Biochem. Biotechnol.*, 178, 2016, pp. 353–367.

[26]. J. C. Gonzalez-Rivera and J. F. Osma, Fabrication of an Amperometric Flow-Injection Microfluidic Biosensor Based on Laccase for in Situ Determination of Phenolic Compounds, *Biomed Res. Int.*, 2015.

[27]. C. Gómez-Anquela, T. García-Mendiola, J. M. Abad, M. Pita, F. Pariente, and E. Lorenzo, Scaffold electrodes based on thioctic acid-capped gold nanoparticles coordinated Alcohol Dehydrogenase and Azure A films for high performance biosensor, *Bioelectrochemistry*, 106, 2015, pp. 335-342.

[28]. B. Liang, S. Zhang, Q. Lang, J. Song, L. Han, and A. Liu, Amperometric l-glutamate biosensor based on bacterial cell-surface displayed glutamate dehydrogenase, *Anal. Chim. Acta*, 884, 2015, pp. 83-89.

[29]. Z. Guo, L. Murphy, V. Stein, W. A. Johnston, S. Alcala-Perez, and K. Alexandrov, Engineered PQQ-Glucose Dehydrogenase as a Universal Biosensor Platform, *J. Am. Chem. Soc.*, 52, 2016, pp. 485-458.

[30]. K. Y. Goud *et al.*, Progress on nanostructured electrochemical sensors and their recognition elements for detection of mycotoxins: A review, *Biosensors and Bioelectronics*, 121, 2018, pp. 205-222.

[31]. C. A. Lee and Y. C. Tsai, Preparation of multiwalled carbon nanotube-chitosan-alcohol dehydrogenase nanobiocomposite for amperometric detection of ethanol, *Sensors Actuators, B Chem.*, 138, 2009, pp. 518-523.

[32]. G. Rocchitta *et al.*, Development and characterization of an implantable biosensor for telemetric monitoring of ethanol in the brain of freely moving rats, *Anal. Chem.*, 84, 2012, pp. 7072-7079.

[33]. C. P. McMahon, G. Rocchitta, P. A. Serra, S. M. Kirwan, J. P. Lowry, and R. D. O'Neill, Control of the oxygen dependence of an implantable polymer/enzyme composite biosensor for glutamate, *Anal. Chem.*, 78, 2006, pp. 2352-2359.

[34]. M. Zhang, C. Liao, C. H. Mak, P. You, C. L. Mak, and F. Yan, Highly sensitive glucose sensors based on enzyme-modified whole-graphene solution-gated transistors, *Sci. Rep.*, 5, 2015, 8311.

[35]. Q. Sheng, D. Zhang, Q. Wu, J. Zheng, and H. Tang, Electrodeposition of Prussian blue nanoparticles on polyaniline coated halloysite nanotubes for nonenzymatic hydrogen peroxide sensing, *Anal. Methods*, 7, 2015, 6896.

[36]. A. A. Karyakin, E. E. Karyakina, and L. Gorton, Prussian-Blue-based amperometric biosensors in flow-injection analysis, *Talanta*, 43, 1996, pp. 1597-1606.

[37]. M. I. Prodromidis and M. I. Karayannis, Enzyme based amperometric biosensors for food analysis, *Electroanalysis*, 14, 2002, pp. 241-261.

[38]. G. Rocchitta *et al.*, Enzyme biosensors for biomedical applications: Strategies for safeguarding analytical performances in biological fluids, *Sensors (Switzerland)*, 16, 6, 2016, 780.

[39]. H. Lee, Y. J. Hong, S. Baik, T. Hyeon, and D. H. Kim, Enzyme-Based Glucose Sensor: From Invasive to Wearable Device, *Adv. Healthc. Mater.*, 7, 2018, e1701150.

[40]. P. N. Bartlett, V. Q. Bradford, and R. G. Whitaker, Enzyme electrode studies of glucose oxidase modified with a redox mediator, *Talanta*, 38, 1991, pp. 57-63.
[41]. A. Chaubey and B. D. Malhotra, Mediated biosensors, *Biosensors and Bioelectronics*, 17, 2002, pp. 441-456.
[42]. J. Wang, Electrochemical glucose biosensors, *Chem. Rev.,* 108, 2008, pp. 814-825.
[43]. F. W. Scheller *et al.*, Second generation biosensors, *Biosens. Bioelectron.*, 6, 1991, pp. 245-253.
[44]. G. Rocchitta *et al.*, Analytical Problems in Exposing Amperometric Enzyme Biosensors to Biological Fluids, *Sensors*, 16, 2016, 780.
[45]. S. V Dzyadevych, V. N. Arkhypova, A. P. Soldatkin, A. V El, C. Martelet, and N. Jaffrezic-renault, Amperometric enzyme biosensors : Past , present and future Biocapteurs enzymatiques à transduction ampérométrique : passé, présent, futur, *ITBM-RBM*, 29, 2008, pp. 171-180.
[46]. R. Devi, M. Thakur, and C. S. Pundir, Construction and application of an amperometric xanthine biosensor based on zinc oxide nanoparticles-polypyrrole composite film, *Biosens. Bioelectron.*, 26, 2011, pp. 3420-3426.
[47]. S. Yadav, A. Kumar, and C. S. Pundir, Amperometric creatinine biosensor based on covalently coimmobilized enzymes onto carboxylated multiwalled carbon nanotubes/polyaniline composite film, *Anal. Biochem.*, 419, 2011, pp. 277-283.
[48]. S. Yadav, R. Devi, S. Kumari, S. Yadav, and C. S. Pundir, An amperometric oxalate biosensor based on sorghum oxalate oxidase bound carboxylated multiwalled carbon nanotubes-polyaniline composite film, *J. Biotechnol.*, 151, 2011, pp. 212-217.
[49]. R. Devi, S. Yadav, and C. S. Pundir, Amperometric determination of xanthine in fish meat by zinc oxide nanoparticle/chitosan/multiwalled carbon nanotube/polyaniline composite film bound xanthine oxidase, *Analyst*, 137, 2012, pp. 754-759.
[50]. R. Devi, S. Yadav, and C. S. Pundir, Electrochemical detection of xanthine in fish meat by xanthine oxidase immobilized on carboxylated multiwalled carbon nanotubes/polyaniline composite film, *Biochem. Eng. J.*, 115, 2, 2011, pp. 207-214.
[51]. P. D'Orazio, Biosensors in clinical chemistry, *Clinica Chimica Acta*, 334, 1-2, 2003, pp. 41-69.
[52]. Y. I. Korpan *et al.*, Development of highly selective and stable potentiometric sensors for formaldehyde determination, *Biosens. Bioelectron.*, 15, 2000, pp. 77-83.
[53]. M. Ben Ali *et al.*, Electrical characterization of functionalized platinum electrodes and ISFET sensors for metal ion detection, *Mater. Sci. Eng. C*, C26, 2006, pp. 149-153.
[54]. S. Borman, Biosensors: Potentiometric and Amperometric, *Anal. Chem.*, 59, 1987, pp. 1091A-1098A.

[55]. R. J. Guo, M. H. Wang, T. L. Tso, and T. P. Perng, Photoelectrochemical properties of sulfidized TiO2 electrodes, *Int. J. Hydrogen Energy*, 7, 1995, pp. 561-566.

[56]. Y. Han, X. Ruan, J. Chen, H. Zhang, H. Zhao, and S. Zhang, Photoelectrochemical properties and its application of nano-tio 2/boron-doped diamond heterojunction electrode material, *Asian J. Chem.*, 62, 2013, pp. 619-625.

[57]. H. Huang, Preparation and photoelectrochemical characterization of nano-participate TiO2 and polyaniline composite film on ρ-aminothiophenol/Au film, *J. Rare Earths*, 23, 2005, pp. 116-121.

[58]. J. Zhang *et al.*, Fluorescent gold nanoclusters based photoelectrochemical sensors for detection of H_2O_2 and glucose, *Biosens. Bioelectron.*, 67, 2015, pp. 296-302.

[59]. D. J. K. Swainsbury, V. M. Friebe, R. N. Frese, and M. R. Jones, Evaluation of a biohybrid photoelectrochemical cell employing the purple bacterial reaction centre as a biosensor for herbicides, *Biosens. Bioelectron.*, 58, 2014, pp. 172-178.

[60]. W. W. Zhao, J. J. Xu, and H. Y. Chen, Photoelectrochemical enzymatic biosensors, *Biosensors and Bioelectronics*, 92, 2017, pp. 294-304.

[61]. F. C. M. Wong, M. Ahmad, L. Y. Heng, and L. B. Peng, An optical biosensor for dichlovos using stacked sol-gel films containing acetylcholinesterase and a lipophilic chromoionophore, *Talanta*, 69, 2006, pp. 888–893.

[62]. Z. Lin, Z. Chen, Y. Liu, J. Wang, and G. Chen, An electrochemiluminescent biosensor for uric acid based on the electrochemiluminescence of bis-[3,4,6-trichloro-2-(pentyloxycarbonyl)-phenyl] oxalate on an ITO electrode modified by an electropolymerized nickel phthalocyanine film, *Analyst*, 133, 2008, pp. 797-801.

[63]. K. L. Brogan and D. R. Walt, Optical fiber-based sensors: Application to chemical biology, *Current Opinion in Chemical Biology*, 9, 5, 2005, pp. 494-500.

[64]. A. Ibraheem and R. E. Campbell, Designs and applications of fluorescent protein-based biosensors, *Current Opinion in Chemical Biology*, 14, 1, 2010, pp. 30-36.

[65]. B. Polyak, E. Bassis, A. Novodvorets, S. Belkin, and R. S. Marks, Bioluminescent whole cell optical fiber sensor to genotoxicants: System optimization, *Sensors and Actuators B: Chemical,* 74, 1–3, 2001, pp. 18-26.

[66]. A. M. Horsburgh *et al.*, On-line microbial biosensing and fingerprinting of water pollutants, *Biosens. Bioelectron.*, 17, 6-7, 2002, pp. 495-501.

[67]. Y. S. Fung and C. C. W. Wong, Determination of carbon monoxide in ambient air using piezoelectric crystal sorption detection, *Anal. Chim. Acta*, 456, 2, 2002, pp. 227-239.

[68]. Z. Su, L. Ye, and X. Bu, A damage identification technique for CF/EP composite laminates using distributed piezoelectric transducers, *Compos. Struct.*, 57, 14, 2002, pp. 465–471.
[69]. S. K. Arya, P. R. Solanki, R. P. Singh, M. K. Pandey, M. Datta, and B. D. Malhotra, Application of octadecanethiol self-assembled monolayer to cholesterol biosensor based on surface plasmon resonance technique, *Talanta*, 69, 4, 2006, pp. 918-926.
[70]. Y. Zhang and S. Tadigadapa, Calorimetric biosensors with integrated microfluidic channels, *Biosens. Bioelectron.*, 19, 12, 2004, pp. 1733-1743.
[71]. D. R. Thévenot, K. Toth, R. A. Durst, and G. S. Wilson, Electrochemical biosensors: Recommended definitions and classification, *Biosens. Bioelectron.*, 16, 1-2, 2001, pp. 121-131.
[72]. A. Amine, F. Arduini, D. Moscone, and G. Palleschi, Recent advances in biosensors based on enzyme inhibition, *Biosens. Bioelectron.*, 76, 2016, pp. 180-194.
[73]. J. Wang, Electrochemical biosensors: Towards point-of-care cancer diagnostics, *Biosens Bioelectron*, 21, 10, 2006, pp. 1887-1892.
[74]. D. Grieshaber, R. MacKenzie, J. Vörös, and E. Reimhult, Electrochemical biosensors - Sensor principles and architectures, *Sensors*, 8, 2008, 1400.
[75]. R. A Copeland, Enzymes: A Practical Introduction to Structure, Mechanism, and Data Analysis, 2nd ed., *Wiley-VCH,* 2000.
[76]. T. Monteiro and M. G. Almeida, Electrochemical Enzyme Biosensors Revisited: Old Solutions for New Problems, *Critical Reviews in Analytical Chemistry*, 49, 2019, pp. 44-66.
[77]. N. Wisniewski and M. Reichert, Methods for reducing biosensor membrane biofouling, *Colloids Surfaces B Biointerfaces*, 18, 2000, pp. 197-219.
[78]. M. D. Gouda, M. S. Thakur, and N. G. Karanth, Reversible denaturation behavior of immobilized glucose oxidase, 102-103, 1-6, 2002, pp. 471-80.
[79]. Y. Cui *et al.*, Prevalence and causes of low vision and blindness in a Chinese population with type 2 diabetes: The Dongguan Eye Study, *Sci. Rep.*, 7, 2017, 11195.
[80]. C. S. Fox *et al.*, Update on prevention of cardiovascular disease in adults with type 2 diabetes mellitus in light of recent evidence: A scientific statement from the American Heart Association and the American diabetes association, *Diabetes Care*, 38, 9, 2015, pp. 1777-1803.
[81]. K. K. Aung, C. Lorenzo, M. A. Hinojosa, and S. M. Haffner, Risk of developing diabetes and cardiovascular disease in metabolically unhealthy normal-weight and metabolically healthy obese individuals, *J. Clin. Endocrinol. Metab.*, 99, 2014, 462.
[82]. S. L. Appleton *et al.*, Diabetes and cardiovascular disease outcomes in the metabolically healthy obese phenotype: A cohort study, *Diabetes Care*, 36, 2013, 2388.

[83]. C. Wanner, S. E. Inzucchi, and B. Zinman, The authors reply: Empagliflozin and progression of kidney disease in Type 2 diabetes, *New England Journal of Medicine*, 375, 2016, 323.
[84]. M. Afkarian *et al.*, Kidney disease and increased mortality risk in type 2 diabetes, *J. Am. Soc. Nephrol.*, 24, 2013, 302.
[85]. A. Harper and M. R. Anderson, Electrochemical glucose sensors-developments using electrostatic assembly and carbon nanotubes for biosensor construction, *Sensors*, 10, 2010, 8248.
[86]. T. F. Tseng, Y. L. Yang, Y. J. Lin, and S. L. Lou, Effects of electric potential treatment of a chromium hexacyanoferrate modified biosensor based on PQQ-dependent glucose dehydrogenase, *Sensors*, 10, 2010, 6347.
[87]. S. Abdellaoui, R. D. Milton, T. Quah, and S. D. Minteer, NAD-dependent dehydrogenase bioelectrocatalysis: The ability of a naphthoquinone redox polymer to regenerate NAD, *Chem. Commun.*, 52, 2016, 1147.
[88]. S. J. Updike and G. P. Hicks, The enzyme electrode, *Nature*, 214, 1967, 986.
[89]. J. Wang and X. Zhang, Needle-type dual microsensor for the simultaneous monitoring of glucose and insulin, *Anal. Chem.*, 73, 4, 2001, pp. 844-847.
[90]. G. Palleschi, M. Mascini, L. Bernardi, and P. Zeppilli, Lactate and glucose electrochemical biosensors for the evaluation of the aerobic and anaerobic threshold in runners, *Med. Biol. Eng. Comput.*, 28, 1990, B25.
[91]. J. W. Mo and W. Smart, Lactate biosensors for continuous monitoring., *Frontiers in Bioscience : a Journal and Virtual Library*, 9, 2004, 3384.
[92]. J. Boldt, Clinical review: Hemodynamic monitoring in the intensive care unit, *Critical Care*, 6, 1, 2002, p. 52.
[93]. C. J. E. Ingram, C. A. Mulcare, Y. Itan, M. G. Thomas, and D. M. Swallow, Lactose digestion and the evolutionary genetics of lactase persistence, *Human Genetics*, 124, 2009, pp. 579-591.
[94]. M. Leonardi, P. Gerbault, M. G. Thomas, and J. Burger, The evolution of lactase persistence in Europe. A synthesis of archaeological and genetic evidence, *International Dairy Journal*, 22, 2012, pp. 88-97.
[95]. N. Ghéczy, A. Küchler, and P. Walde, Proteinase K activity determination with β-galactosidase as sensitive macromolecular substrate, *Anal. Biochem.*, 513, 2016, pp. 54-60.
[96]. Z. Grosová, M. Rosenberg, and M. Rebroš, Perspectives and applications of immobilised β-galactosidase in food industry - A review, *Czech Journal of Food Sciences*. 2008, 26, 1-14.
[97]. S. K. Sharma *et al.*, β-Galactosidase Langmuir Monolayer at Air/X-gal Subphase Interface, *J. Phys. Chem. B*, 120, 2016, pp. 12279-12286.
[98]. E. Watanabe, M. Takagi, S. Takei, M. Hoshi, and C. Shu-gui, Development of biosensors for the simultaneous determination of sucrose and glucose, lactose and glucose, and starch and glucose, *Biotechnol. Bioeng.*, 38, 1991, pp. 99-103.

[99]. R. J. M. Lourenço, M. L. M. Serralheiro, and M. J. F. Rebelo, Development of a New Amperometric Biosensor for Lactose Determination, *Port. Electrochim. Acta*, 21, 2003, pp. 171-177.
[100]. N. E. Miller, HDL Cholesterol, Tissue Cholesterol and Coronary Atherosclerosis: Epidemiological Correlations, in Atherosclerosis V, Gotto A. M., Smith L. C., Allen B. (Eds.), *Springer,* New York, NY, 1980, pp. 500-503.
[101]. M. Kratz, Dietary cholesterol, atherosclerosis and coronary heart disease, *Handb. Exp. Pharmacol.*, 170, 2005, pp. 195-213.
[102]. A. Vrielink, Cholesterol Oxidase: Structure and Function, *Subcell. Biochem.*, 51, 2010, pp. 137-158.
[103]. G. V. Vahouny and C. R. Treadwell, Enzymatic synthesis and hydrolysis of cholesterol esters., *Methods of Biochemical Analysis*, 16, 1968, pp. 219-272.
[104]. A. Gahlaut, A. Gothwal, A. K. Chhillar, and V. Hooda, Electrochemical Biosensors for Determination of Organophosphorus Compounds: Review, *Open J. Appl. Biosens.*, 1, 2012, pp. 1-8.
[105]. L. L. Smith, Cholesterolautoxidation 1981-1986, *Chem. Phys. Lipids*, 44, 1987, pp. 87–125.
[106]. A. L. Ghindilis, P. Atanasov, and E. Wilkins, Enzyme-Catalyzed Direct Electron Transfer: Fundamentals and Analytical Applications, *Electroanalysis*, 9, 1997, pp. 661-674.
[107]. E. E. Ferapontova, Electrochemical Analysis of Dopamine: Perspectives of Specific In Vivo Detection, *Electrochim. Acta*, 245, 2017, pp. 664-671.
[108]. I. Cesarino, H. V. Galesco, F. C. Moraes, M. R. V. Lanza, and S. A. S. Machado, Biosensor Based on Electrocodeposition of Carbon Nanotubes/Polypyrrole/Laccase for Neurotransmitter Detection, *Electroanalysis*, 25, 2, 2013, pp. 394-400.
[109]. C. Wang *et al.*, A facile electrochemical sensor based on reduced graphene oxide and Au nanoplates modified glassy carbon electrode for simultaneous detection of ascorbic acid, dopamine and uric acid, *Sensors Actuators, B Chem.*, 204, 2014, pp. 302–309.
[110]. Y. Ferry and D. Leech, Amperometric detection of catecholamine neurotransmitters using electrocatalytic substrate recycling at a laccase electrode, *Electroanalysis*, 17, 2, 2005, pp. 113 – 119.
[111]. A. C. Skulas-Ray, P. M. Kris-Etherton, W. S. Harris, J. P. Vanden Heuvel, P. R. Wagner, and S. G. West, Dose-response effects of omega-3 fatty acids on triglycerides, inflammation, and endothelial function in healthy persons with moderate hypertriglyceridemia, *Am. J. Clin. Nutr.*, 93, 2011, pp. 243-252.
[112]. B. L. Burgess *et al.*, Elevated plasma triglyceride levels precede amyloid deposition in Alzheimer's disease mouse models with abundant Aβ in plasma, *Neurobiol. Dis.*, 24, 2006, pp. 114-127.

[113]. N. Sarwar *et al.*, Triglycerides and the risk of coronary heart disease: 10 158 Incident cases among 262 525 participants in 29 Western prospective studies, *Circulation*, 115, 2007, pp. 450-458.
[114]. C. S. Pundir, V. Narwal, and B. Batra, Determination of lactic acid with special emphasis on biosensing methods: A review, *Biosensors and Bioelectronics*, 86, 2016, pp. 777-790.
[115]. S. Sadeghi and A. Garmroodi, A highly sensitive and selective electrochemical sensor for determination of Cr(VI) in the presence of Cr(III) using modified multi-walled carbon nanotubes/quercetin screen-printed electrode, *Mater. Sci. Eng. C*, 33, 8, 2013, pp. 4972-4977.
[116]. P. Das, M. Das, S. R. Chinnadayyala, I. M. Singha, and P. Goswami, Recent advances on developing 3rd generation enzyme electrode for biosensor applications, *Biosensors and Bioelectronics*, 79, 2016, pp. 386-397.
[117]. I. Grabowska, M. Chudy, A. Dybko, and Z. Brzozka, Uric acid determination in a miniaturized flow system with dual optical detection, *Sensors Actuators, B Chem.*, 130, 2008, pp. 508-513.
[118]. R. Kand'ár, P. Žáková, and V. Mužáková, Monitoring of antioxidant properties of uric acid in humans for a consideration measuring of levels of allantoin in plasma by liquid chromatography, *Clin. Chim. Acta*, 365, 2006, pp. 249-256.
[119]. G. F. Falasca, Metabolic diseases: gout, *Clin. Dermatol.*, 24, 2006, pp. 498-508.
[120]. T. R. Merriman and N. Dalbeth, The genetic basis of hyperuricaemia and gout, *Joint Bone Spine*, 78, 2011, pp. 35-40.
[121]. T. Nakagawa *et al.*, Unearthing uric acid: An ancient factor with recently found significance in renal and cardiovascular disease, *Kidney International*, 69, 2006, pp. 1722-1725.
[122]. W. L. Nyhan, The recognition of Lesch-Nyhan syndrome as an inborn error of purine metabolism, *J. Inherit Metab Dis.,* 20, 1997, pp. 171-178.
[123]. P. J. Cannon, W. B. Stason, F. E. Demartini, S. C. Sommers, and J. H. Laragh, Hyperuricemia in primary and renal hypertension., *N. Engl. J. Med.*, 275, 1966, pp. 457-464.
[124]. F. Jossa *et al.*, Serum uric acid and hypertension: The Olivetti heart study, *J. Hum. Hypertens.*, 8, 1994, pp. 677-681.
[125]. V. Lohsoonthorn, B. Dhanamun, and M. A. Williams, Prevalence of Hyperuricemia and its Relationship with Metabolic Syndrome in Thai Adults Receiving Annual Health Exams, *Arch. Med. Res.*, 37, 2006, pp. 883-889.
[126]. A. C. M. Gagliardi, M. H. Miname, and R. D. Santos, Uric acid: A marker of increased cardiovascular risk, *Atherosclerosis*, 202, 2009, pp. 11-17.
[127]. J. Fang and M. H. Alderman, Serum uric acid and cardiovascular mortality the NHANES I epidemiologic follow-up study, 1971-1992. National Health and Nutrition Examination Survey., *JAMA*, 283, 2000, pp. 2404-2410.

[128]. G. Lippi, M. Montagnana, M. Franchini, E. J. Favaloro, and G. Targher, The paradoxical relationship between serum uric acid and cardiovascular disease, *Clinica Chimica Acta*, 392, 2008, pp. 1-7.
[129]. E. Akyilmaz, M. K. Sezgintürk, and E. Dinçkaya, A biosensor based on urate oxidase-peroxidase coupled enzyme system for uric acid determination in urine, *Talanta*, 61, 2003, pp. 73-79.
[130]. E. Miland, A. J. Miranda Ordieres, P. Tuñón Blanco, M. R. Smyth, and C. Ó. Fágáin, Poly(o-aminophenol)-modified bienzyme carbon paste electrode for the detection of uric acid, *Talanta*, 43, 1996, pp. 785-796.
[131]. J. Kan, X. Pan, and C. Chen, Polyaniline-uricase biosensor prepared with template process, *Biosens. Bioelectron.*, 19, 2004, pp. 1635-1640.
[132]. J. Motonaka, K. Miyata, and L. R. Faulkner, Micro Enzyme-Sensor with Osmium Complex and a Porous Carbon for Measuring Uric Acid, *Anal. Lett.*, 27, 1994, pp. 1-13.
[133]. M. Niculescu, T. Erichsen, V. Sukharev, Z. Kerenyi, E. Csöregi, and W. Schuhmann, Quinohemoprotein alcohol dehydrogenase-based reagentless amperometric biosensor for ethanol monitoring during wine fermentation, *Anal. Chim. Acta*, 463, 1, 2002, pp. 39–51.
[134]. A. S. Santos, A. C. Pereira, N. Durán, and L. T. Kubota, Amperometric biosensor for ethanol based on co-immobilization of alcohol dehydrogenase and Meldola's Blue on multi-wall carbon nanotube, *Electrochim. Acta*, 52, 2006, pp. 215-220.
[135]. A. S. Santos, R. S. Freire, and L. T. Kubota, Highly stable amperometric biosensor for ethanol based on Meldola's blue adsorbed on silica gel modified with niobium oxide, *J. Electroanal. Chem.*, 547, 2003, pp. 135-142.
[136]. J. Vonck and E. F. J. Van Bruggen, Architecture of peroxisomal alcohol oxidase crystals from the methylotrophic yeast Hansenula polymorpha as deduced by electron microscopy, *J. Bacteriol.*, 74, 16, 1992, pp. 5391-5399.
[137]. A. Gahlaut, V. Dhull, M. Dahiya, and R. Dabur, Analytical Techniques in Forensic Science: MS & Bio-Sensor based diagnostics, *Int. J. Chem. Anal. Sci.*, 5, 1, 2014, pp. 6-10.
[138]. S. Zhen *et al.*, A novel microassay for measuring blood alcohol concentration using a disposable biosensor strip, *Forensic Sci. Int.*, 207, 2011, pp. 177-182.
[139]. T. S. Anthonymuthu, E. M. Kenny, and H. Bayır, Therapies targeting lipid peroxidation in traumatic brain injury, *Brain Research*, 1640, 2016, pp. 57-76.
[140]. S. C. Barber, R. J. Mead, and P. J. Shaw, Oxidative stress in ALS: A mechanism of neurodegeneration and a therapeutic target, *Biochimica et Biophysica Acta - Molecular Basis of Disease*, 1762, 11-12, 2006, pp. 1051-67.
[141]. O. Hwang, Role of Oxidative Stress in Parkinson's Disease, *Exp. Neurobiol.*, 22, 1, 2013, pp. 11-7.

[142]. C. Cheignon, M. Tomas, D. Bonnefont-Rousselot, P. Faller, C. Hureau, and F. Collin, Oxidative stress and the amyloid beta peptide in Alzheimer's disease, *Redox Biology*, 14, 2018, pp. 450–464.
[143]. P. Rocha-Pereira, A. Santos-Silva, I. Rebelo, A. Figueiredo, A. Quintanilha, and F. Teixeira, Dislipidemia and oxidative stress in mild and in severe psoriasis as a risk for cardiovascular disease, *Clin. Chim. Acta*, 303, 1-2, 2001, pp. 33-39.
[144]. N. S. Dhalla, R. M. Temsah, and T. Netticadan, Role of oxidative stress in cardiovascular diseases, *Journal of Hypertension*, 18, 6, 2000, pp. 655-673.
[145]. B. Uttara, A. Singh, P. Zamboni, and R. Mahajan, Oxidative Stress and Neurodegenerative Diseases: A Review of Upstream and Downstream Antioxidant Therapeutic Options, *Curr. Neuropharmacol.*, 7, 1, 2009, pp. 65–74.
[146]. E. Emregül, Development of a new biosensor for superoxide radicals, *Anal. Bioanal. Chem.*, 383, 2005, pp. 947–954.
[147]. K. Endo *et al.*, Development of a superoxide sensor by immobilization of superoxide dismutase, *Sensors and Actuators B Chemical*, 83, 2002, pp. 30–34.
[148]. M. B. Colovic, D. Z. Krstic, T. D. Lazarevic-Pasti, A. M. Bondzic, and V. M. Vasic, Acetylcholinesterase Inhibitors: Pharmacology and Toxicology, *Curr. Neuropharmacol.*, 11, 2013, pp. 315-335.
[149]. W. E. Lee, H. G. Thompson, J. G. Hall, and D. E. Bader, Rapid detection and identification of biological and chemical agents by immunoassay, gene probe assay and enzyme inhibition using a silicon-based biosensor, *Biosens. Bioelectron.*, 14, 2000, pp. 795-804.
[150]. S. Upadhyay, G. R. Rao, M. K. Sharma, B. K. Bhattacharya, V. K. Rao, and R. Vijayaraghavan, Immobilization of acetylcholineesterase-choline oxidase on a gold-platinum bimetallic nanoparticles modified glassy carbon electrode for the sensitive detection of organophosphate pesticides, carbamates and nerve agents, *Biosens. Bioelectron.*, 25, 2009, pp. 832-838.
[151]. L. Kenar, The use of biosensors for the detection of chemical and biological weapons, *Turkish Journal of Biochemistry*, 35, 2010, pp. 72-74.
[152]. T. Hansmann, B. Sanson, J. Stojan, M. Weik, J. L. Marty, and D. Fournier, Kinetic insight into the mechanism of cholinesterasterase inhibition by aflatoxin B1 to develop biosensors, *Biosens. Bioelectron.*, 24, 2009, pp. 2119-2124.
[153]. I. Ben Rejeb *et al.*, Development of a bio-electrochemical assay for AFB1 detection in olive oil, *Biosens. Bioelectron.*, 24, 2009, pp. 1962-1968.
[154]. F. Villatte, H. Schulze, R. D. Schmid, and T. T. Bachmann, A disposable acetylcholinesterase-based electrode biosensor to detect anatoxin-a(s) in water, *Fresenius. J. Anal. Chem.*, 372, 2002, pp. 322-326.

[155]. E. Devic *et al.*, Detection of anatoxin-a(s) in environmental samples of cyanobacteria by using a biosensor with engineered acetylcholinesterases, *Appl. Environ. Microbiol.*, 68, 2002, pp. 4102-4106.
[156]. M. A. Espinoza, G. Istamboulie, A. Chira, T. Noguer, M. Stoytcheva, and J. L. Marty, Detection of glycoalkaloids using disposable biosensors based on genetically modified enzymes, *Anal. Biochem.*, 457, 2014, pp. 85-90.
[157]. A. Yarman, U. Wollenberger, and F. W. Scheller, Sensors based on cytochrome P450 and CYP mimicking systems, *Electrochim. Acta*, 110, 2013, pp. 63-72.
[158]. D. De Venuto, S. Carrara, A. Cavallini, and G. De Micheli, PH sensing with temperature compensation in a molecular biosensor for drugs detection, in *Proceedings of the 12th International Symposium on Quality Electronic Design (ISQED 2011),* Santa Clara, California, USA, 14-16 March 2011, p. 326.
[159]. S. Liu, L. Peng, X. Yang, Y. Wu, and L. He, Electrochemistry of cytochrome P450 enzyme on nanoparticle-containing membrane-coated electrode and its applications for drug sensing, *Anal. Biochem.*, 375, 2, 2008, pp. 209-216.
[160]. P. Panicco, V. R. Dodhia, A. Fantuzzi, and G. Gilardi, Enzyme-based amperometric platform to determine the polymorphic response in drug metabolism by cytochromes P450, *Anal. Chem.*, 83, 6, 2011, pp. 2179-2186.
[161]. M. Yang *et al.*, Electrocatalytic drug metabolism by CYP2C9 bonded to A self-assembled monolayer-modified electrode, *Drug Metab. Dispos.*, 37, 4, 2009, pp. 892-9.
[162]. P. Skládal, G. S. Nunes, H. Yamanaka, and M. L. Ribeiro, Detection of Carbamate Pesticides in Vegetable Samples Using Cholinesterase-Based Biosensors, *Electroanalysis*, 9, 1997, pp. 1083-1087.
[163]. A. F. S. Amaral, Pesticides and asthma: Challenges for epidemiology, *Front. Public Heal.*, 2, 6, 2014, 24479117.
[164]. K. Kuroda, Y. Yamaguchi, and G. Endo, Mitotic toxicity, sister chromatid exchange, and rec assay of pesticides, *Arch. Environ. Contam. Toxicol.*, 23, 1992, pp. 13-18.
[165]. G. Liu and Y. Lin, Biosensor based on self-assembling acetylcholinesterase on carbon nanotubes for flow injection/amperometric detection of organophosphate pesticides and nerve agents, *Anal. Chem.*, 78, 3, 2006, pp. 835–843.
[166]. Y. D. Tanimoto de Albuquerque and L. F. Ferreira, Amperometric biosensing of carbamate and organophosphate pesticides utilizing screen-printed tyrosinase-modified electrodes, *Anal. Chim. Acta*, 596, 2007, pp. 210-221.
[167]. W. J. Donarski, D. P. Dumas, D. P. Heitmeyer, V. E. Lewis, and F. M. Raushel, Structure-Activity Relationships in the Hydrolysis of

Substrates by the Phosphotriesterase from Pseudomonas diminuta, *Biochemistry*, 28, 11, 1989, pp. 4650-4655.
[168]. S. Chapalamadugu and G. R. Chaudhry, Microbiological and biotechnological aspects of metabolism of carbamates and organophosphates, *Crit. Rev. Biotechnol.*, 12, 1992, pp. 357-389.
[169]. N. Jaffrezic-Renault, New trends in biosensors for organophosphorus pesticides, *Sensors*, 1, 2, 2001, pp. 60-74.
[170]. M. Trojanowicz, Determination of pesticides using electrochemical enzymatic biosensors, *Electroanalysis*, 14, 19, 2002, pp. 1311-1328.
[171]. I. Palchetti, A. Cagnini, M. Del Carlo, C. Coppi, M. Mascini, and A. P. F. Turner, Determination of anticholinesterase pesticides in real samples using a disposable biosensor, *Anal. Chim. Acta*, 337, 1997, pp. 351-321.
[172]. J. Diehl-Faxon, A. L. Ghindilis, P. Atanasov, and E. Wilkins, Direct electron transfer based tri-enzyme electrode for monitoring of organophosphorus pesticides, *Sensors Actuators, B Chem.*, 35, 1996, pp. 448-457.
[173]. G. Palleschi, M. Bernabei, C. Cremisini, and M. Mascini, Determination of organophosphorus insecticides with a choline electrochemical biosensor, *Sensors Actuators B. Chem.*, 7, 1992, pp. 513-517.
[174]. M. Trojanowicz and M. L. Hitchman, Determination of pesticides using electrochemical biosensors, *TrAC - Trends Anal. Chem.*, 15, 1996, pp. 38-45.
[175]. D. P. Dumas, H. D. Durst, W. G. Landis, F. M. Raushel, and J. R. Wild, Inactivation of organophosphorus nerve agents by the phosphotriesterase from Pseudomonas diminuta, *Arch. Biochem. Biophys.*, 227, 1990, pp. 155-159.
[176]. X. Tang *et al.*, Sensitive electrochemical microbial biosensor for p-nitrophenylorganophosphates based on electrode modified with cell surface-displayed organophosphorus hydrolase and ordered mesopore carbons, *Biosens. Bioelectron.*, 60, 2014, pp. 137-142.
[177]. T. M. B. F. Oliveira *et al.*, Laccase-Prussian blue film-graphene doped carbon paste modified electrode for carbamate pesticides quantification, *Biosens. Bioelectron.*, 47, 2013, pp. 292–299.
[178]. T. M. B. F. Oliveira *et al.*, Biosensor based on multi-walled carbon nanotubes paste electrode modified with laccase for pirimicarb pesticide quantification, *Talanta*, 106, 2013, pp. 137-143.
[179]. M. Stoytcheva, V. Sharkova, and M. Panayotova, Electrochemical approach in studying the inhibition of acetylcholinesterase by arsenate(III): Analytical characterisation and application for arsenic determination, *Anal. Chim. Acta*, 364, 1998, pp. 195-201.
[180]. S. Sanllorente-Méndez, O. Domínguez-Renedo, and M. Julia Arcos-Martínez, Immobilization of acetylcholinesterase on screen-printed electrodes. Application to the determination of arsenic(III), *Sensors*, 10, 2010, pp. 2119-2128.

[181]. C. Malitesta and M. R. Guascito, Heavy metal determination by biosensors based on enzyme immobilised by electropolymerisation, *Biosens Bioelectron*., 20, 8, 2005, pp. 1643-1637.
[182]. R. A. Doong and H. C. Tsai, Immobilization and characterization of sol-gel-encapsulated acetylcholinesterase fiber-optic biosensor, *Anal. Chim. Acta*, 434, 2, 2001, pp. 239-246.
[183]. H. C. Tsai and R. A. Doong, Simultaneous determination of pH, urea, acetylcholine and heavy metals using array-based enzymatic optical biosensor, *Biosens. Bioelectron.*, 20, 9, 2005, pp. 1796-1804.
[184]. S. V. Mohan and J. Karthikeyan, Removal of lignin and tannin colour from aqueous solution by adsorption onto activated charcoal, *Environ. Pollut.*, 97, 1997, pp. 183-187.
[185]. D. Mohan and C. U. Pittman, Activated carbons and low cost adsorbents for remediation of tri- and hexavalent chromium from water, *Journal of Hazardous Materials*., 137, 2, 2006, pp. 762-811.
[186]. S. P. *et al.*, Groundwater Contaminated with Hexavalent Chromium [Cr (VI)]: A Health Survey and Clinical Examination of Community Inhabitants (Kanpur, India), *PLoS One*, 7, 10, 2012, e47877.
[187]. C. Michel, F. Battaglia-Brunet, C. T. Minh, M. Bruschi, and I. Ignatiadis, Amperometric cytochrome c3-based biosensor for chromate determination, *Biosens. Bioelectron.*, 19, 4, 2003, pp. 345-352.
[188]. A. M. Aiken, B. M. Peyton, W. A. Apel, and J. N. Petersen, Heavy metal-induced inhibition of Aspergillus niger nitrate reductase: Applications for rapid contaminant detection in aqueous samples, *Anal. Chim. Acta*, 480, 2003, pp. 131–142.
[189]. N. J. Nepomuscene, D. Daniel, and A. Krastanov, Biosensor to detect chromium in wastewater, *Biotechnol. Biotechnol. Equip.*, 21, 2007, pp. 377-381.
[190]. D. Mani and C. Kumar, Biotechnological advances in bioremediation of heavy metals contaminated ecosystems: An overview with special reference to phytoremediation, *International Journal of Environmental Science and Technology*, 11, 2014, pp. 843-872.
[191]. T. Boningari and P. G. Smirniotis, Impact of nitrogen oxides on the environment and human health: Mn-based materials for the NOx abatement, *Current Opinion in Chemical Engineering*, 13, 2016, pp. 133-141.
[192]. D. M. Zurcher, Y. J. Adhia, J. D. Romero, and A. J. McNeil, Modifying a known gelator scaffold for nitrite detection, *Chem. Commun.*, 50, 2014, pp. 7813-7816.
[193]. H. Chen, C. Mousty, L. Chen, and S. Cosnier, A new approach for nitrite determination based on a HRP/catalase biosensor, *Mater. Sci. Eng. C*, 28, 2008, pp. 726-730.
[194]. A. Zazoua, M. Hnaien, S. Cosnier, N. Jaffrezic-Renault, and R. Kherrat, A new HRP/catalase biosensor based on microconductometric transduction for nitrite determination, *Mater. Sci. Eng. C*, 29, 2009, pp. 191-1922.

[195]. H. Liu *et al.*, A novel Nitrite biosensor based on direct electrochemistry of horseradish peroxidase immobilized on porous Co_3O_4 nanosheets and reduced graphene oxide composite modifide electrode, *Sens. Acurator B Chem.*, 238, 2017, pp. 249-256.
[196]. S. Rajesh, A. K. Kanugula, K. Bhargava, G. Ilavazhagan, S. Kotamraju, and C. Karunakaran, Simultaneous electrochemical determination of superoxide anion radical and nitrite using Cu,ZnSOD immobilized on carbon nanotube in polypyrrole matrix, *Biosens. Bioelectron.*, 26, 2010, pp. 689-695.
[197]. A. Gerssen, I. E. Pol-Hofstad, M. Poelman, P. P. J. Mulder, H. J. van den Top, and J. Dde Boer, Marine toxins: Chemistry, toxicity, occurrence and detection, with special reference to the dutch situation, *Toxins*., 2, 2010, pp. 878-904.
[198]. A. Zingone and H. Oksfeldt Enevoldsen, The diversity of harmful algal blooms: A challenge for science and management, *Ocean Coast. Manag.*, 43, 2000, pp. 725-748.
[199]. D. L. Anderson, Screening of foods and related products for toxic elements with a portable X-ray tube analyzer, *J. Radioanal. Nucl. Chem.*, 282, 2009, pp. 415–418.
[200]. C. Vale *et al.*, In vitro and in vivo evaluation of paralytic shellfish poisoning toxin potency and the influence of the pH of extraction, *Anal. Chem.*, 80, 5, 2008, pp. 1770-1776.
[201]. L. E. Llewellyn, The behavior of mixtures of paralytic shellfish toxins in competitive binding assays, *Chem. Res. Toxicol.*, 19, 5, 2006, pp. 661-667.
[202]. P. Visciano, M. Schirone, M. Berti, A. Milandri, R. Tofalo, and G. Suzzi, Marine Biotoxins: Occurrence, Toxicity, Regulatory Limits and Reference Methods, *Front. Microbiol.*, 7, 2016, pp. 1-10.
[203]. J. F. Lawrence *et al.*, Quantitative determination of paralytic shellfish poisoning toxins in shellfish using prechromatographic oxidation and liquid chromatography with fluorescence detection: Collaborative study, *J. AOAC Int.*, 88, 2005, pp. 1714-1732.
[204]. M. G. N. Cruz *et al.*, Determination of paralytic shellfish toxins using potentiometric electronic tongue, *Sensors Actuators, B Chem.*, 263, 2018, pp. 550-556.
[205]. M. Raposo, M. J. Botelho, S. T. Costa, M. T. S. R. Gomes, and A. Rudnitskaya, A carbamoylase-based bioassay for the detection of paralytic shellfish poisoning toxins, *Sensors (Switzerland)*, 20, 2, 2020, p. 507.
[206]. H. P. Lin, Y. Cho, H. Yashiro, T. Yamada, and Y. Oshima, Purification and characterization of paralytic shellfish toxin transforming enzyme from Mactra chinensis, *Toxicon*, 44, 2004, pp. 657-668.
[207]. Y. Cho, N. Ogawa, M. Takahashi, H. P. Lin, and Y. Oshima, Purification and characterization of paralytic shellfish toxin-transforming enzyme, sulfocarbamoylase I, from the Japanese bivalve Peronidia venulosa,

Biochim. Biophys. Acta - Proteins Proteomics, 1784, 2008, pp. 1277-1285.

[208]. F. Arslan, A. Yaşar, and E. Kiliç, An amperometric biosensor for xanthine determination prepared from xanthine oxidase immobilized in polypyrrole film, *Artif. Cells, Blood Substitutes, Biotechnol.*, 34, 2006, pp. 113-128.

[209]. H. S. Nakatani *et al.*, Biosensor Based on Xanthine Oxidase for Monitoring Hypoxanthine in Fish Meat, *Am. J. Biochem. Biotechnol.*, 1, 2005, pp. 85-89.

[210]. L. Agüí, J. Manso, P. Yáñez-Sedeño, and J. M. Pingarrón, Amperometric biosensor for hypoxanthine based on immobilized xanthine oxidase on nanocrystal gold-carbon paste electrodes, *Sensors Actuators, B Chem.*, 113, 1, 2006, pp. 272-280.

[211]. S. Hu and C. C. Liu, Development of a Hypoxanthine Biosensor Based on Immobilized Xanthine Oxidase Chemically Modified Electrode, *Electroanalysis*, 9, 5, 1997, pp. 372-377.

[212]. J. Niu and J. Y. Lee, Bulk-modified amperometric biosensors for hypoxanthine based on sol-gel technique, *Sensors Actuators, B Chem.*, 62, 3, 2000, pp. 190-198.

[213]. H. Okuma and E. Watanabe, Flow system for fish freshness determination based on double multi-enzyme reactor electrodes, *Biosens. Bioelectron.*, 17, 5, 2002, pp. 367-372.

[214]. M. J. Sweeney and A. D. W. Dobson, Mycotoxin production by Aspergillus, Fusarium and Penicillium species, *International Journal of Food Microbiology,* 43, 3, 1998, pp. 141-158.

[215]. S. Marin, A. J. Ramos, G. Cano-Sancho, and V. Sanchis, Mycotoxins: Occurrence, toxicology, and exposure assessment, *Food and Chemical Toxicology*, 60, 2013, pp. 218-237.

[216]. H. P. van Egmond, R. C. Schothorst, and M. A. Jonker, Regulations relating to mycotoxins in food, *Anal. Bioanal. Chem.*, 389, 2007, pp. 1505–1523.

[217]. Y. C. Wong and R. J. Lewis (Eds.), Analysis of Food Toxins and Toxicants, *John Wiley & Sons*, 2017.

[218]. I. F. F. Benzie, Y. T. Szeto, J. J. Strain, and B. Tomlinson, Consumption of green tea causes rapid increase in plasma antioxidant power in humans, *Nutr. Cancer*, 34, 1, 1999, pp. 83-7.

[219]. E. Sharpe, F. Hua, S. Schuckers, S. Andreescu, and R. Bradley, Effects of brewing conditions on the antioxidant capacity of twenty-four commercial green tea varieties, *Food Chem.*, 192, 2016, pp. 380–387.

[220]. M. R. Montereali, L. Della Seta, W. Vastarella, and R. Pilloton, A disposable Laccase-Tyrosinase based biosensor for amperometric detection of phenolic compounds in must and wine, *J. Mol. Catal. B Enzym.*, 64, 2010, pp. 189-194.

[221]. M. Di Fusco, C. Tortolini, D. Deriu, and F. Mazzei, Laccase-based biosensor for the determination of polyphenol index in wine, *Talanta*, 81, 1-2, 2010, pp. 235-240.

[222]. A. L. Ghindilis, V. P. Gavrilova, and A. I. Yaropolov, Laccase-based biosensor for determination of polyphenols: determination of catechols in tea, *Biosens. Bioelectron.*, 7, 2, 1992, pp. 127-31.
[223]. C. Zhang, L. Gong, Q. Mao, P. Han, X. Lu, and J. Qu, Laccase immobilization and surface modification of activated carbon fibers by bio-inspired poly-dopamine, *RSC Adv.*, 8, 2018, pp. 14414-14421.
[224]. S. Zhang, Z. Wu, G. Chen, and Z. Wang, An improved method to encapsulate laccase from trametes versicolor with enhanced stability and catalytic activity, *Catalysts*, 8, 7, 2018, p. 286.
[225]. F. W. P. Ribeiro *et al.*, Simple laccase-based biosensor for formetanate hydrochloride quantification in fruits, *Bioelectrochemistry*, 97, 2014, pp. 7-14.
[226]. A. Dabhade, S. Jayaraman, and B. Paramasivan, Colorimetric paper bioassay by horseradish peroxidase for the detection of catechol and resorcinol in aqueous samples, *Prep. Biochem. Biotechnol.*, 7, 1-8, 2020, pp. 849-856.

Chapter 9

Nanobiosensors

Sandeep Yadav, Ashok Saini and Kavita Vasdev

9.1. Introduction

The concept of biosensors is just five decades old and the feasibility of biosensing was first demonstrated by an American scientist Leland C. Clark in 1962. Leland C. Clark introduced the principle of the first enzyme electrode with immobilized glucose oxidase. He described how to make electrochemical sensors more intelligent by adding "enzyme transducers as membrane enclosed sandwiches" (See Fig. 8.1) [1].

Biosensors are the analytical tools that consist of a substrate and a selective interface in closed proximicity or integrated with a transducer, therefore, the substrates and transducers are important components of the analytical tools which contain an immobilized biologically active compound such as proteins (e.g., cell receptors, enzymes, antibodies), oligo- or polynucleotides, microorganisms, or even whole biological tissues that interact with specific species of interest. This reaction between the bioactive substance and the species (substrates) produces a product in the form of a biological or chemical substance electrochemical, heat, light or sound, then a transducer such as an electrode electrochemical, semiconductor, thermistor, counter or sound detector changes the product of the reaction into usable data [2-4]. Rapid development of electrochemical devices has provided convenience and capability for disease diagnosis or food applications [3, 5-8]. The main requirements for a biosensor approach in terms of research and

Kavita Vasdev
Department of Microbiology, Gargi College, University of Delhi, New Delhi, India

commercial applications are the identification of a target molecule, availability of a suitable biological recognition element and the potential for disposable portable detection systems. Biosensors have certain disadvantages involving low sensitivity & selectivity, elimination of interferences, limited electron communication, and complexity of immobilization, long incubation time, high operational potential and low sensor stability that are still to be improved or solved.

The performance of the biosensors has been enhanced after the emergence of nanotechnology. Nanotechnology is a branch of science in which various techniques are used for construction, measurement and imaging of nanoscale objects. Nanotechnology is now used to develop variety of sensors that can interact with analytes made up of extremely small molecules. Advances in nanotechnology have led to the development of nanobiosensors with high sensitivity, stability and versatility. The ultimate goal of nanobiosensors is mainly to detect any biochemical and biophysical signal associated with a specific disease at the level of a single molecule or cell.

Nanotechnology based biosensors known as "**nanobiosensors**" in which biological function are integrated with nanofabrication techniques. A lot of novel nanomaterials have been fabricated with the development of nanotechnology in recent years and their novel properties are being gradually discovered and their applications have also greatly advanced in biosensors [9-10]. Biosensors represent an especially exciting opportunity for high-impact applications benefiting from "nano" attributes. The unique properties of nanoscale materials offer excellent prospects for interfacing biological recognition events with electronic signal transduction and for designing a new generation of bioelectronics devices exhibiting novel functions. Nanomaterials, provide a promising way to increase the effective bio-recognition area i.e. the area actually interacting with the analyte, is one of the important parameters that determines the sensitivity of a biosensor because of the high surface to volume ratio of nanomaterials which provides a large number of sites available for molecular interactions. Nanobiosensors have generated a great deal of excitement due to their ability to detect a wide range of materials at incredibly small concentrations. Researchers tend to integrate nanoparticles into the materials used for biosensor construction in order to improve the performance of the system in both existing and potential sensing applications. The ultimate goal of nanobiosensors is to detect any biochemical and biophysical signal related to a specific disease at the level of a single molecule or cell [8, 11-19].

As the nanotechnology field matures, it seems highly likely that the diagnostic techniques of today will soon become antiquated and a new class of low cost, robust, reliable, easy-to-use and ultrasensitive diagnostics will become available. This integration of nanoscale with other medical instruments may even spur a dramatic increase in the number of point-of-care diagnostics, as well as diagnostic tools by reducing instrumentation size that can be used by patients on their own. Reduction in sensor size provides great versatility for incorporation into multiplexed, transportable, portable, wearable, and even implantable medical devices. Nanobiosensor technology will enable early diagnosis of chronic debilitating diseases, ultrasensitive detection of pathogens, and long-term monitoring of patients using biocompatible integrated medical instrumentation by revolutionizing conventional medical practices.

There are different strategies:

i) Use of a completely new class of nanomaterial for sensing purposes;

ii) New immobilization strategies; and

iii) New nanotechnological approaches can be used for creating the next generation nanobiosensor devices.

Microorganisms in various samples, metabolites in body fluids and tissue pathology can be detected/monitored by applying the nanobiosensors but they can be used in the laboratory setting as well [20]. The ability to detect disease-associated biomolecules, such as disease-specific metabolites, nucleic acids, proteins, pathogens, and cells such as circulating tumor cells, is essential not only for disease diagnosis in the clinical setting but also for biomedical research involving drug discovery and development. This book chapter surveys the various types of nanobiosensors, their applications, current trends and future prospects of nanobiosensors.

9.2. Types of Nanobiosensors based on Nanostructured Materials

With the emergence of nanomaterials having unique physico-chemical properties, a new class of biosensors (nano-biosensors) based on nanoparticles (NPs) and nanotubes has been developed. Several nanobiosensors- architecture based mechanical devices, optical resonators, functionalised nanoparticles, nanowires, nanotubes and

nanofibers have been in use. In particular, nanomaterials such as gold nanoparticles, carbon nanotubes, magnetic nanoparticles and quantum dots have being actively investigated for their application in biosensors, which have become a new interdisciplinary frontier between biological detection and material science.

Table 9.1. Overview of Nanostructured Materials used in improving biosensor technology.

Sr. No.	Nanomaterial used	Key Benefits	References
1.	Carbon Nanotubes	Large length-to diameter aspect ratios, mediate fast electron-transfer kinetics, ability to be functionalized, effective matrices for the immobilisation, less surface fouling effects	[11, 21-22]
2.	Graphene	High mechanical strength, high surface area, excellent conductivity, exceptional biocompatibility, easy to functionalized, produce in mass quantity	[14, 17,23]
3.	Metal nanoparticles	Physiochemical malleability, and high surface areas, aid in immobilization, Enhanced electron-transfer kinetics and high adsorption capability	[12, 18,24]
4.	Metal oxide nanomaterials based nanobiosensors	Good electrical and sensing properties for bio and chemical sensing, better charge conductor, can be coupled in MEMS and induced specific field response	[13, 15, 16]
5.	Enzyme nanoparticles	Large surface to volume ratio, unique optical, thermal and chemical than native enzymes	[19]

9.2.1. Carbon Nanotubes Based Nanobiosensors

Carbon nanotubes (CNTs) have attracted much attention as an electrode material for electrochemical biosensors during the past few years due to their several unique properties viz. electrochemically stable in aqueous and nonaqueous solutions and high thermal conductivity, a large edge plane/basal plane ratio, rapid electron kinetics, semi- and superconducting electron transport, high tensile strength composites, hollow core suitable for storing guest molecules and excellent mechanical strength [11, 21, 25-27]. CNT have been considered to be the best-suited nanomaterials for transduction of the signals associated with the biorecognition analytes, metabolites, or disease biomarkers, and can serve as effective matrices for the immobilization of biomolecules in biosensors.

A CNT is a hollow carbon structure, with one or more walls, having a nanometre-scale diameter and an approximate length. It is a well-ordered arrangement of carbon atoms linked *via* sp2 bonds, which gives it the stiffest and strongest fibres. CNTs can be classified as a SWCNT or a MWCNT according to the number of graphitic layers as the CNT skeleton comprises of a seamless hollow tube composed of a 'rolling' graphite sheet [28-29]. In short, SWCNT is a single molecular nanomaterial composed of a single layer that rolls a single sheet of graphite into a seamless molecular cylinder [30]. The diameter is 0.75–3 nm whereas the length is l–50 nm [31]. On the other hand, MWCNT have more than two layers of a 'curly' graphite sheet, with a diameter of 2–30 nm (some may be >l00 nm), and the distance between each layer is ≈0.42 nm. CNTs, also called buckytubes were first reported by Iijima and co-workers in 1991 [32]. Since his first report on multi-walled carbon nanotubes (MWNTs), in 1993, these researchers reported the single-walled carbon nanotubes (SWNTs) [33]. After this discovery, CNTs have emerged as one of the most intensively investigated nanostructured materials [34], with thousands of papers published every year, offering promises for new applications which have attracted both academic and industrial interest. CNTs offer great promises for a wide range of applications, including fabrication of ultrasensitive biosensors as compared to other nanomaterials lies in a unique combination of an ultra-high specific surface area, and outstanding electrical, magnetic, optical, mechanical, and chemical properties [35-36]. CNTS serve as an ideal material for high sensitive nanoscale biosensor devices due to their remarkable sensitivity toward their surface [37-38]. But, the strong intermolecular π-π interactions, and hydrophobic nature of CNTs is a

major obstacle for developing CNTs-based biosensors. In order to improve their solubility and stability, different functionalities of the CNTs have been improved by functionalizing through chemical adsorption [39]. Many reports have emerged over the last decade showing that functionalized CNTs have an ability to address several concerns related to biocompatibility and toxicology [40]. Although, CNTs poses several attractive properties and advantages, dispersion activated by the high surface energy of the CNTs marks as an obstruction to progress any further and CNTs becomes insoluble in water and other common solvents poses due to their high hydrophobicity. Therefore, depending on application, CNTs needs to be functionalized to improve their solubility and other functional properties [41]. Biological barriers such as the cell membrane and penetrate individual cells can be effectively crossed by the functionalized CNTs [42]. This feature and the mechanism of internalization and release of CNTs from the cells are of major interest for biological and in particular intracellular biosensing applications.

CNTs offer diverse features of interest to engineer new generation probes in CNTs-based biosensors due to their remarkable structural, optical, electronic and mechanical properties. An ideal biosensor should have good physical and chemical as well as biological properties. CNTs could easily cross the biological membranes which makes them applicable in vivo. By using various dispersion and functionalization methods, CNTs can be made biocompatible. To examine an extensive range of CNTS various nanobiosensors have been established till date using the CNTs [8, 25, 43-50]. Carrara *et al.,* (2008) developed a biosensor to detect the cholesterol by depositing Multi-walled carbon nanotubes onto the rhodium–graphite electrodes by drop casting along with cytochrome P450scc [51]. Cyclic voltammetry indicated largest enhanced activity of the enzyme at the MWCNT modified surface. Systems based on the cytochromes P450s integrated with nanostructures present improvements of orders of magnitude in the sensitivity of cholesterol biosensors, while systems based on oxidases do not show such an improvement. Presence of carbon nanotubes improved the response of linearity of the detection. Li *et al.,* (2009) developed biocomposite film for the electrocatalysis combines the advantages of ease of fabrication, high reproducibility, and sufficient long-term stability using MWCNTs, PNDGA, and PChi (MWCNTs–PNDGAChi) at gold and SPCE electrode surfaces, which are more stable in PBS [52]. In his work they presented the experimental methods of CV and FIA with biocomposite film biosensor integrated into the gold electrode and SPCE, provide an

opportunity for qualitative and quantitative characterization. Tarley *et al.,* (2009) reported a new electroanalytical method for simultaneous determination of zinc, cadmium and lead by using the combination of PSA with the unique properties of MWCNT [53]. This electrode satisfactory applied without severe interference even in complex environmental water samples; sufficient sensitivity for simultaneous metal ions monitoring in aqueous effluent according to CONAMA, being an effective replacement to those methods based on AAS; simplicity in the building of the electrode; excellent reproducibility of measurements; reduced time of analysis compared to other electrochemical stripping methods and low operation cost. Yadav *et al.,* (2011a,b) have used the conducting c-MWCNT/PANI composite film for the development of amperometric biosensors with improved analytical responses in terms of high specificity, sensitivity, stability, and less response times for the determination of oxalate and creatinine in human urine and serum samples [54-55] (Fig 9.1 a, b). Application of CNTs for biomedical tests faces a variety of challenges prerequisites like synthesis of CNTs with tailored functionalities and uniform morphology; modification of CNTs to make them compatible with biological systems; detailed study of their interaction with biological environments (toxicity, interaction with single cells); and in vivo testing for specific therapeutic and diagnostic purposes.

Functionalization of CNTs has become a prerequisite in order to enable facile fabrication of nanodevices. Non-covalent and covalent surface modifications are two commonly used methods for the functionalization approaches. The main advantage of non-covalent functionalization is that their structure and their original properties remain the same, and it becomes extremely difficult to modify further. Direct covalent functionalization can significantly alter the solubility and compatibility of CNTs [56]. Mananghaya et al. reported that functionalized CNTs (f-CNTs) significantly improved the solubility [57] and thereby performance and lowered their toxicity [58]. But the disadvantage of covalent functionalization is that the structural homogeneity and other original properties of CNTs are changed thereby effecting mechanical properties [59]. Devi at al., 2011 immobilized xanthine oxidase on the c-MWCNT/PANI surfaces through the amide bonds between the unbound –COOH groups of c-MWCNT/PANI film and the $–NH_2$ groups on the surface of enzyme using the EDC–NHS chemistry [60] (Fig. 9.2). EDC and NHS activate the free –COOH groups of c-MWCNT/PANI composite layer.

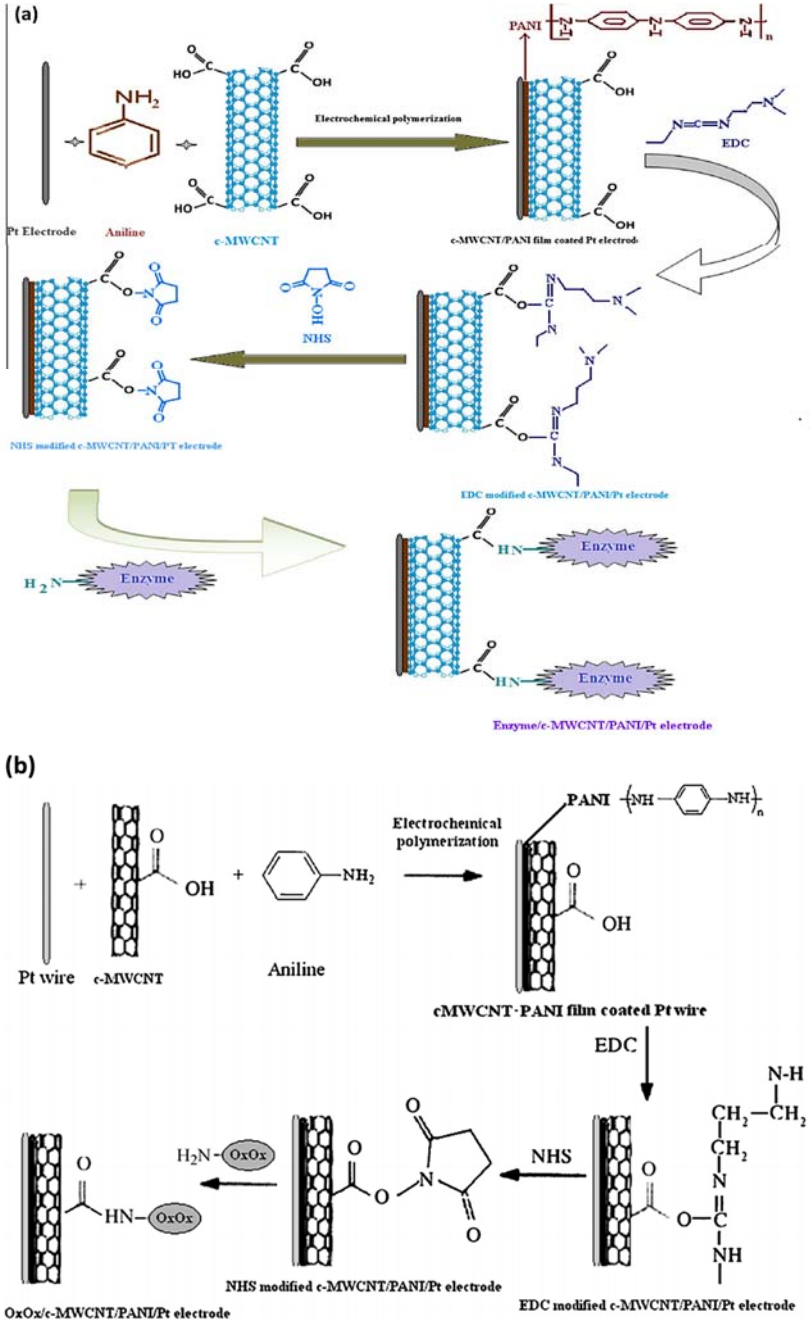

Fig. 9.1. Schematic presentation for the fabrication of (a) Creatinin biosensor and (b) Oxalate biosensor based on c-MWCNT/PANI composite film. [54-55].

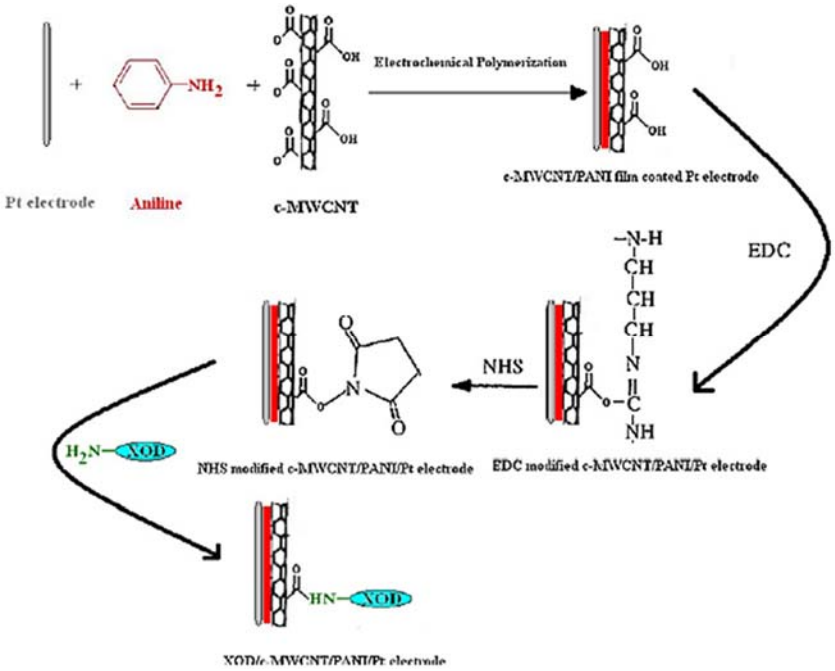

Fig. 9.2. Schematic presentation for the fabrication of xanthine biosensor based on functionalized CNTs. [60].

Yamada *et al.,* (2014) fabricated high-performance disposable junction biosensor for detection of foodborne pathogens *Escherichia coli* K-12 by integrating the single walled carbon nanotubes (SWCNTs) and immobilized antibodies into a disposable bio-nano combinatorial junction sensor [61]. Gold tungsten wires (50 mm diameter) coated with polyethylenimine (PEI) and SWCNTs were aligned to form a crossbar junction, which was functionalized with streptavidin and biotinylated antibodies to allow for enhanced specificity towards targeted microbes. The sensor performance was evaluated by monitoring the changes in electrical current (DI) after bioaffinity reactions between bacterial cells (*E. coli* K-12) and antibodies on the SWCNT surface. The averaged DI increased from 33.13 nA to 290.9 nA with the presence of SWCNTs in a 108 CFU/mL concentration of *E. coli*, thus showing an improvement in sensing magnitude. Current decreased as cell concentrations increased, due to increased bacterial resistance on the bio-nano modified surface. The detection limit of the developed sensor was 102 CFU/mL with a detection time of less than 5 min with nanotubes. Choi *et*

al.,(2017) demonstrated that the SWCNT-based biosensor could be useful for the detection of food borne pathogens such as S. aureus [62]. The indirect ELISA confirmed that the anti-*S. aureus* polyclonal antibodies were specific enough to bind to the target *S. aureus* cells among the tested bacteria. The gold electrodes fabricated on the silicon wafer were assembled with single-walled carbon nanotubes. The optimum concentration of assembled SWCNTs was determined to be 0.1 mg/mL. 1-Pyrenebutanoic acid, succinimidyl ester was selected as a linker to bind between SWCNTs and pAbs. As PBASE and pAbs were immobilized on the biosensor platform, the resistance of the SWCNT-based biosensor increased. The bacteria detected by the biosensor were observed using a scanning electron microscope (SEM). Tung *et al.,* (2017) presented the first demonstration of highly selective and sensitive biosensor for detection of Cathepsin E (CatE) in serum based on a peptide aptamer-modifed SWCNT [63]. The minimal detectable CatE concentration was 10 ng/mL in human serum; this value is three orders of magnitude lower than that of the conventional ELISA method using the same peptide aptamer. The high specificity originates from selective binding of the peptide aptamer to the target CatE. Our results suggest that the integration of a highly specific peptide aptamer and a SWCNT FET transducer can be a platform for near-patient detection of biomarkers and thus could be widely used for human health monitoring and early disease diagnosis, such as breast cancer diagnosis. Madadi (2019) simulated the adsorption behaviors of Fe-SWCNT and Fe-N-SWCNT (8, 0) upon dopamine molecule addition to detect dopamine with DFT approach [64]. The interactions between the Fe-SWCNT and Fe-N-SWCNT and dopamine were exothermic; however, the adsorption energy of Fe-N-SWCNT was more satisfactory. The theoretical calculation results inferred that Fe-N-SWCNT can have good sensitivity to the dopamine molecule. Thus, both Fe-SWCNT and Fe-N-SWCNT (8, 0) can be suitable options for dopamine molecule detection. These results are helpful in the development of CNT-based sensors and provide a theoretical basis for developing Fe-N-SWCNT-based sensors; the outcomes also indicated that the Fe- and N-doped adsorbents had a superior sensing property. Guo *et al.,* (2020) designed a disposable paper-based microanalysis device using graphite doped with multi-walled carbon nanotubes for in vitro evaluation of fluorene cytotoxicity [65]. Developing a cost-effective and simple micro-analysis tool has long been an important objective in the toxicological detection of fluorene. They investigated the feasibility of the designed MWCNTs/μ-PAD as a cell-sensing platform using voltammetry measurements. Advantages such as the simplicity of manufacture, low consumption, low

cost, rapid detection, and disposability, suggest that the MWCNTs/μ-PAD could provide new opportunities and directions for *in vitro* microanalysis.

CNTs have been attracting a great deal of interest in many sensing applications, due to their small size and excellent electrochemical properties. The electronic properties of CNTs are extremely well suited for electrochemical, amperometric, impedometric or field-effect transduction of signals, but their particular optical properties and their ability to penetrate readily through biological membranes also make them suitable candidates for the development of photoacoustic imaging sensors as well. CNTs therefore constitute versatile and multifunctional nanostructures which combine the potential to serve for diagnostic and therapeutic applications. Many biosensors based on the CNTS have been developed but still there are many challenges ahead to further improve their material performance. In the future, efforts will need to be directed toward preventing nonspecific adsorption of biomolecules onto the tube walls, although promising advances have already been made in this direction. There is sufficient scope to exploit the outstanding properties of CNT networks that promise to have a long-lasting impact on future technologies for biosensing.

9.2.2. Graphene Based Nanobiosensors

Graphene has emerged as a champion material for a variety of applications cutting across multiple disciplines in science and engineering. As a representative two-dimensional (2D) nanomaterial with an atomic thickness, graphene has received considerable attention for biosensing applications due to its unique physicochemical properties mainly its large surface to volume ratio, excellent thermal and electrical conductivity, biocompatibility, ease of functionalization, flexibility as well as broad electrochemical potential. Because of its unique physicochemical properties graphene is the most promising nanostructured carbon material that is used in the bioanalytical area and has stimulated intense research, thus, providing more specific sites to capture foreign moieties with high sensitivity [14, 17, 23]. The surface-to-volume ratio and conduction channel area increases drastically, as the dimensions of the particle decreases from micro to nanometer regime to particularly graphene. For micro and nanoparticles, only a part of their volume is exposed to the analyte molecule, and therefore minimizing the sensing effect. On the other hand, the planar topology of graphene offers

enhanced specific surface area and allows even a single molecule to be captured. Consequently, the electron transport pathway through graphene becomes highly sensitive to the adsorbed molecules and makes it more apt for low-level detection [66].

Biosensor research accelerated after advent of graphene in 2004, by adding new-dimensions in terms of high loading efficiency, good stability, biocompatibility, fast response time, low production cost, and consistent signal amplification even under the harsh environmental conditions that brings important advantages over many other nanomaterials. Graphene-based materials particularly graphene oxide and reduced graphene oxide are widely utilized in various applications ranging from food industry, environmental monitoring and biomedical fields as well as in the development of various types of biosensing devices. Their widespread use in making biosensors has opened up new possibilities for early diagnosis of life-threatening diseases and real-time health monitoring. The richness in oxygen functional groups in the materials serves as a catalysis for the development of biosensors/electrochemical biosensors which promotes for an attachment of biological recognition elements, surface functionalization and compatible with micro- and nano- bio-environment [8, 67-73].

Graphene due to its remarkable high surface-to-volume ratio to capture even a single molecule and electrical conductivity that modulates as soon as the foreign entity binds to it along with the chemical and thermal stability is fundamentally suitable for detecting organic molecules, ions, biomolecules, gas molecules and living organisms with high sensitivity. Strategies to attach these biomolecules onto the surface of graphene have been employed based on its chemical composition. These methods include covalent bonding, such as the coupling of the biomolecules via the 1-ethyl-3-(3-dimethylaminopropyl) carbodiimide hydrochloride and N-hydroxysuccinimide reactions, and physisorption [17]. Various electrochemical biosensors have been developed using the graphene nanomaterial including graphene oxide, reduced graphene oxide, CVD graphene, and various graphene based nanostructures including nanomesh, nanowalls, etc. in healthcare related applications and in clinical diagnosis for detection of proteins (disease biomarkers), nucleic acids (mutation analysis in genetic diseases), small molecules (disease metabolites like glucose, lactic acid etc.), and pathogens (bacterial and viral infections) [49, 74]. Consequently, graphene continues to be a focus of research for the futuristic goal of multiplexed clinical diagnostic

biosensors to provide early detection of many deadly diseases. The specific and sensitive detection of pathogenic microorganisms remains a big scientific challenge and a practical problem of enormous significance. Pathogen diagnosis is currently based on culturing the microorganism on agar plates with the disadvantage of being long (minimum of 24 h) and ignoring viable but non-culturable cells. G-FET biosensors have been successfully applied for the detection of bacteria and their metabolic activities. Huang *et al.,* (2011) used CVD graphene modified with anti-Escherichia coli antibodies allowed to detect E. coli concentrations as low as 10 cfu/ml [75]. Morales-Narvaez *et al.,* (2013) developed graphene oxide in combination with E. coli O157:H7 antibody-conjugated quantum dots and used as a pathogen-revealing agent by exploiting the universal highly efficient long-range quenching properties of GO; an LOD of 3.8_103 cfu/ml achieved [76]. Graphene printed onto water-soluble silk and modified with antimicrobial peptides allowed bioselective detection of bacteria at single-cell levels remotely. Graphene-based platforms have been demonstrated for the detection of Escherichia coli (E. coli) bacteria, glucose, and various proteins by functionalizing the graphene-based materials with gold nanoparticle (NP)-antibody conjugates to develop an electronic biosensor and used as a conducting channel in a field-effect transistor (FET). Electrical detection of protein binding is accomplished through FET and direct current (dc) measurements. Highly electrocatalytic metal oxides are also combined with graphene-based materials to offer both a high electrocatalytic activity and a high electrical conductivity for enzymeless electrochemical biosensing. Biomolecules are then detected through electrochemical measurements such as cyclic voltammetry. Field-effect transistors (FETs) based on large-area graphene and other 2D materials can potentially be used as low-cost and flexible potentiometric biological sensors. However, there have been few attempts to use these devices for quantifying molecular interactions and to compare their performance to established sensor technology. Huang et al. (2010) proposed various Graphene-based glucose sensors, which are generally built by immobilizing glucose oxidase (GOx) onto the graphene surface, such as the graphene–FET. In this work, GOx was covalently linked via its amine groups to 1-pyrenebutanoic acid succinimidyl ester, where the pyrene end is firmly attached to graphene through p–p stacking interactions [77]. Li *et al.,* (2013) proposed a different non-enzymatic glucose-sensing approach based on the use of GQDs modified with boronic acid-substituted bipyridine ligands, which serve as a fluorescence quencher upon electrostatic interaction with grapheme quantum dots [78]. Mani *et al.,* (2013) fabricated an electrochemically

reduced graphene oxide–multiwalled carbon nanotubes hybrid (ERGO–MWCNT) modified glassy carbon electrode (GCE) for determination glucose oxidase (GOx) by direct electrochemistry after immobilizing GOx onto the ERGO–MWCNT hybrid film [79]. UV–Vis absorption spectroscopy have been used to revealed the π–π stacking interaction operating between the MWCNT and graphene oxide (GO). This hybrid film have 2.1 fold higher peak current and very low peak to peak separation (Δ*E*p) of 26 mV as compared with pristine MWCNT, demonstrating faster electron transfer between GOx and the modified electrode surface. The fabricated biosensor exhibits low detection limit of 4.7 μM with wide linear range of 0.01–6.5 mM and acquires excellent storage and operational stabilities. The promising feature of graphene with metal nanoparticles nanocomposite favors the selective and sensitive determination of biological recognition elements with improved analytical capabilities. Xu *et al.,* (2014) used the metal nanoparticles for improvement for nanocomposite response and developed glucose biosensor was based on the direct electrochemistry of glucose oxidase (GOD) adsorbed in graphene/polyaniline/gold nanoparticles (AuNPs) nanocomposite modified glassy carbonelectrode (GCE) [80]. The graphene/ PANI/AuNPs nanocomposite was more biocompatible and it offered a favorable microenvironment for facilitating the direct electron transfer between GOD and electrode as compared with graphene, polyanilline (PANI) or graphene/PANI. The adsorbed GOD displayed a pair of well-defined quasi-reversible redox peaks with a formal potential of −0.477 V (vs. SCE) and an apparent electron transfer rate constant (*ks*) of 4.8 s−1 in 0.1 M pH 7.0 PBS solution. The apparent Michaelis–Menten constant of the adsorbed GOD was 0.60 mM, implying a fabulous catalytic activity and a remarkable affinity of the adsorbed GOD for glucose. The amperometric response of GOD-graphene/PANI/AuNPs modified electrode was linearly proportional to the concentration of glucose in the range of 4.0 μM to 1.12 mM with a low detection limit of 0.6 μM at signal-to-noise of 3. The role of the graphene transducer is to simply amplify surface potential changes caused by adsorption of molecules on the gold surface to measure the binding affinity of a specific protein–antibody interaction in nanocomposite of a gold-coated graphene FETs. Having a gold surface gives access to well-known thiol chemistry for the self-assembly of linker molecules. The estimated dissociation constants are in excellent agreement for all sensor types as long as the active surfaces are the same (gold) [81]. Sakr and Serry, (2015) fabricated a novel mediator-free, non-enzymatic electrochemical sensor, based on a graphene-Schottky

junction for glucose detection [82]. The sensor offers a promising alternative to the conventional enzyme-catalyzed electrochemical continuous glucose monitoring systems (CGM), as it overcomes many of the drawbacks attributed to the enzymatic nature; namely, irreversibility, drift, and interference with body fluids, which affect their accuracy, reliability and longevity. Enhanced performance of the sensors is demonstrated through the band interaction at the graphene-Schottky junction, which yields stronger forward/reverse currents in response to 50 μL glucose drop. The results indicated that the proposed sensor provided a highly sensitive, more facile method with good reproducibility for continuous glucose detection.

Graphene oxide (GO) and graphene quantum dots (GQDs) display advantageous characteristics with interest for building innovative biosensing platforms and even smart devices such as nano/micromotors for a myriad of uses including sensing. Li *et al.,* (2015) devised a GQD-based fluorometric sensor to detect acetylcholinesterase (AChE, a critical enzyme in central nervous system and neuromuscular junctions) with an ultralow detection limit (0.58 pM with S/N of 5.0), using a photoluminescence 'turn-off' mechanism [83]. This simple 'mix-and-detect' platform can also be employed to sense a variety of compounds that can directly or indirectly inhibit the enzymatic activities of AChE, such as nerve gases, pesticides, and therapeutic drugs. Quenching of the fluorescence induced by GO or photoluminescence of GQDs can easily operate in synergy with various other nanomaterials and platforms opening the way to several unprecedented biosensing strategies and unique nanomotor technologies. He *et al.,* (2015, 2017) demonstrated that post-functionalization of GO-modified electrodes by simple immersion into a solution of folic acid allowed for the development of an electrochemical-based sensor for folic acid protein with an LOD of 1 pM and a plasmonic sensor with a 5 fM LOD [84,85]. Levels of folic acid protein in serum can increase up to 22 pM in metastic diseases. Given that human serum is free of folic acid proteins, detection of this protein in serum serves as an early stage cancer diagnostic step. Altuntas *et al.,* (2016) prepared and characterized the graphene sheets and three different graphene-metallic nanocomposites including graphene-copper (graphene-Cu), graphene-nickel (graphene-Ni) and graphene-platinum (graphene-Pt) and tested these nanocomposites in glucose biosensor transducers, which were formed by combining these metallic nanocomposites with glucose oxidase enzyme and glassy carbon paste electrode (GCPE) [86]. This is the first work that includes the usage of these graphene-Me nanocomposites as a part of glucose biosensor

transducer. Taniselass, *et al* (2019) developed electrochemical biosensors based on recent advancement (e.g.; the surface modification and analytical performances), based on grapheme and the utilized such biosensors to monitor the noncommunicable diseases [70]. The detection performances of the graphene-based electrochemical biosensors are in the range of ng/mL and have reached up to fg/mL in detecting the targets of NCDs with higher selectivity, sensitivity and stability with good reproducibility attributes.

Although the field of graphene, its derivatives and hybrids, is rapidly progressing from its theoretical projection to practical implementation is an excellent electrode material for sensing applications in the medical field, novel methods for well-controlled synthesis and processing of grapheme need more attention and should be investigated in future studies. Numerous graphene-based biosensors have shown remarkable performance from diagnosis of disease to their treatment and have begun to make their way to the market place. Although graphene-based materials are considered to have no significant toxicity in many biomedical applications, however, more elaborative studies are still needed before considering it as a reliable material for implantable devices. This would include monitoring the interaction of graphene with genetic molecules, acute toxicity studies (long term toxicity), intracellular metabolic pathway, and excretion studies from biological systems. Nevertheless, the sensing platform may be further refined to avoid the adsorption of unwanted molecules on graphene and improve the orientation of biomolecules on graphene platforms. These experimental studies are essential to design graphene based biosensors that will help us better understand the metastatic cancer, molecular basis underlying the brain function, developing prostheses for injured organs, hepatitis, oxidative stress, autophagy, apoptosis etc. This could enable early detection and lead to better treatment strategies by monitoring the progress of the disease in response to treatment. Thus, more fundamental and detailed research is required to resolve many clinical hurdles, in order, to bring graphene-based flexible and implantable biosensors in the market by next decade [14, 17].

9.2.3. Metal Nanoparticles Based Nanobiosensors

The intelligent use of nanomaterials in the last decade has been having a great impact in biosensing and the interest in the fabrication of electrochemical biosensors with high sensitivity, selectivity, efficiency

and lower detection limits of several orders of magnitudes is rapidly growing. In the era of nanotechnology, noble metal nanoparticles (NPs) have played an important role in the development of new biosensors and/or in the enhancement of existing biosensing techniques with extraordinary conductivity, large surface-to-volume ratio and biocompatibility, have been extensively employed for developing novel electrochemical sensing platforms and improving their performances to fulfil the demand for more specific and highly sensitive biomolecular diagnostics [87-88]. In fact, NPs are, in general, one of the most common nanotechnology-based approaches for developing biosensors, due to their simplicity, physiochemical malleability and high surface areas. They can measure between 1 to 100 nm in diameter, have different shapes and can be composed of one or more inorganic compounds, such as noble metals, heavy metals, iron, etc. [89-90]. The majority of them exhibitsize-related properties that differ significantly from those observed in microparticles or bulk materials [91-92]. Further, metal NPs may be composed of one or more inorganic compounds, such as noble metals, heavy metals, or iron. Interesting properties, such as quantum confinement (semiconductor nanocrystals), surface plasmon resonance (SPR) (metal NP) superparamagnetism (magnetic materials) may observed due to different size and composition of metal NPs [93]. Metal NPs are synthesized by using various techniques such as including chemical and photochemical reduction, co-precipitation, thermal decomposition, hydrolysis, vapour deposition, laser ablation, and grinding [94-96].Two distinct nanofabrication methods have been used to synthesis of metallic NPs such as:

i) **Top-down approaches**: These approaches involve physical processes such as lithography or chemical processes controlled by external experimental parameters to create nanoscale structures starting from larger dimensions to the nanometer range [97]. This can be achieved by milling or high pressure homogenization [98]. Most used techniques for metal NPs synthesis are chemical techniques and, usually involved the reduction of the noble metal ion by chemical reducing agents, such as sodium borohydride, sodium citrate, etc. These type of chemically synthesized metal NPs are very unstable and prone to form aggregates, thus required the addition of a stabilizer, which can functionalize the metal NPs.

ii) **The bottom-up approaches**: These approaches use atoms or small molecules as the building blocks of multi-level structures to build up more complex nanoscale assemblies or directed self-assemblies that

perform various operations [99]. This method is extremely valuable since it is free of waste or unused materials [100]. This can be achieved by controlled precipitation (or crystallization) and evaporation from a precursor [98, 101].

Crystalline NPs are generally produced by top-down techniques but to achieve nanometer range comminution, high energy or pressure is required to, which may also lead to contamination if a milling medium is used. In contrast, bottom-up processes involve dissolution, followed by precipitation or drying. The mechanical energy input is thus minimal, and the resulting NPs can be crystalline or amorphous, depending on the synthesis conditions [102-104]. In general, chemical synthesis has little control on the metal NPs size, electrochemical and photochemical techniques emerging as a new alternative since they allow precise control of the particle size, morphology and density, by controlling the deposition parameters, such as the applied potential, the pulse time for both nucleation and growth processes, etc. [97, 105-107]. The ultimate goal of these techniques is to obtain metal NPs with an apparent homogeneity and to provide excellent control over size, shape, and surface properties so that their unique physico-chemical properties can be used for biosensing. Metal NPs can be used alone and in combination with other classes of nanostructures and biosensors based on metal NPs leads to significant signal amplification, higher sensitivity, and great improvements in the detection and quantification of biomolecules and different ions [12]. Noble metal NPs show unique physicochemical properties (such as ease of functionalization via simple chemistry and high surface-to-volume ratios) that allied with their unique spectral and optical properties have prompted the development of a plethora of biosensing platforms. Additionally, they also provide an additional or enhanced layer of application for commonly used techniques, such as fluorescence, infrared and Raman spectroscopy. In particular, the unique physicochemical properties of noble metal nanoparticles at the nanoscale have allowed for the development of a wide variety of new biosensors platforms such as: for point of care diagnostics, in vivo sensing, imaging, cell tracking and monitoring disease pathogenesis or disease pathogenesis and other nanotechnology tools that benefit scientific research on basic biology with enhanced capabilities in the specific detection of bioanalytes [8, 87, 108-112]. One general advantage of all nanomaterials is the high specific surface thus already enabling the immobilization of an enhanced amount of bioreceptor units. Putzbach and Ronkainen, (2013) have summarized the efficient methods for biofunctionalization of nanomaterials as the technique used to

immobilize the enzyme is one of the key factor in developing a reliable biosensor because one of the constant challenges is the immobilization strategy used to conjugate intimately the bio-specific entity onto such nanomaterials [113]. There are various approaches for biofunctionalization of nanomaterials such as

(i) Non-covalent approaches representing electrostatic interaction, π–π stacking, entrapment in polymers, or vander Waals forces between the nano material and the biological entity. These principles preserve all specific properties of both, nanomaterials and biomolecule.

(ii) Covalent binding: the strategy to attached covalently biomolecules to nanomaterials has an advantage in terms of stability and reproducibility of the surface functionalization and lowers unspecific physisorption. Covalent links can be formed, e.g., by classic amide coupling reactions, cross-linking, or click chemistry. One drawback is the uncontrolled anchoring of the biomolecule which can affect the domain which is responsible for the recognition event.

(iii) The immobilization of biomolecules via supramolecular or coordinative interactions: this technique has achieved wide acceptance in recent years in binding biological species to surfaces. The advantage of such systems, compared to the other immobilization methods, is the reversibility, enabling the possibility to regenerate the transducer element. Such functionalization not only allows the reproducible immobilization of bioreceptor units but can also increase the biocompatibility of these materials [36, 88].

The metal NPs have been involved into biorecognition elements such as enzymes, antibodies, aptamers, DNA sequences, and whole cells by conjugating with various biomolecules, chemical labels and other nanomaterials, achieving the signal transduction and amplification. The metal NPS not only participate into biorecognition but also act as electroactive tags to enhance the signal output readouts like electrochemical (amperometric and voltametric), optical (surface plasmon resonance, colorimetric, chemiluminescence, photoelectrochemical, etc.) and piezoelectric to provide a snapshot of recent advances in the design of electrochemical biosensing platforms. Metal NPs have received attention for applications in biosensing

amplificationas well as, including enzyme/protein sensors focused on their direct electrochemistry on metal NPs-modified electrode surface; immunosensors and gene sensors due to their unique heterostructures and fascinating properties [114-115]. These properties include a large surface area that enhances biorecognizers and receptor immobilization, good ability for reaction catalysis and electron transfer, and good biocompatibility.

Among the various noble metal NPs such as gold (Au), silver (Ag), platinum (Pt) and palladium (Pd), in particular gold and silver NPs, are among the most extensively studied nanomaterials because they show several interesting properties [116-119]. Moreover, AuNP can permit fast and direct electron transfer among a wide range of electroactive species and electrode materials and have led to the development of numerous techniques and methods for molecular diagnostics, imaging, drug delivery and therapeutics [41, 120].These can be conjugated with biomolecules, thus maintaining the biochemical activity of the tagged biomolecules, and hence can be excellent transducers for several biorecognition applications [121-122]. One of the most characteristic physical properties of metallic NPs is the localized surface plasmon resonance (LSPR), which is responsible for the bright color of the nanoparticle colloidal suspensions [117, 123-126]. AuNPs and AgNPs are specifically investigated for their optical properties because of light-scattering properties and the enhancement ability of the local electromagnetic field to be use as signal-amplification tags in various biosensors [127-130]. Other properties, such as an electron dense core, highly resonant particle plasmons, direct visualisation of single nanoclusters by scattered light, and catalytic size enhancement by Ag deposition, have made AuNP attractive materials for several applications in biotechnology [131-132]. Through distinct surface modification strategies (e.g. self-assembly, layer-by-layer, hybridization and sol-gel technology), metal NPSs provide well control over the microenvironment of biological molecules retaining their activity, and facilitate the electron transfer between the redox center of biomolecules and electrode surface.

Selective biosensing of molecules using functionalized nanoparticles has become a major research interdisciplinary area between chemistry, biology and material science. The unique physicochemical properties of noble metal NPs that have been explored for the development of new highly sensitive and specific biosensing techniques, favoring those that have already been successfully tested with biological samples. Most of

their unique physicochemical properties at the nanoscale, such as Localized Surface Plasmon Resonance (LSPR) i.e. collective oscillation of metal NPs when irradiated at a specific wavelength resulting in the appearance of the electromagnetic field localized on the NPs, have been explored for the development of new biosensors such as molecular diagnostics and therapy [110] or cancer applications [133], and others have focused on the bio-applications of a specific type of noble metal NP, mostly gold NPs The property of LSPR as a consequence of the confinement of the electric field within a small metallic sphere whose radius is much smaller than the wavelength, can be tuned by controlling parameters such as shape, size, uniformity and surface coating [117-118, 123, 134]. On one side of the particle where the plasmons oscillate in resonance with the light frequency, the electron density is polarized. This phenomenon was described applying the Mie theory [135-136] and is strongly dependent on the size, shape of the nanoparticle and the dielectric constant of its environment. This environmental dependency represents a great advantage for (bio)-analytics since the recognition event can result in a change of the oscillation frequency and therefore to a color change of the gold nanoparticles observable with bare eye. In this context, a wide series of efficient colorimetric biosensors were developed for DNA or oligonucleotide detection, or immunosensors [137-139]. The advantages of Au NPs have also demonstrated in bioanalysis using SPR transduction and this method is usually based on the change of the dielectric constant of propagating surface plasmons' environment of gold films where the detection of the analyte can be recorded in different ways like the changes of the angle, intensity, or phase of the reflected light [140-141]. The optimal configuration of this approach was determined for gold nanoparticles smaller than 40 nm at a distance to the gold film surface of 5 nm [142]. In this case, gold nanoparticles serve as labels when attached to secondary antibodies or DNA strands. Zhang *et al.,* (2013) demonstrated an Au-graphene (Au-Gra) nanohybrids and Ag-graphene (Ag-Gra) nanohybrids to develop a novel surface plasmon resonance (SPR) biosensors for the detection of mouse IgG [143]. Au-Gra and Ag-Gra nanohybrids were synthesized in a simple, effective and rapid way, and further characterized by X-ray photoelectron spectroscopy (XPS), transmission electron microscopy(TEM) and UV–vis absorption spectroscopy. These nanohybrids were assembled on the Au film through 1,6-hexanedithiol by covalent attachment. The biosensors based on Au-Gra nanohybrids and Ag-Gra nanohybrids show a good response to mouse IgG in the concentration range of 0.30–40.00 μg mL^{-1} and 0.15–40.00 μg mL^{-1}, respectively. While, the biosensor unmodified with nanohybrids shows

a response to mouse IgG in the concentration range of 2.50–40.00μg mL^{-1}.

AgNPs also played an important role in the development of the latest plasmonic applications, owing to its unique properties [18]. For this purpose, AgNPs of different shapes and sizes, from the simplest to the most sophisticated, can be readily obtained by using a large range of techniques. Batra *et al.,* (2012) fabricated a nanocomposite of citric acid-capped silver nanoparticles bound to surface of Au electrode through cysteine self-assembled monolayer for the development of an amperometric tyramine biosensor by covalently immobilizing tyramine oxidase [144]. The enzyme electrode was characterized by scanning electron microscopy, Fourier transform infrared spectroscopy, and cyclic voltammetry. The enzyme electrode has resulted into an improved analytic performance of tyramine biosensor in terms of lower detection limit (0.01 mM), fast response time (8 s), and long storage stability (60 days). Devi *et al.,* (2013a) developed a method for construction of an amperometric xanthine biosensor based on covalent immobilization of xanthine oxidase (XOD) onto citrate capped silver nanoparticles deposited on Au electrode surface through cysteine self-assembled monolayers (SAM) [145] (Fig. 9.3)**.** The use of silver nanoparticles/cysteine on the surface of an Au electrode as a support for immobilization of XOD has resulted into improved performance of xanthine biosensor. The silver nanoparticles/cysteine provides very sensitive and reliable biocompatible environment for the enzyme. Owing to their plasmonic properties, metallic nanoparticles are also responsible for enhancing Raman scattering of molecules adsorbed at their surface, giving rise to the so-called surface enhanced Raman spectroscopy (SERS) [124], It is worthy to note that this phenomenon is very different from propagative SPR or surface plasmon polariton (SPP) that occurs at the plane surface of large metallic structures, or on metallic nanowires, on which one direction is regarded as infinite. The position of the LSPR band of AuNPs and AgNPs depends on their size, uniformity, shape, dispersion, composition (ratio Au:Ag), and also on the dielectric constant of the surrounding medium [105, 118, 124, 146]. Two formats are typically encountered for colorimetric and plasmonic biosensors, i.e., aggregation-based assays and LSPR-based ones [128, 147]. The refractive index sensitivity (RIS), expressed in nm/refractive index unit (RIU) (nanometer per refractive index unit) is a measure of the shift in wavelength of the LSPR peak: the more the peak is shifted for small variations of refractive index (RI), the more sensitive the biosensor is (i.e., the highest the sensitivity is). AgNPs are described as more

sensitive than AuNPs for the second biosensing strategy. Indeed, a study showed that the RIS for AgNPs and AuNPs increased from 153 to 265 nm/RIU and 128 to 233 nm/RIU, respectively, for sizes 5 to 50 nm [148]. However, combining the two metals is very attractive and offers a wide range of possibilities.

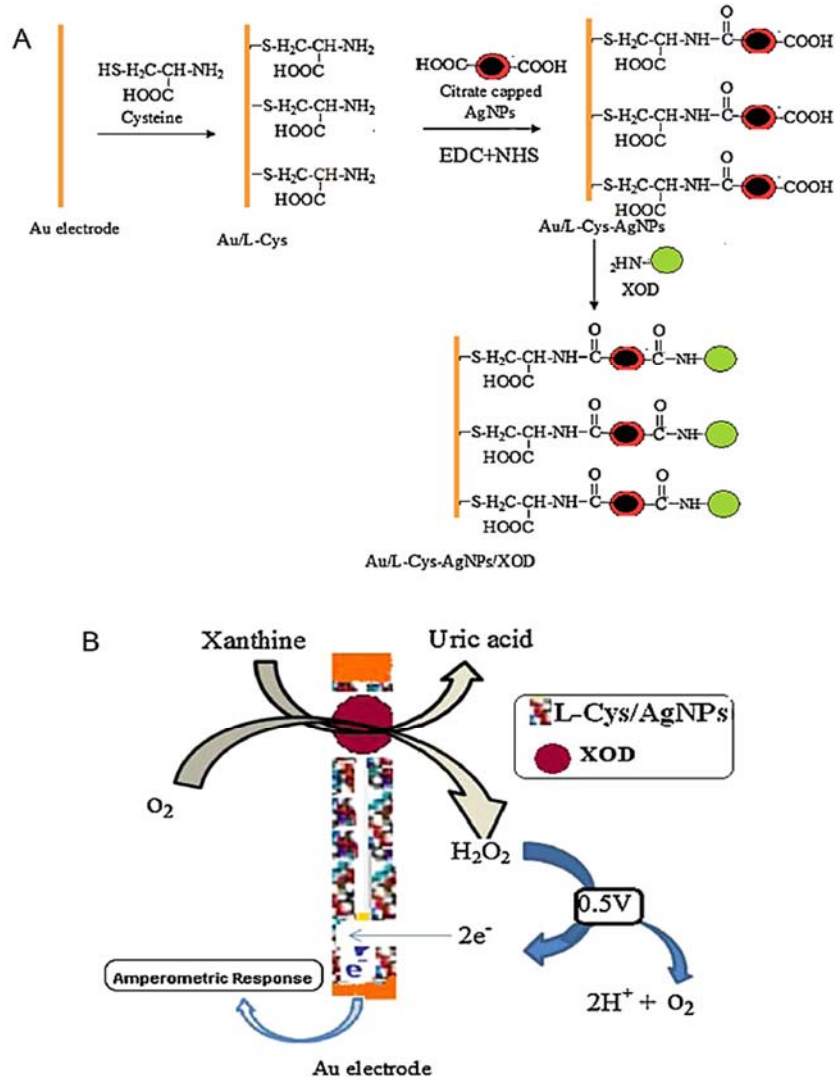

Fig. 9.3. A scheme showing the chemical reactions involved in the fabrication of XOD electrode (A) and mechanism of electron exchange between XOD and electrode surface (B) [145].

Metal NPs have also been extensively used to improve layer-by-layer (LbL) or self-assembled layers biosensor performance, especially noble metal nanoparticles (NP), e.g. AuNP, AgNP, PtNP and PdNP, since they possess high stability, conductivity, biocompatibility and size-related electronic, magnetic and optical properties. LbL methodology has been widely used to incorporate the metallic nanomaterials with controlled molecular architecture, in order to improve electronic communication between the biomolecule and the immobilize biomolecules without affecting their native conformation. The use of metal NPs incorporated in self-assembled LbL architectures allows the development of well-organized biosensor architectures, leading to more efficient biosensor platforms with enhanced performance. The incorporation of metal NPs into self-assembled multilayers leads to an overall increase in electronic conductivity and electroactive surface area of the modified electrodes, enabling an improvement in the analytical performances of the corresponding biosensors [149].Beside noble metal NP, iron NP have been widely employed in electrochemical biosensors, offering the same advantages as the noble NP such as an increase in enzymatic enzyme apparent activity and reduction of the difficulties associated with mass transfer, but with lower cost and easier preparation. A new trend is the adsorption of metal nanoparticles on porous micro-capsules of controllable size, which can be synthesized using a combination of polyelectrolytes [150-151].

To improve the performance, metal NPs have been reported in various combinations with viz. conductive polymers, graphene, chitosan and graphene oxide carbon nanotubes etc., which endow high electrical conductivity, effective surface area, and fast electron-transfer rate. The electrobiochemical sensor efficiency mainly depends on the modification of working electrode surface with different electro active coating materials [24, 88, 152]. The addition of nanoparticles (NPs) to the CNTs films could generate new nanostructures with excellent behavior in the fields of optics, electronics, and electrocatalysis. An amperometric oxalate biosensor was developed by using nanohybrid film of multi-walled carbon nanotubes (MWCNTs) and gold colloidal nanoparticles (GNPs) via carbodiimide chemistry by forming amide linkages between carboxylic acid groups on the CNTs and amine residues of cysteamine self-assembled monolayer (SAM) [153]. The enzyme nanocomposite electrode had improved performance in terms of response time (7s), sensitivity ($0.50 mA mM^{-1}$ in 1–800μM), reusability (more than 100 times) and stability (5months). A novel strategy is reported for developing a composite bio electrode consisting of

NiO-NPs/cMWCNT/PANI/Au, which showed remarkably enhanced sensitivity and selectivity for hydrogen peroxide in the presence of interference by dopamine, ascorbic acid, l-cysteine, and glucose [154]. The non-enzymatic biosensor showed relatively rapid response, broad linear range, low detection limit (0.2 μM), good reproducibility and long stability.

Magnetic NPs are promising alternatives to fluorescent labels in biosensor devices. Nanosized magnetic NPs due to the reduced number of magnetic domains (regions of parallel oriented magnetic moments caused by interacting unpaired electrons of an atom) shows different magnetic behaviors compared to its bulk material leading to so called superparamagnetic behavior. This means that magnetization can flip the direction randomly within very short time (Neel's relaxation time) and the magnetization appears in average zero in absence of an external magnetic field. This temperature dependent phenomenon disappears by applying an external magnetic field aligning the magnetic moments. Even when this effect seems to be similar to this of classic paramagnetic materials, the magnetic susceptibility of superparamagnets are much higher [155]. Such superparamagnetic behavior prevents therefore from attractive or repulsive forces between the magnetic nanoparticles as long as no external magnetic field is applied. A high-performance amperometric fructosyl valine (FV) biosensor was developed by immobilizing of fructosyl amino-acid oxidase (FAO) on core–shell magnetic bionanoparticles modified gold electrode [156]. Chitosan was used to introduce amino groups onto the surface of core–shell magnetic bionanoparticles (MNPs). The sensor showed high sensitivity, linearity, reproducibility and stability and fast response time. This biosensor prototype could be used effectively as the basis for HbA1c detection for diabetic patient’s medical management. The gold layers with their excellent compatibility with biomolecules and non-toxic property provide the stability to the Fe-NPs in solution; also create a suitable surface for the binding of Fe-NPs with various chemical and biological agents, which extend the application scope of Fe-NPs in various potential fields of bionanotechnology [157]. An amperometric biosensor for determination of xanthine was constructed by covalently immobilizing xanthine oxidase onto chitosan bound gold coated iron nanoparticles (CHIT/Fe-NPs@Au) nanocomposte on the surface of pencil graphite electrode (PGE) [158] (Fig. 9.4). The enzyme electrode was characterized by scanning electron microscopy (SEM), Fourier transform infrared (FTIR) spectroscopy and electrochemical impedance spectroscopy (EIS). The biosensor exhibited optimum current response

within 3 s at pH 7.4, 35 °C and working range 0.1–300 μM, when polarized at 0.5 V vs Ag/AgCl. The biosensor showed only 25 % loss in its initial activity after its 100 uses over 100 days, when stored at 4 °C.

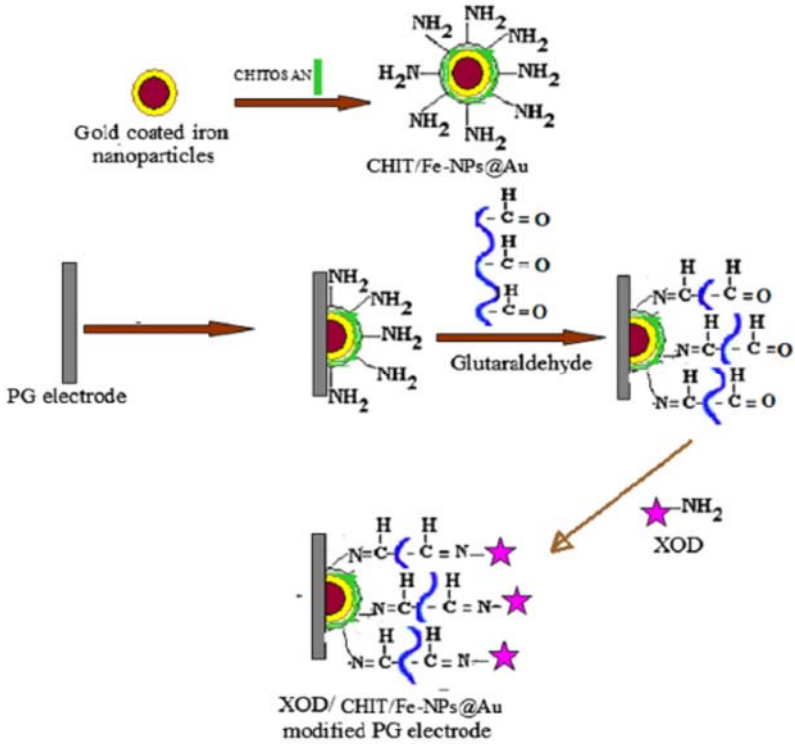

Fig. 9.4. Schematic representation of chemical reaction involved in the fabrication of XOD/CHIT/Fe-NPs@Au/PG electrode [158].

The use of metal NPs incorporated in self-assembled LbL architectures allows the development of well-organized biosensor architectures, leading to more efficient biosensor platforms with enhanced performance. The use of metal NPs in LbL architectures allowed the increase in sensitivity of optical sensors, also enabling exact control of the plasmonic properties of such devices, by varying Metal NPs size and distribution. The tailoring of nanomaterials such as metal nanoparticles in thin multilayers can bring further developments in the area of biosensors for their application in food/environmental industry, point-of-care diagnosis and fuel cells [149].

9.2.4. Metal Oxide Nanomaterials based Nanobiosensors

Many techniques have been proposed to design nanomaterials, to take advantage of their optical, catalytic, magnetic and adsorption properties for the fabrication of highly sensitive, selective and efficient biosensors. Nanostructured metal oxides have recently emerged as a useful platform for their high stability, low cost, unique physical properties, versatility in chemical properties and catalytic properties [159-160]. The structures or materials at the nanometer scale can be categories into four types of dimensions classified as:

- 0D (zero dimension) if all three spatial dimensions are in the nanometric range, i.e. nanoparticles or clusters [161-162];
- 1D (one dimension) if two dimensions are in the nanometric range, like nanotubes, nanorods and nanowires [163-166];
- 2D (two dimensions) if only one spatial dimension is nanometric, such as in thin films or nanosheets [165, 167-169];
- 3D (three dimensional) materials implies that the 0D, 1D and 2D elements are in close contact forming interfaces, for example compact polycrystals with nanosized grains or 3D porous nanostructures [170].

The electronic, physical and chemical properties of metal oxide can be engineered by modifying their size, structure, composition, stoichiometry and by doping [164]. Metal oxides can exhibit metallic, semiconductor or insulator characteristics [163] and are ionic compounds composed by positive metallic and negative oxygen ions [162]. In metal oxides, although the s-shells of positive metallic ions are always fully filled by electrons, their d-shells may not be completely filled [165]. Semiconductor metal oxides can either be classified as n-type, in which electrons are the majority charge carriers, or p-type, in which the majority charge carriers are holes. Nevertheless, the electronic structure range of these materials is extensive, being divided into two main categories, i.e. transition and non-transition metal oxides, where the latter englobes the pre- and post-transition metal oxides. Nevertheless, the sensing technology has evolved over the last years and continues to grow to guarantee human well-being, quality and safety from food to air, but also for environmental protection. Metal oxide nanostructures exhibit functional biocompatibility and non-toxic properties but are relatively inexpensive to produce. Meanwhile, nanostructured metal oxides possess a high surface area and isoelectric

point (IEP), which provide a suitable and reliable surface for immobilization of low IEP enzymes. Several high IEP metal oxide nanomaterials used are zinc oxide (ZnO) [171-173], iron oxide (Fe_3O_4) [174], titanium dioxide (TiO_2) [175-176], copper oxide (CuO) [177-178], cerium oxide (CeO_2) [179] and zirconia (ZrO_2) [180-181] in several kinds of sensors, *e.g.* gas, humidity, UV and biological sensors to reveal fascinating nano-morphological, functional biocompatible, non-toxic and catalytic properties [182]. These materials can adopt the most distinct structures at the nanoscale, ranging from nanowires to nanospheres or nanosheets, which will directly facilitate enhanced electron-transfer kinetics and high adsorption capability, thus providing suitable microenvironments for the immobilisation of biomolecules, resulting in improved biosensing characteristics [8, 183-184]. By using various methods, including soft templates (nanorods and nanofibres), sol–gel technique (three-dimensional ordered nanostructures), radio-frequency sputtering and hydrothermal methods, different morphologies of metal oxide nanoparticles have been synthesised [185-187]. The controlled methods lead to the fabrication of novel biosensing devices with enhanced signal amplification for bioaffinity assays, efficient charge transfer with redox species, and immobilised biomolecules [188]. These metal oxide nanoparticles provide an excellent pathway for immobilising the desired biological recognition molecules with an electronic signal transduction that leads to the design of a new generation of bioelectronics devices that may exhibit novel functions with exceptional optical and electrical properties due to electron and phonon confinement, high surface to volume ratios, surface reaction activity, catalytic efficiency and strong adsorption ability [189]. It is desirable to select suitable metal oxide nanoparticles to fabricate an efficient biosensor by immobilizing biomolecules as the binding between an metal oxide nanoparticles and a biomolecule (at the interface) is known to affect the performance of a biosensor [190]. The designing of a suitable metal oxide nanoparticles based bio-interface provides a biocompatible microenvironment that helps a biorecognition element to retain its biological activity with high stability. Various surface architectures have been used to fabricate a wide number of electrochemical biosensing devices that show improved sensitivity and selectivity.

The unique properties of ZnO combined with metal oxide nanostructures play important roles as the active sites where biological events occur and were recently demonstrated to be an efficient approach for sensor device fabrication, creating new avenues for diagnosis, disease management

and therapeutics. The biosensors developed using ZnO-based nanostructures have immense potential for biomedical applications owing to their effective surface area combined with its biocompatible nature, ease of synthesis with controlled morphologies and pore sizes, and high electron communication. In addition, owing to its excellent film forming and adhesion capability, large surface area, strong adsorption ability due to high isoelectric point (~9.5), improved catalytic efficiency (oxygen storage capacity), better chemical stability, resistant against corrosion and oxidation, and small grain size, makes it highly amenable to biomolecular sensing applications [13, 15, 16, 191]. ZnO nanostructures that exhibit high crystallinity create direct electron conduction tunnels between enzyme sites and electrode surfaces. Functionalization with metal oxides nanostructures not only improves the biosensor device stability, but also enhances selectivity, sensitivity and lowers detection limits of the desired biosensor. A combination of quantum mechanics, surface physics, biology, bioengineering, and electrical engineering may be required to create highly sensitive, highly specific, multianalysis, and nanoscale biosensors and bioelectronics, which would greatly benefit early diagnostics and health care [192-194]. ZnO, an n-type semiconductor metal oxide with a wide direct band gap of 3.37 eV, a large exciton binding energy of 60 meV, and enhanced electron mobility, that has gathered attention for a broad range of applications in biomedical and clinical sciences. ZnO nanostructures are suitable choice for surface functionalization and interfacing with chemical/biological compounds at various temperature and pH levels because of its biocompatible nature [195]. Hence, nanohybrids can be regarded as a promising new multifunctional material for high performance device fabrication. The features of ZnO for the sensing of biomolecules can be further improved by modifying the ZnO with metal oxide nanomaterials, as metal oxide nanomaterials make great catalysts due to their high surface ratio of atoms with free valences of the total atoms in the cluster, which also may lead to electrochemical reversibility for redox reactions [196-197]. Therefore, the integration of ZnO with metal oxide nanomaterials can provide new avenues for the development of highly sensitive biosensors, where the surface functionalized-metal oxides serve as active sites for improving specificity and sensitivity, and the ZnO offers rapid electron transfer in an electrochemical reaction [159]. A new zinc oxide nanoparticles/chitosan/carboxylated multiwall carbonnanotube/polyaniline(ZnONPs/CHIT/c-MWCNT/PANI) composite film has been synthesized on platinum (Pt) electrode using electrochemical techniques and have been used for the fabrication of creatinine and xanthjine biosensors by immobilizing enzymes [171-172].

The enzyme electrode was characterized by scanning electron microscopy (SEM), Fourier transform infrared (FTIR) spectroscopy and electrochemical impedance spectroscopy (EIS) (Fig. 9.5). The sensor exhibited high sensitivity, fast response time and good reproducibility.

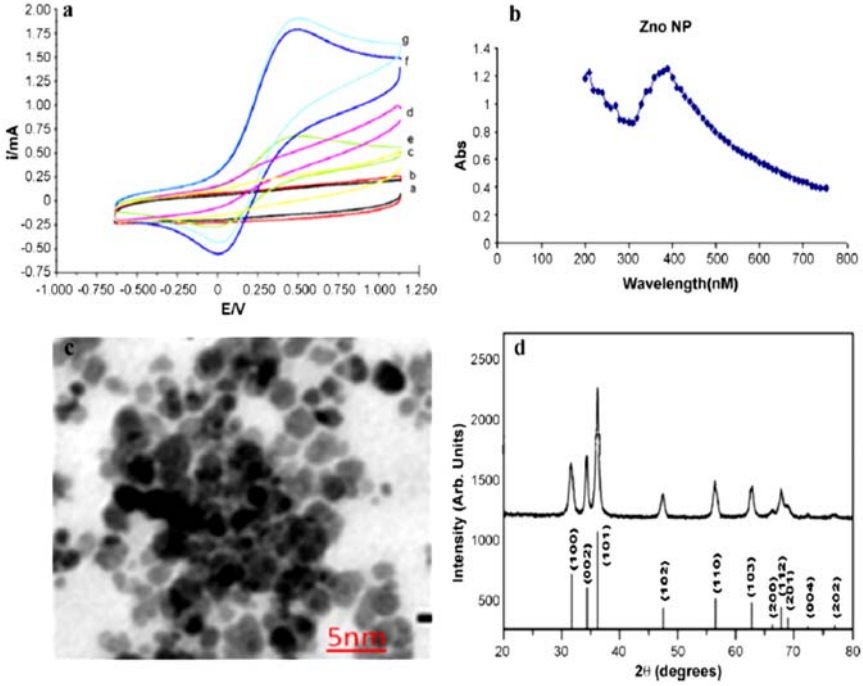

Fig. 9.5. (a) Cyclic voltammograms of amperometric response studies as a function of enzymes/ZnO-NPs/CHIT/c-MWCNT/PANI/Pt electrode in creatinine concentration from (a = 1 to g = 300 μM) using 0.05 M PB, pH 7.5. (b) UV spectrum of ZnO-NPs. (c) Transmission electron microscopic (TEM) images of ZnO-NPs. (d) X-ray diffraction (XRD) pattern ZnO-NPs [171].

Due to the clean interface and easy surface modification, the ZnO nanorod sensors can easily detect streptavidin binding down to a concentration of 25 nM, which is more sensitive than previously reported one-dimensional (1D) nanostructure electrical biosensors. Jin *et al.,* (2006) reported the fabrication of electrical biosensors based on functionalized ZnO nanorod surfaces with biotin for highly sensitive detection of biological molecules. In addition, the unique device structure with a micrometer-scale hole at the center of the ZnO nanorod's

conducting channel reduces the leakage current from the aqueous solution, hence enhancing device sensitivity [198]. Nanoflake ZnO with a wall thickness around 200 nm was grown on the tip of a borosilicate glass capillary and used as a selective intracellular glucose biosensor for the measurement of glucose concentrations in human adipocytes and frog oocytes. Fulati *et al.,* (2010) fabricated, a potentiometric intracellular glucose biosensor by immobilization of glucose oxidase on nanoflake ZnO. The results showed a fast response within 4 s and a logarithmic linear glucose-dependent electrochemical potential difference over a wide range of glucose concentration (500 nM–10 mM) [199]. The nanoflake ZnO material provided 1.8 times higher sensitivity than previously used ZnO nanorods under the same conditions. All these results demonstrate that the nanoflake ZnO can provide a promising material for reliable measurements of intracellular glucose concentrations within single living cells. Qualitative and quantitative detection of biological and chemical species is crucial in many areas, ranging from clinical diagnosis to homeland security. Due to the advantages of ultralow detection limit, label-free, fast readout and easy fabrication over the traditional detection systems, semiconductor nanowire based electronic devices have emerged as a potential platform. Electrodeposition of ZnO NWs on the conducting PET substrate was carried out at 70 °C in an aqueous electrolyte consisting of zinc nitrate mixed with potassium chloride. Pradhan *et al.,* (2010) demonstrated the fabrication and performance of an enzymatic glucose biosensor based on ZnO nanowires (NWs) deposited on an Au-coated polyester (PET) substrate [200]. Glucose oxidase (GOx) was subsequently immobilized on the synthesized ZnO NWs, and the electrocatalytic properties of GOx-immobilized ZnO NWs were evaluated by amperometry. The resulting GOx/ZnO-NWs/Au/PET bioelectrode exhibits excellent electrocatalytic performance with a high sensitivity of 19.5 μA mM−1 cm−2, a low Michaelis-Menten constant of 1.57 mM, and a fast response time of <5 s for the amperometric detection of glucose. Liu *et al.,* (2013), fabricated a single ZnO nanowire-based biologically sensitive field-effect transistors (bioFETs) for detection of different concentrations of uric acid solution at the same time [201]. The addition of uric acid with the concentrations from 1 pM to 0.5 mM resulted in the electrical conductance changes of up to 227 nS, and the response time turns out to be in the order of millisecond. The ZnO NW biosensor could easily detect as low as 1 pM of the uric acid with 14.7 nS of conductance increase, which implied that the detection limit of the biosensor can be as low as 1 pM. Ahmad *et al.,* (2012) developed a amperometric glucose biosensors using aspect-ratio (AR) controlled

zinc oxidenanorods (ZnO NRs) grown directly on Si/Ag electrodes, which showed a high performance in terms of selectivity, response time, linear range and repeatability [202]. Especially, the glucose biosensor with AR = 60 demonstrates the highest sensitivity of 110.76 μA/mM cm^2 and a wide linear range of 0.01–23.0 mM with ultrafast response time (<1 s). Such high performance is due to more immobilization on the well-aligned ZnO NRs arrays and direct electron conduction between the NRs and the electrodes.

Because of their outstanding properties that contribute to enhanced sensor performance, iron oxide nanostructures have gained wide interest for development of biosensors. Iron oxide has several advantages, such as chemical and biological stability, low toxicity, super paramagnetic property, and low cost for large-scale production. Iron oxide nanostructures also offer high conductivity and catalytic properties, which render them as suitable electronic wires to enhance electron transfer. This agglomeration can be prevented by functionalization of iron oxide with organic, inorganic, and biopolymeric materials, such as chitosan, silica, polymers, and carbon. Iron oxide can either be useful or undesirable depending on their phases, compositions, and functions. Among all iron oxide compounds, hydroxide and oxide–hydroxide and magnetite (Fe_3O_4) and maghemite (γ-Fe_2O_3) phases are the most important [203-204]. Fe_3O_4-NPs have been considered as interesting for the immobilization of desired biomolecules due to biocompatibility, strong superparamagnetic behavior which provide better contact and low toxicity. Immobilization of bioactive molecules onto a surface charged with superparamagnetic nanoparticles is of special interest, since the magnetic behavior of these bioconjugates may result in improved delivery and recovery of biomolecules for desired biosensing applications. An iron oxide nanoparticles/chitosangraft-polyaniline (Fe3O4-NPs/CHIT-g-PANI) composite film electrodeposited on surface of Pt electrode was fabricated and used for the development of creatinine biosensor by immobilizing enzymes on the nanocomposite film through glutaraldehyde coupling [174]. Transmission electron microscopy (TEM) was used for characterization of Fe_3O_4-NPs (Fig 9.6)**.** The use of Fe_3O_4-NPs/CHIT-g-PANI composite film for construction of amperometric creatinine biosensor has resulted in improved analytical performance in terms of relatively rapid response (2 s), higher sensitivity (3.9 $\mu A \mu M^{-1} cm^{-2}$), broad linear range (1–800 μM), good reproducibility and long term stability (200 days) of the biosensor.

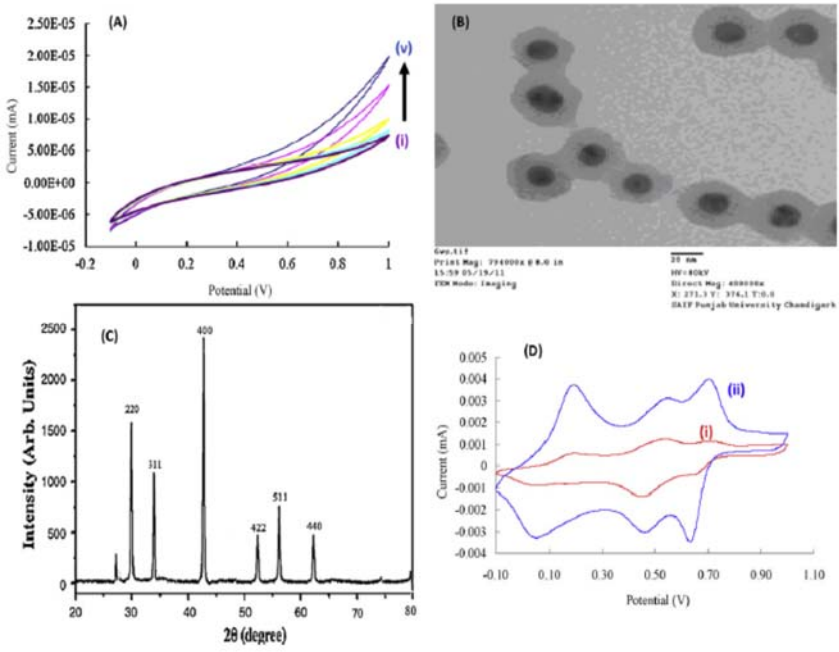

Fig. 9.6. (A) Cyclic voltammograms of amperometric response studies as a function of Enzymes/Fe_3O_4-NPs/CHIT-g-PANI/Pt electrode in creatinine concentration from (i = 50 to v = 250 μM) using 0.05 M PB, pH 7.5. (B) Transmission electron microscopic (TEM) images of Fe_3O_4-NPs dispersed in CHIT. (C) X-ray diffraction (XRD) pattern of Fe_3O_4-NPs. (D) Current responses curves of CHIT-g-PANI (curve i) and Fe3O4-NPs/CHIT-g-PANI composite (curve ii) films at 100 μM creatinine [174].

Uhlirova *et al.,* (2018) prepared superparamagnetic iron oxide nanoparticles (SPIONs) with different modified surface area. Nanoparticles (NPs) were modified by chitosan (CS), and sarcosine oxidase (SOX) [205]. The obtained NPs were characterized by physicochemical methods. The size of the NPs determined by the dynamic light scattering method was as follows: SPIONs/Au/NPs (100–300 nm), SPIONs/Au/CS/NPs (300–700 nm), and SPIONs/Au/CS/SOX/NPs (600–1500 nm). The amount of CS deposited on the NP surface was found to be 48 mg/mL for SPIONs/Au/CS/NPs and 39 mg/mL for SPIONs/Au/CS/SOX/NPs, and repeatability varied around 10%. The smallest amount of NPs that was able to detect sarcosine was 0.2 mg/well (200 μL of total volume) with the correlation coefficient

r = 0.9992, relative standard deviation (RSD) 6.35%, limit of detection (LOD) 5 μM. The proposed detection system allows the analysis of sarcosine at micromolar concentrations and to monitor changes in its levels as a potential prostate cancer marker. The whole system is suitable for low-cost miniaturization and point-of-care testing technology and diagnostic systems. This system is simple, inexpensive, and convenient for screening tests and telemedicine applications. The designed detection system was tested in artificial urine specimens and also applied to real urine specimens. The proposed procedure enables the analysis of sarcosine at micromolar levels, and is very sensitive, affordable, and suitable for monitoring urine sarcosine concentrations in prostate cancer patients, and could also be used for screening testing.

Cerium oxide nanoparticles or nanoceria particles have attracted much interest in building amperometric biosensors owing to their high isoelectric point (IEP) (~9.0), biocompatibility, chemical stability, high oxygen storage capacity, attractive catalytic and electrochemical features [206-208]. Cerium oxide nanoparticles act as an excellent nanomaterial for co-immobilization of a variety of oxidase and peroxidase enzymes such as horseradish peroxidase, glutamate oxidase [209-211]. Its catalytic activity can be exploited to develop for the fabrication of third generation biosensors and highly sensitive, enzymeless H_2O_2 sensors [212-213]. Ceria has high oxygen mobility at its surface and a large oxygen diffusion coefficient, which facilitates the conversion between valance states Ce4+/Ce3+ that allow oxygen to be released or stored in its crystalline structure [214-216]. Cerium oxide nanoparticles have also been used to immobilize multienzyme, including superoxide oxidase, catalase and oxidase, and mimetic properties, and emerged as a fascinating material in biological fields, such as in bioanalysis, biomedicine, and drug delivery [217-224]. Catalytically active nanoceria offer several advantages over natural enzymes, such as controlled synthesis at low cost, tunable catalytic activities and high stability against severe physiological conditions [225]. A single-use electrochemical screen-printed electrode is reported based on biomimetic properties of nanoceria particles. The developed tool showed an easy approach compared to the classical spectrophotometric methods reported in literature in terms of ease of use, cost, portability, and unnecessary secondary reagents. The sensor allowed the detection of the total antioxidant capacity (TAC) in wine samples. The sensor has been optimized and characterized electrochemically and then tested with antioxidant compounds occurred in wine samples. The electrochemical CeNPs modified sensor has been used for detection of TAC in white and

red commercial wines and the data compared to the 2,20-azino-bis (3-ethylbenzthiazoline-6-sulphonic acid (ABTS)-based spectrophotometric method. Finally, the obtained results have demonstrated that the proposed sensor was suitable for the simple and quick evaluation of TAC in beverage samples [226]. A simple and sensitive enzymatic electrochemical biosensor was developed to detect rutin by cyclic voltammetry (CV), differential pulse voltammetry (DPV) and square wave voltammetry (SWV) using a carbon paste electrode modified with a multiwall carbon nanotube (MWCNT),cerium oxide nanoparticle, and crude extract source of peroxidase enzyme (PO_x) composite [227]. The electrochemical parameters and experimental conditions were optimized and evaluated. The enzymatic electrochemical biosensor showed excellent electrocatalytic activity towards the detection of rutin. The surface physical characteristics of the modified electrode were studied by scanning electron microscopy (SEM) and transmission electron microscopy (TEM). This biosensor demonstrated selectivity, stability, and reproducibility, which was further applied to detect rutin in medicine tablets and capsules with recoveries in the range of 97-102%. The cerium dioxide and carbon nanotubes effectively facilitate the electrocatalysis of rutin and the electron transfer on the electrode surface. These materials also increase the sensitivity of the sensor, which shows good linearity as a function of concentration. The capability of the modified electrode in terms of selectivity, linearity, limit of detection, quantification, and repeatability are comparable with the analytical parameters of other reported modified electrodes.

Copper oxides nanomaterials oxides are abundant materials, eco-friendly, non-toxic and are compatible with wet-chemical synthesis routes that originate low-cost devices [228]. There are two most common copper oxides such as

- Copper (I) oxide or cuprous oxide (Cu_2O), reddish material;
- Copper (II) oxide or cupric oxide (CuO), black material.

Copper oxides nanoparticles have been used in fabrication of nanobiosensors [229-232]. A biosensor for detection of glucose and hydrogen peroxide based on Cu_2O nanocubes wrapped by graphene nanosheets was reported [230]. The biosensor showed a linear response for glucose in the range of 0.3 to 3.3 mM with a detection limit of 3.3 μM, high selectivity and short response time (< 9 s). The enzymeless biosensor also exhibited good response toward H_2O_2, with the linear response ranging from 0.3 to 7.8 mM at −0.4 V and detection limit of

20.8 μM. By using hydrothermal synthesis Cu_2O shuriken-like nanostructures were synthesized and used for fabrication of nonenzymatic glucose biosensors [231]. In another study carbon quantum dots/octahedral Cu_2O nanocomposites were fabricated and tested as non-enzymatic glucose and hydrogen peroxide amperometric sensors [233]. Leaf-like CuO nanoparticles and CuO nanotube arrays were also fabricated and used for development of glucose biosensors [234-235]. Copper oxides nanoparticles were also tested as biosensors in film form. Inkjet-printed CuO nanoparticles to produce films were integrated in nonenzymatic glucose biosensors [236]. A uric acid biosensor was developed based on CuO thin film, have good linearity over a wide uric acid concentration range of 0.05 mM to 1.0 mM with enhanced response of 2.7 $mAmM^{-1}$ and long shelf life (> 14 weeks) [229]. Batra *et al.,* (2015) demonstrated a ZnO–CuO composite matrix based biosensor for detection of total cholesterol, for which sensitivity was reported to be 680 $\mu AmM^{-1}cm{-}2$ and 760 $\mu AmM^{-1}cm^{-2}$ towards free cholesterol and total cholesterol respectively with response time of 5 s, with long shelf life [237]. A high-performance nonenzymatic glucose biosensor was developed by using vertically-aligned ZnO nanorods decorated with CuO [232]. The fabricated electrodes exhibited high sensitivity (2961.7 $\mu AmM^{-1}cm^{-2}$), linear range up to 8.45mM, low limit of detection (0.40 μM) and short response time < 2 s. The selected metal oxides have in common the fact that these are earth abundant, low-cost, nontoxic and compatible with wet-chemical synthesis routes. In terms of future perspectives, the scientific community has been focused on the development of innovative synthesis strategies capable of specifically tuning the metal oxide structures at the nanoscale, as well as their intrinsic properties for developing biosensing devices that may lead to the evolution of new strategies for bio-affinity assays and efficient electrical communication.

9.2.5. Enzyme Nanoparticles based Nanobiosensors

There was a little knowledge about the enzyme attachment on the nanoparticles and creation of enzyme nanoparticles (ENPs) but due to their potential outcomes, this area of nanobiosensors based on ENPs has also seen development in recent times. Enzyme nanoparticles (ENPs) are the aggregated forms of enzymic molecules in an appropriate configuration in nano scale ranges between 10 and 100 nm [238-239]. ENPs have enhanced the functional activities of enzyme based devices such as biosensors because these have various excellent features such as

optical, electronic, electrical, thermal, chemical, mechanical, catalytic and large surface area than native enzymes. Biosensor based ENPs have exhibited better analytical performance such as limit of detection, working range, reproducibility as well as repeatability. These biosensors have been used for the diagnosis of various diseases such as cardiovascular diseases, renal disorders, diabetes, environment monitoring, and biochemical engineering and reused up to 8–200 times over a period of 60–240 days while stored dry at 4°C [19]. ENPs based electrochemical biosensors have exhibited novel fascinating features including exceptional selectivity, analytical signalling, and sensitivity, high surface area, better electrical properties, unique optical properties, and nanoscale structures. These biosensors have shown high sensitivity and detection of specific compounds timely, whereas conventional detection techniques including chromatography are not easy to operate and time consuming. Various types of enzyme nanoparticles have been used for the construction of biosensors for the detection of specific analyte such as horse radish peroxidase (HRP) [240], glucose oxidase (GOD) [241], uricase [242], cholesterol oxidase (ChO_x)/cholesterol esterase (ChE) NPs [243], lipase/glycerol kinase/glycerol-3-phosphate oxidase NPs [244], creatinine (CA)/creatine (CI)/sarcosine oxidase (SO_x) NPs [245], haemoglobin NPs [246] and urease NPs [247].

Liu *et al.,* (2005) developed a simple and effective method to immobilize horseradish peroxidase ENPs directly onto the gold electrode surface, used to develop reagentless electronic biosensors for H_2O_2 detection without promoters and mediators and offer great potential to develop enzyme-based electronic biosensors [240]. The nanoparticle (NP) aggregates of glucose oxidase (GOD) were prepared with 117 nm diameter, by desolvation method and characterized by UV, transmission electron microscopic (TEM) and Fourier transform infrared (FTIR) spectra (Fig 9.7). GOD-NP aggregates were more stable, active and had a higher shelf life than that of free enzyme. The immobilized NP aggregates of enzyme showed higher activity, thermostability and lower apparent Km as compared to free enzyme and employed for DO metric determination of serum glucose [241].

Uricase NPs (100 nm in size) were prepared and immobilized onto the Au electrode to construct an amperometric uric acid biosensor [242]. The enzyme electrode was characterized by scanning electron microscopy (SEM), Fourier transform infrared (FTIR) spectroscopy, and electrochemical impedance spectroscopy (EIS). The enzyme electrode detected uric acid level as low as 5.0 μM at a signal-to-noise ratio of 3,

within 7 s at pH 8.5 and 40 °C. The biosensor showed a linear working range, 0.005 to 0.8 mM for uric acid with a sensitivity of 0.03 $mA\mu M^{-1}cm^{-2}$. Cholesterol esterase nanoparticles (ChENPs) and cholesterol oxidase nanoparticles (ChO_xNPs) aggregates were prepared and functionalized with glutaraldehyde cross-linking to an improved amperometric determination of serum total cholesterol [243]. Transmission electron microscope (TEM) images of ChENPs and ChO_xNPs showed their spherical shape and average size of 35.40 and 56.97 nm, respectively. The biosensor exhibited optimal response at pH 5.5 and 40 °C within 5 s when polarized at +0.25 V versus Ag/AgCl. The working/linear range of the biosensor was 10–700 mg/dl for cholesterol. The sensor showed high sensitivity and measured total cholesterol as low as 0.1 mg/dl. Kumar *et al.,* (2017) developed an improved amperometric biosensor for detection of creatinine based on immobilization of nanoparticles (NPs) of creatininase (CA), creatinase (CI), and sarcosine oxidase (SOx) onto glassy carbon (GC) electrode [245]. The biosensor showed optimum response within 2s at pH 6.0 in 0.1 M sodium phosphate buffer and 25 °C, when operated at 1.0 V against Ag/AgCl. Biosensor exhibited wider linear range from 0.01 μM to 12 μM with a limit of detection (LOD) of 0.01 μM. Lipase, glycerol kinase (GK) and glycerol-3-phosphate oxidase (GPO) NPs aggregates were prepared by desolvation and glutaraldehyde crosslinking and functionalized by cysteamine and used in the fabrication of amperometric triglyceride (TG) bionanosensor by co-immobilizing the ENPs aggregates covalently onto polycrystalline Au electrode through thiolated bond [244]. Biosensor showed optimum current at 1.2 V within 5s, with linear relationship of triolein concentration in lower concentration range, 10–100 mg/dL and higher concentration range, 100–500 mg/dL and limit of detection (LOD) of bionanosensor was 1.0 μg/ml. Yadav *et al.,* (2018b) prepared NPs of haemoglobin (HbNPs) by desolvation method and characterized by transmission electron microscopy (TEM),UV–vis spectroscopy, Fourier transformation infra-red (FTIR) spectroscopy and X-ray diffraction (XRD) and atomic force microscopy (AFM). An amperometric acrylamide biosensor was constructed by immobilizing covalently HbNPs onto polycrystalline Au electrode [246]. The biosensor showed optimum current response within 2 s at 0.26 V, pH 5.0 at room temperature (20° C). The working range of biosensor was 0.1nm–100mM with a limit of detection (LOD) as low as 0.1nM. ENPs aggregates of urease were prepared by desolvation and glutaraldehyde crosslinking and functionalized by cysteamine dihydrochloride, characterization and applied for construction of an improved potentiometric urea biosensor [247]. The biosensor displayed a low

detection limit of 1 μM/L with a wide working range of 2–80 μM/L (0.002–0.08 mM) and sensitivity of 23mV/decade.

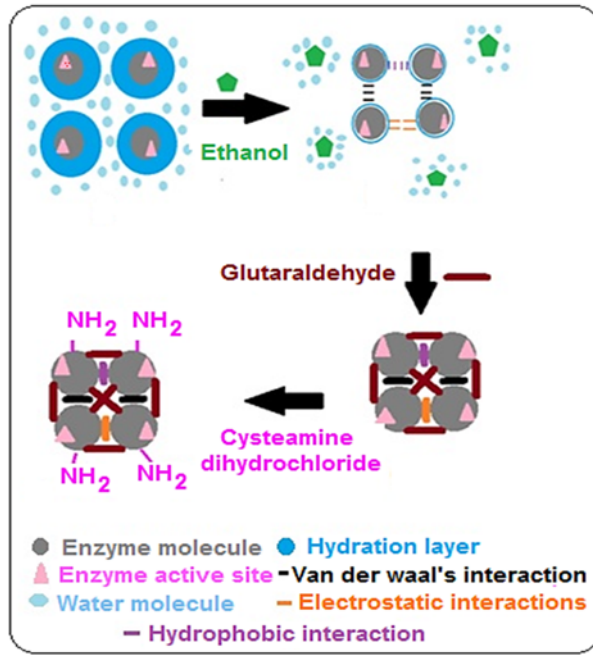

Fig. 9.7. Scheme of cross-linked GOD-NP aggregates formation by desolvation process [241].

In another novel method, single enzyme nanoparticles (SENs) by attaching the anchor covalently over the single enzyme and growing the organic/inorganic network for making ENPs. In an instance the enzyme were entrapped in a thin layer of nanoparticles just by drying the mixture of specified concentration of enzyme and nanoparticles at room temperature [248]. Unlike ENPs, single enzyme nanoparticles (SENs) are comprised of monomeric enzyme coated with organic or inorganic macromolecules of nano range. Sensors employing SENs have increased the electrochemical activity and stability at high temperature. Single-enzyme (SENs) with excellent activity and stability were successfully fabricated via the surface modification and in situ aqueous polymerization of separate urease molecule. A novel piezo-electric biosensor was developed for urea determination based on SENs immobilization onto nanoporous alumina membranes prepared by

electrical anodization. The process of SENs immobilization was optimized and the performance of the developed urea biosensor was evaluated. The high selectivity, shorter response time (12 s), wider linear range (0.08 μM–1 mM) and lower limit of detection (LOD, 0.05 μM) were observed for the present biosensor. Moreover, a stability study showed a very high stability over time for the frequency response of the biosensor with separated porous alumina/SENs electrode, testifying for the protective nature of the nanoporous alumina membranes and the interest of SENs. [249]. Therefore, the future research should be focused to understand the interaction of ENPs with their analyte and further improvement and commercialization of ENPs based biosensor.

9.3. Applications of Nanobiosensors

The definition and description of the concept of operation of nanobiosensors do not leave any room for their application as they are highly versatile and multifunctional. The nanotechnology based biosensor or nanobiosensor technology is not only revolutionizing the health care industry but nanobiosensors are also being used for environment monitoring of pollutants, toxicants and physical aspects like humidity, heavy metal toxicity, in food and beverage industry, determination of drug residues in food and even presence of their carcinogens etc. [8].

9.3.1. Biomedical and Diagnostic Application

Emerging technological innovations enabled by next-generation sensors will define the landscape for the future commercialization of medical devices. Nanobiosensors have been used for routine application in diagnosis such as biological detection of serum antigen and carcinogens, detection of glucose, cholesterol, allergic responses, pathogenic viruses, and pathogenic bacteria [20, 250]. The advent of biosensors has really improved the diagnosis of all these diseases and related malfunctions. With the addition of nanoscale interventions, disease diagnosis has further been benefited and made more precise. The incorporation of nanomaterials has enabled the detecting enzyme system to be immobilized, and this has allowed the recycling and reuse of costly enzymes. Prior to the use of nanobiosensors, the detection and diagnosis of these diseases were very difficult, time consuming and costly. Besides this, nanobiosensors have improved sensitivity and accuracies that make

them good candidate for diagnosis. The implementation of nanoscale innovations like NEMS and MEMS has added several advantages to the overall testing procedure. Biochips and microarray based technique has enabled the testing of many diseases, simultaneously in no time. Significant advancements have been made in the development of nanosensors for point-of-care diagnostics for cancer, diabetes, malaria, HIV, and bilharzias. With controlled synthesis, even magnetic nanoparticles have been synthesised and used for isolation and heavy metal resembling in properties with iron from the blood serum of living organisms. Therapeutic gene sequences are controlled by biosensor-activated control switches to provide the proper amount of gene therapy on a single-cell basis. [76].

9.3.2. Environmental Applications

There is a big demand for fast, reliable, and low-cost systems for the detection, monitoring, and diagnosis of pollutant in the environment and agriculture. A wide range of new biosensors (an analytical device for the quantitative detection of analyte with a biologically active element) are being developed. Several of these biosensors rely on nanotechnological platforms [251]. This is a relatively broader area of application, as environment undergoes so many rapid scale changes almost every second. The sensors based on nanomaterials can be very versatile in terms of their detection and monitoring of pollutants, toxic intermediates, heavy metals from waste streams and the monitoring of weather conditions like the estimation of humidity and many other vital features are really highly detailed and comprehensive tasks. The nanomaterials based sensing tools can be used to find the particular kind of damaging extent of a material present or prevailing in the environment, at any given time. Carcinogens and harmful intermediates leading to the disruption of proper hormonal systems in the living beings have been isolated through the use of highly sophisticated and specific compounds, particularly named as endocrine-disrupting compounds. Using the substrate specific detection mechanism, biosensors have been developed for detection of nitrates, inorganic phosphates [252], and biological oxygen demand like parameters and have been proved to be environmentally restoring in their working mechanisms. These applications can be integrated and a single sensor can be developed by the use of nanomaterials which can sense the different contaminants equally well in only a single operation. In this manner, there are endless environmental parameters for the evaluation of which the nanobiosensors can be used and developed. These

applications are highly energy saving, economical and time saving in nature [20].

9.3.3. Food Contamination Monitoring Applications

Nanobiosensors have tremendous potential applications in various food industry due to the potential feasibility of practical on-site detection of foodborne pathogens biotoxin, and agrochemicals as rapid detection methods. The unique optical, electrical, and electrochemical properties of the nanomaterials provide novel interesting alternatives to conventional platforms for biosensor development, with improved stability, sensitivity, selectivity, and indirect detection [253-255]. Electrochemical biosensors are particularly attractive as a selective, sensitive, and reliable analytical methods due to their low-cost, high sensitivity and selectivity to overcome the key challenges to both control foodstuff composition and detect chemical or biological contaminants in food. They can be easily miniaturized and integrated in high density arrays for multianalyte and high throughput analysis [256]. The incorporation of nanosensors into food packaging has resulted in various advantages over conventional sensors such as improved sensitivity and specificity, speed of analysis, increased sample throughput (multiplex systems), reduced assay complexity, and reduced cost. A variety of nanosensor designs for the same analyte may be found, which typically provide different levels of sensitivity and specificity [257].

9.3.4. Miscellaneous Applications

Nanobiosensors can also be employed to optimize several other detections. In the industrial operations, feeding of nutrient media and substrate mixtures into the bioreactors for diverse applications can be regulated using these sensors. On an industrial scale, many commercial preparations and separations can be enhanced with these sensors. For instance, in the metallurgical operations requiring separation of impurities existing in a complexed form combined in the form of ores, nanobiosensors can be used to separate the impurities selectively by trying out different configurations of the sensing enzymes. Developing microbiological and biochemical assays coupled with bioengineering based innovations are really very handy applications of these sensing materials [20].

9.4. Conclusion and Future Prospects

There is a big demand for fast, reliable and low-cost systems for the detection, monitoring and diagnosis of biological molecules and diseases in medicine. This demand exists in the areas of environmental pollutant monitoring, detection of foodborne pathogens, and the potential danger of bioterrorism. The development of ultra-sensitive biological and chemical sensors is one of the grand scientific, engineering, and educational challenges of the 21st century. The next generation biosensor platforms require significant improvements in sensitivity and specificity, in order to meet the needs in a variety of fields including in vitro medical diagnostics, pharmaceutical discovery and pathogen detection. Considering all of these aspects, it can be stated that with the advent of nanotechnology and its impact on developing ultrasensitive devices, nanobiosensors offer the possibility of diagnostic tools with increased sensitivity, specificity, and reliability for in vivo and in vitro analytical applications. Nanobiosensor research focuses on developing innovative technologies that have the ability to make significant contributions in the areas of human and animal disease marker detection, promising therapeutic compound identification and analysis, nano-and biomaterials characterization, and biocatalyst development and the transduction mechanisms have been significantly improved with the use nanomaterials and nanostructures like those of quantum dots, nanoparticles for enzyme immobilization, and hybrid nanostructure with multiple functionalities. The increasing advancement of miniaturization and nanomaterials research has stimulated the application of these materials for sensing several key pathways and regulatory events. Even though a wide range of nanobiosensors have been developed in the past two decades,, however, nanobiosensors still need to achieve the confidence of potential users, especially considering that the commercialization of new devices is the aim of nanobiosensor technology development, the futuristic goal of low-cost, high throughput, multiplexed clinical diagnostic lab-on-a-chip devices is yet to be truly realized. Additionally, miniaturization and production of compact biosensors for diagnostic purposes is an emergent need in sensor technology since it requires development of reliable, reproducible, and cost-effective sensors with high accuracy, sensitivity, and specificity. Well-structured interdisciplinary research programs that involve, life science researchers, engineers and physicians have to be conducted, to reveal more refined and affordable biosensors [17].

References

[1]. L. C. Clark, C. Lyons Biosensors - A Practical Approach, *J. Amn. N. Y. Acad. Sci*.,102, 1962, pp. 29-45.

[2]. M. Mehrvar, C. Bis, J. M. Scharer, M. Moo-Young and J. H., Loung Fiber optic biosensors-Trends and advances, *Anal. Sci.,*16, 2000, pp. 677-691.

[3]. Y. Zhang and S Tadigadapa, Calorimetric biosensors with integrated microfluidic channels, *Biosens. Bioelectron.,*19, 2004, pp. 1733-1743.

[4]. C. S. Pundir, S. Yadav and A. Kumar, Creatinine sensors, *Trends in Anal. Chem*.,50, 2013, pp. 42-52.

[5]. S. F. D'Souza, Microbial biosensors, *Biosens Bioelectron*.,16, 2001, pp. 337-353.

[6]. S. Brahim, D. Narinesingh and A. Guseppi-Elie, Polypyrrole-hydrogel composites for the construction of clinically important biosensors, *Biosens. Bielectrons*.,17, 2002, pp. 53-59.

[7]. P. D'Orazio, Biosensors in clinical chemistry, *Clin. Chim. Acta*.,334, 2003, pp. 41-69.

[8]. B. D. Malhotra and C. M. Pandey, Biosensors: Fundamentals and Applications, *Smithers Rapra Technology Ltd.*, 2017, pp. 55-96.

[9]. A. Munawar, Y. Ong, R. Schirhagl, M. A. Tahir, W. S. Khanae and S. Z. Bajwa, Nanosensors for diagnosis with optical, electric and mechanical transducers, *RSC Adv.,*9, 2019, pp. 6793–6803.

[10]. N. M. Noah and P. M. Ndangili, Current Trends of Nanobiosensors for Point-of-Care Diagnostics, *J Anal. Methods Chem*., 2019, art. 2179718.

[11]. C-M. Tîlmaciu and M. C. Morris, Carbon nano tube biosensors, *Front. Chem.,*3, 2015, pp. 1-21.

[12]. H. Malekzad, P. S. Zangabad, H. Mirshekari, M. Karimi and M. Hamblin, Noble metal nanoparticles in biosensors: Recent studies and applications, *Nanotechnol. Reviews*, 6, 3, 2017, pp. 301–329.

[13]. C. Y. Chen, Y. R. Liu, S. S. Lin, L. J. Hsu and S. L. Tsai, Role of annealing temperature on the formation of aligned zinc oxide nanorod arrays for efficient photocatalysts and photodetectors, *Sci. Adv. Mater*.,8, 2016, pp. 2197–2203.

[14]. N. Chauhan and K. D. N. Sakthi, Graphene based biosensors—Accelerating medical diagnostics to new-dimensions, *J. Mater. Resear*., 32, 2017, pp. 2860-2882.

[15]. M. Mazaheri, H. Aashuri and A. Simchi, Three-dimensional hybrid graphene/nickel electrodes on zinc oxide nanorod arrays as non-enzymatic glucose biosensors, *Sens. Actuators B: Chem*.,251, 2017, pp. 462–471.

[16]. W. Raza and K. Ahmad, A highly selective Fe@ZnO modified disposable screen printed electrode based non-enzymatic glucose sensor (SPE/Fe@ ZnO), *Mater. Lett*., 212, 2018, pp. 231–234.

[17]. J. Pena‐Bahamonde, H. N. Nguyen, S. K. Fanourakis and D. F. Rodrigues, Recent advances in graphene‐based biosensor technology with applications in life sciences, *J Nanobiotechnol.,*16, 2018, 75.
[18]. A. Loiseau, V. Asila, G. Boitel-Aullen, M. Lam, M. Salmain and S. Boujday, Silver-Based Plasmonic Nanoparticles for and Their Use in Biosensing, *Biosens.,*9, 2019, 78.
[19]. Neelam, A. K. Chhillar and J. S. Rana, Enzyme nanoparticles and their biosensing applications: A review, *Anal. Biochem*, 581, 2019, 113345.
[20]. S. Pandit, D. Dasgupta, N. Dewan and P. Ahmed, Nanotechnology based biosensors and its application, *The Pharma Innova. J*., 5, 2016, pp. 18-25.
[21]. B. Q. Wei, R. Vajtai and P. M. Ajayan, Reliability and current carrying capacity of carbon nanotubes, *Appl. Phys. Lett*.,79, 2001, pp. 1172–1174.
[22]. K. Balasubramanian and M. Burghard, Biosensors based on carbon nanotubes, *Anal. Bioanal. Chem*., 385, 2006, pp. 452–468.
[23]. S. Szunerits and R. Boukherroub, Graphene-based biosensors, *Interf. Focus*, 8, 2018, 20160132.
[24]. S. Shrivastava, N. Jadon and R. Jain, Next-generation polymer nanocomposite-based electrochemical sensors and biosensors: A review, *Trends in Anal. Chem*., 82, 2016, pp. 55-67.
[25]. M. Sireesha, B. V. Jagadeesh, K. A. S. Kranthi and S. Ramakrishna, A review on carbon nanotubes in biosensor devices and their applications in medicine, *Nanocompos.,*4, 2018, pp. 36-57.
[26]. B. Peng, M. Locascio, P., Zapol *et al.,*Measurements of near-ultimate strength for multiwalled carbon nanotubes and irradiation-induced cross-linking improvements, *Nat Nanotechnol*.,3, 2008, pp. 626–631.
[27]. E. Pop, D. Mann, Q., Wang *et al.,*Thermal conductance of an individual single-wall carbon nanotube above room temperature, *Nano Lett*, 6, 2006, pp. 96–100.
[28]. A. Charlier, E. McRae, R. Heyd, M. Charlier and D. Moretti, Classification for double-walled carbon nanotubes, *Carbon*, 37, 1999, 1779.
[29]. M. Endo, M. S. Strano and P. M. Ajayan, Carbon Nanotubes, *Springer*, Berlin, Germany, 2007, p. 13.
[30]. A. Aqel, K. M. M. A. El-Nour, R. A. A. Ammar and A. Al-Warthan, Carbon nanotubes, science and technology part (I) structure, synthesis and characterization, *Arab. J. Chem*., 5, 1, 2012, pp. 1-23.
[31]. P. L. McEuen, Single-wall carbon nanotubes, *Physics World*, 2000, 13, pp. 31-36.
[32]. S. Iijima, Helical micro tubules of graphitic carbon, *Nature*, 354, 1991, pp. 56–58.
[33]. S. Iijima and T. Ichihashi, Single-shell carbon nanotubes of 1-nm diameter, *Nature*, 363, 1993, pp. 603-605.

[34]. K. Balasubramanian and M. Burghard, Chemically functionalized carbon nanotubes, *Small*, 1, 2005, pp. 180–192.
[35]. A. LeGoff, M. Holzinger and S. Cosnier, Enzymatic biosensors based on SWCNT-conducting polymer electrodes, *Analyst*, 136, 2011, pp. 1279–1287.
[36]. V. Biju, Chemical modifications and bioconjugate reactions of nanomaterials for sensing, imaging, drug delivery and therapy, *Chem. Soc. Rev*.,43, 2014, pp. 744–764.
[37]. B. Thirumalraj, S. Kubendhiran, S-M., Chen *et al*., Highly sensitive electrochemical detection of palmatine using a biocompatible multiwalled carbon nanotube/poly-l-lysine composite, *J Colloid Interface Sci*.,498, 2017, pp. 144–152.
[38]. Y. Yun, Z. Dong, V. Shanov, *et al*., Nanotube electrodes and biosensors, *Nano Today*, 2, 2007, pp. 30–37.
[39]. S. Vardharajula, S. Z. Ali, P. M. Tiwari, *et al*., Functionalized carbon nanotubes: biomedical applications, *Int. J. Nanomed*., 7, 2012, pp. 5361–5374.
[40]. A. Erdely, M. Dahm, B. T. Chen, *et al.,* Carbon nanotube dosimetry: from workplace exposure assessment to inhalation toxicology, *Part Fibre Toxicol*., 10, 1, 2013, 53.
[41]. T. K. Sau, A. L. Rogach, F. Jackel, T. A. Klar and J. Feldmann, Properties and applications of colloidal nonspherical noble metal nanoparticles, *Advanced Materials*, 2010, 22, 16, pp. 1805-1825.
[42]. D. Pantarotto, R. Singh, D. McCarthy, M. Erhardt, J-P. Briand, M. Prato, *et al.,* Functionalized carbon nanotubes for plasmid DNA gene delivery, *Angew. Chem. Int. Ed*., 43, 2004, pp. 5242–5246.
[43]. J. V. Veetil and K. Ye, Development of immunosensors using carbon nanotubes, *Biotechnol. Prog*., 23, 2007, pp. 517–531.
[44]. Y. E. Choi, J. W. Kwak and J. W. Park, Nanotechnology for early cancer detection, *Sens. (Basel),*10, 2010, pp. 428–455.
[45]. Z. Wang and Z. Dai, Carbon nanomaterial-based electrochemical biosensors: an overview, *Nanoscale*., 7, 2015, pp. 6420–6431.
[46]. A. Jain, A. Homayoun, C. W. Bannister, *et al*., Singlewalled carbon nanotubes as near-infrared optical biosensors for life sciences and biomedicine, *Biotechnol J.,* 10, 2015, pp. 447–459.
[47]. N. Yang, X. Chen, T. Ren, and D. Yang, Carbon nanotube based biosensors, *Sens. Actuators B: Chem*., 207, 2015, pp. 690-715.
[48]. G. Ijeomah, F. Obite and O. Rahman, Development of carbon nanotube-based biosensors, *Int. J. Nano. Biomater*. , 6, 2016, pp. 83-109.
[49]. Z. Zhu, An Overview of Carbon Nanotubes and Graphene for Biosensing Applications, *Nano-Micro Lett*. , 9, 2017, 25.
[50]. S. Same and G. Samee, Carbon Nanotube Biosensor for Diabetes Disease, *Cres. J. Med. Biolog. Sci.,* 5, 2018, pp. 1–6.
[51]. S. Carrara, V. V. Shumyantsev, A. I. Archakov, B. Samor, Screen-printed electrodes based on carbon nanotubes and cytochrome P450scc

for highly sensitive cholesterol biosensors, *Biosens. Bioelectronics*. , 24, 2008, pp. 148–150.

[52]. Y. Li, Y. Umasankar and S-M. Chen, Multiwalled carbon nanotubes with poly(NDGAChi) biocomposite film for the electrocatalysis of epinephrine and norepinephrine, *Anal. Biochem*., 388, 2009, pp. 288–295.

[53]. Y-Q. Tian, N-B. Li and H-Q Luo, Simultaneous Determination of Trace Zinc(II) and Cadmium(II) by Differential Pulse Anodic Stripping Voltammetry Using a MWCNTs–NaDBS Modified Stannum Film Electrode, *Elctroanalysis,*21, pp 2009,. 2584-2589

[54]. S. Yadav, R. Devi, S. Kumari, S. Yadav and C. S. Pundir, An amperometric oxalate biosensor based on sorghum oxalate oxidase bound carboxylated multiwalled carbon nanotubes–polyaniline composite film, *J. Biotechnol*.,151, 2011a, pp. 212-217.

[55]. S. Yadav, A. Kumar and C. S. Pundir, Amperometric creatinine biosensor based on covalently coimmobilized enzymes onto carboxylated multiwalled carbon nanotubes/polyaniline composite film, *Anal. Biochem*., 419, 2011b, pp. 277–283.

[56]. A. Di Crescenzo, V. Ettorre and A. Fontana, Non-covalent and reversible functionalization of carbon nanotubes, *Beilstein J. Nanotechnol*, 5, 2014, pp. 1675–1690.

[57]. M. R. Mananghaya, G. N. Santos and D. N. Yu, Solubility of amide functionalized single wall carbon nanotubes: a quantum mechanical study, *J. Mol. Liquids*.,242, 2017, pp. 1208–1214.

[58]. F. A. Girardi, G. E. Bruch, C. S. Peixoto, *et al.,* Toxicity of single-wall carbon nanotubes functionalized with polyethylene glycol in zebrafish (Danio rerio) embryos, *J. Appl. Toxicol*.,37, 2017, pp. 214–221.

[59]. V. Mittal, Carbon nanotubes surface modifications: an overview, In: Mittal V, Ed., Surface modification of nanotube fillers, *Wiley Interscience*, Vol. 1,2011, p. 316.

[60]. R. Devi, S. Yadav and C. S. Pundir, Electrochemical detection of xanthine in fish meat by xanthine oxidase immobilized on carboxylated multiwalled carbon nanotubes/polyaniline composite film, *Biochem. Eng. J. ,* 58–59, 2011, pp. 148–153.

[61]. K. Yamada, C-T. Kim, J-H. Kim, J-H. Chung, H. G. Lee and S. Jun, Single Walled Carbon Nanotube-Based Junction Biosensor for Detection of *Escherichia coli*, *PLOS ONE*, 9, 2014, pp. e105767-e105773

[62]. H-K. Choi, J. Lee, M-K. Park and J-H. Oh, Development of Single-Walled Carbon Nanotube-Based Biosensor for the Detection of Staphylococcus aureus, *J. Food Qual*., 2017, pp. 1-8

[63]. N. T. Tung, P. T. Tue, T. Thi, N. Lien, Y. Ohno, K. Maehashi, K. Matsumoto, K. Nishigaki, M. Biyani and Y. Takamura, Peptide aptamer-modifed single walled carbon nanotube-based transistors for high-performance biosensors, *Sci. Reports*, 7, 2017, pp. 17881-17889.

[64]. M. N. Madadi, Dopamine detection by doped single-walled carbon nanotube biosensors: A theoretical study, *J. Res. Pharm*., 23, 2019, pp. 785-791.
[65]. Z. Guo, S. Zhou, J. Li, X. Guo, J. Cu and D. Wu, Development of a paper-based microanalysis device doped with multi-walled carbon nanotubes for in vitro evaluation of fluorene cytotoxicity, *Bioelectrochem*.,135, 2020, 107552.
[66]. A. C. Ferrari, F. Bonaccorso, V. Fal'ko, K. S. Novoselov, *et al.,*Science and technology roadmap for graphene, related two-dimensional crystals, and hybrid systems, *Nanoscale*, 7, 2015, 4598.
[67]. M. Pumera, Graphene in biosensing, *Mater. Today*, 14, 2011, pp. 308-315.
[68]. Q. Zheng, H. Wu, N. Wang, R. Yan, *et al*., Graphene-based Biosensors for Biomolecules Detection, *Curr. Nanosci*., 10, 2014, pp. 627-637.
[69]. P. Suvarnaphaet and S. Pechprasarn, Graphene-Based Materials for Biosensors: A Review, *Sens*., 17, 2017, 2161.
[70]. S. Taniselass, M. K. Md. Arshad,Subash and C. B. Gopinath, Graphene-based electrochemical biosensors for monitoring noncommunicable disease biomarkers, *Biosens. Bioelectrons*., 130, 2019, pp. 276-292.
[71]. L. Xu, Y. Wen, S. Pandit, V. R. S. S. Mokkapati, *et al*., Graphene‐based biosensors for the detection of prostate cancer protein biomarkers: a review, *BMC Chem*., 13, 2019, 112.
[72]. H. Huang, S. Su, N. Wu, H. Wan, *et al*., Graphene-Based Sensors for Human Health Monitoring, *Front. Chem*., 7, 2019, 399.
[73]. Y. Bai, T. Xu and X. Zhang, Graphene-Based Biosensors for Detection of Biomarkers, *Micromach*., 11, 2020, 60.
[74]. T-T. Trupti, B. Sushmee and M. Ashok, Graphene-Based Biosensors for Detection of Biomarkers, *J. Mater. Resear*., 32, 2017, pp. 2905-2929.
[75]. Y. X. Huang, X. C. Dong, Y. Liu, L-J. Li and P. Chen, Graphene-based biosensors for detection of bacteria and their metabolic activities, *J. Mater. Chem*., 21, 2011, 12358.
[76]. E. Morales-Narvaez, A-R. Hassan and A. Merkoci, Graphene oxide as a pathogen-revealing agent: sensing with a digital-like response, *Angew. Chem. Int. Ed*., 52, 2013, pp. 13779–13783.
[77]. Y. X. Huang, X. C. Dong, Y. Shi, C. M. Li, L-J. Li and P. Chen, Nanoelectronic biosensors based on CVD grown graphene, *Nanoscale,*2, 2010, pp. 1485–1488.
[78]. Y-H. Li, L. Zhang, J. Huang, R-P. Liang and J-D. Qiu, Fluorescent graphene quantum dots with a boronic acid appended bipyridinium salt to sense monosaccharides in aqueous solution, *Chem. Commun*., 49, 2013, 5180.
[79]. V. Maniand S-M. Chen, Direct electrochemistry of glucose oxidase at electrochemically reduced graphene oxide-multiwalled carbon nanotubes hybrid material modified electrode for glucose biosensor, *Biosens. Bioelectrons.,* 41, 2013, pp. 309-315.

[80]. Q. Xu, S-X. Gu, L. Jin, Y. Zhou, *et al*., Graphene/polyaniline/gold nanoparticles nanocomposite for the direct electron transfer of glucose oxidase and glucose biosensing, *Sens. Actuators B: Chem*.,190, 2014, pp. 562-569.
[81]. A. Tarasov, M-Y. Tsai, E. M. Flynn, C. A. Joiner, *et al*., Gold-coated graphene field-effect transistors for quantitative analysis of protein–antibody interactions, *2D Material*s,2, 4, 2015, 044008.
[82]. M. A. Sakr and M. Serry, Non-enzymatic graphene-based biosensors for continous glucose monitoring, *IEEE SENS*., 2015, pp. 1-4.
[83]. N. Li, X. Wang, J. Chen, L. Sun and P. Chen, Graphene quantum dots for ultrasensitive detection of acetylcholinesterase and its inhibitors, *2D Materials*, 2, 3, 2015.
[84]. L. He, Q. Wang, D. Mandler, M. Li, *et al*., Detection of folic acid protein in human serum using reduced graphene oxide electrodes modified by folic-acid, *Biosens. Bioelectron*., 75, 2015, pp. 389–395.
[85]. L. He, Q. Pagneux, I. Larroulet, S-A. Yanguas, *et al*., Label-free femtomolar cancer biomarker detection in human serum using graphene-coated surface plasmon resonance chips, *Biosens. Bioelectron.,* 89, 2017, pp. 606–611.
[86]. D. B. Altuntas, Y. Tepeli and U. Anik, Graphene-metallic nanocomposites as modifiers in electrochemical glucose biosensor transducers, *2D Materials*, 3, 3, 2016, 034001.
[87]. G. Doria, J. Conde, B. Veigas,L. Giestas, *et al*., Noble Metal Nanoparticles for Biosensing Applications, *Sens. (Basel),*12, 2012, pp. 1657–1687.
[88]. M. Holzinger, A. Le Goff and S. Cosnier, Nanomaterials for biosensing applications: a review, *Front. Chem*.,2, 2014, pp. 1-10.
[89]. J. Wang, Nanomaterial-Based Electrochemical Biosensors, *Analyst*, 130, 2005, pp. 421-426.
[90]. C. N. R. Rao, A. Muller and A. K. Cheetham, The Chemistry of Nanomaterials: Synthesis, Properties and Applications, *John Wiley & Sons,* Hoboken, NJ, USA, 2006.
[91]. T. M. Tritt, Thermal Conductivity: Theory, Properties, and Applications, *Springer Science & Business Media*, Berlin, Germany, 2005.
[92]. G. Zhang and B. Li, Impacts of doping on thermal and thermoelectric properties of nanomaterials, *Nanoscale*, 2, 2010, pp. 1058-1068.
[93]. D. T. T. Nguyen, T. H. Au, Q. C. Tong, M. H. Luong, *et al.,* Coupling of a single active nanoparticle to a polymer-based photonic structure, *J. Sci. Adv. Mater. Devices,* 1, 2016, pp. 18-30.
[94]. S. T. Aruna and A. S. Mukasyan, Combustion synthesis and nanomaterials, *Curr. Opinion Sol. State Material. Sci*., 12, 2008, pp. 44-50.
[95]. Z. Liu, B. Han, in Handbook of Green Chemistry, *Wiley Online Library*, *John Wiley & Sons, Inc.,* Hoboken, NJ, USA, 2010.
[96]. S. K. Kulkarni, Nanotechnology: Principles and Practices, *Springer International Publishing AG,* Cham, Switzerland, 2015, p. 55.

[97]. H. D. Yu, M. D. Regulacio, E. Ye and M. Y. Han, Chemical routes to top-down nanofabrication, *Chem. Chem. Soc. Rev*., 42, 2013, pp. 6006–6018.
[98]. K-I. Chen, B-R. Li and Y-T. Chen, Silicon nanowire field-effect transistor-based biosensors for biomedical diagnosis and cellular recording investigation, *Nano Today*, 6, 2011, pp. 131-154.
[99]. K. Ariga, Y. Yamauchi, G. Rydzek, Q. Ji, *et al*., Layer-by-layer nanoarchitectonics: Invention, innovation, and evolution, *Chem. Lett.,* 43, 2013, pp. 36–68.
[100]. A. Biswas, I. S. Bayer, A. S. Biris, T. Wang, *et al*., Advances in top–down and bottom–up surface nanofabrication: Techniques, applications & future prospects, *Adv. Colloid Interface Sci*.,170, 2012, pp. 2–27.
[101]. F. Sanchez and K. Sobolev, Nanotechnology in concrete—A review, *Constr. Build. Mater.,* 24, 2010, pp. 2060–2071.
[102]. G. Cao, Nanostructures & Nanomaterials: Synthesis, Properties & Applications, *Imperial College Press,* London, UK, 2004.
[103]. X. Zhang, Q. Guo and D. Cui, Recent Advances in nanotechnology applied to biosensors, *Sens.,* 9, 2009, pp. 1033-1053.
[104]. J. Verma, S. Lal and C. J. van Noorden, Inorganic nanoparticles for the theranostics of cancer, *Eur. J. Nanomed*., 7, 2015, pp. 271–287.
[105]. M. I. Stockman, Nanoplasmonics: physics behind the applications, *Phys. Today*, 64, 2011, pp. 39–44.
[106]. K. Purohit, P. Khitoliya and R. Purohit, Recent advances in nanotechnology, *Int. J. Sci. Eng. Res*., 3, 2012.
[107]. L. Catherine, P. Olivier, Gold Nanoparticles for Physics, Chemistry and Biology, *World Scientific*, London, UK, 2017.
[108]. K. K. Jain, Nanomedicine: Application of nanobiotechnology in medical practice, *Med. Princ. Pract*., 17, 2008, pp. 89–101.
[109]. J Conde, J. Rosa, J. C. Lima and P. V. Baptista, Nanophotonics for Molecular Diagnostics and Therapy Applications, *Int. J. Photoenergy*., 2012, 2011, 619530.
[110]. P. V. Baptista, G. Doria, P. Quaresma, M. Cavadas, *et al*., Nanoparticles in molecular diagnostics, *Prog. Mol. Biol. Transl. Sci.,* 104, 2011, pp. 427-488.
[111]. J. Xie, X. Zhang, H. Wang, H. Zheng and Y. Huang, Analytical and environmental applications of nanoparticles as enzyme mimetics, *Trends in Anal. Chemi*., 39, 2012, pp. 114-129.
[112]. M. A. Eckert, P. Q. Vu, K. Zhang, D. Kang, *et al*., Novel Molecular and Nanosensors for In Vivo Sensing, *Theranostics*, 3, 2013, pp. 583-594.
[113]. W. Putzbach and N. Ronkainen, Immobilization techniques in the fabrication of nanomaterial-based electrochemical biosensors: a review, *Sens*., 13, 2013, pp. 4811–4840.
[114]. J. Wang, Electrochemical biosensing based on noble metal nanoparticles, *Microchim. Acta*, 177, 2012, pp. 245–270.
[115]. Y. Fang, Y. Xu and P. He, DNA Biosensors Based on Metal Nanoparticles, *J. Biomed. Nanotechnol*., 1, 2005, pp. 276-285.

[116]. E. Boisselier and D. Astruc, Gold nanoparticles in nanomedicine: Preparations, imaging, diagnostics, therapies and toxicity, *Chem. Soc. Rev.,* 38, 2009, pp. 1759–1782.
[117]. K. M. Mayer and J. H. Hafner, Localized surface plasmon resonance sensors, *Chem. Rev*., 111, 2011, pp. 3828–3857.
[118]. M. Rycenga, C. M. Cobley, J. Zeng, W. Li, *et al*., Controlling the synthesis and assembly of silver nanostructures for plasmonic applications, *Chem. Rev*., 111, 2011, pp. 3669–3712.
[119]. E. C. Dreaden, A. M. Alkilany, X. Huang, C. J. Murphy and M. A. El-Sayed, The golden age: Gold nanoparticles for biomedicine, *Chem. Soc. Rev.,* 41, 2012, pp. 2740–2779.
[120]. V. V. Mody, R. Siwale, A. Singh and H. R. Mody, Introduction to metallic nanoparticles, *J. Pharm. Bioallied Sci.,*2, 2010, pp. 282-289.
[121]. P. Pandey, S. K. Arya, Z. Matharu, S. P. Singh, M. Datta and B. D. Malhotra, Polythiophene gold nanoparticles composite film for application to glucose sensor, *J. Applied Poly. Sci*., 110, 2008, pp. 988-994.
[122]. R. Chauhan, J. Singh, P. R. Solanki, T. Manaka, M. Iwamoto, T. Basu and B. D. Malhotra, Label-free piezoelectric immunosensor decorated with gold nanoparticles: Kinetic analysis and biosensing application, *Sens. Actuators B: Chem*., 222, 2016, pp. 804-814.
[123]. S. Unser, I. Bruzas, J. He and L. Sagle, Localized surface plasmon resonance biosensing: Current challenges and approaches, *Sens*., 15, 2015, 15684.
[124]. S. Hui, Plasmonic nanoparticles: Towards the fabrication of biosensors, *IOP Conf. Ser. Mater. Sci. Eng*., 87, 2015, 012009.
[125]. P. Chen, N. T. Tran, X. Wen, Q. Xiong and B. Liedberg, Inflection Point of the localized surface plasmon resonance peak: A General method to improve the sensitivity, *ACS Sens*., 2, 2017, pp. 235–242.
[126]. P. Chen, X. Liu, G. Goyal, N. T. Tran, *et al*., Nanoplasmonic Sensing from the human vision perspective, *Anal. Chem*., 90, 2018, pp. 4916–4924.
[127]. A. Sharma, Z. Matharu, G. Sumana, P. R. Solanki, C. G. Kim and B. D. Malhotra, Antibody immobilized cysteamine functionalized-gold nanoparticles for aflatoxin detection, *Thin Solid Films*, 519, 2010, pp. 1213-1218.
[128]. A. Steinbrück, O. Stranik, A. Csaki and W. Fritzsche, Sensoric potential of gold–silver core–shell nanoparticles, *Anal. Bioanal. Chem*., 401, 2011, 1241.
[129]. H. Huang, S. Huang, S. Yuan, C. Qu, *et al*., High-sensitivity biosensors fabricated by tailoring the localized surface plasmon resonance property of core-shell goldnanorods, *Anal. Chim. Acta,* 683, 2011,pp. 242–247.
[130]. L. Lu, G. Burkey, I. Halaciuga and D. V. Goia, Core-shell gold/silver nanoparticles: Synthesis and optical properties, *J. Colloid Int. Sci*., 392, 2013, pp. 90–95.

[131]. X. Cao, Y. Ye and S. Liu, Gold nanoparticle-based signal amplification for biosensing, *Anal Biochem*., 417, 2011, pp. 1-16.
[132]. A. Kumar, B. Mazinder Boruah and X-J., Liang Gold nanoparticles: promising nanomaterials for the diagnosis of cancer and HIV/AIDS, *J. Nanomater*., 17, 2011, 202187.
[133]. J. Conde, G. Doria and P. Baptista, Noble metal nanoparticles applications in cancer, *J. Drug. Deliv*., 2012, 751075.
[134]. K. A. Willets and R. P. van Duyne, Localized surface plasmon resonance spectroscopy and sensing, *Ann. Rev. Phys. Chem*., 58, 2007, pp. 267–297.
[135]. P. Mulvaney, Surface plasmon spectroscopy of nano sized metal particles, *Langmuir*, 12, 1996, pp. 788–800.
[136]. E. Hao, G. C. Schatz and J. T. Hupp, Synthesis and optical properties of an isotropic metal nanoparticles, *J. Fluoresc*., 14, 2004, pp. 331–341.
[137]. S. J. Oldenburg, C. C. Genick, K. A. Clark and D. A. Schultz, Base pair mismatch recognition using plasmon resonant particle labels, *Anal. Biochem*., 309, 2002, pp. 109–116.
[138]. J. Liu and Y. Lu, Colorimetric biosensors based on DNAzyme assembled gold nanoparticles, *J. Fluoresc*., 14, 2004, pp. 343–354.
[139]. W. Xu, X. Xue, T. Li, H. Zeng and X. Liu, Ultrasensitive and selective col orimetric DNA detection by nicking endonuclease assisted nanoparticle amplification, *Angew. Chem. Int. Ed*., 48, 2009, pp. 6849–6852.
[140]. E. Wijaya, C. Lenaerts, S. Maricot, J. Hastanin, *et. al*., Surface plasmon resonance based biosensors: from the development of different SPR structures to novel surface functionalization strategies, *Curr. Opin. Solid State Mater. Sci.,* 15, 2011, pp. 208–224
[141]. X. Guo, Surface plasmon resonance based biosensor technique: a review, *J. Biophotonics*, 5, 2012, pp. 483–501.
[142]. S. Zeng, X. Yu, W-C. Law, Y. Zhang, *et. al.,* Size dependence of AuNP enhanced surface plasmon resonance based on differential phase measurement, *Sens. Actuators B Chem*., 176, 2013, pp. 1128–1133.
[143]. H. Zhang, D. Song, S. Gao, J. Zhang, H. Zhang andY. Sun, Novel SPR biosensors based on metal nanoparticles decorated with graphene for immunoassay, *Sens. Actuators B: Chem.,*188, 2013, pp. 548-554.
[144]. B. Batra, S. Lata, R. Devi, S. Yadav and C. S. Pundir, Fabrication of an amperometric tyramine biosensor based on immobilization of tyramine oxidase on AgNPs/L-Cys-modified Au electrode, *J. Solid State Electrochem*., 16, 2012, pp. 3869–3876.
[145]. R. Devi, B. Batra, S. Lata, S. Yadav and C. S. Pundir, A method for determination of xanthine in meat by amperometric biosensor based on silver nanoparticles/cysteine modified Au electrode, *Proces. Biochem*., 48, 2013a, pp. 242–249
[146]. X. Huang and M. A. El-Sayed, Gold nanoparticles: Optical properties and implementations in cancer diagnosis and photothermal therapy, *J. Adv. Res*.,1, 2010, pp. 13–28.

[147]. C. J. Murphy, A. M. Gole, S. E. Hunyadi, J. W. Stone, *et al*., Chemical sensing and imaging with metallic nanorods, *Chem. Commun*., 8, 2008, pp. 544–557.
[148]. M. P. Navas and R. K. Soni, Laser-generated bimetallic Ag-Au and Ag-Cu core-shell nanoparticles for refractive index sensing, *Plasmonics*, 10, 2015, pp. 681–690.
[149]. M. M. Barsan and C. M. A. Brett, Recent advances in layer-by-layer strategies for biosensors incorporating metal nanoparticles, *Trends Anal. Chem*., 79, 2016, pp. 286–296.
[150]. J. Yu, W. C. Guo, M. Yang, Y. Luan, J. Z. Tao and X. W. Zhang, Synthesis of hierarchical polystyrene/polyaniline@Au nanostructures of different surface states and studies of their catalytic properties, *Sci. China Chem*., 57, 2014, pp. 1211–1217.
[151]. M. Hasanzadeh, N Shadjou., M. de la Guardia *Trend. Anal. Chem*., 72, 2015, pp. 1–9.
[152]. S. Mehtab, M. G. H. Zaidi and P. Joshi, Metal Nanoparticles Based Electrochemical Biosensors for Cholesterol, *J. Nanomed. Nanotech*., 11, 1, 2020, 540.
[153]. C. S. Pundir, N. Chauhan, Rajneesh and M. Verma, A novel amperometric biosensor for oxalate determination using multi-walled carbon nanotube-gold nanoparticle composite, *Sens. Actuators B: Chem*., 155, 2011, pp. 796–803.
[154]. S. Lata, B. Batra, N. Karwasra and C. S. Pundir, An amperometric H2O2 biosensor based on cytochrome c immobilized onto nickel oxide nanoparticles/carboxylated multiwalled carbon nanotubes/polyaniline modified gold electrode, *Proc. Biochem*., 47, 2012, pp. 992–998.
[155]. K. J. M. Bishop, C. E. Wilmer, S. Soh and B. A. Grzybowski, Nano scale forces and their uses in self-assembly', *Small*, 5, 2009, pp. 1600–1630.
[156]. S. Chawla and C. S. Pundir, An electrochemical biosensor for fructosyl valine for glycosylated hemoglobin detection based on core–shell magnetic bionanoparticles modified gold electrode, *Biosens. Bioelectrons*., 26, 2011, pp. 3438–3443.
[157]. Z. Zhong, S. Patskovskyy, P. Bouvrette, J. H. T. Luong and A. Gedanken, The surface chemistry of Au colloids and their interactions with functional amino acids, *J. Phys. Chem. B,* 108, 2004, pp. 4046–4052.
[158]. R. Devi, S. Yadav, R. Nehra, S. Yadav and C. S. Pundir, Electrochemical biosensor based on gold coated iron nanoparticles/chitosan composite bound xanthine oxidase for detection of xanthine in fish meat, *J. Food Eng*.,115, 2013b, pp. 207–214.
[159]. P. R. Solanki, A. Kaushik, V. V. Agrawal and B. D. Malhotra, Nanostructured metal oxide-based biosensors, *NPG Asia Materials*, 3, 2011, pp. 17-24.
[160]. X. Shi, W. Gu, B. Li, N. Chen, K. Zhao andY. Xian, Enzymatic biosensors based on the use of metal oxide nanoparticles, *Microchimica Acta*, 181, 2014, pp. 1–22.

[161]. B. Gu, C. Xu, C. Yang, S. Liu and M. Wang, ZnO quantum dot labeled immunosensor for carbohydrate antigen, *Biosens*. *Bioelectron*., 26, 2011, pp. 2720–2723.
[162]. R. Sadeghi, H. Karimi-Maleh, A. Bahari and M. Taghavi, A novel biosensor based on ZnO nanoparticle/1,3-dipropylimidazolium bromide ionic liquid-modified carbon paste electrode for square-wave voltammetric determination of epinephrine, *Phys. Chem. Liq*., 51, 2013, pp. 704–714.
[163]. F. Zhou, W. Jing, P. Liu, D. Han, Z. Jiang and Z Wei, Doping Ag in ZnO Nanorods to Improve the Performance of Related Enzymatic Glucose Sensors, *Sens*., 17, 2017, 2214.
[164]. S. M. Sultan, M. R. R. De Planque, P. Ashburn and H. M. H. Chong, Effect of Phosphate Buffered Saline Solutions on Top-Down Fabricated ZnO Nanowire Field Effect Transistor, J. *Nanomater*., 7, 2017, p. 5413705.
[165]. X. Wang, X. Ma, J. Church, S. Jung, Y. Son, W. H. Lee and H. J. Cho, ZnO nanoflakes as a template for in-situ electrodeposition of nanostructured cobalt electrodes as amperometric phosphate sensors, *Mater. Lett*., 192, 2017, pp. 107–110.
[166]. C. Aydin, Synthesis of Pd: ZnO nanofibers and their optical characterization dependent on modified morphological properties, *J. Alloy. Compd*., 777, 2019, pp. 145–151.
[167]. S. Hussain, T. Liu, N. Aslam, M. Kashif, *et al*., Polymer-assisted co-axial multi-layered circular ZnO nanodisks, *Mater. Lett*., 152, 2015, pp. 260–263.
[168]. L. Yu, F. Guo, S. Liu, B. Yang, *et al*., Both oxygen vacancies defects and porosity facilitated NO2 gas sensing response in 2D ZnO nanowalls at room temperature, *J. Alloy. Compd*., 682, 2016, pp. 352–356.
[169]. H. Tian, H. Fan, J. Ma, L. Ma and G. Dong, Noble metal-free modified electrode of exfoliated graphitic carbon nitride/ZnO nanosheets for highly efficient hydrogen peroxide sensing, *Electrochim. Acta*, 247, 2017, pp. 787–794.
[170]. Y. Wang, H. Deng, C. Huangfu, Z. Lu, *et al*., Research of protein adsorption on the different surface topography of the zinc oxide, *Surf. Interface Anal*., 47, 2015, pp. 245–252.
[171]. S. Yadav, R. Devi, A. Kumar and C. S. Pundir, Tri-enzyme functionalized ZnO-NPs/CHIT/c-MWCNT/PANI composite film for amperometric determination of creatinine, *Biosens. Bioelectrons*,. 28, 2011c, pp. 64-70.
[172]. R. Devi, S. Yadav and C. S. Pundir, Amperometric determination of xanthine in fish meat by zinc oxide nanoparticle/chitosan/multiwalled carbon nanotube/polyaniline composite film bound xanthine oxidase, *Analyst*, 137, 2012, pp. 754-759.
[173]. Ç. Atan, Karaku and Emine, Novel Zinc Oxide Nanorod and Chitosan-Based Electrochemical Glucose Biosensors for Glucose Assay in Human Serum Samples, *Sens. Lett*., 12, 2014, pp. 1613-1619.

[174]. S. Yadav, R. Devi, P. Bhar, S. Singhla and C. S. Pundir, A creatinine biosensor based on iron oxide nanoparticles/chitosan-g-polyaniline composite film electrodeposited on Pt electrode, *Enz. Microb. Technol*., 50, 2012, pp. 247-254.

[175]. Z. Yang, Y. Xu, J. Li, Z. Jian, *et al*., An enzymatic glucose biosensor based on a glassy carbon electrode modified with cylinder-shaped titanium dioxide nanorods, *Microchimica Acta*, 182, 2015, pp. 1841-1848.

[176]. N. Haghighi, R. Hallaj and A. Salimi, Immobilization of glucose oxidase onto a novel platform based on modified TiO2 and graphene oxide, direct electrochemistry, catalytic and photocatalytic activity, *Materials Sci. Eng. C*., 73, 2017, pp. 417-424.

[177]. F. Huang, Y. Zhong, J. Chen, S. Li, Y. Li, F. Wang and S. Feng, Nonenzymatic glucose sensor based on three different CuO nanomaterials, *Anal. Methods*., 5, 2013, pp. 3050-3055.

[178]. S. Liu, Z. Wang, F. Wang, B. Yu and T. Zhang, High surface area mesoporous CuO: A high-performance electrocatalyst for non-enzymatic glucose biosensing, *RSC Advances*., 4, 2014, pp. 33327-33331.

[179]. D. Patil, N. Q. Dung, H. Jung, S. Y. Ahn, D. M. Jang and D. Kim, Enzymatic glucose biosensor based on CeO_2 nanorods synthesized by non-isothermal precipitation, *Biosens. Bioelectrons*., 31, 2012, pp. 176-181.

[180]. C. J. Cai, M. W. Xu, S. J. Bao, C. Lei and D. Z. Jia, A facile route for constructing a graphene-chitosan-ZrO_2 composite for direct electron transfer and glucose sensing, *RSC Advancs*., 2, 2012, pp. 8172-8178.

[181]. A. T. E. Vilian, S. M. Chen, M. A. Ali and F. M. A. Al-Hemaid, Direct electrochemistry of glucose oxidase immobilized on ZrO_2 nanoparticles-decorated reduced graphene oxide sheets for a glucose biosensor, *RSC Adv*., 4, 2014, pp. 30358-30367.

[182]. J. Jiang, Y. Li, J. Liu, X. Huang, C. Yuan and X. W. D. Lou, Recent advances in metal oxide-based electrode architecture design for electrochemical energy storage, *Advan. Mater*., 24, 2012, pp. 5166-5180.

[183]. W. He, Y. Huang and J. Wu, Enzyme-Free Glucose Biosensors Based on MoS2 Nanocomposites, *Nanoscale Res. Letts*., 15, 60, 2020.

[184]. L. Lu, X. Hu, Z. Zhu, D. Li, S. Tian and Z. Chen, Electrochemical Sensors and Biosensors Modified with Binary Nanocomposite for Food Safety, *J. Electrochem. Soc*., 167, 2020, 037512.

[185]. M-M. Titirici, M. Antonietti and A. Thomas, A Generalized Synthesis of Metal Oxide Hollow Spheres Using a Hydrothermal Approach, *Chem. Mater*., 18, 16, 2006, pp. 3808–3812.

[186]. J. S. Hu, L. S. Zhong, W. G. Song and L. J. Wan, Synthesis of hierarchically structured metal oxides and their application in heavy metal ion removal, *Advanc. Mater*., 20, 15, 2008, pp. 2977-2982.

[187]. Y. Ren, Z. Ma and P. G. Bruce, Ordered mesoporous metal oxides: synthesis and applications, *Chem. Soc. Reviews*, 41, 2012, pp. 4909-4927.
[188]. J. Hu, Y. Qian, X. Wang, T. Liu and S. Liu, Drug-Loaded and Superparamagnetic Iron Oxide Nanoparticle Surface-Embedded Amphiphilic Block Copolymer Micelles for Integrated Chemotherapeutic Drug Delivery and MR Imaging, *Langmuir*, 28, 4, 2012, pp. 2073–2082.
[189]. P. Kofstad, Defects and transport properties of metal oxides, *Oxid. Metals*, 44, 3, 1995, pp. 3–27.
[190]. A. E. Nel, L. Madler, D. Velegol, T. Xia, *et al*., Understanding biophysicochemical interactions at the nano–bio interface, *Nature Mater*., 8, 2009, pp. 543–557.
[191]. R. Ahmad, N. Tripathy, J-H. Park and Y-B. Hahn, A comprehensive biosensor integrated with a ZnO nanorod FET array for selective detection of glucose, cholesterol and urea, *Chem. Comm*., 51, 2015, pp. 11968–11971.
[192]. A. Tereshchenko, M. Bechelany, R. Viter, V. Khranovskyy, *et al*., Optical Biosensors Based on ZnO Nanostructures: Advantages and Perspectives. A Review, *Sens. Actuators B: Chem.,* 229, 2016, pp. 664-677.
[193]. M. L. Mohd Napi, S. Mohd Sultan, R. Ismail, K. Wei How and M. K. Ahmad, Electrochemical-Based Biosensors on Different Zinc Oxide Nanostructures: A Review, *Mater.,* 12, 2019, 2985.
[194]. B. Liu and J. Liu, Sensors and biosensors based on metal oxide nanomaterials, *Trend. Anal. Chem*., 121, 2019, 115690.
[195]. J. Geng, G. H. Song, X. D. Jia, F. F. Cheng and J. J. Zhu, Fast one-step synthesis of biocompatible ZnO/Au nanocomposites with hollow doughnut-like and other controlled morphologies, *J. Phys. Chem. C*, 116, 2012, pp. 4517–4525.
[196]. S. Hrapovic, E. Majid, Y. Liu, Y. Male and J. H. T. Luong, Metallic nanoparticle carbon nanotube composites for electrochemical determination of explosive nitroaromatic compounds, *Anal. Chem*., 78, 2006, pp. 5504–5512.
[197]. M. M. Rahman, A. J. S. Ahammad, J. H. Jin, S. J. Ahn and J. J. Lee, A comprehensive review of glucose biosensors based on nanostructured metal-oxides, *Sens.,*10, 2010, pp. 4588–4886.
[198]. S-K. Jin, P. Won, L. Chul-Ho and Y. Gyu-Chul, ZnO Nanorod Biosensor for Highly Sensitive Detection of Specific Protein Binding, *J. Korean Phys. Soc*., 49, 2006, 1635.
[199]. A. Fulati, S. M. Usman Ali, M. H. Asif, Hassan Alvi *etal*., An intracellular glucose biosensor based on nanoflake ZnO, *Sens. Actuators B: Chem.,*150, 2010, pp. 673-680.
[200]. D. Pradhan, F. Niroui and K. T. Leung, High-Performance, Flexible Enzymatic Glucose Biosensor Based on ZnO Nanowires Supported on a

Gold-Coated Polyester Substrate, *Appl. Mater. Interfaces*, 2, 2010, pp. 2409–2412.

[201]. M. Liu, R. Liu and W. Chen, Graphene wrapped Cu2O nanocubes: Non-enzymatic electrochemical sensors for the detection of glucose and hydrogen peroxide with enhanced stability, *Biosens. Bioelectrons*., 45, 2013, pp. 206-212.

[202]. R. Ahmad, N. Tripathy, J. H. Kim and Y-B. Hahn, Highly selective wide linear-range detecting glucose biosensors based on aspect-ratio controlled ZnO nanorods directly grown on electrodes, *Sens. Actuators B: Chem*., 174, 2012, pp. 195-201.

[203]. R. M. Cornell and U. Schwertmann, Introduction to the Iron Oxides, in The Iron Oxides, *Wiley-VCH Verlag GmbH & Co. KGaA*,2004, p. 1-7.

[204]. A. K. Gupta and M. Gupta, Synthesis and surface engineering of iron oxide nanoparticles for biomedical applications, *Biomaterials*, 26, 2005, pp. 3995-4021.

[205]. D. Uhlirova, M. Stankova, M. Docekalova, B. Hosnedlova, *et al*., A Rapid Method for the Detection of Sarcosine Using SPIONs/Au/CS/SOX/NPs for Prostate Cancer Sensing, *Int. J. Mol. Sci*.,19, 2018, 3722.

[206]. P. Nayak, P. N. Santhosh and S. Ramaprabhu, Cerium oxide nanoparticles decorated graphene nanosheets for selective detection of dopamine, *J. Nanosci. Nanotechnol*.,15, 7, 2015, pp. 4855-4862.

[207]. Y. Zhang and Q. Wei, The role of nanomaterials in electroanalytical biosensors: A mini review, *J. Electroanal. Chem*.,781, 2016, pp. 401-409.

[208]. C. I. L. Justino, A. R. Gomes, A. C. Freitas, A. C. Duarte and T. A. P. Rocha-Santos, Graphene based sensors and biosensors, *Trend. Anal. Chem.,* 91, 2017*,* pp. 53-56.

[209]. A. A. Ansari, P. R. Solanki and B. D. Malhotra, Hydrogen peroxide sensor based on horseradish peroxidase immobilized nanostructured cerium oxide film, *J. Biotechnol*.,142, 2009, pp. 179–184.

[210]. X. L. Xiao, Q. F. Luan, X. Yao and K. B. Zhou, Single-crystal CeO2 nanocubes used for the direct electron transfer and electrocatalysis of horseradish peroxidase, *Biosens. Bioelectron*., 24, 2010, pp. 2447–2451.

[211]. R. E. Özel, C. Ispas, M. Ganesana, J. C. Leiter and S. Andreescu, Glutamate oxidase biosensor based on mixed ceria and titania nanoparticles for the detection of glutamate in hypoxic environments, *Biosens. Bioelectron*., 52, 2014, pp. 397–402.

[212]. C. Ispas, J. Njagi, M. Cates and S. Andreescu, Electrochemical Studies of Ceria as Electrode Material for Sensing and Biosensing Applications, *J. Electrochem. Soc*., 155, 2008, pp. F169–F176.

[213]. X. Yang, Y. Ouyang, F. Wu, Y. Hu, H. Zhang and Z. Wu, In situ & controlled preparation of platinum nanoparticles dopping into graphene sheets @cerium oxide nanocomposites sensitized screen printed electrode for nonenzymatic electrochemical sensing of hydrogen peroxide, *J. Electroanal. Chem*., 777, 2016, pp. 85–91.

[214]. J. Xu, J. Harmer, G. Li, T. Chapman, P. Collier, S. Longworth and S. C. Tsang, Size dependent oxygen buffering capacity of ceria nanocrystals, *Chem. Commun.,*46, 2010, pp. 1887–1889.

[215]. D. Wang, Y. Kang, V. Doan-Nguyen, J. Chen, *et al*., Synthesis and oxygen storage capacity of two-dimensional ceria nanocrystals, *Angew. Chem. Int. Ed. Engl*., 50, 2011, pp. 4378–4381.

[216]. G. Preda, A. Migani, K. M. Neyman, S. T. Bromley, F. Illas and G. Pacchioni, Formation of superoxide anions on ceria nanoparticles by interaction of molecular oxygen with Ce^{3+} sites, *J. Phys. Chem. C,*115, 2011, pp. 5817–5822.

[217]. T. Pirmohamed, J. M. Dowding, S. Singh, B. Wasserman, *et al*., Nanoceria exhibit redox state-dependent catalase mimetic activity, *Chem. Commun*., 46, 2010, pp. 2736–2738.

[218]. A. Asati, C. Kaittanis, S. Santra and J. M. Perez, The pH-tunable oxidase-like activity of cerium oxide nanoparticles achieves sensitive fluorigenic detection of cancer biomarkers at neutral pH, *Anal. Chem*., 83, 2011, pp. 2547–2553.

[219]. M. Ornatska, E. Sharpe, D. Andreescu and S. Andreescu, Paper bioassay based on ceria nanoparticles as colorimetric probes, *Anal. Chem*., 83, 2011, pp. 4273–4280.

[220]. X. Li, L. Sun, A. Ge and Y. Guo, Enhanced chemiluminescence detection of thrombin based on cerium oxide nanoparticles, *Chem. Commun*.,47, 2011, pp. 947–949.

[221]. C. Kaittanis, S. Santra, A. Asati and J. M. Perez, A cerium oxide nanoparticle based device for the detection of chronic inflammation via optical and magnetic resonance imaging, *Nanoscale*, 4, 2012, pp. 2117–2123.

[222]. Y. Lin, C. Xu, J. Ren and X. Qu, Using thermally regenerable cerium oxide nanoparticles in biocomputing to perform label-free, resettable, and colorimetric logic operations, *Angew. Chem. Int. Ed. Engl*., 51, 2012, pp. 12579–12583.

[223]. M. Li, P. Shi, C. Xu, J. Ren and X. Qu, Cerium oxide caged metal chelator: Anti-aggregation and anti-oxidation integrated H_2O_2-responsive controlled drug release for potential Alzheimer's disease treatment, *Chem. Sci.,*4, 2013, pp. 2536–2542.

[224]. C. Xu, Y. Lin, J. Wang, L. Wu, W. Wei, J. Ren and X. Qu, Nanoceria-triggered synergetic drug release based on CeO(2)-capped mesoporous silica host–guest interactions and switchable enzymatic activity and cellular effects of CeO(2), *Adv. Healthc. Mater.,* 2, 2013, pp. 1591–1599.

[225]. S. Singh, Cerium oxide based nanozymes: Redox phenomenon at biointerfaces, *Biointerphases*, 11, 2016, 04B202.

[226]. C. Tortolini, P. Bollella, R. Zumpano, G. Favero, F. Mazzei and R. Antiochia, Metal Oxide Nanoparticle Based Electrochemical Sensor for Total Antioxidant Capacity (TAC) Detection in Wine Samples, *Biosens.,* 8, 2018, 108.

[227]. S. R. Benjamin, R. S. Vilela, H. S. de Camargo, M. I. F. Guedes, K. F. Fernandes and F. Colmati, Enzymatic Electrochemical Biosensor Based on Multiwall Carbon Nanotubes and Cerium Dioxide Nanoparticles for Rutin Detection, *Int. J. Electrochem. Sci*., 13, 2018, pp. 563-586.

[228]. D. Nunes, L. Santos, P. Duarte, A. Pimentel, *et al*., Room Temperature Synthesis of Cu_2O Nanospheres Optical Properties and Thermal Behavior, *Microsco. Microanal*., 21, 2014, pp. 108-119.

[229]. K. Jindal, M. Tomar and V. Gupta, CuO thin film based uric acid biosensor with enhanced response characteristics, *Biosens. Bioelectrons*., 38, 2012, pp. 11-8.

[230]. X. Liu, P. Lin, X. Yan, Z. Kang, *et al*., Enzyme-coated single ZnO nanowire FET biosensor for detection of uric acid, *Sens. Actuators B: Chem.,*176, 2013, pp. 22-27.

[231]. R. Khan, R. Ahmad, P. Rai, L-W. Jang, *et al*., Glucose-assisted synthesis of Cu_2O shuriken-like nanostructures and their application as nonenzymatic glucose biosensors, *Sensors Sens. Actuators B: Chem.,*203, 2014, pp. 471-476.

[232]. R. Ahmad, N. Tripathy, M-S. Ahn, K. S Bhat, *et al*., Highly efficient non-enzymatic glucose sensor based on CuO modified vertically-grown ZnO nanorods on electrode, *Scientific Reports*, 7, 2017, 5715.

[233]. Y. Li, Y. Zhong, Y. Zhang, W. Weng and S. Li, Carbon quantum dots/octahedral Cu_2O nanocomposites for non-enzymatic glucose and hydrogen peroxide amperometric sensor, *Sens. Actuators B: Chem.,*206, 2015, pp. 735-743.

[234]. Y. Li, Y. Wei, G. Shi, Y. Xian and L. Jin, Facile Synthesis of Leaf Like CuO Nanoparticles and Their Application on Glucose Biosensor, *Electroanal*., 23, 2010, pp. 497-502.

[235]. L. Xu, Q. Yang, X. Liu, J. Liu and X. Sun, One-dimensional copper oxide nanotube arrays: biosensors for glucose detection, *RSC Adv*., 4, 2014, pp. 1449-1455.

[236]. R. Ahmad, M. Vaseem, N. Tripathy and Y-B. Hahn, Wide Linear-Range Detecting Nonenzymatic Glucose Biosensor Based on CuO Nanoparticles Inkjet-Printed on Electrodes, *Anal. Chem*., 85, 2013, pp. 10448-10454.

[237]. N. Batra, M. Tomar and V. Gupta, ZnO–CuO composite matrix based reagentless biosensor for detection of total cholesterol, *Biosens. Bioelectrons*., 67, 2015, pp. 263-271.

[238]. C. S. Pundir, Introduction to enzyme and nanotechnology, Enzyme Nanoparticles: Preparation, Characterization, Properties, and Applications, (Micro and Nanotechnology Series), *Elsevier*, Oxford, UK, 2015.

[239]. N. Yadav, J. Narang, A. K. Chhillar and C. S. Pundir, Preparation, characterization, and application of enzyme nanoparticles, *Meth. Enzymol*., 609, 2018a, pp. 171–196.

[240]. G. Liu, Y. Lin, V. Ostatna and J. Wang, Enzyme nanoparticles based electronic biosensor, *Chem. Commun*., 27, 2005, pp. 3481–3483.
[241]. N. Kundu, S. Yadav and C. S. Pundir, Preparation and characterization of glucose oxidase nanoparticles and their application in DO metric determination of serum glucose, *Nanosci. Nanotechnol*., 13, 2012, pp. 1710–1716.
[242]. N. Chauhan, A. Kumar and C. S. Pundir, Construction of an uricase nanoparticles modified Au electrode for amperometric determination of uric acid, *Appl. Biochem. Biotechnol*., 174, 2014, pp. 1683–1694.
[243]. V. Aggarwal, J. Malik, A. Prashant, P. K. Jaiwal and C. S. Pundir, Amperometric determination of serum total cholesterol with nanoparticles of cholesterol esterase and cholesterol oxidase, *Anal. Biochem*., 500, 2016, pp. 6–11.
[244]. C. S. Pundir and V. Aggarwal, Amperometric triglyceride bionanosensor based on nanoparticles of lipase, glycerol kinase, glycerol-3-phosphate oxidase, *Anal. Biochem*., 517, 2017, pp. 56–63.
[245]. P. Kumar, R. Jaiwal and C. S. Pundir, An improved amperometric creatinine biosensor based on nanoparticles of creatininase, creatinase and sarcosine oxidase, *Anal. Biochem*., 537, 2017, pp. 41–49.
[246]. N. Yadav, A. K. Chhillar and C. S. Pundir, Preparation, characterization and application of haemoglobin nanoparticles for detection of acrylamide in processed foods, *Int. J. Biol. Macromol*.,107, 2018b, pp. 1000–1013
[247]. S. Jakhar and C. S. Pundir, Preparation, characterization and application of urease nanoparticles for construction of an improved potentiometric urea biosensor, *Biosens. Bioelectron*., 100, 2018, pp. 242–250.
[248]. A. Khosravi, M. Vossoughi, S. Sharokhian and I. Alemzadeh, Synthesis and stability evaluation of HRP single enzyme nanoparticles, *Proceed. Internat. Conf. Nanostruct. (ICNS4)*, 2012, pp. 857–869.
[249]. Z. Yang and C. Zhang, Single-enzyme nanoparticles based urea biosensor, *Sens. Actuators B: Chem*., 188, 2013, pp. 313-317.
[250]. R. K. Mishra and R. Rajakumari, Nanobiosensors for Biomedical Application: Present and Future Prospects: Characterization and Biology of Nanomaterials for Drug Delivery, *Nanosci. Nanotechnol. in Drug Delivery: Micro and Nano Technol.,*1, 2019, pp. 1-23.
[251]. M. Salouti and F. K. Derakhshan, Biosensors and Nanobiosensors in Environmental Applications, *Biogenic Nano-Particles and their Use in Agro-ecosystems,* 515, 2020, pp. 515-591.
[252]. P. Malik, V. Katyal, V. Malik, A. Asatkar, G. Inwati and T. K. Mukherjee, Nanobiosensors: concepts and variations, *ISRN Nanomat.,* 2013, pp. 1-9.
[253]. S. Devi and T. L. Robert, Emerging trends in the application of nanobiosensors in the food industry: Novel Approaches of Nanotechnology in Food, *Nanotechnol. Agri-Food Indust*., 1, 2013, pp. 663-696.

[254]. R. Genç, Nanomaterial-based sensor platforms for facile detection of food contaminants, *Nanobiosens.*, 10, 2017, pp. 391-427.
[255]. S. Neethirajan, V. Ragavan, X. Weng and R. Chand, Biosensors for Sustainable Food Engineering: Challenges and Perspectives, *Biosens*., 8, 1, 2018, 23.
[256]. F. Dridi, M. Marrakchi, M. Gargouri, J. Saulnier, N. Jaffrezic-Renault and F. Lagarde, Nanomaterial-based electrochemical biosensors for food safety and quality assessment, *Nanobiosens*., 5, 2017, pp. 167-204.
[257]. T. Caon, M. S. Maria and F. F. Matta, New trends in the food industry: application of nanosensors in food packaging, *Nanobiosens*., 18, 2017, pp. 773-804.

Index

β-phase, 66

A

Acetylcholinesterase, 248, 249
Active site, 229
actuators, 65
AgNPs, 294
Alcohol
  dehydrogenase (ADH), 246
  oxidase (AOX), 246
Amperometric biosensor, 235
Amyloid polyneuropathy
  (TTR-FAP), 188
Analyte, 223, 224, 226, 229, 230,
  232-235, 237, 240, 241, 245,
  255
Anxiety, treatment, 12, 216
Anxiolytic, effect of. *Anxiety*
artificial and electronic skins, 67
AuNP, 292
autonomic
  function, 188, 191
  nervous system, 149, 186
  adrenergic, 152, 172, 190
  cholinergic, 150, 152-154, 159,
    190
  Muscarinic, 152
  sympathetic, 151, 172, 183

B

Biological, method, 215
Biomarkers, 244
biomedical sensors, 67
biomimetic, 72, 74
Blood glucose, 241, 242

C

C fibers, 150, 151, 179, 191
Carbon
  nanotubes, 276-278, 281, 282,
  286, 296, 307
  NPs, 67
Cardiovascular
  autonomic reflex tests
  (CARTs), 187
  disease, 243
Cell-based olfactory biosensor, 24
CFTR, 152, 153, 159, 192
chemical
  bath deposition, 90, 98
  precipitation, synthesis, 211
Chemiluminescence, 236
Chlorides, 156
Cholesterol
  esterase, 243
  oxidase, 243
chronoamperometry, 87
chronovoltammetry, 155, 173
CNT. *See* Nanobiosensors
composite films, 67, 69, 70, 72, 73
  Constancy, 163
conductivity, 68, 70, 71
Conductometric biosensor, 235
Crystal, structure of, 210
Current
  Axial, 160
  Axial Almost Piecewise Linear,
    168
  Capacitive wall, 159
  Cross-wall, 158
cyclic voltammetry, 87

D

Degrading enzymes, 22–23
diabetes, 81, 82, 153, 178, 179,
  181-183, 185-187, 190
dielectric
  constant, 68-71, 73
  loss, 68-71
  permittivity, 68
dimethylformamide (DMF), 67
dipole orientation, 68
Drag force, 162
dynamic tactile sensing, 66

dysautonomia, 188, 189

E

electric field, 160, 162, 202
Electrochemical Hairless Skin Model, 154
electrode, 153, 156, 162, 163, 169, 172, 176-178
  anode, 156, 158, 164, 165, 172-176, 202
  cathode, 156, 164, 165, 173-177
  nickel, 156, 172
  stainless steel, 156, 172, 174, 178
Electrode passivation, 240
electrodeposition, 90, 94-96, 99
Electronic nose, 16, 19, *See also Olfactory biosensors and bioelectronic noses*
energy harvesting, 65, 67, 68, 70, 72, 75
Enzyme Biosensors, 223
  Advantages, 239
  Applications, 241
    cholesterol detection, 237, 243
    detection of neurotransmitters, 244
    detection of phenolic compounds, 254
    detection of triglycerides, 245
    diabetes, 241
    drugs screening, 248
    ethanol detection, 246
    food industry, 252
    heavy metals detection, 250
    lactose intolerance, 242
    nitrite detection, 251
    pesticides detection, 249
    reactive oxygen species, 247
    toxin detection, 252
    uric acid detection, 245
  Classification, 230
    1st generation, 231
    2nd generation, 232
    3rd generation, 233
  Immobilization methods, 226
  Monitoring method, 237
  Transducing mechanism, 234
    electrochemical, 234
    optical-detection, 236
    piezoelectric, 237
    thermal-detection, 237

F

Fear, 205
ferroelectric, 65, 70
Field-Effect Transistor (FET), 285
figure-of-merit, 69-71, 73
flexible pressure monitoring system, 75
Fluorescence, 236
functional aspects, 108

G

Gallium nitrate, 66
Gauge Factor, 69
glucose, 81-98
  dehydrogenases, 242
  oxidase, 82
  oxidase (GO_x), 241
Glycerol kinase (GK), 245
G-protein-coupled receptors. *See* signaliging process
graphene, 83, 96, 98, 99
  oxide, 287

H

healing, 150, 151, 179
Heavy metal, 250
hierarchical structures, 94
hydrothermal, 89, 90, 98
Hyperuricemia, 245

I

Immobilization, 226
individual grip force profiles, 117

infrared sensing, 68, 70
interfacial polarization, 71
intraepidermal nerve fiber density (ENFD), 183
Iron oxide, 304

L

Lab-on-a-Chip, 315
Lactate, 242
Law of Conservation, 156, 196
  Mass, 160
  Momentum, 162
lead magnesium niobate-lead titanate (PMN-PT), 66
lead zirconate titanate (PZT), 66
limit of detection, 89
Lipase, 245
Lorentz force, 162
Luminescence, 236

M

Magnetic NPs, 297
Mechanochemical, method, 12, 213
Mediator, 232
medical and industrial applications, 65
Membrane
  biofouling, 240
  fractions, 28
metal organic frameworks, 83
methyl-ethyl-ketone (MEK), 67
Mood disorders, 206
MWCNT, 278
Mycotoxin, 253

N

nano
  nano-zinc, 12, 206, 210
Nanobiosensors, 273
  Applications
    biomedical and diagnostic, 312
    environmental, 313
    food contamination monitoring, 314
  Types, 275
    carbon nanotubes, 277
    enzyme nanoparticles, 308
    graphene based, 283
    metal nanoparticles, 288
    metal oxide, 299
nanocomposite thick films, 73
Nanodiscs, 38
nanoflakes, 89, 94-99
nanofoam, 91-94, 97-99
Nanomaterials, 274, 299
Nanoparticle, 209
nanoparticles, 65-67, 71, 89, 91, 97-99
Nanoparticles, 274, 275, 286, 292, 294, 296, 297, 300, 301, 304, 305, 308
  Cerium oxide, 306
  Cholesterol esterase, 310
  Copper oxides, 307
  Enzyme nanoparticles, 276, 308, 311
  Metal Nanoparticles, 288
nanorods, 84, 94, 95, 98, 99
nanosheets, 89-91, 98
nanotechnology, 84
Nanotechnology, 274, 275, 289, 290, 312
Nanovesicles, 33
nanowalls, 89-94, 97, 98
Nernst's law, 159
Neurotransmitters, 244
  Catecholamine, 244
  Dopamine (DA), 244
nickel, 81, 83, 85-99
  hydroxide, 85
  oxide, 85
non-enzymatic Glucose Detection, 81, 83, 89

O

Odor discrimination, 18–19
Odorant binding proteins

structure and role, 21–22
Odors, 15
Ohm's law, 160, 161, 166, 202, 204
Olfactory biosensors and bioelectronic noses, 23
odorant binding protein based, 44–51
olfactory receptor based, 26–44
Olfactory
neurons, 17
receptors, 17, 19
signaling process, 20–21
system
structure, 17–18
tissues based biosensor, 24
Optical sensing, 236
oxidation, 82, 84, 86-88, 90, 94, 99
Oxidative Stress, 247

P

Peripheral neuropathie
small fiber (SFN), 179
Peripheral
neuropathies, 149
Peripheral neuropathy
Cardiac autonomic (CAN), 186
diabetic (DPN), 183, 185
permittivity, 68
Pesticides, 249
Photoelectrochemical (PEC), 235
piezoelectric, 65, 66, 70, 75-77
piezoelectric pressure sensor, 76
Piezoelectricity, 66
piezoresistive, 65, 67, 73
Piezoresistivity, 65
Pollutant in the environment and agriculture, 313
Polymer Composite Films, 67
polymer-composite films, 67
polyvinylidene
difluoride (PVDF), 66
fluoride, 66
porous structures, 89
Potentiometric biosensor, 235
Prehensile synergies, 121
pressure sensors, 65, 69, 73, 75, 76
proton, 156, 165
PVDF
film, 74, 77
sensing film, 77
pyroelectric, 65, 66, 68-71, 73, 74
device, 71
Pyroelectricity, 66
Pyrolysis, methods, 12, 212

Q

QSART, 153, 182, 183
Quantum dots, 287
Questionnaires, 190

R

Reactive Oxygen Species, 247
regenerate, 151, 190
reverse iontophoresis, 154, 173
robot assisted minimally invasive surgical training, 112

S

selectivity, 84
Semipermeable membrane, 232
sensitivity, 84, 97
sensors, 65, 66, 69, 70, 72-77
Skin Conductance
detachement ratio, 177
dynamic, 176
Electrochemical (ESC), 169
ESC thresholds, 181
Gland Wall Ion Permeability, 169
hand to foot ratio, 177
high, 177
low, 176, 177
Normalization, 170
Normative ESC values, 181
reproducibility, 178, 182, 191
Sol-gel, method, 212
solution-cast technique, 67

spatiotemporal grip force profiles, 107
SSR, 154
Steady, 163, 165, 166
  solutions, 163
Stokes coefficient, 163
strain sensors, 69
Stress, 206, 207
structural materials, 65
Sudoscan
  accuracy, 181, 183, 187
  clinical utility, 153, 180, 181, 189
  Medical Device, 173
  patent, 174
  Schematic circuit of the measure, 174
  technology, 154, 173, 180, 182, 184, 191
Superoxide Desmutases (SODs), 247
Supplements, 209
Surface plasmon resonance, 25, 289
  imaging, 48
surgical expertise, 121
SWCNTs, 281
Sweat Glands, 150
  coil, 150, 157, 158, 164, 166, 167
  duct, 153, 157-159, 164, 166
  electrical stimulation, 154, 180
  excretory portion, 157
  secretory portion, 150, 157, 172
  Sudomor function, 151
  sweat function, 153, 179-181, 191

T

tactile sensors, 66
Tactile sensors, 65
tactile technology, 66
Thermistors, 237
Transducers, 226
Triglycerides, 245

U

Uric acid, 245, 246
Uricase, 246

V

velocities, 157
Volatile organic compounds, 15
voltage, 150, 154-160, 165, 166, 169, 171-178, 191
  inside the Gland Almost Constant, 167

W

wearable
  electronics, 66
  sensor, 74
wearable sensor systems, 107

X

Xanthine oxidase, 253

Z

zinc oxide, 66, 83, 94-96, 98, 99, 210
ZnO, 300

Advances in Biosensors: Reviews Volume 3

Sergey Y. Yurish, Editor

The 3rd volume of 'Advances in Biosensors: Book Series contains 9 chapters written by 27 authors from 9 countries: France, India, Italy, Malaysia, Turkey and USA. But is is not the set of reviews. As usually, it is extended state-of-the arts followed by novel, unpublished before, results.

Like the first two volumes of this Book Series, the 3rd volume also has been organized by topics of high interest. In order to offer a fast and easy reading of the state of the art of each topic, every chapter in this book is independent and self-contained. All chapters have the same structure: first an introduction to specific topic under study; second particular field description including sensing applications. Each of chapter is ending by well selected list of references with books, journals, conference proceedings and web sites.

This book ensures that our readers will stay at the cutting edge of the field and get the right and effective start point and road map for the further researches and developments.

With this unique combination of information in each volume, the 'Advances in Biosensors: Reviews' book Series will be of value for scientists and engineers in industry and at universities, to biosensors developers and users.

IFSA

ISBN 978-84-09-25124-7

9 788409 251247